Granular Structures with Shear Interactions : Discrete Versus Nonlocal Approaches

Sina Massoumi

THÈSE DE DOCTORAT

NNT : 2022UPAST010

Granular Structures with Shear Interactions; Discrete and Nonlocal Approaches

Structures Granulaires avec les Interactions de Cisaillement : Approches Discrètes et Nonlocaux

Thèse de doctorat de l'université Paris-Saclay

École doctorale n° 579 Sciences Mécaniques et Energétiques, Matériaux et Géosciences
Spécialité de doctorat : Mécanique du Solide
Graduate School : Sciences de l'ingénierie et des systèmes. Référent : Université d'Evry Val d'Essonne

Thèse préparée dans l'unité de recherche **Université Paris-Saclay, CNRS, Univ Evry, Laboratoire de Mathématiques et Modélisation d'Evry, 91037, Evry-Courcouronnes, France,** sous la direction de **Jean LERBET**, Professeur, la co-direction de **Noël CHALLAMEL**, Professeur

Thèse soutenue à Paris-Saclay, le 03 Février 2022, par

Sina MASSOUMI

Composition du Jury

Samuel FOREST Professeur, MINES ParisTech, PSL University, Centre des Materiaux (CMAT), CNRS 7633, Evry, France.	Rapporteur
Luigi GAMBAROTTA Professeur, Department of Civil, Chemical and Environmental Engineering, University of Genova, Genova, Italy.	Rapporteur
Ahmer WADEE Professeur, Department of Civil and Environmental Engineering, Imperial College London, London, United Kingdom.	Rapporteur
Francesco DELL'ISOLA Professeur, International Research Center on Mathematics and Mechanics of Complex Systems (M&MoCS), University of L'Aquila, Italy.	Examinateur
Djimedo KONDO Professeur, Institut Jean le Rond d'Alembert, Sorbonne Université, UPMC, CNRS 7190, Paris, France.	Examinateur
Noël CHALLAMEL Professeur, IRDL – UBS – UMR CNRS 6027, Univ. Bretagne Sud Lorient, Franc.	Directeur de thèse
Jean LERBET Professeur, Laboratoire de Mathématiques et Modélisation d'Evry, CNRS 8071, Univ Evry, Université Paris-Saclay, Evry, France.	Directeur de thèse

université PARIS-SACLAY

ÉCOLE DOCTORALE
Sciences mécaniques et énergétiques, matériaux et géosciences (SMEMAG)

Title : Granular Structures with Shear Interactions; Discrete and Nonlocal Approaches

Keywords : Granular chain, Micropolar continuum mechanic, Discrete Cosserat formulation, Wave dispersion, Nonlocal beams, DEM

ABSTRACT:

This study is an attempt towards a better understanding of the length scale effects on the bending response of the granular beams. The current work allows to investigate the interactions between the theoretical models, granular materials and the included effective parameters. To this aim first, a unidimensional discrete granular chain resting on the Winkler foundation is considered. This problem can be considered as a simple model to rigorously study the effects of the microstructure on the static and dynamic behavior of the equivalent continuum structural model. The unidimensional granular chain consists of uniform rigid grains confined by discrete elastic interactions with both shear and rotational springs, to take into account the lateral granular contributions. The presented repetitive discrete system can be referred to elastic lattice model or discrete Cosserat chain with two independent degrees of freedom (DOF) (the transversal displacement and the rotation) for each grain with the consideration of shear interaction. Accordingly, the deformation of this granular model subjected to a uniform distributed loading, are investigated theoretically for various boundary conditions defined at the grain level. Such a discrete model permits to introduce the size effect (grain dimension) in the bending formulation of a microstructured granular beam. The length scale at which the system is probed is an important issue bridging together multi-scale behavior and heterogeneity. It is shown that for an infinite number of grains, the difference equations governed to the discrete system asymptotically converge towards the differential equations of the Bresse-Timoshenko continuum beam (neglecting the length scale) resting on Winkler foundation (also classified as a continuous Cosserat beam model). Next, a twin numerical problem is studied to compare the exact analytical results with the numerical ones simulated by the discrete element method (DEM). The natural frequencies of free vibrational granular model are analytically calculated for whatever modes. The results clarify the dependency of the beam dynamic responses to the beam length ratio. In the presence of internal (microstructural) length scales, the elastic wave propagation problem involves an interplay between wave dispersion and structural features. The wave dispersive properties of this discrete model are investigated also in the Brillouin zone. Eventually, through the continualization of the coupled difference equations system governing the discrete beam, a nonlocal elasticity Cosserat continuum model is obtained. The process of continualization consists in approaching the difference operators by differential operators applied either by the polynomial or by the rational development of initial differential operators in which a length scale appears. It is shown that both the granular model and the nonlocal beam model give very close which underlines the relevance of our approach. In the end, a two-dimensional granular model connected elastically to the lateral and diagonal neighbors, is studied. The equation of the motion of this 2D system is obtained and continualized using six material parameters. Furthermore, we investigate an efficient formulation of nonlinear micropolar continuum model based on a new contribution of the relative micro rotations. Thus, a novel relative rotation tensor is used as a measure of deformation in addition to the classical strain tensor and the wryness tensor. The consequences of the proposed micropolar model are then discussed with the aid of numerical examples. To this aim, several numerical applications of 2D plate specimens subjected to in-plane loads are considered by performing a finite element code based on a variational formulation. Some new key features of the novel model, in comparison with the classical one, are illustrated by the sensitive numerical analysis.

Titre : Structures granulaires avec les interactions de cisaillement : approches discrètes et non locales

Mots clés : Chaîne granulaire, Mécanique du continu micropolaire, Formulation discrète de Cosserat, Dispersion des ondes, Poutres non locaux, DEM

Résumé : L'objectif de ce travail est d'obtenir une meilleure compréhension des effets d'échelle de longueur sur la réponse en flexion des poutres granulaires. Cette étude nous permet de mieux comprendre les liens entre les modèles théoriques, les matériaux granulaires et les paramètres effectifs inclus. Dans ce but on considère tout d'abord, une chaîne granulaire discrète unidimensionnelle reposant sur la fondation de Winkler. Ce problème peut être considéré comme un modèle simple pour étudier rigoureusement les effets de la microstructure sur le comportement statique et dynamique du modèle structurel continu équivalent. La chaîne granulaire unidimensionnelle est constituée de grains rigides uniformes confinés par des interactions élastiques discrètes avec des ressorts de cisaillement et de rotation, pour prendre en compte les contributions granulaires latérales. Le système discret répétitif présenté peut être appelé modèle de réseau élastique ou chaîne de Cosserat discrète avec deux degrés de liberté (DOF) indépendants pour chaque grain en tenant compte de l'interaction de cisaillement. Les déformations d'un tel modèle granulaire soumis à un chargement réparti uniforme, sont étudiées théoriquement pour différentes conditions aux limites. Un tel modèle discret permet d'introduire l'effet de taille (dimension de grain) dans la formulation de flexion d'une poutre granulaire micro-structurée. L'échelle de longueur à laquelle le système est sondé est un problème important associant comportement multi-échelle et hétérogénéité. On montre que pour un nombre infini de grains, les équations aux différences régies par le système discret convergent asymptotiquement vers les équations différentielles de la poutre continue de Bresse-Timoshenko (en négligeant l'échelle de longueur) reposant sur la fondation de Winkler (également classée comme poutre continue de Cosserat). Ensuite, un problème numérique jumeau est étudié pour comparer les résultats analytiques exacts avec ceux numériques simulés par la méthode des éléments discrets (DEM). Les fréquences naturelles d'un tel modèle granulaire sont calculées analytiquement pour tous les modes. Les résultats obtenus clarifient la dépendance des réponses dynamiques de la poutre avec sa longueur. En présence d'échelles de longueur internes (microstructurales), le problème de propagation des ondes élastiques implique une interaction entre la dispersion des ondes et les caractéristiques structurelles. Les propriétés de dispersion des vagues de ce modèle discret sont également étudiées dans la zone de Brillouin. Finalement, grâce à la continualisation du système d'équations aux différences couplées régissant l'évolution de la poutre discrète, un modèle continu de Cosserat à élasticité non locale est obtenu. Le processus de continualisation consiste à approcher les opérateurs aux différences impliqués dans les équations du système discret par des opérateurs différentiels obtenus soit par troncature polynômiale, soit par développements approchés rationnels dans lesquels apparaît une échelle de longueur. Enfin, un modèle granulaire bidimensionnel reliés élastiquement aux voisins latéraux et diagonaux, est étudié. Les équations du mouvement sont obtenues et continualisées par six paramètres de liaisons intergranulaires. De plus, nous étudions une formulation efficace d'un modèle de continuum micropolaire non linéaire basé sur une nouvelle contribution des micro-rotations relatives. Ainsi, un nouveau tenseur de rotation relative est utilisé comme mesure de déformation en plus du tenseur de déformation classique et du tenseur de torsion. Les conséquences du modèle micropolaire proposé sont ensuite discutées à l'aide d'exemples numériques. Dans ce but, plusieurs applications numériques d'éprouvettes de plaques 2D soumises à des charges dans le plan sont envisagées en réalisant un code d'éléments finis basé sur une formulation variationnelle

DEDICATION

This work is dedicated to:

My respectful parents, Soheila and Bahram Massoumi who has supported, encouraged and helped me attentively with their fullest attention,

My dear aunt and uncle, Karine and Shahram Massoumi who supported me particularly during my stay in France,

My beloved grandparents whom I always appreciate for all they have done especially by inspiring me,

My great friends and all the people in my life who touch my heart and affected my thinking and living style: S. M. Zia Abadi, Sheikh H. Ansarian, Prof. M. M. Shokrieh and Prof. H. Elahi Ghomshei.

ACKNOWLEDGMENTS

I would like to express my sincere gratitude to my supervisors Prof. Jean Lerbet and Prof. Noël Challamel for their consistent support, thoughtful comments and recommendations on this dissertation. I would like to thank Prof. François Nicot and Prof. Felix Darve for their guidance during this research. To Dr. Antoine Wautier for his contribution in numerical analysis. Furthermore, I would also like to acknowledge Prof. Francesco Dell'Isola and his research team for the collaboration in the continuum analysis. Finally, I would like to appreciate my family for supporting me during the compilation of this dissertation.

Sina MASSOUMI
B.Sc., IRAN UNIVERSITY OF SCIENCE AND TECHNOLOGY
M.Sc., IRAN UNIVERSITY OF SCIENCE AND TECHNOLOGY
M.Sc., ECOLE NATIONALE SUPERIEURE D'ARTS ET METIERS
Ph.D., UNIVERSITY OF PARIS-SACLAY (EVRY)
Directed by: Professor Noël Challamel and Professor Jean Lerbet

List of Publications

1. S. Massoumi, N. Challamel and J. Lerbet, Exact solutions for the vibration of finite granular beam using discrete and gradient elasticity Cosserat models, *Journal of Sound and Vibration*, 494, 2021.

2. S. Massoumi, N. Challamel and J. Lerbet, Bending/Shear Wave Dispersion Analysis of Granular Chains – Discrete and Enriched Continuous Cosserat Modelling, *International Journal of Solids and Structures,* 2021.

3. S. Massoumi, G. La Valle, Static Analysis of 2D Micropolar Model for Describing Granular Media by Considering Relative Rotations, *Mechanics Research Communications*, 2021.

4. G. La Valle, S. Massoumi, A new deformation measure for micropolar plates subjected to in-plane loads, *Continuum Mechanics and Thermodynamics*, 2021.

5. S. Massoumi, N. Challamel, A. Wautier, F. Nicot, F. Darve and J. Lerbet., Static bending of granular beam: Exact discrete and nonlocal solutions, in Revision, *Meccanica*, 2021.

6. S. Massoumi, N. Challamel, J. Lerbet, A. Wautier, F.Nicot and F. Darve, Shear vibration modes of granular structures for general boundary conditions, in Preparation, 2022.

Conference Presentations

1. Massoumi S., Challamel N. et Lerbet J., Dynamique d'une chaîne granulaire - Modèles discrets et continus, *Congrès Français de Mécanique*, 26-30 Août 2019, Brest, France.
2. Massoumi S., Challamel N. et Lerbet J., Discrete and gradient elasticity Cosserat modelling of granular chains, *Powder and Granular Materials*, 6-7 June 2019, Montpellier, France.
3. Massoumi S., Challamel N. et Lerbet J., Wave dispersion analysis of discrete granular chains: discrete versus non-local approaches, *ASCE-EMI* 2019, 3-5 July 2019, Lyon, France.
4. Massoumi S., Challamel N. et Lerbet J., Vibration and wave dispersion analysis of finite granular chains - discrete versus non-local approaches, *14th World Congress in Computational Mechanics (WCCM)*, 19-24 July 2020, Paris, France.
5. Massoumi S., Challamel N. and Lerbet J., On the wave dispersion analysis of granular chain surrounded by elastic media using an exact discrete approach, *ASCE-EMI* 2021, 25-28 May 2021, New-York, USA.
6. Massoumi S., Challamel N. et Lerbet J., Dynamic analysis of granular chain using Cosserat discrete modeling, *International Congress of Theoretical and Applied Mechanics.* 22-27 August 2021, Milan, Italy.

TABLE OF CONTENTS

Page

ABSTRACT:..... ii

ACKNOWLEDGMENTS v

List of Publications vi

LIST OF TABLES..... xi

LIST OF FIGURES xii

Introduction.....1

1. Background.....1
2. Literature Review.....4
3. Motivation and Statement of the Problem 11

Static Bending of Granular Beam.....15

1. Introduction.....15
2. Discrete Granular Model.....16
3. Simply Supported (S-S) Granular Beam.....21
   - 3.1. Exact Analytical Solution 21
   - 3.2. Numerical Simulations (DEM) 26
     - 3.2.1. Collision Detection 27
     - 3.2.2. Interactions.....28
     - 3.2.3. Explicit Dynamic Algorithm.....30
     - 3.2.4. Numerical Results.....31
4. Nonlocal Continuum Approach 31
   - 4.1. Continualization of the Boundary Conditions with Static Variables 33
   - 4.2. Continualization of the Boundary Conditions Based on Deflection.....34
5. Conclusion and Outlook 36

Vibration Analysis of Granular Beam 39

1. Introduction.....39
2. Granular Model.....40
3. Resolution of The Difference Equation 46
   - 3.1. General Solution of The Difference Equation 55
   - 3.2. Antisymmetric Boundary Conditions on Deflection 59
   - 3.3. Explicit Method: Granular Beam Composed of Three Grains 64
   - 3.4. Continuum Solution.....66

4. Nonlocal Approximate Solutions - Continuous Approach 73
4.1. Polynomial Expansion (Taylor Series Approximant)....74
4.2. Rational Expansion (Padé Approximant) 78
5. Discussion 83
6. Conclusion 87
Wave Dispersion Analysis of Granular Beam 90

1. Introduction 90
2. Discrete Approach via Exact Solution 91
3. Continuous Approach 101
3.1. Exact Solution 101
3.2. Approximate Solution via Polynomial Expansion....102
3.3. Approximate Solution via Rational Expansion....109
4. Discussion 117
5. Conclusions 121
Two-Dimensional Plane: Discrete and Continuum Modelling....124

1. Introduction 124
2. In-Plane Granular Model 125
3. Linear Isotropic Micropolar Elasticity Theory 133
4. Two-dimensional Micropolar Continuum Model 136
4.1. The Cauchy-Green Strain Tensor 137
4.2. Relative Rotation Tensor 137
4.3. The Wryness Tensor 138
5. Energy Approach 138
5.1. Deformation Energy Function for Isotropic Materials 139
5.2. Boundary Conditions 139
6. Numerical Simulations....140
6.1. Compression Test....141
6.2. Biaxial Shear Test 142
6.3. Parametric Analysis for Tensile Test 144
7. Conclusion and Summary 147
Conclusion and Perspective 150

1. Conclusion and Summary 150
2. Outlook 154
APPENDIX A. Exact solution of the static deflection of the discrete granular beam –

General solution 156

APPENDIX B. Exact solution of the static deflection of the discrete granular beam for

various boundary conditions 157

I. Clamped-Simply (C-S) Supported Granular Beam 157
II. Clamped – Clamped (C-C) Granular Beam....159

III. Clamped-Free (C-F) Granular Beam 161
APPENDIX C. Exact solution of the static deflection of the continuous nonlocal granular beam 164

APPENDIX D. Alternative methods of the static analysis of the continuous nonlocal granular beam.....165

I. Continualization of Discrete Bending Moment 165
II. Continualization of the Kinematic Boundary Conditions.....165
III. Continualization of Discrete Bending Moment 165
IV. Continualization of the Static Boundary Conditions with Cinematic Variables 166
APPENDIX E. Nonlocal static analysis of the granular beam for various boundary conditions.....167

I. Clamped-Simply Nonlocal Model 167
II. Clamped-Clamped Nonlocal Model 168
III. Clamped-Free Nonlocal Model.....169
APPENDIX F. Comparison of the numerical DEM model and the exact discrete approach of the static deflection of the granular beam.....171

BIBLIOGRAPHY.....172

LIST OF TABLES

Table Page

Table 1: Comparison of the maximum deflection values (μm) for the discrete granular beam with simply supported (S-S), clamped-simply (C-S), clamped-clamped (C-C) and clamped-free (C-F); exact analytical solutions and the numerical ones (DEM)..... 171

Table 2: Comparison of the maximum rotation values ($\mu\, degree$) for the discrete granular beam with simply supported (S-S), clamped-simply (C-S), clamped-clamped (C-C) and clamped-free (C-F); exact analytical solutions and the numerical ones (DEM)..... 171

Table 3: Material parameters used in energy definition of the medium..... 171

LIST OF FIGURES

Figure Page

Figure 1. A discrete granular beam with length L (a) Non-deformed discretized beam (b) Deformed beam composed of $n + 1$ rigid grain; $L = na$ 17

Figure 2. Static bending granular beam solution for 11 number of grains (a) Deflection and (b) Rotation 25

Figure 3. Parametric analysis of the continuum and discrete differences (ϵ) with regards to the grain number values for a simply supported granular beam by varying (a) Rotational spring rigidity, (b) Shear spring rigidity, and (c) Beam length 26

Figure 4. Comparison of the exact discrete approach with the nonlocal ones based on discrete model (1st nonlocal approximation) and based on the development of the continuum formulations (2nd nonlocal approximation) for 11 number of granular elements (a) Deflection and (b) Rotation 36

Figure 5. A discrete shear granular chain model composed of n+1 grain; (a) undeformed and (b) deformed. 41

Figure 6. Schematic behavior of the wave vector regarding the eigenfrequencies for finite grain number (n=50). (a), (c), (e) and (g) correspond to the real part and (b), (d), (f) and (h) correspond to the imaginary part of the wave vector 52

Figure 7. The effects of the eigenfrequencies on the wave behavior for a general discrete beam contains an infinite grain number ($n \to \infty$). (a), (c), (e) and (g) correspond to the real part and (b), (d), (f) and (h) correspond to the imaginary part of the wave vector 53

Figure 8. Comparison of the first branch natural frequencies for the discrete exact, Duan et al. [12] and continuum solutions with respect to the mode number (p) and grain number: (a) $n = 5$, (b) $n = 20$, (c) $n = 35$ and (d) $n = 50$ for $\mu s = 4.28$, $r^* = 0.007$ and $k^* = 0$. 68

Figure 9. Comparison of the second branch natural frequencies for the discrete exact, Duan et al. [12] and continuum solutions with respect to the mode number (p) and grain number: (a) $n = 5$, (b) $n = 20$, (c) $n = 35$ and (d) $n = 50$ for $\mu s = 4.28$, $r^* = 0.07$ and $k^* = 0$. 70

Figure 10. Comparison of the first branch natural frequencies for the discrete exact, Duan et al. [12] and continuum solutions with respect to the mode

number (p) and grain number: (a) $r^* = 0.004$, (b) $r^* = 0.022$, (c) $r^* = 0.04$ and (d) $r^* = 0.058$ for $n = 20$, $\mu s = 4.28$ and $k^* = 0$. 71

Figure 11. Comparison of the second branch natural frequencies for the discrete exact, Duan et al. [12] and continuum solutions with respect to the mode number (p) and grain number: (a) $r^* = 0.004$, (b) $r^* = 0.022$, (c) $r^* = 0.04$ and (d) $r^* = 0.058$ for $n = 20$, $\mu s = 4.28$ and $k^* = 0$. 72

Figure 12. Analysis of the grain number effect on the frequencies (discrete exact solution) for the mode number (a) $p = 1$ and (b) $p = 10$ with respect to the length ratio ($r^* = 0.029$) for $\mu s = 4.28$ and $k^* = 1.87$..... 73

Figure 13. Comparison of the natural frequencies for the nonlocal Taylor and continuum solutions with respect to the mode number (p) and grain number: (a) $n = 5$ and $r^* = 0.058$, (b) $n = 20$ and $r^* = 0.014$, (c) $n = 35$ and $r^* = 0.0082$ and (d) $n = 50$ and $r^* = 0.0058$ for $\mu s = 4.28$. 78

Figure 14. Analysis of the grain number effect on the frequencies (nonlocal Taylor) for the mode number (a) $p = 1$ and (b) $p = 10$ with respect to the length ratio for $\mu s = 4.28$ and $k^* = 1.87$..... 78

Figure 15. Comparison of the natural frequencies for the nonlocal Padé and continuum solutions with respect to the mode number (p) and grain number: (a) $n = 5$ and $r^* = 0.058$, (b) $n = 20$ and $r^* = 0.014$, (c) $n = 35$ and $r^* = 0.0082$ and (d) $n = 50$ and $r^* = 0.0058$ for $\mu s = 4.28$. 83

Figure 16. Analysis of the grain number effect on the frequencies (nonlocal Padé) with respect to the length ratio ($r^* = 0.029$) for mode number: (a) $p = 1$ and (b) $p = 10$ $\mu s = 4.28$..... 83

Figure 17. Comparison of the first branch natural frequencies for different approaches as a function of mode number (p) with respect to the grain number: (a) $n = 5$, (b) $n = 20$, (c) $n = 35$ and (d) $n = 50$ for $\mu s = 4.28$. 84

Figure 18. Comparison of the second branch natural frequencies for different approaches as a function of mode number (p) with respect to the grain number: (a) $n = 5$ and $r^* = 0.058$, (b) $n = 20$ and $r^* = 0.014$, (c) $n = 35$ and $r^* = 0.0082$ and (d) $n = 50$ and $r^* = 0.0058$ for $\mu s = 4.28$. 85

Figure 19. Comparison of the natural frequencies of the first branch for different approaches as a function of mode number (p) with respect to the grain number: (a) $n = 5$ and $r^* = 0.058$, (b) $n = 20$ and $r^* = 0.014$, (c)

$n = 35$ and $r^* = 0.0082$ and (d) $n = 50$ and $r^* = 0.0058$ for $\mu s \to \infty$ (weak shear interaction). 85

Figure 20. Comparison of the natural frequencies of the second branch for different approaches as a function of mode number (p) with respect to the grain number: (a) $n = 5$ and $r^* = 0.058$, (b) $n = 20$ and $r^* = 0.014$, (c) $n = 35$ and $r^* = 0.0082$ and (d) $n = 50$ and $r^* = 0.0058$ for $\mu s \to \infty$ (weak shear interaction). 86

Figure 21. Correction in the first branch natural frequencies regarding Winkler foundation effect. 87

Figure 22. Dispersive curves for one-dimensional compression wave of (a) the first branch and (b) the second branch according to bending nondimensional parameter for $\mu s = 4.28$, $r^* = 0.289$ and $k^* = 0.02$. 107

Figure 23. The complex results of nonlocal Taylor development (a) 2^{nd}-order first branch, (b) 2^{nd}-order second branch, (c) 4^{th}-order first branch, (d) 4^{th}-order second branch, (e) 6^{th}-order first branch and (f) 6^{th} -order second branch according to bending nondimensional parameter for $\mu s = 4.28$, $r^* = 0.289$ and $k^* = 0.02$. 109

Figure 24. Dispersive curves for one-dimensional compression wave of (a) the first branch and (b) the second branch according to bending nondimensional parameter for $\mu s = 4.28$, $r^* = 0.289$ and $k^* = 0.02$. 116

Figure 25. Dispersive curves for one-dimensional compression wave of (a) first branch or the acoustic mode and (b)second branch or the optical mode according to shear nondimensional parameter- various approaches for $\mu s = 4.28$, $r^* = 0.289$ and $k^* = 1.03$. 118

Figure 26. Comparison of the first branch of natural frequency for the different values of Young modulus in 1D media: (a) $c0 = 3162$ m/s^2 and $\mu s = 1.71$, (b) $c0 = 4183$ m/s^2 and $\mu s = 2.99$, (c) $c0 = 5000$ m/s^2 and $\mu s = 4.28$ and (d) $c0 = 8660$ m/s^2 and $\mu s = 12.85$ for $r^* = 0.289$ and $k^* = 0$. 119

Figure 27. Comparison of the second branch of natural frequency for the different values of Young modulus in 1D media: (a) $c0 = 3160$ m/s2 and $\mu s = 1.71$, (b) $c0 = 4183$ m/s2 and $\mu s = 2.99$, (c) $c0 = 5000$ m/s^2 and $\mu s = 4.28$ and (d) $c0 = 8660$ m/s2 and $\mu s = 12.85$ for $r^* = 0.289$ and $k^* = 0$. 120

Figure 28. Comparison of the different approaches with the molecular dynamics results of Wang and Hu [133]: (a) (5,5) and (b) (10,10) armchair CNT - various approaches 121

Figure 29. A discrete shear granular plane of dimension L1 × L2 composed of $(n + 1) \times (m + 1)$ grains of diameter a and mass m 125

Figure 30. Compression test with a clamped bottom side (a) distribution of the vertical strain (b) distribution of the horizontal strain (c) distribution of the microrotation 142

Figure 31. Biaxial shear test with fixed microrotation on the sides (a) distribution of the macro-rotation (b) distribution of the micro-rotation Q_{21} (c) distribution of the relative rotation R_{21} 143

Figure 32. Distribution of the lateral displacement for parametric analysis on $\mu\Gamma\Gamma T$ for tensile test (a) $\mu\Gamma\Gamma T/\mu\Gamma\Gamma T0 = 0.001$ (b) $\mu\Gamma\Gamma T/\mu\Gamma\Gamma T0 = 0.1$ 145

Figure 33. Distribution of the micro rotation for parametric analysis on $\mu\Gamma\Gamma T$ for tensile test (a) $\mu\Gamma\Gamma T/\mu\Gamma\Gamma T0 = 0.001$ (b) $\mu\Gamma\Gamma T/\mu\Gamma\Gamma T0 = 0.1$ 146

Figure 34. Distribution of reactions along the clamped boundary (a) Horizontal reaction (along x-direction) (b) Vertical reaction (along y-direction) 147

CHAPTER 1

Introduction

1. Background

Due to the importance of processing scale, using particulate material has become more and more popular. Large number of raw materials entering the industries are granular in nature. According to the huge applications of granular material in diverse industries such as pharmaceutical powders, food engineering, and agricultural grains, minerals, civil engineering, it is important to identify the characteristic behavior of such materials, when externally excited. Despite the simplicity of the granular medium by introducing the simple interactions at the micro scale, sophisticated nonlinear features emerge at the macro scale both in mechanical and morphological aspects (Nicot and Darve [1], Vardoulakis. [2]).

Classical continuum mechanics suffer from the absence of internal scale effects. This might be insufficient for analyzing the granular media, in which both the nonlocal effects (internal length) of the interactions and grain rotation may play an important role in the response of the system. In order to adapt a standard continuum theory to granular materials, it is necessary to introduce the independent rotational degrees of freedom (DOF) in addition to the conventional translational ones. This helps to describe accurately the relative movements between the microstructure and the average macroscopic deformations. One may obtain higher-order gradient continua with additional degrees of freedom. One may also obtain Cosserat modeling that consequently leads to a non-classical continuum or polar continuum theories (Cosserat type theories, *e.g.* Cosserat and Cosserat

[3]; Nowacki [4]). Voigt [5] was the pioneer of developing this concept who first showed the existence of couple–stress in materials.

Basically, as it was mentioned above, to deal with granular media, it may be necessary to define additional degrees of freedom or higher-order gradients (for instance Mindlin [6] and Aifantis [7]) which permits also to study the nonlocal effects and capture the internal length scale of the material (Truesdell and Noll [8], Toupin [9] and Truesdell [10]). This leads to the enriched formulations of Cosserat-type or micro-polar type theories which possess both rotational degrees of freedom in addition to the conventional translational ones. Many studies have been done recently to study granular media using micropolar models ((Pasternak and Mühlhaus [11], Duan et al. [12], Challamel et al. [13], Poorsolhjouy and Misra [14] and Misra et al. [15])).

In beam analysis, the Bresse-Timoshenko model takes into account both beam shear flexibility and rotatory inertia (Bresse [16] and Timoshenko [17, [18]). The effects of shear and rotational inertia can be significant in the case of calculating eigenfrequencies for short beams, or in the case of sufficiently small shear modulus.

On the other hand, in presence of length scales, the elastic wave propagation problem involves an interplay between wave dispersion and structural features. The wave propagation characteristics of conventional forms of matter are well understood and well documented. In contrast, waves in granular media are more complex due to the discrete nature of these systems, which may include nonlinear interactions. Considerable interest in the dynamic response of granular media exists in the geomechanics community typically involving acoustics and wave propagation in sand, gravel and rock materials. Mechanical energy is transferred through a structured wave-guide network which is created by granular

media. The key element in the mechanics of a granular system is the force chain. It is along these preferentially stressed chains of particles that waves are transmitted. These nonlinear chains are heavily dependent on the geometry of the bed and are prone to rearrangement even by the slightest of forces.

Dispersion is a real issue in wave propagation since each granular element acts as a filter for the frequencies (letting the low frequencies or large wave-lengths pass through). In addition to dispersion, the material can delay or block the high frequencies (short wavelengths). Classical elasticity theories are not suitable for capturing the wave dispersion in granular materials when the microstructured influence is predominant in the wave propagation. For these cases, the long-range interactions are important to take into account in the deformation process (for instance the book of Bagdoev et al. [19] or Vardoulakis [20]).

It is noteworthy to mention that one of the efficient approaches to simulate granular media consists in a discrete element method (DEM). This method was first applied in granular media for a class of problems that cannot be solved through analytical or continuous methods (Cundall and Strack [21], Serrano and Rodriguez-Ortiz [22]). Using this method to analyze the behavior of continuum media provides new insights into the mechanical behavior of these materials. Newton's second law is applied to determine the displacements and rotations of each particle. Today, there are many open-source and commercial DEM programs available. YADE is an open-source DEM software that uses object-oriented (OO) programming techniques. The location and trajectory of each individual particle are calculated through Newton's second law. The forces and movements of particles are calculated basically from their contact interactions. In DEM, the

interactions between the particles are obtained from simple contact laws while the interaction forces are deducted through the interatomic potential in the molecular dynamics simulations.

2. Literature Review

Cosserat continuum theories belong to the larger class of generalized continua which introduce intrinsic length scales into continuum mechanics via higher-order gradients or additional degrees of freedom (Eringen [23, [24], Forest [25]). Feng [26] analyzed the behavior of the granular medium considering normal, shear and rotation interactions. In contrast, the classical continuum mechanics ignore the rotational interactions among particles and neglect the size effect of material particles. Micropolar models could interpret both the complex discrete and continuum microstructures such as granular media (Pasternak and Mühlhaus [11], Duan et al. [12], Challamel et al. [13], Poorsolhjouy and Misra [14], Massoumi et al. [27] and Misra et al. [15]), soils (Matsushima et al. [28] and Bourrier et al. [29]), metamaterials (Barchiesi et al. [30], Vescovo and Giorgio [31], Giorgio et al. [32] and Misra et al. [33]).

In a physical sense, each point of the material could be asymptotically equivalent to a rigid body. As a result, three degrees of freedom can be defined for a rigid body in 2D analysis. The ideas of the micropolar continuum were presented at the end of the 19th century by Kelvin, Helmholtz, Duhem, Voigt and Cosserat and Cosserat [34]. A new aspect of this theory is the introduction of couple stresses in addition to the conventional ones (Truesdell and Toupin [35]). Several researchers like Aero and Kuvshinskii [36, [37], Toupin [9], Mindlin and Tiersten [38] and Eringen [39, [40] investigated the linear Cosserat theory. On the other hand, the non-linear micropolar continuum was studied in the early

publications by Toupin [41], and more recently by Pietraszkiewicz and Eremeyev [42] (see also Eremeyev and Pietraszkiewicz [43] and La-Valle and Massoumi [44]).

The deformation of the micropolar continuum could be defined through the position vector and the three orthonormal directors which model the orientation changes. This method could be used only for small deformation (Grioli [45], Kafadar and Eringen [46] and Ramezani and Naghdabadi [47]). Usually, the strain measures are presented by the Cosserat deformation and wryness tensors (Kafadar and Eringen [46] and Eringen and Kafadar [48]).

Modeling continuum media with granular models (Cosserat discrete) which involve intrinsically the influence of size effects (grain diameter), allows for taking into account the nonlocal effect. The approaches for solving repetitive cell structures problems is applying finite difference calculus and obtaining the exact solutions and then making a continuous approximation (Bažant and Christensen [49]). Continualizing such a discrete system composed of repetitive periodical cells leads to the nonlocal continuum models (Bacigalupo and Gambarotta [50], Bacigalupo and Gambarotta [51] and Picandet et al. [52]). For an infinite number of grains when this internal length approaches zero, the nonlocal continualized model converges asymptotically toward the local continuum one.

The advantage of discrete models in comparison with the continuum ones is their ability to describe better the inhomogeneous effects at the particle level. In recent decades, several models have been developed on the granular chains in order to understand deeper the static and dynamic behavior of these structures and predict more precisely the wave dispersion. Microstructural models of granular media based on both translation and rotational degrees of freedom have been initially investigated for regular granular packing

by Duffy [53] and for random granular packing by Digby [54] and Chang [55]. Mühlhaus and Vardoulakis [56] analyzed the influence of additional degrees of freedom on the familiar translational motion (Cosserat-type theories). This has led to formulations of the micro-polar type or Cosserat-type theories for random packing of granulates (Suiker et al. [57]). Chang and Ma [58] studied the random packing of grains based on linear elastic contact interactions with the isotropic distribution. Using the same concept for static analysis, the buckling behavior of the granular chain has recently been investigated by Challamel et al. [13]. Schwartz et al. [59] studied the vibrational behavior of solid grains by having particle rotation and translation together (Cosserat discrete model) while assuming only shear elastic interaction for both ordered and disordered packings. The model of Schwartz et al. [59] has been generalized using a discrete Cosserat model with the consideration of both shear and rotation interactions (Pasternak and Mühlhaus [11], Pichard et al. [60], Vasiliev et al. [61] and Massoumi et al. [27] for instance). In particular, Pasternak and Mühlhaus [11] studied both the dispersive wave propagation properties in the granular chain with both bending and shear interactions, and also the static response of the finite granular beam under distributed lateral forces. Furthermore, wave propagation properties of the infinite and a semi-infinite granular chain were investigated by Pichard et al. [60].

The Bresse-Timoshenko beam model is also a generalization of the Euler-Bernoulli model and admits kinematics with two independent fields, a field of transverse displacement and a field of rotation. Timoshenko pointed out that the effects of cross-sectional dimensions on the beam dynamic behavior and frequencies could be significant. Timoshenko [17, [18] calculated the exact eigenfrequencies for such a beam with two

degrees of freedom resting on two simple supports. Several lattice models have been developed based on microstructured Timoshenko in order to go further in understanding the structure behavior (see Ostoja-Starzewski [62] and Attar et al. [63]). The static and dynamic properties of a Cosserat-type lattice interface were studied by Vasiliev et al. [61]. Calculation of eigenfrequencies for a Bresse-Timoshenko beam with any boundary conditions and elastic interaction with a rigid medium is obtained by Wang and Stephens [64], Manevich [65] or Elishakoff et al. [66] (see more recently Elishakoff [67] and Challamel and Elishakoff [68]). Bresse-Timoshenko beam theory is merely a one-dimensional Cosserat continuum medium by considering two independent translational and rotational degrees of freedom (Rubin [69] and Exadaktylos [70]). Thus, there is a fundamental link between these two continuum theories. In this thesis, we will develop a bridge between a discrete Cosserat theory for the granular system and an equivalent continuous one.

In the past few years, several studies focused on the investigation of the equivalent continua formulations from the lattice model by discretizing a continuum beam through periodic discrete elements. The granular models are able to predict both the static and dynamic response of lattice by taking into account the effects of the motions of the neighborhood (Eringen [71, [23, [24]). Although the lattice models propose a very large number of degrees of freedom for complicated geometry but in many cases, they permit to obtain analytical results simply. The nonlocal continuum models are derived by continualizing the Lagrangian difference equations governing the granular model. To this aim, the higher order continuum differential equations are obtained eventually through the approximations of difference equations by using the polynomial expansions based on the

Taylor series (see for instance Kruskal and Zabusky [72] or more recently by Gul et al. [73]) or rational expansions based on Padé approximants (Askes and Metrikine [74], Andrianov et al. [75]). Challamel et al. [76] investigated the nonlocal model for an axial lattice loaded by distributed forces and in interaction with an elastic medium.

In the literature, there are several general strategies to model the microstructure of a one-dimensional granular beam for bending. One strategy is based on pure rotational interactions, which consider only the elastic rotational springs, and take into account the bending effect; they are referred to as Hencky's chain model (Hencky [77] and Naschie [78]) and lead to an equivalent Euler-Bernoulli continuum beam. Challamel et al. [79] studied the bending response of nonlocal Euler-Bernoulli under lateral loads using the nonlocal elastic model of Eringen. Gomez-Silva and Zaera [80] investigated different continualization methods for a one-dimensional Hencky beam model assuming only bending interactions. Another approach to model the microstructure of a beam consists in including the shear springs in addition to the rotational ones in order to simulate the shear interactions which are leading to an equivalent Timoshenko nonlocal beam (Bresse [16] and Timoshenko [17, [18]). Wave propagation of the granular beam assuming only shear effects has been studied by Schwartz et al. [59] and for axial, shear, and rotational interactions by Feng [26] (see also Nejadsadeghi et al. [81], Misra and Nejadsadeghi [82] and Nejadsadeghi and Misra [83]). The wave dispersion properties of the discrete granular beam under a discrete Winkler-type foundation has been studied by Massoumi et al. [84], which can be viewed as a discrete formulation of a Bresse-Timoshenko beam under a distributed Winkler-type foundation, as investigated by Manevich [65] also in term of wave dispersion properties.

Due to the importance of dynamic properties and functions of one-dimensional granular media, several studies have been done in various domains. Toward this aim, studying the phenomena involved using simple analytical models is beneficial. Starosvetsky et al. [85] studied the dynamic behavior of nonlinear granular chains with Hertz interaction. The problem of nonlinear perturbations in the one-dimensional granular chain is investigated by Nesterenko [86] in Hertzian contact. Herbold et al. [87] analyzed the formation and propagation of nonstationary signals in linear and nonlinear diatomic periodic one-dimensional granular chains. The free vibration of a granular chain with both bending and shear granular interactions rested on simply supported boundary conditions resting on Winkler elastic foundations is studied by Massoumi et al. [88]. In the present study, the same discrete Cosserat model with both rotation and shear elastic interactions will be considered, which could be understood as an equivalent discrete Bresse-Timoshenko model (Bresse [16] and Timoshenko [17, [18]- see also Challamel and Elishakoff [68]).

It is noteworthy to mention that detecting the constitutive equations and consequently identifying the material parameters, is one of the most important points of the micropolar theories. While studying the classical continuum model in isotropic materials only is needed to present two Lamé parameters, this might vary to six or more material moduli for the micropolar models. Generally, there exist two major strategies to obtain these material parameters. The first approach concerns defining various experimental tests based upon measuring size effects that have been reported (Gauthier and Jahsman [89], Lakes [90], Mora and Waas [91] and Beveridge et al. [92]). To this aim, the specimens of similar material and geometry are tested for various sizes to identify any

variation in stiffness with size. Lakes et al. [93] presented a method that can identify micropolar materials without testing the various sample size. An alternative method is using different homogenization procedures (Cielecka et al. [94], Larsson and Zhang [95] and Ostoja-Starzewski [62]). Accordingly, these approaches attempt to represent materials at the microstructural level basically using lattice structure by an assembly of individual elements.

Many studies have been done to investigate the micropolar continuum models for plates and shells. Eringen [96], Eringen [97] and Altenbach and Eremeyev [98], Altenbach and Eremeyev [99] studied the application of the linear micropolar model for plates. Giorgio et al. [100] introduced an extended Cosserat model that accounts for the coupling between stretching deformations and the micro-rotation for 2D plates. Casolo [101] investigated the macroscopic modeling of the in-plane elastic behavior of composite solids and expounds the theoretical relationship between the orthotropic Cosserat continuum and the proposed rigid elements. Besides, many researchers investigated the in-plane stress of 2D continuum plates using granular elements: Ouali et al. [102] studied the stress concentrations of plates with notches and holes using granular micromechanics, Turco et al. [103] formulated a nonlinear Lagrangian model for 2d elastic interacting grains, Placidi et al. [104] and Timofeev et al. [105] developed the continuum theories to interpret 2d granular microstructures. Hasanyan and Waas [106] investigated the buckling of a single strip of material, modeled as a two-dimensional (2D) micropolar solid. Misra and Poorsolhjouy [107] studied the discrete micropolar theory for 2D granular models in order to develop a 2D micromorphic continuum model. Giorgio et al. [108] used a nonlinear 2D Biot-Cosserat to study a micromorphic medium.

The comprehensive literature review that was presented above not only permits us to understand better the problem namely the discrete and continuum micropolar theory as well as prepare the proper background knowledge of the nonlocal models but also gives us an effective perspective to orient the future works. Besides, analyzing the related works in this area allows recognizing some absent aspects of the topic which also emphasize the importance of the doing current thesis.

3. Motivation and Statement of the Problem

This study is an attempt towards a better understanding of the length scale effects on the bending response of the granular beams. To this aim, first, a unidimensional discrete granular chain composed of a finite number of rigid grains connected elastically is studied. It is assumed that shear and rotational interactions exist at the rigid grain interfaces. This granular model can be classified also as a discrete Cosserat chain with two independent degrees of freedom (DOF) for each grain (the deflection and the rotation). Subsequently, such a discrete model permits to introduce the size effect (grain dimension) in the bending formulation of a microstructured granular beam. It is shown that for an infinite number of grains, the difference equations that govern the behaviour of the discrete granular beam converge towards the differential equations of the Bresse-Timoshenko beam resting on Winkler foundation (also classified as a continuous Cosserat beam model on Winkler foundation). A gradient Bresse-Timoshenko model is constructed from the continualization of the difference equations. The continuous gradient elasticity Cosserat model is obtained from a polynomial or a rational expansion of the pseudo-differential operators in which scale effects of the granular chain would be captured.

The exact solutions of this granular model subjected to a uniform distributed loading, are investigated in static conditions for various boundary conditions which are defined at the grain level. The performance of the Discrete Element Method (DEM) for simulating such a problem is investigated as well. Accordingly, a twin numerical problem is studied to compare the exact analytical results with the numerical ones simulated by DEM. Furthermore, the natural frequencies of a free vibrating granular beam with simply supported boundary conditions are analytically calculated for whatever modes.

In chapter 3, we studied the free vibrations of granular-microstructured beams using the Cosserat discrete model. To this end, the dynamic responses of the one-dimensional granular beam have been investigated for simply supported boundary conditions through the analytical resolution of the exact problem. The effective parameters and the constitutive equations defined in the interactions are described in detail. Next, the governing equations of motion and variationally-based boundary conditions are derived through the Lagrangian of the system and Hamilton's principle. For simply supported granular beams, the equivalency of the exact boundary conditions with an alternative problem (half boundary density with antisymmetric deflection) has been checked. Besides, the problem is simulated by DEM. The responses of the numerical approach are compared with the exact results of the analytical solutions which present a quite well accuracy. Some interesting features of the results such as the critical frequencies of the discrete model and the pure shear modes are discussed through the numerical sensitive analysis.

This work is motivated also by the detection of standing waves and negative velocity of acoustic and optical waves observed in discrete granular models. This study allows us to understand better the incorporation between the theoretical models, granular

materials and the included effective parameters. Concerning wave propagation, granular elements create a structured wave-guide network through which mechanical energy is transferred. In the presence of internal (microstructural) length scales, the elastic wave propagation problem involves an interplay between wave dispersion and structural features.

The last chapter is dedicated to the study of the same methodology (micropolar theory) for two-dimensional plates starting from the 2d granular arrangement and continuing to obtain an enrich continuum model. Accordingly, the in-plane deformation of the plate (using plane stress) is taken into account by using a comprehensive discrete granular model for a regular packing of grains including horizontal, vertical and diagonal interactions. To this aim, in order to analyze the in-plane deformation of the system. we consider the normal, shear and rotational interactions. First, the constitutive relationships and governing equations of motion are derived using the Lagrangian equation of the discrete system. Next, the continualized model is compared with the literature and the material parameters are determined according to the discrete model. In the end, novel nonlinear deformation energy based on 2d continuum micropolar theory is presented with regards to the new measure of deformation.

CHAPTER 2

Static Bending of Granular Beam

1. Introduction

In this chapter, the bending behavior of the granular beam is investigated for a uniform distributed loading. The purpose is a deep analysis of discrete mechanics versus continuous ones which therefore leads to capture the internal length scale (grain diameter) and give some clues to check the ability of DEM (for instance using YADE) to account for the 1D Cosserat chain. Assuming that the number of granular elements is large enough, DEM with basic contact laws can describe enriched continuum mechanics. The local and non-local continuum models converge to each other for negligible length scale parameters. Within this perspective, comparisons between DEM and exact analytical Cosserat discrete solution through the static analysis of granular chain are carried out. Accordingly, the discrete system is considered as the reference model to be studied. This granular model could be considered as the discrete Cosserat model or discrete Bresse-Timoshenko model which takes into account the effects of the length scale. It is shown that for an infinite number of grains this model converges to the local continuum model of Cosserat which is merely the local continuum model of Bresse-Timoshenko. This model is called local in the sense that the generalized variables of bending moment and shearing force depend on the variables of generalized deformations namely the curvature and sliding in a local way and without scale effects.

This chapter is organized as follows. First, the governing equations of such a granular chain are obtained assuming shear and rotational interactions between the grains.

Each grain is supposed to comprise two independent degrees of freedom which is in accordance with the Cosserat discrete theory. The model could be considered the same as the one investigated by Pasternak and Mühlhaus [11] or more recently by Vasiliev et al. [61] for a static case under uniformly distributed loading. The novel aspects of this analysis are studying the granular model presented by Pasternak and Mühlhaus [11] for four various boundary conditions of simply supported, clamped, clamped-simply supported and clamped-free, the exact solutions of the bending discrete beam are studied. Also, the nonlocal continuum beam is investigated originally for the aforementioned boundary conditions and the results are compared well by the ones of the discrete model. Next, the same problem is simulated by DEM using YADE open-source software. The numerical results obtained by DEM are verified well with the exact analytical results of the granular model for the deflection and micro rotations. A significant accuracy was obtained between the results of these two approaches. Finally, the nonlocal continuum model is achieved through the continualization of the problem by virtue of the Taylor series.

2. Discrete Granular Model

In this section, the microstructure of a beam of length L is considered. The discretized beam is composed of $n+1$ spherical rigid grains of size a connected elastically by rotational springs of stiffness k_r and shear springs of stiffness k_s. The normal interactions between the grains are neglected to study the shear and bending response of the system. This model was used also by Pasternak and Mühlhaus [11] or more recent by Massoumi et al. [88]. The micro rolling rigidity and the micro shear stiffness relate to some macro parameters of the continuum beam, namely to the Young modulus E, the shear modulus G, the second moment of area I, the area of the cross-section A and the shear

coefficient of the Bresse-Timoshenko beam $\mathcal{K}$ that depends on the Poisson's ratio (Cowper [109]).

$$k_r = \frac{EI}{a}, \quad k_s = \frac{\mathcal{K}GA}{a} \tag{1}$$

The proposed model behaves as a discrete Cosserat model or equivalently as a discrete Bresse-Timoshenko one. The model is loaded by distributed vertical uniform forces denoted by $Q = qa$ concentrated at the center of each grain. This model allows for capturing an intrinsic length scale a and can be shown in Figure 1. Assuming two degrees of freedom (DOF) for each grain (vertical displacement (W_i) in addition to the rotation (Θ_i)) in the 1D study let us apply Cosserat discrete theory by considering a system of $2(n+1)$ DOF.

(a)

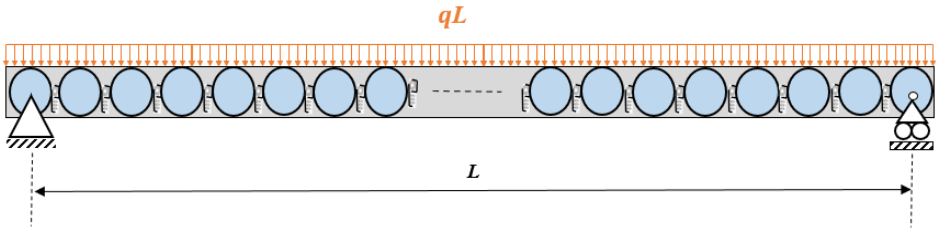

(b)

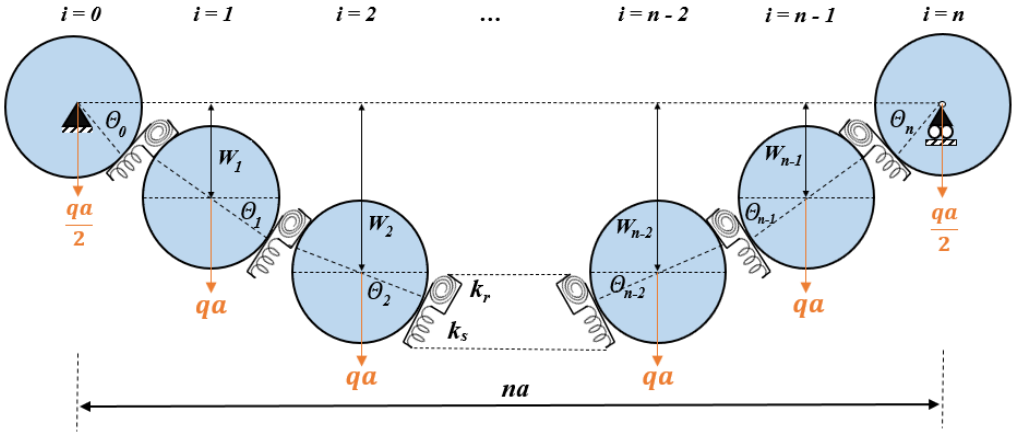

Figure 1. A discrete granular beam with length L (a) Non-deformed discretized beam (b) Deformed beam composed of $n+1$ rigid grain; $L = na$

The Lagrangian of the system may be defined as $L = -(U_s + U_b + U_Q)$, where U_s and U_b are respectively the elastic potential energies of deformed shear and rotational springs and U_Q concerns the work done by the transverse distributed load. With the substitution of the potential terms, the Lagrangian or equivalently the energy functional may be expressed as:

$$L = -\left[\frac{1}{2}\sum_{i=0}^{n-1} k_s\left(W_{i+1} - W_i - a\frac{\Theta_{i+1} + \Theta_i}{2}\right)^2 + \frac{1}{2}\sum_{i=0}^{n-1} k_r(\Theta_{i+1} - \Theta_i)^2 - \sum_{i=0}^{n} Q_i W_i\right] \tag{2}$$

where $W_i = W(x = ia)$. The system of difference equations for both the discrete displacement and rotation fields is obtained from the application of Hamilton's principle for the static case, given by:

$$\int_{t_1}^{t_2} \boldsymbol{\delta L}\, \boldsymbol{dt} = \int_{t_1}^{t_2} (-\boldsymbol{\delta U})\, \boldsymbol{dt} = \mathbf{0} \tag{3}$$

The contact forces $V_{i+1/2}$ and contact bending moment $M_{i+1/2}$ derived from the potential energy of the system can be expressed as

$$\begin{aligned} \boldsymbol{V_{i+1/2}} &= \boldsymbol{k_s}\left(\boldsymbol{W_{i+1}} - \boldsymbol{W_i} - \frac{\boldsymbol{a}}{\mathbf{2}}(\boldsymbol{\Theta_{i+1}} + \boldsymbol{\Theta_i})\right), \\ \boldsymbol{M_{i+1/2}} &= \boldsymbol{k_r}(\boldsymbol{\Theta_{i+1}} - \boldsymbol{\Theta_i}) \end{aligned} \tag{4}$$

for $i = 0, \dots, n-1$ while for the grain i two contact position $i \pm \frac{1}{2}$ could be defined (the subscript $i \pm \frac{1}{2}$ refers to the contact position at $ai \pm \frac{a}{2}$). Using Eq. (3) based on the energy function of Eq. (2) leads to the following difference equation system

$$\boldsymbol{k_s}(\boldsymbol{W_{i+1}} + \boldsymbol{W_{i-1}} - \mathbf{2}\boldsymbol{W_i}) - \frac{\boldsymbol{a}}{\mathbf{2}}\boldsymbol{k_s}(\boldsymbol{\theta_{i+1}} - \boldsymbol{\theta_{i-1}}) = -\boldsymbol{Q_i} \quad (\boldsymbol{i} = \mathbf{1}, \dots, \boldsymbol{n} - \mathbf{1}) \tag{5}$$

$$\frac{\boldsymbol{a}}{\boldsymbol{2}}\boldsymbol{k_s}(\boldsymbol{W_{i+1}}-\boldsymbol{W_{i-1}})-\frac{\boldsymbol{a^2}}{\boldsymbol{4}}\boldsymbol{k_s}(\boldsymbol{\theta_{i+1}}+\boldsymbol{\theta_{i-1}}+\boldsymbol{2\theta_i})+\boldsymbol{k_r}(\boldsymbol{\theta_{i+1}}+\boldsymbol{\theta_{i-1}}-\boldsymbol{2\theta_i})=\boldsymbol{0}\quad(\boldsymbol{i}=\boldsymbol{1},\dots,\boldsymbol{n-1})$$

This equation could be compared well for static case by Pasternak and Mühlhaus [11] and Vasiliev et al. [61] for free beam. Also neglecting the rotational interactions ($C = 0$) leads to the static equilibrium equations of Schwartz et al. [59]. Eq. (5) might be generalized and rewritten compactly through the introduction of the following difference operators

$$\boldsymbol{\delta_0 W_i}=\frac{\boldsymbol{W_{i+1}}+\boldsymbol{2W_i}+\boldsymbol{W_{i-1}}}{\boldsymbol{4}},\quad \boldsymbol{\delta_1 W_i}=\frac{\boldsymbol{W_{i+1}}-\boldsymbol{W_{i-1}}}{\boldsymbol{2a}},\quad \boldsymbol{\delta_2 W_i}=\frac{\boldsymbol{W_{i+1}}-\boldsymbol{2W_i}+\boldsymbol{W_{i-1}}}{\boldsymbol{a^2}} \tag{6}$$

It is noteworthy to mention that the boundary interactions are expressed as

$$\begin{gathered}\boldsymbol{M_{1/2}}=\boldsymbol{k_r}(\boldsymbol{\Theta_1}-\boldsymbol{\Theta_0}),\quad \boldsymbol{V_{1/2}}=\boldsymbol{k_s}\left(\boldsymbol{W_1}-\boldsymbol{W_0}-\frac{\boldsymbol{a}}{\boldsymbol{2}}(\boldsymbol{\Theta_1}+\boldsymbol{\Theta_0})\right);\\ \boldsymbol{M_{n-1/2}}=\boldsymbol{k_r}(\boldsymbol{\Theta_n}-\boldsymbol{\Theta_{n-1}}),\quad \boldsymbol{V_{n-1/2}}=\boldsymbol{k_s}\left(\boldsymbol{W_n}-\boldsymbol{W_{n-1}}-\frac{\boldsymbol{a}}{\boldsymbol{2}}(\boldsymbol{\Theta_n}+\boldsymbol{\Theta_{n-1}})\right)\end{gathered} \tag{7}$$

Thus, the coupled difference equations of the static bending of the granular chain could be obtained in the matrix form:

$$\begin{pmatrix}-\boldsymbol{k_s\delta_1} & +\boldsymbol{k_s\delta_2}\\ \boldsymbol{k_r\delta_2}-\boldsymbol{k_s\delta_0} & \boldsymbol{k_s\delta_1}\end{pmatrix}\begin{pmatrix}\boldsymbol{\Theta_i}\\ \boldsymbol{W_i}\end{pmatrix}=\begin{pmatrix}\boldsymbol{-Q}\\ \frac{\boldsymbol{-Q}}{\boldsymbol{a^2}}\\ \boldsymbol{0}\end{pmatrix} \tag{8}$$

The uncoupled difference equations could be obtained as follows

$$\begin{gathered}\boldsymbol{k_r\delta_2\delta_2\Theta_i}-\boldsymbol{k_s\delta_0\delta_2\Theta_i}-\boldsymbol{\delta_1}\frac{\boldsymbol{Q}}{\boldsymbol{a^2}}+\boldsymbol{k_s\delta_1\delta_1\Theta_i}=\boldsymbol{0};\\ \boldsymbol{k_r\delta_2}\left(\frac{\boldsymbol{Q}}{\boldsymbol{k_s a^2}}+\boldsymbol{\delta_2 W_i}\right)-\boldsymbol{k_s\delta_0}\left(\frac{\boldsymbol{Q}}{\boldsymbol{k_s a^2}}+\boldsymbol{\delta_2 W_i}\right)+\boldsymbol{k_s\delta_1\delta_1 W_i}=\boldsymbol{0}\end{gathered} \tag{9}$$

Knowing the following relationship between the difference operators defined in Eq. (6) which is true also for the equivalent pseudo-differential operators

$$\boldsymbol{\delta_0\delta_2}=\boldsymbol{\delta_2\delta_0}=\boldsymbol{\delta_1\delta_1} \tag{10}$$

the fourth-order difference equation for the displacement and rotation of the granular beam could be obtained from Eq. (**9**) as follows:

$$\boldsymbol{k_r{\delta_2}^2 W_i = \left(\delta_0 - \frac{k_r}{k_s}\delta_2\right)\frac{Q}{a^2}},\quad \boldsymbol{k_r{\delta_1}^3\theta_i = {\delta_0}^2\frac{Q}{a^2}} \tag{11}$$

Assuming a constant uniform load distribution (q) on the beam which is equivalent for the discrete model as the point load $(Q = aq)$ applied to the center of the grain. Accordingly, the aforementioned difference equations could be simplified

$$\boldsymbol{EI{\delta_2}^2 W_i = q},\quad \boldsymbol{EI{\delta_1}^3\theta_i = q} \tag{12}$$

The displacement and rotation equations of each grain can be exactly obtained for the granular beam with distributed uniform loading as follows (see details in Appendix A)

$$\begin{aligned} \boldsymbol{W_i} &= \boldsymbol{W_0 + \left(a\theta_0 + \left(\frac{a}{6} - \frac{2k_r}{k_s a}\right)\beta\right)i + \left(\frac{a}{2}\alpha\right)i^2 + \left(\frac{a}{3}\beta\right)i^3 + \left(\frac{a^2 Q}{24k_r}\right)i^4} \\ &\quad \boldsymbol{+ \left(\frac{a^2 Q}{24k_r} - \frac{Q}{2k_s}\right)i^2}; \\ \boldsymbol{\theta_i} &= \boldsymbol{\theta_0 + \alpha i + \beta i^2 + \frac{aQ}{6k_r}i^3} \end{aligned} \tag{13}$$

where W_0, θ_0, α and β are constants that are obtained through the boundary conditions. Furthermore, the shear and bending moment constitutive law is given by:

$$\begin{aligned} \boldsymbol{V_i} &= \boldsymbol{k_s\left(W_{i+1/2} - W_{i-1/2} - \frac{a}{2}(\Theta_{i+1/2} + \Theta_{i-1/2})\right) = ak_s(\sqrt{\delta_2}W_i - \sqrt{\delta_0}\Theta_i)}; \\ \boldsymbol{M_i} &= \boldsymbol{k_r(\Theta_{i+1/2} - \Theta_{i-1/2}) = ak_r\sqrt{\delta_2}\Theta_i} \end{aligned} \tag{14}$$

where the mean difference operators are defined by

$$\boldsymbol{\sqrt{\delta_0}W_i = \frac{W_{i+1/2} + W_{i-1/2}}{2}},\quad \boldsymbol{\sqrt{\delta_2}W_i = \frac{W_{i+1/2} - W_{i-1/2}}{a}} \tag{15}$$

The balance equations of the discrete granular system read

$$\boldsymbol{V_{i+1/2} - V_{i-1/2} = -Q};$$
$$\boldsymbol{M_{i+1/2} - M_{i-1/2} + \frac{a}{2}\left(V_{i+1/2} + V_{i-1/2}\right) = 0} \tag{16}$$

where V is the shear force and M is the bending moment. In view of Eq. (12), the recent equation leads to

$$\boldsymbol{\sqrt{\delta_2}V_i = -q\,,\ \ \delta_0\delta_1\sqrt{\delta_2}M_i = q} \tag{17}$$

The general solutions of the bending and shear distributions in the discrete model could be considered as follows:

$$\boldsymbol{V_{i+1/2} = -Q\left(i + \frac{1}{2} + \sigma\right),\ \ M_{i+1/2} = \frac{aQ}{2}\left((i + \frac{1}{2})^2 + 2\sigma(i + \frac{1}{2}) + \gamma\right)} \tag{18}$$

where σ and γ are the unknown which might be obtained from the boundary reaction forces.

3. Simply Supported (S-S) Granular Beam

In this section, the bending responses of the granular beam are investigated analytically and numerically (using DEM) for simply supported boundary conditions. Accordingly, the deflection and rotation equations of the system are obtained as a function of grain number by considering the exact discrete conditions for the boundary grains. Next, the model is simulated in YADE open-source software to estimate the accuracy of the numerical computations.

3.1. Exact Analytical Solution

Let's consider a simply supported granular beam under uniformly distributed point load of intensity Q. The reaction forces could be obtained from the equilibrium equations of the granular system as follows

$$\boldsymbol{F_{ry}^1 + F_{ry}^2 - nQ = 0}\,;$$
$$\boldsymbol{(an)F_{ry}^2 - \left(\frac{an}{2}\right)(nQ) = 0} \tag{19}$$

Note that F_{ry}^1 and F_{ry}^2 are the vertical reaction forces of the left and right boundaries and are found by $F_{ry}^1 = F_{ry}^2 = \frac{nQ}{2}$. Also, using the equilibrium conditions for the boundary grains individually leads to

$$\boldsymbol{F_{ry}^1 - \frac{Q}{2} - V_{1/2} = 0}\,,\quad \boldsymbol{-\left(\frac{a}{2}\right)V_{1/2} - M_{1/2} = 0}\,;$$
$$\boldsymbol{F_{ry}^2 - \frac{Q}{2} + V_{n-1/2} = 0}\,,\ \boldsymbol{M_{n-1/2} - \left(\frac{a}{2}\right)V_{n-1/2} = 0} \tag{20}$$

Therefore, the shear and bending interactions of the boundary grains could be obtained as follows

$$\boldsymbol{V_{1/2} = \frac{Q}{2}(n-1),\ \ M_{1/2} = -\frac{aQ}{4}(n-1)}\,;$$
$$\boldsymbol{V_{n-1/2} = -\frac{Q}{2}(n-1),\ \ M_{n-1/2} = -\frac{aQ}{4}(n-1)} \tag{21}$$

Applying the values of Eq. (21) into Eq. (18), the distribution of bending moment and shear forces on the discrete granular beam could be obtained

$$\boldsymbol{V_{i+1/2} = -Q\left(i + \frac{1}{2} - \frac{n}{2}\right),\ \ M_{i+1/2} = \frac{aQ}{2}\left((i+\frac{1}{2})^2 - n(i+\frac{1}{2}) + \frac{1}{4}\right)} \tag{22}$$

For an infinite number of grains ($n \to \infty$), the corresponding local bending solutions of the Timoshenko continuum beam are found as follows (Timoshenko [110] and Wang et al. [111])

$$\boldsymbol{V(x) = -q\left(x - \frac{L}{2}\right),\ \ M(x) = \frac{q}{2}(x^2 - Lx)} \tag{23}$$

The exact simply supported boundary conditions for such a granular system are defined by considering the sides grains could rotate freely while their vertical displacements are

blocked. Thus, the proposed boundary conditions based on the finite difference beam model are obtained from Eq. (20) by replacing the interactions of Eq. (7) as follows:

$$\begin{gathered} \boldsymbol{W_0 = 0,\ \ ak_sW_1 - \frac{a^2}{2}k_s(\theta_1 + \theta_0) + 2k_r(\theta_1 - \theta_0) = 0}\ ; \\ \boldsymbol{W_n = 0,\ \ -ak_sW_{n-1} - \frac{a^2}{2}k_s(\theta_{n-1} + \theta_n) + 2k_r(\theta_{n-1} - \theta_n) = 0} \end{gathered} \tag{24}$$

On the other hand, based on Hamilton's principle, using the variationally-based boundary conditions, the same properties could be obtained as follows

$$\begin{gathered} \boldsymbol{\left[k_s\left(W_1 - W_0 - \frac{a}{2}(\theta_1 + \theta_0)\right)\right]\delta W_0 = 0}\ ; \\ \boldsymbol{\left[k_s\left(W_n - W_{n-1} - \frac{a}{2}(\theta_n + \theta_{n-1})\right)\right]\delta W_n = 0}\ ; \\ \boldsymbol{\left[k_r(\theta_1 - \theta_0) + \frac{a}{2}k_s(W_1 - W_0) - \frac{a^2}{4}k_s(\theta_1 + \theta_0)\right]\delta\theta_0 = 0}\ ; \\ \boldsymbol{\left[-k_r(\theta_{n-1} - \theta_n) - \frac{a}{2}k_s(W_n - W_{n-1}) + \frac{a^2}{4}k_s(\theta_n + \theta_{n-1})\right]\delta\theta_n = 0} \end{gathered} \tag{25}$$

The substitution of general solutions of Eq. (13) into boundary conditions (24) leads to the displacement and rotation equations of the simply supported granular chain which could be expressed as follows:

$$\begin{gathered} \boldsymbol{W_i = \left(\left(\frac{a^2Q}{24k_r}\right)(n^3 - 2n) + \frac{Qn}{2k_s}\right)i - \left(\frac{a^2nQ}{12k_r}\right)i^3 + \left(\frac{a^2Q}{24k_r}\right)i^4 + \left(\frac{a^2Q}{12k_r} - \frac{Q}{2k_s}\right)i^2}; \\ \boldsymbol{\theta_i = \left(\frac{aQ}{24k_r}\right)(n^3 - n) + \frac{aQ}{12k_r}i - \frac{aQn}{4k_r}i^2 + \frac{aQ}{6k_r}i^3} \end{gathered} \tag{26}$$

Recalling the continuum terms ($x = ai,\ k_s = \frac{\mathcal{K}GA}{a},\ k_r = \frac{EI}{a}$), leads to

$$\begin{gathered} \boldsymbol{W(x) = \frac{qL^4}{24EI}\left[\left(1 + \frac{12EI}{\mathcal{K}GAL^2}\right)\left(\frac{x}{L}\right) - 2\left(\frac{x}{L}\right)^3 + \left(\frac{x}{L}\right)^4 - \left(\frac{12EI}{\mathcal{K}GAL^2}\right)\left(\frac{x}{L}\right)^2 - \frac{2a^2}{L^2}\left(1 - \frac{x}{L}\right)\left(\frac{x}{L}\right)\right]}; \\ \boldsymbol{\theta(x) = \frac{qL^3}{24EI}\left[1 - 6\left(\frac{x}{L}\right)^2 + 4\left(\frac{x}{L}\right)^3 - \frac{a^2}{L^2}\left(1 - 2\left(\frac{x}{L}\right)\right)\right]} \end{gathered} \tag{27}$$

It is worthwhile to note that the scale effect leads to the smaller values of deflection and micro rotation which concludes the hardening behavior of the beam. Assuming an infinite number of grains when $a \to 0$ for the continuum model**,** Eq. (27) leads to

$$\begin{gathered} \boldsymbol{W(x) = \frac{qL^4}{24EI}\left[\left(1 + \frac{12EI}{\mathcal{K}GAL^2}\right)\left(\frac{x}{L}\right) - 2\left(\frac{x}{L}\right)^3 + \left(\frac{x}{L}\right)^4 - \left(\frac{12EI}{\mathcal{K}GAL^2}\right)\left(\frac{x}{L}\right)^2\right];} \\ \boldsymbol{\theta(x) = \frac{qL^3}{24EI}\left[1 - 6\left(\frac{x}{L}\right)^2 + 4\left(\frac{x}{L}\right)^3\right]} \end{gathered} \tag{28}$$

These equations could be compared well by the equivalent local continuum model of Timoshenko [110]. The maximum deflection and micro rotation angle which occur respectively at the middle ($x = \frac{L}{2}$) and on the boundaries ($x = 0, L$) are given by

$$\begin{gathered} \boldsymbol{W_{max} = \frac{qL^4}{24EI}\left[\frac{5}{16} - \frac{1}{2n^2} + \frac{3EI}{\mathcal{K}GAL^2}\right] < f_{SS}^{\infty};} \\ \boldsymbol{\theta_{max} = \frac{qL^3}{24EI}\left[1 - \frac{1}{n^2}\right]} \end{gathered} \tag{29}$$

f_{SS}^{∞} refers to the maximum bending displacement of the S-S continuum Timoshenko beam which is given by Eq. (30). For an infinite number of grains ($a \to 0$) the discrete solutions converge to the local continuum deflection results obtained by Timoshenko [110]:

$$\boldsymbol{\frac{EI}{qL^4} f_{SS}^{\infty} = \frac{5}{384} + \frac{EI}{8\mathcal{K}GAL^2}} \tag{30}$$

It could be concluded that the nonlocal terms that affect the granular beam contribute to a stiffening effect, as compared to the so-called local continuum solution. The response of the system for clamped-simply, clamped-clamped and clamped-free boundary conditions are discussed in Appendix B.

The deflection and rotation of the granular beam subjected to distributed loading are shown in Figure 2 for various boundary conditions presented above. The results are

obtained for the numerical problem of section 3.2 while the typical value of grain number is fixed to 11.

(a) **(b)**

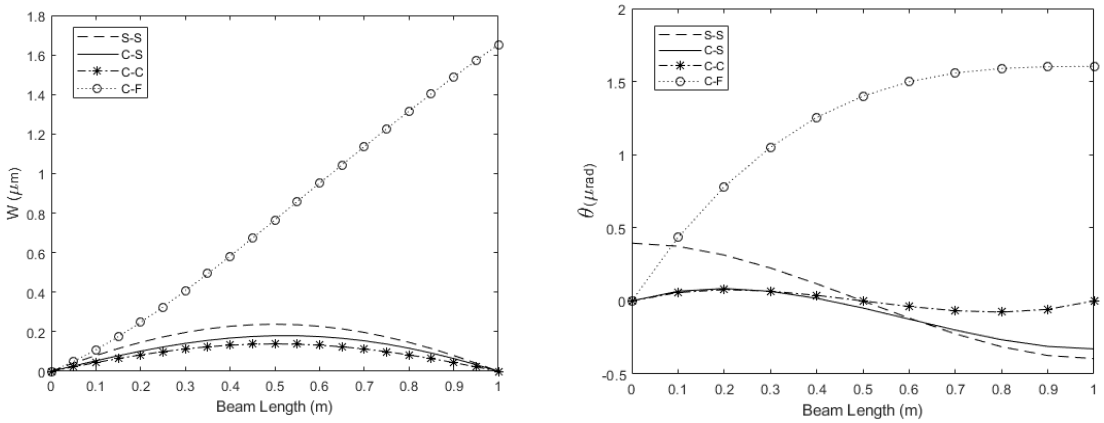

Figure 2. Static bending granular beam solution for 11 number of grains (a) Deflection and (b) Rotation

Figure 3 studies the effect of the grain number on the exact solution of the simply supported granular beam (Eq. (26)). The difference between the discrete and continuum solutions parameterized by ($\epsilon = \frac{W^{Continuum} - W^{Discrete}}{W^{Continuum}} \times 100$) are plotted. The effects of the rotational and shear spring rigidity and the beam length are also investigated. As it was expected, the discrete results converge to the continuum ones by increasing the grain number or decreasing the length scale. For this specific numerical problem (introduced in section) ϵ is less than *1%* when the grain number is more than *10*. It could be concluded that either the decrease of bending stiffness or the increase of the shear stiffness leads to the larger difference values of the discrete and continuum models.

(a) **(b)**

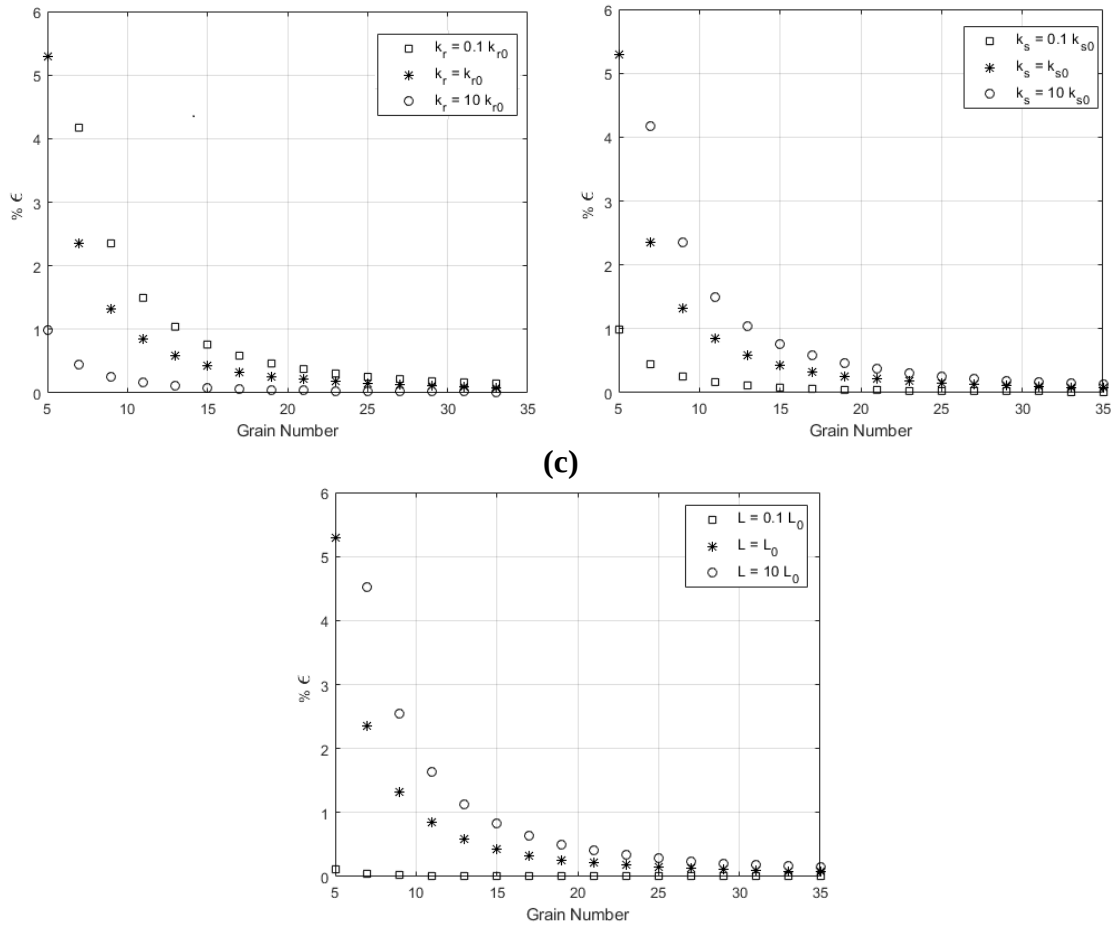

Figure 3. Parametric analysis of the continuum and discrete differences ($\boldsymbol{\epsilon}$) with regards to the grain number values for a simply supported granular beam by varying (a) Rotational spring rigidity, (b) Shear spring rigidity, and (c) Beam length

3.2. Numerical Simulations (DEM)

In this section, a granular beam of length L similar to Figure 2, is studied for different values of grain number. The open-source software YADE (Šmilauer et al. [112]) is used for numerical simulations. This model embeds parameters such as the number of grains, initial positions, density, and radius. To model the contact behavior of the grains, an elastic contact relation will be used thereafter. The contact stiffnesses are defined as follows

$$\boldsymbol{k_n = Ea},\ \ \boldsymbol{k_s = \vartheta_m k_n},\ \ \boldsymbol{k_b = \alpha_b k_s \left(\frac{a}{2}\right)^2} \tag{31}$$

Note that k_n, k_s and k_b are associated with normal, shear, and bending stiffness. ϑ_m and $\alpha_b$are respectively the contact stiffness ratio and the dimensionless rolling stiffness which can be defined as follows with regards to the discrete model presented in section 2.

$$\boldsymbol{\vartheta_m = \frac{2\mathcal{K}GA}{Ea^2}, \quad \alpha_b = \frac{8EI}{E\vartheta_m a^4}} \tag{32}$$

The micromechanical properties of the beam are calculated for Titanium with the mechanical properties of $E = 116\ GPa$ and $G = 43\ GPa$. The beam geometry is introduced by $L = 1\ m, A = 0.3\ m^2$ and $I = 0.009\ m^4$. Thus, ones could be obtained as below:

$$\boldsymbol{k_s = 11.22n\ \frac{N}{m}, \quad k_b = 1.04n\ N.m, \quad Q = \frac{10}{n}\ kN} \tag{33}$$

where n is the grain number. The problem is investigated for a rectangular cross-section beam. The shear coefficient of the Bresse-Timoshenko beam could be estimated from $\mathcal{K} = \frac{5(1+\vartheta)}{6+5\vartheta}$ (Challamel and Elishakoff [68]). Once the mechanical and geometrical parameters of the model are defined completely, the physical law and the mechanical principles of the system need to be introduced (collision physics and the contact law).

3.2.1. Collision Detection

There exist several efficient ways to determine approximately the contacts between discrete element pairs such as nearest neighbor contact detection scheme, neighboring cell contact detection scheme and sweep and prune. Depending on particles' arrangement or their shape, each method has its own advantages or disadvantages.

The sweep and prune algorithm is used for collision detection in Yade through the consideration of the bounding box. This general approach deals more efficiently with high density systems while permitting to handle poly-sized particle distributions. To this aim,

each particle is surrounded by a bounding box with edges aligned with the reference coordinate system. In order to detect the collision between particles only it is needed to check the overlapping of the bounding boxes. The sweep and prune algorithm is optimized with Verlet's distance (Verlet [113]). Accordingly, this permits to introduce a relative length to enlarge the bounding boxes.

3.2.2. Interactions

Once the elements which are in contact are detected, it is needed to find the exact collision depending on the geometry of the individual particle. Since at every timestep the grains can move or rotate, exact collision detection must be run at every step. Let us consider two identical grains (with diameter a) in the non-deformed configuration. The position vectors are presented by r_1 and r_2. The two spheres enter in when the distance (u_n) between the spheres is negative, with

$$\boldsymbol{u_n} = \|\boldsymbol{r_2} - \boldsymbol{r_1}\| - \boldsymbol{a} \tag{34}$$

The unit normal orientation (n) at the contact is obtained by

$$\boldsymbol{n} = \frac{\boldsymbol{r_2} - \boldsymbol{r_1}}{\|\boldsymbol{r_2} - \boldsymbol{r_1}\|} \tag{35}$$

Regarding the problem investigated in this chapter, the normal relative displacement is null, only the shear and bending relative displacement of two grains in contact are computed. The shear displacement contains two parts, namely the motion of the interaction in global space and the relative motion of spheres. At each step, the shear displacement u_s is updated as follows

$$\boldsymbol{u_s^{t+\Delta t}} = \boldsymbol{u_s^t} + (\boldsymbol{\delta_s})_1 + (\boldsymbol{\delta_s})_2 + (\boldsymbol{\delta_s})_3 \tag{36}$$

where $(\delta_s)_1$ and $(\delta_s)_2$ refer to the contact displacements due to changes in the spheres' positions and $(\delta_s)_3$ is the relative motion of spheres. These terms could be obtained respectively by

$$\begin{gathered}(\boldsymbol{\delta_s})_1 = -\boldsymbol{\delta_s^{t-\Delta t}} \times (\boldsymbol{n^{t-\Delta t}} \times \boldsymbol{n^t});\\ (\boldsymbol{\delta_s})_2 = -\boldsymbol{\delta_s^{t-\Delta t}} \times \left(\frac{\boldsymbol{\Delta t}}{\boldsymbol{2}} \boldsymbol{n^t}.\left(\boldsymbol{\omega_1^{t-\frac{\Delta t}{2}}} + \boldsymbol{\omega_2^{t-\frac{\Delta t}{2}}}\right)\right)\boldsymbol{n^t};\\ (\boldsymbol{\delta_s})_3 = -\boldsymbol{\Delta t}\, \boldsymbol{v_{12}^{\perp}}\end{gathered} \tag{37}$$

Note that Δt is the time step and the superscript t refers to the current time. $v_{12}^{\perp}$ is the relative velocity perpendicular to the interaction normal vector and could be computed as follows

$$\begin{gathered}\boldsymbol{v_{12}^{\perp}} = \boldsymbol{v_{12}} - (\boldsymbol{v_{12}}.\boldsymbol{n^t})\boldsymbol{n^t};\\ \boldsymbol{v_{12}} = \left(\boldsymbol{v_2^{t-\Delta t/2}} - \boldsymbol{v_1^{t-\Delta t/2}}\right) - \frac{\boldsymbol{a}}{\boldsymbol{2}}\left(\boldsymbol{\omega_1^{t-\Delta t/2}} + \boldsymbol{\omega_2^{t-\Delta t/2}}\right) \times \boldsymbol{n^t}\end{gathered} \tag{38}$$

The relative rotation of each grain sphere is expressed by

$$\boldsymbol{\delta_b} = \boldsymbol{\Delta t}\, (\boldsymbol{\omega_2^t} - \boldsymbol{\omega_1^t}) \times \boldsymbol{n^t} \tag{39}$$

Once all kinematics components of the contact interaction are introduced and also the exact contact location (for instance $r_1 + \frac{a}{2}n$) is detected, the physical properties of the contact can be defined. To this aim, the following contact model is adopted, in which the normal, shear and bending forces and also the bending moment are defined by

$$\boldsymbol{F_n} = \boldsymbol{k_n \delta_n}, \quad \boldsymbol{F_s} = \boldsymbol{k_s \delta_s}, \quad \boldsymbol{M_b} = \boldsymbol{k_b \delta_b} \tag{40}$$

where δ_n, δ_s correspond to relative displacements in the normal and tangential direction and δ_b is the relative rotation. It is worth mentioning that the friction angle (φ) which controls the relative sliding, is fixed to 90 degrees.

3.2.3. Explicit Dynamic Algorithm

The numerical resolution is based on an explicit integration scheme based on a Velocity Verlet scheme well adapted to DEM simulation. Once, the shear forces and bending moments at the interactions are computed, the accelerations of each particle can be estimated from the second Newton's law (Eq. (41)). In order to update the grain positions at the next timestep ($u^{t+\Delta t}$) from the current position (u^t), the current acceleration ($\ddot{u}^t$) is integrated by time as follows.

$$\ddot{\boldsymbol{u}}^{\boldsymbol{t}} = \boldsymbol{\delta}_{\boldsymbol{2t}}\boldsymbol{u} = \frac{\boldsymbol{F}}{\boldsymbol{m}} \tag{41}$$

where the time differences operator of δ_{2t} is defined

$$\boldsymbol{\delta}_{\boldsymbol{2t}}\boldsymbol{u} = \frac{\boldsymbol{u}^{\boldsymbol{t+\Delta t}} + \boldsymbol{u}^{\boldsymbol{t-\Delta t}} - \boldsymbol{2u}^{\boldsymbol{t}}}{\boldsymbol{\Delta t^2}} \tag{42}$$

So, the position of the next timestep might be expressed by

$$\boldsymbol{u}^{\boldsymbol{t+\Delta t}} = \boldsymbol{u}^{\boldsymbol{t}} + \boldsymbol{\Delta t}\left(\frac{\boldsymbol{u}^{\boldsymbol{t}} - \boldsymbol{u}^{\boldsymbol{t-\Delta t}}}{\boldsymbol{\Delta t}} + \ddot{\boldsymbol{u}}^{\boldsymbol{t}}\boldsymbol{\Delta t}\right) \tag{43}$$

Since only the current position (u^t) is known, the mean terms could be defined as follows

$$\dot{\boldsymbol{u}}^{\boldsymbol{t-\Delta t/2}} = \frac{\boldsymbol{u}^{\boldsymbol{t}} - \boldsymbol{u}^{\boldsymbol{t-\Delta t}}}{\boldsymbol{\Delta t}} \tag{44}$$

The mean velocity during the previous step is known, thus,

$$\boldsymbol{u}^{\boldsymbol{t+\Delta t}} = \boldsymbol{u}^{\boldsymbol{t}} + \boldsymbol{\Delta t}\left(\dot{\boldsymbol{u}}^{\boldsymbol{t-\Delta t/2}} + \ddot{\boldsymbol{u}}^{\boldsymbol{t}}\boldsymbol{\Delta t}\right) \tag{45}$$

The current mean velocity ($\dot{u}^{t+\Delta t/2}$) is needed for the next step and obtained from the following equation

$$\ddot{\boldsymbol{u}}^{\boldsymbol{t}} = \frac{\dot{\boldsymbol{u}}^{\boldsymbol{t+\Delta t/2}} - \dot{\boldsymbol{u}}^{\boldsymbol{t-\Delta t/2}}}{\boldsymbol{\Delta t}} \tag{46}$$

3.2.4. Numerical Results

The discrete granular beam has been simulated by DEM for various boundary conditions. It could be demonstrated that the DEM numerical results have a significant accuracy with the exact analytical ones for the four types of boundary conditions S-S, C-C, S-C, and C-F. The maximum deflection and micro-rotation of the granular beam are reported respectively in Table 1 and Table 2. Although the numerical simulation includes dynamical effects (based on Newton's equation of motion) and so hysteresis effects may appear due to incremental formulation of the contact law, a significant accuracy (nearly 0.01%) has been obtained for the numerical results in comparison with the exact analytical ones.

4. Nonlocal Continuum Approach

Nonlocal continuum theories stem from the substitution of the local axiom action by the principle of weakening neighborhood. This states that the mechanical behavior of each element is affected significantly by the rotation and displacement of a finite-size neighborhood. Subsequently, internal characteristic length and scale effects can be introduced through gradient elasticity or nonlocal elasticity. Furthermore, discrete granular structured systems (Cosserat discrete) behave as nonlocal structural systems in which the continualization leads to the nonlocal continuum models.

In this section, a more refined Cosserat continuum that accounts for the internal nonlocal effects is proposed through the continualization of the difference governing coupled equation of the Cosserat discrete chain (Eq. (8)) using polynomial or rational expansions. Accordingly, the governing differential equations are given with the variationally-based boundary conditions. It is worth mentioning that for clamped ends, the

nonlocal boundary conditions are the same as the discrete ones. The nonlocal boundary conditions of C-S, C-C and C-F boundaries are also investigated in Appendix E. For simply supported boundary conditions, several different strategies are followed to obtain the nonlocal solutions. The nonlocal boundary conditions could be investigated from various approaches: the first approximation is based on the development of the continuum equilibrium equations of the boundaries independently from the discrete model. Alternative approaches are based on the discrete model formulations (2nd nonlocal approximation) such as continualization of the exact cinematic conditions, continualization of the bending moment, or continualization of the static boundary conditions.

The coupled balance equations of Eq. (8) could be continualized using the Taylor series in the function of the small length scale noted by $\boldsymbol{a}$. The governing differential equations of the nonlocal continuum beam could be stated by

$$\boldsymbol{EI\Theta'''} = \boldsymbol{q}, \;\; \boldsymbol{EIW''''} = \boldsymbol{q} \tag{47}$$

The details are given in Appendix C. Accordingly, the governing equations of the nonlocal beam could be obtained the same as the local continuum beam from the coupled differential equations. Since the second gradient of the external load (a uniformly distributed load) is null, the governing differential equations of the nonlocal model are identical to the ones that have been obtained for the local continuum Bresse-Timoshenko beam (Timoshenko [110]). The general solution reads in a quartic and cubic form respectively for the deflection and micro rotation as

$$\boldsymbol{W(x)} = \boldsymbol{\bar{A}_1} + \boldsymbol{\bar{B}_1 x} + \boldsymbol{\bar{C}_1 x^2} + \boldsymbol{\bar{D}_1 x^3} + \frac{\boldsymbol{q}}{\boldsymbol{24EI}}\boldsymbol{x^4}; \tag{48}$$

$$\boldsymbol{\Theta(x)} = \boldsymbol{\bar{A}_2} + \boldsymbol{\bar{B}_2 x} + \boldsymbol{\bar{C}_2 x^2} + \frac{\boldsymbol{q}}{\boldsymbol{6EI}}\boldsymbol{x^3}$$

$\bar{A}_1, \bar{B}_1, \bar{C}_1, \bar{D}_1, \bar{A}_2, \bar{B}_2$ and $\bar{C}_2$ are constants. Replacing Eq. (48) in the coupled balance equations of the nonlocal model presented by Eq. (C.2) leads to

$$\begin{gathered} \boldsymbol{W(x) = \overline{W}_0 + \left(\bar{\theta}_0 + \frac{a^2}{6}\mu - \frac{2EI}{\mathcal{K}GA}\mu\right)x + \left(\frac{\lambda}{2} + \frac{a^2 q}{24EI} - \frac{q}{2\mathcal{K}GA}\right)x^2 + \left(\frac{\mu}{3}\right)x^3 + \frac{q}{24EI}x^4;} \\ \boldsymbol{\Theta(x) = \bar{\theta}_0 + \lambda x + \mu x^2 + \frac{q}{6EI}x^3} \end{gathered} \tag{49}$$

where $\bar{W}_0, \bar{\theta}_0, \mu$ and λ are constants. These constant parameters would be obtained by applying the boundary conditions. On the other hand, the nonlocal shear and bending moment of the beam could be obtained from the continualization of Eq. (14) through the rational expansion of second order for the difference operator as follows

$$\boldsymbol{V(x) = \mathcal{K}GA\left(W'(x) - \Theta(x) - \frac{a^2}{12}W'''(x)\right)} \tag{50}$$

$$\boldsymbol{M(x) - \frac{a^2}{24}M''(x) = EI\Theta'(x)} \tag{51}$$

Furthermore, in view of the continualization of Eq. (17), $M''(x) = q$. Thus, Eq. (51) might be rewritten eventually as follows

$$\boldsymbol{M(x) = EI\Theta'(x) + \frac{a^2}{24}q} \tag{52}$$

4.1. Continualization of the Boundary Conditions with Static Variables

This method stems from the direct continualization of the equilibrium equations of the continuum beam. Developing the equilibrium equations of the boundaries (See Appendix D, Eq. (D.4)) by Taylor series and ignoring the higher order of terms a^3 leads to

$$\begin{gathered} \boldsymbol{M(0) + \frac{a}{2}M'(0) + \frac{a^2}{8}M''(0) + \frac{a}{2}\left(V(0) + \frac{a}{2}V'(0) + \frac{a^2}{8}V''(0)\right) = 0;} \\ \boldsymbol{M(L) - \frac{a}{2}M'(L) + \frac{a^2}{8}M''(L) + \frac{a}{2}\left(V(L) - \frac{a}{2}V'(L) + \frac{a^2}{8}V''(L)\right) = 0} \end{gathered} \tag{53}$$

Knowing $V(x) = -M'(x)$ and $V'(x) = -M''(x) = -q$, the abovementioned equations could be simplified as follows

$$\boldsymbol{M(0) + \frac{a^2}{8}(q - 2q) = 0;\ \ M(L) + \frac{a^2}{8}(q - 2q) = 0} \tag{54}$$

It is noteworthy to conclude that despite the simply supported boundary conditions the nonlocal bending moments on the pinned boundaries are not zero and is equal to $M(0) = M(L) = \frac{a^2 q}{8}$. Thus, based on the nonlocal bending moment presented by Eq. (52), the nonlocal boundary conditions could be obtained independently from the discrete model as follows

$$\boldsymbol{W(0) = 0\ ;\ \ \Theta'(0) = \frac{a^2 q}{12EI}\ ;\ \ W(L) = 0\ ;\ \ \Theta'(L) = \frac{a^2 q}{12EI}} \tag{55}$$

The constant of the nonlocal general solutions of Eq. (49) could be obtained concerning the aforementioned set of conditions. Accordingly, the solutions are given

$$\boldsymbol{W(x) = \frac{qL^4}{24EI}\left[\left(1 - \frac{2a^2}{L^2} + \frac{12EI}{\mathcal{K}GAL^2}\right)\left(\frac{x}{L}\right) + \left(\frac{2a^2}{L^2} - \frac{12EI}{\mathcal{K}GAL^2}\right)\left(\frac{x}{L}\right)^2 - 2\left(\frac{x}{L}\right)^3 + \left(\frac{x}{L}\right)^4\right];}$$

$$\boldsymbol{\Theta(x) = \frac{qL^3}{24EI}\left[1 - \frac{a^2}{L^2} + \frac{2a^2}{L^2}\left(\frac{x}{L}\right) - 6\left(\frac{x}{L}\right)^2 + 4\left(\frac{x}{L}\right)^3\right]} \tag{56}$$

These nonlocal solutions are exactly the same as those presented in Eq. (27) from the discrete model. For instance, the maximum deflection values are expressed by

$$\boldsymbol{W_{max} = \frac{qL^4}{24EI}\left[\frac{5}{16} - \frac{a^2}{2L^2} + \frac{3EI}{\mathcal{K}GAL^2}\right]} \tag{57}$$

which can be compared well also by the results of the granular beam by Eq. (29).

4.2. Continualization of the Boundary Conditions Based on Deflection

An alternative approach based only on the deflection equation could be considered as follows. The differential deflection equation of the continuum beam could be expressed

by $EIW'''' = q$. In order to investigate the deflection equation of the problem, we have to consider four boundary values based on the deflection. From the discrete medium, it could be written

$$(\boldsymbol{\delta_0 - k_r/k_s\,\delta_2})\boldsymbol{\Theta_i = \delta_1 W_i} \tag{58}$$

Using the rational expansion for the rotation ($\Theta_i = \frac{M}{EI\sqrt{\delta_2}}$), it can be found

$$(\boldsymbol{\delta_0 - \frac{EI}{\mathcal{K}GA}\delta_2})\boldsymbol{M = EI\delta_1\sqrt{\delta_2}W} \tag{59}$$

Through the polynomial development of the difference operators (using Taylor series by neglecting the higher-order terms in $\boldsymbol{a}^4$), this can be continualized as

$$\left(\left(\mathbf{1}+\frac{\boldsymbol{a^2D_x^2}}{\mathbf{4}}\right)-\frac{\boldsymbol{EI}}{\boldsymbol{\mathcal{K}GA}}\left(\mathbf{1}+\frac{\boldsymbol{a^2D_x^2}}{\mathbf{12}}\right)\boldsymbol{D_x^2}\right)\boldsymbol{M} = \boldsymbol{EI}\left(\mathbf{1}+\frac{\boldsymbol{a^2D_x^2}}{\mathbf{6}}\right)\left(\mathbf{1}+\frac{\boldsymbol{a^2D_x^2}}{\mathbf{24}}\right)\boldsymbol{D_x^2W} \tag{60}$$

Considering the general solution of deflection given by Eq. (48) and knowing $M''(x) = q$, the nonlocal moment could be obtained

$$\boldsymbol{M(x)} = -\frac{\boldsymbol{a^2q}}{\mathbf{4}}+\frac{\boldsymbol{EIq}}{\boldsymbol{\mathcal{K}GA}}+\boldsymbol{EI}\left(\mathbf{1}+\frac{\mathbf{5}\boldsymbol{a^2D_x^2}}{\mathbf{24}}\right)\boldsymbol{D_x^2W} \tag{61}$$

Here, the simply supported continuum beam is introduced with the nonlocal boundary conditions depending only on the displacement which may be written by:

$$\begin{aligned}&\boldsymbol{W(0) = 0\,;\quad W''(0)+\frac{5a^2}{24}W''''(0) = \frac{3a^2q}{8EI}-\frac{q}{\mathcal{K}GA}\,;}\\ &\boldsymbol{W(L) = 0\,;\quad W''(L)+\frac{5a^2}{24}W''''(L) = \frac{3a^2q}{8EI}-\frac{q}{\mathcal{K}GA}}\end{aligned} \tag{62}$$

Again, this set of boundary conditions lead to the same deflection equation as the one obtained by Eq. (56). Also, the alternative approaches for studying nonlocal beams are given in Appendix D. The results of these two nonlocal approaches and also the ones of

the exact analytical discrete beam are plotted in Figure 4. The results of the other boundary conditions are presented in Appendix E.

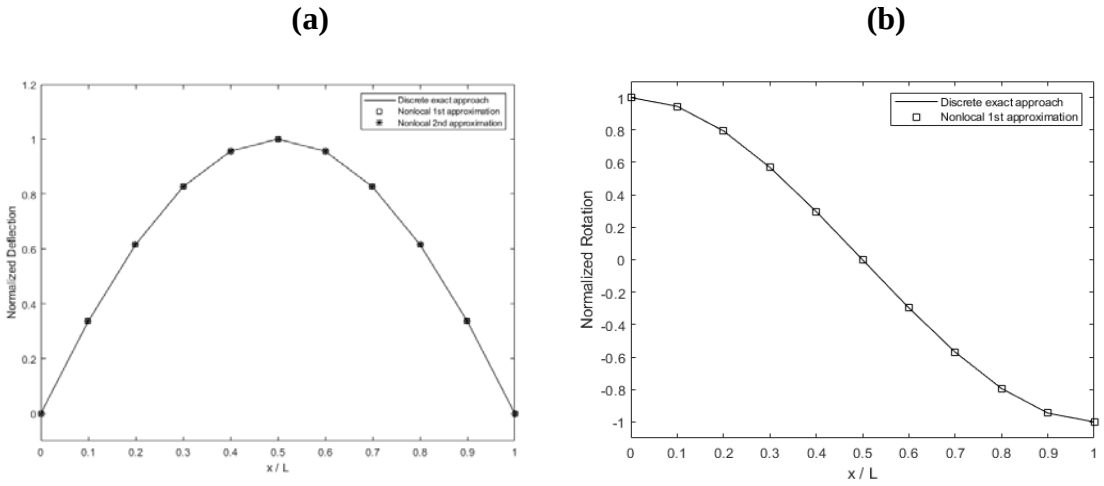

Figure 4. Comparison of the exact discrete approach with the nonlocal ones based on discrete model (1st nonlocal approximation) and based on the development of the continuum formulations (2nd nonlocal approximation) for 11 number of granular elements (a) Deflection and (b) Rotation

5. Conclusion and Outlook

This study represents an effort to investigate theoretically the scale effect upon the bending deformation of a granular beam which can be viewed as a discrete Bresse-Timoshenko beam in static conditions. A unidimensional granular chain consisting of rigid grains connected elastically with rotation and shear springs is considered. Thus, the mechanical properties of the system are characterized by the grain diameter (length scale). The proposed system can be considered as a discrete Cosserat chain with two independent degrees of freedom, namely the deflection and the rotation of each grain. Once the kinematics and Lagrangian energy of the model have been introduced, we have obtained the general solutions of the static granular chain under distributed vertical loads ruled by a coupled system of difference equations. The problem is postulated for four conventional boundary conditions, namely simply supported, clamped, clamped-simply and clamped-free. For each case, the exact displacement and rotation of the granular beam are found

through the exact discrete conditions defined for the boundary grains. The solution of the simply supported discrete system is compared to the one of a continuous Cosserat chain asymptotically obtained for an infinite number of grains when only the local neighbor effects are taken into account. For this case, the discrete solution converges asymptotically towards the local continuum one of a Bresse-Timoshenko beam. Then, the gradient elasticity Cosserat continuum is developed through the continualization of the difference equations using two equivalent strategies. The nonlocal models are able to reproduce the scale effects. The distinguishing features of these two refined continuous models basically stem from the continualization of the bending moment valid for the discrete Cosserat media which could be defined either by displacement or rotation parameters. It was shown that both nonlocal solutions coincide with the exact discrete one. Finally, a numerical asymptotic problem of a cantilever beam under distributed loading is studied for various boundary conditions. The problem is simulated by the open-source framework of Yade based on DEM. The DEM numerical results are exactly the same as the ones obtained by the exact analytical discrete approach. As the relevance of this discrete numerical model was checked for elementary cases, it would be of great interest to use it for investigating more complicated problems involving disordered discrete structures subjected to various types of loading including dynamic and vibration effects in 2D and 3D.

CHAPTER 3

Vibration Analysis of Granular Beam

1. Introduction

The present study focuses on the vibration of a granular beam with both bending and shear granular interactions. The granular beam is assumed to interact elastically with a rigid elastic support, a discrete elastic foundation labeled as a discrete Winkler foundation (Winkler [114]). Note that the difference equations governed to the model coincide with the ones of Cosserat granular model of Pasternak and Mühlhaus [11] in the absence of an elastic foundation, but differ from the ones of the discrete shear model studied by Duan et al. [12]. However, for some specific bending/ shear interaction modeling, the model developed by Bacigalupo and Gambarotta [115] can be mathematically reformulated with the difference equation presented in this chapter.

This chapter is arranged as follows: First, a discrete granular beam model is introduced from a geometrical and mechanical point of view. The grain interaction and material parameters are defined in detail. Then from the dynamic analysis of the lattice beam model, the deflection equations of the finite granular beam are derived. This fourth-order linear difference equation is solved by using the exact resolution of the difference equation. For an infinite number of grains, the deflection equation of a continuous beam (a fourth-order linear differential equation) is obtained asymptotically. Next, the eigenfrequencies of the discrete granular model and the continuous one, are obtained and compared as well. In the end, two asymptotic continualization methods are used to investigate continuous beam from the discrete lattice problem. With this aim, the polynomial expansion of Taylor and the rational expansion of Padé (with involved pseudo-

differential operators) are used to derive new enriched beam models. These two nonlocal continualization approaches with the introduction of the gradient terms engage the neighbor influences which allow the passage from discrete results to continuous ones and simultaneously capture the length effect.

2. Granular Model

A granular beam of length *L* resting on two simple supports is modeled by a finite number of grains interacting together. Such a model could be presented by considering the microstructured granular chain comprising *n+1* rigid grains with diameter *a* (*a=L/n*) that are connected by n shear and rotational springs, as shown in Figure 5. It is assumed that the elastic support springs are located at the center of each rigid grain. Each grain has two degrees of freedom which are denoted by W_i for the deflection and Θ_i for the rotation. This model is slightly different from the one of Challamel et al. [116] where the nodal kinematics and the Winkler elastic foundation are located at the grain interface. The aim of this study consists in finding the vibration equation of this granular chain and then trying to obtain the natural frequencies.

(a)

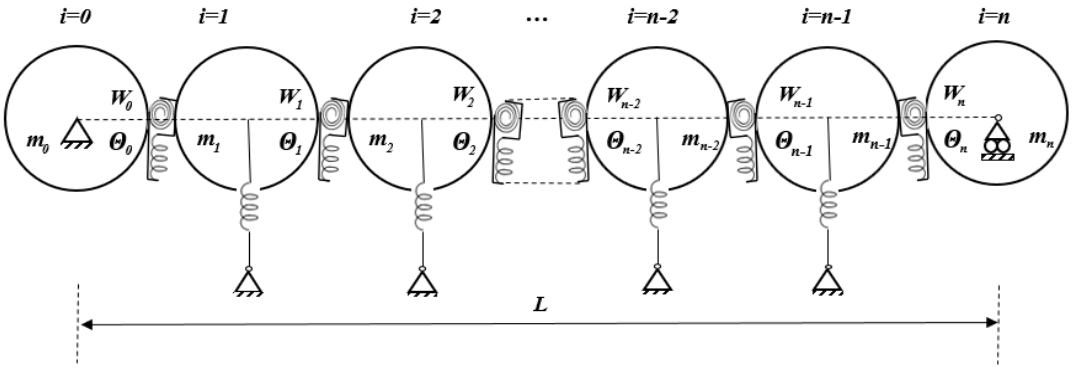

(b)

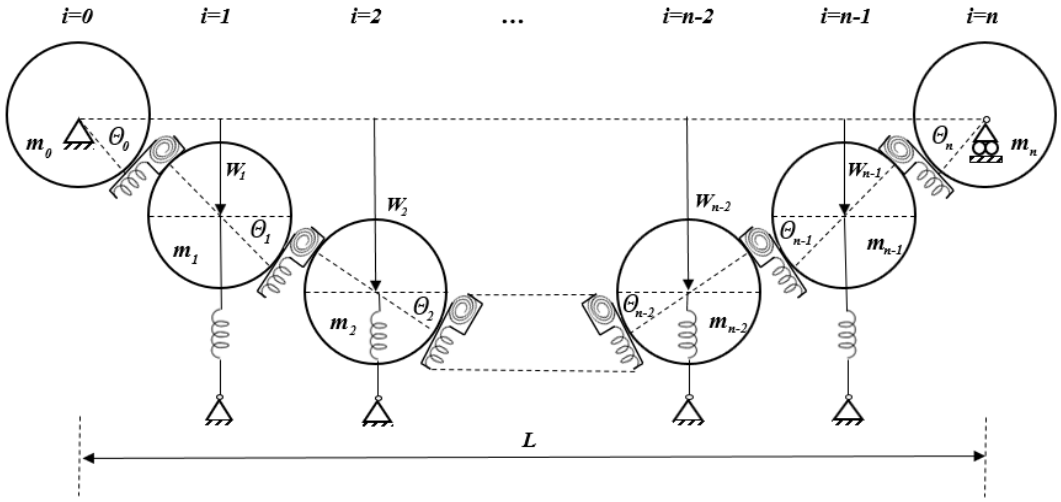

Figure 5. A discrete shear granular chain model composed of n+1 grain; (a) undeformed and (b) deformed.

The total kinetic energy of the model may be expressed as follows:

$$T = \frac{1}{2}\sum_{i=0}^{n} m_i \dot{W}_i^{\,2} + \frac{1}{2}\sum_{i=0}^{n} I_{m_i}\dot{\theta}_i^2 \tag{63}$$

where for i in [1, n-1], $I_{m_i} = \frac{\rho IL}{n} = \rho Ia$ is the second moment of inertia of the beam segment and m_i is the mass term for each grain that is defined for the inter grains by $m_i = \rho a$.

The strain energy function due to deformed shear spring (shear term) is given by

$$\boldsymbol{U_s = \frac{1}{2}\sum_{i=0}^{n-1} S\left(W_{i+1} - W_i - a\frac{\Theta_{i+1} + \Theta_i}{2}\right)^2} \tag{64}$$

where S is the shear stiffness which can be expressed with respect to the shear stiffness K_sGA of the equivalent beam. The shear stiffness parameter could be defined as $S = \frac{K_sGA}{a} = \frac{nK_sGA}{L}$ in which G is the shear modulus, A is the cross-sectional area of the beam and K_s is an equivalent shear correction coefficient.

In the present formulation, the kinematic variables are measured at nodes *i* located at the center of each grain, which is consistent with the approach followed for instance by Pasternak and Mühlhaus [11].

The strain energy function due to deformed rotational springs (bending term) may be obtained by

$$\boldsymbol{U_b = \frac{1}{2}\sum_{i=0}^{n-1} C(\Theta_{i+1} - \Theta_i)^2} \tag{65}$$

where *C* is the rotational stiffness located at the connection between each grain. This discrete stiffness can be expressed with respect to the bending stiffness *EI* of the equivalent beam and thus would be defined as $C = \frac{EI}{a} = \frac{nEI}{L}$. where *E* is Young's modulus and *I* is the second moment of area.

The elastic energy in the discrete elastic support (Winkler [114]) is given by

$$U_{Winkler} = \frac{1}{2}\sum_{i=0}^{n} KW_i^2 \tag{66}$$

where *K=ka* is the discrete stiffness of the elastic support and is attached to the center of each grain.

The Lagrangian of the system may be defined as $L = T - (U_s + U_b + U_{Winkler})$ which slightly differs from the shear lattice model considered by Ostoja-Starzewski [62] for the shear term. By substituting the kinetic and potential terms, the Lagrangian may be expressed as:

$$L = \left[\frac{1}{2}\sum_{i=0}^{n} m_i \dot{W_i}^2 + \frac{1}{2}\sum_{i=0}^{n} I_{m_i}\dot{\Theta}_i^2\right] - \left[\frac{1}{2}\sum_{i=0}^{n-1} S\left(W_{i+1} - W_i - a\frac{\Theta_{i+1}+\Theta_i}{2}\right)^2 + \frac{1}{2}\sum_{i=0}^{n-1} C(\Theta_{i+1} - \Theta_i)^2 + \frac{1}{2}\sum_{i=0}^{n} KW_i^2\right] \tag{67}$$

The system of difference equations for both the discrete displacement and rotation fields is obtained from the application of Hamilton's principle, given by:

$$\int_{t_1}^{t_2} \boldsymbol{\delta L}\, \boldsymbol{dt} = \int_{t_1}^{t_2} (\boldsymbol{\delta T} - \boldsymbol{\delta U})\, \boldsymbol{dt} = \mathbf{0} \tag{68}$$

Using Eq. (3) based on the energy function of Eq. (67) leads to the following difference equation system

$$\begin{gathered} \boldsymbol{S}(\boldsymbol{W}_{i+1} + \boldsymbol{W}_{i-1} - 2\boldsymbol{W}_i) - \frac{\boldsymbol{a}}{\mathbf{2}}\boldsymbol{S}(\boldsymbol{\Theta}_{i+1} - \boldsymbol{\Theta}_{i-1}) - \boldsymbol{kaW}_i - \boldsymbol{m}_i\ddot{\boldsymbol{W}}_i = \mathbf{0} \quad (\boldsymbol{i} = \mathbf{1}, \dots, \boldsymbol{n} - \mathbf{1}) \\ \boldsymbol{C}(\boldsymbol{\Theta}_{i+1} + \boldsymbol{\Theta}_{i-1} - 2\boldsymbol{\Theta}_i) + \frac{\boldsymbol{a}}{\mathbf{2}}\boldsymbol{S}(\boldsymbol{W}_{i+1} - \boldsymbol{W}_{i-1}) - \frac{\boldsymbol{a}^2}{\mathbf{4}}\boldsymbol{S}(\boldsymbol{\Theta}_{i+1} + \boldsymbol{\Theta}_{i-1} + 2\boldsymbol{\Theta}_i) - \boldsymbol{I}_{m_i}\ddot{\boldsymbol{\Theta}}_i = \mathbf{0} \quad (\boldsymbol{i} = \mathbf{1}, \dots, \boldsymbol{n} - \mathbf{1}) \end{gathered} \tag{69}$$

where for the variationally-based boundary conditions, the following four equations could be obtained

$$\begin{gathered} \left[\boldsymbol{S}\left(\boldsymbol{W}_1 - \boldsymbol{W}_0 - \frac{\boldsymbol{a}}{\mathbf{2}}(\boldsymbol{\Theta}_1 + \boldsymbol{\Theta}_0)\right) - \boldsymbol{kaW}_0 - \boldsymbol{m}_0\ddot{\boldsymbol{W}}_0\right]\boldsymbol{\delta W}_0 = \mathbf{0}; \\ \left[\boldsymbol{S}\left(\boldsymbol{W}_n - \boldsymbol{W}_{n-1} - \frac{\boldsymbol{a}}{\mathbf{2}}(\boldsymbol{\Theta}_n + \boldsymbol{\Theta}_{n-1})\right) + \boldsymbol{kaW}_n + \boldsymbol{m}_n\ddot{\boldsymbol{W}}_n\right]\boldsymbol{\delta W}_n = \mathbf{0}; \\ \left[\boldsymbol{C}(\boldsymbol{\Theta}_1 - \boldsymbol{\Theta}_0) + \frac{\boldsymbol{a}}{\mathbf{2}}\boldsymbol{S}(\boldsymbol{W}_1 - \boldsymbol{W}_0) - \frac{\boldsymbol{a}^2}{\mathbf{4}}\boldsymbol{S}(\boldsymbol{\Theta}_1 + \boldsymbol{\Theta}_0) - \boldsymbol{I}_{m_0}\ddot{\boldsymbol{\Theta}}_0\right]\boldsymbol{\delta\Theta}_0 = \mathbf{0}; \\ \left[-\boldsymbol{C}(\boldsymbol{\Theta}_{n-1} - \boldsymbol{\Theta}_n) - \frac{\boldsymbol{a}}{\mathbf{2}}\boldsymbol{S}(\boldsymbol{W}_n - \boldsymbol{W}_{n-1}) + \frac{\boldsymbol{a}^2}{\mathbf{4}}\boldsymbol{S}(\boldsymbol{\Theta}_n + \boldsymbol{\Theta}_{n-1}) - \boldsymbol{I}_{m_n}\ddot{\boldsymbol{\Theta}}_n\right]\boldsymbol{\delta\Theta}_n = \mathbf{0} \end{gathered} \tag{70}$$

Introducing the following difference operators,

$$\boldsymbol{\delta_0 W}_i = \frac{\boldsymbol{W}_{i+1} + 2\boldsymbol{W}_i + \boldsymbol{W}_{i-1}}{\mathbf{4}} \quad , \quad \boldsymbol{\delta_1 W}_i = \frac{\boldsymbol{W}_{i+1} - \boldsymbol{W}_{i-1}}{\mathbf{2a}} \quad , \quad \boldsymbol{\delta_2 W}_i = \frac{\boldsymbol{W}_{i+1} - 2\boldsymbol{W}_i + \boldsymbol{W}_{i-1}}{\boldsymbol{a}^2} \tag{71}$$

Eq. (69) might be generalized and rewritten compactly by Eq. (6).

$$\begin{gathered} \boldsymbol{K_s GA}(\boldsymbol{\delta_2 W}_i) - \boldsymbol{K_s GA}(\boldsymbol{\delta_1 \Theta}_i) - \boldsymbol{kW}_i - \boldsymbol{\rho A}\ddot{\boldsymbol{W}}_i = \mathbf{0} \\ \boldsymbol{EI}(\boldsymbol{\delta_2 \Theta}_i) + \boldsymbol{K_s GA}(\boldsymbol{\delta_1 W}_i) - \boldsymbol{K_s GA}(\boldsymbol{\delta_0 \Theta}_i) - \boldsymbol{\rho I}\ddot{\boldsymbol{\Theta}}_\iota = \mathbf{0} \end{gathered} \tag{72}$$

Assuming a small harmonic vibration

$$\boldsymbol{W}_i = \boldsymbol{w}_i e^{\boldsymbol{j\omega t}}, \quad \boldsymbol{\Theta}_i = \boldsymbol{\theta}_i e^{\boldsymbol{j\omega t}} \tag{73}$$

with $j^2 = -1$.w_i and θ_i are the space part of the solution and are the functions of grains number and ω is the angular natural frequency, Eq. (72) may be written in a matrix form

$$\begin{pmatrix} \boldsymbol{EI\delta_2 - K_sGA\delta_0 + \rho I\omega^2} & \boldsymbol{K_sGA\delta_1} \\ \boldsymbol{K_sGA\delta_1} & \boldsymbol{k - K_sGA\delta_2 - \rho A\omega^2} \end{pmatrix} \begin{pmatrix} \boldsymbol{\theta} \\ \boldsymbol{w} \end{pmatrix}_i = \begin{pmatrix} \mathbf{0} \\ \mathbf{0} \end{pmatrix} \tag{74}$$

These difference equations system (74) have been obtained by Pasternak and Mühlhaus [11] neglecting the elastic Winkler foundation *(k=0)*. With consideration of an infinite number of grains ($n \to \infty$) referring to the continuum beam, it converges to the coupled system differential equations Eq. (75) which has been obtained by Bresse [16] and Timoshenko [17, [18] in the absence of a Winkler foundation *(k=0)* and assuming that the shear correction factor to be unity *(K_s=1)*. Eq. (75) valid for a Bresse-Timoshenko beam on elastic foundation have been also obtained by Wang and Stephens [64] and Manevich [65].

$$\begin{pmatrix} \boldsymbol{EI\partial_x^2 - K_sGA + \rho I\omega^2} & \boldsymbol{K_sGA\partial_x} \\ \boldsymbol{K_sGA\partial_x} & \boldsymbol{k - K_sGA\partial_x^2 - \rho A\omega^2} \end{pmatrix} \begin{pmatrix} \boldsymbol{\theta} \\ \boldsymbol{w} \end{pmatrix} = \begin{pmatrix} \mathbf{0} \\ \mathbf{0} \end{pmatrix} \tag{75}$$

It is possible to introduce the following pseudo-differential operators

$$\begin{aligned} \boldsymbol{\delta_0} &= \frac{\boldsymbol{e^{a\partial_x} + 2 + e^{-a\partial_x}}}{\mathbf{4}} = \boldsymbol{cosh^2}\left(\frac{\boldsymbol{a\partial_x}}{\mathbf{2}}\right); \\ \boldsymbol{\delta_1} &= \frac{\boldsymbol{e^{a\partial_x} - e^{-a\partial_x}}}{\boldsymbol{2a}} = \frac{\boldsymbol{sinh\,(a\partial_x)}}{\boldsymbol{a}}; \\ \boldsymbol{\delta_2} &= \frac{\boldsymbol{e^{a\partial_x} - 2 + e^{-a\partial_x}}}{\boldsymbol{a^2}} = \frac{\mathbf{4}}{\boldsymbol{a^2}}\boldsymbol{sinh^2}\left(\frac{\boldsymbol{a\partial_x}}{\mathbf{2}}\right) \end{aligned} \tag{76}$$

The same relations could be obtained for the difference operators of Eq. (6). Going back to the discrete granular beam model Eq. (74), this characteristic equation has nontrivial solutions only if the determinant of the matrix is zero. Using the property of Eq. (10) gives the fourth-order difference equation for the deflection as follows:

$$[EI\delta_2{}^2 + \left(\rho I\omega^2 - \frac{kEI}{K_sGA} + \frac{EI\rho\omega^2}{K_sG}\right)\delta_2 + (k - \rho A\omega^2)\delta_0 - \frac{k\rho I\omega^2}{K_sGA} + \frac{\rho^2 I\omega^4}{K_sG}]w_i = 0 \quad (77)$$

$$[EI\delta_2{}^2 + \left(\rho I\omega^2 - \frac{kEI}{K_sGA} + \frac{EI\rho\omega^2}{K_sG}\right)\delta_2 + (k - \rho A\omega^2)\delta_0 - \frac{k\rho I\omega^2}{K_sGA} + \frac{\rho^2 I\omega^4}{K_sG}]\theta_i = 0 \quad (78)$$

Neglecting the Winkler elastic foundation (*k=0*), Eq. (11) leads to

$$[\delta_2{}^2 + \omega^2\left(\frac{\rho}{E} + \frac{\rho}{K_sG}\right)\delta_2 - \omega^2(\frac{\rho A}{EI}\delta_0 - \frac{\rho^2\omega^2}{EK_sG})]w_i = 0 \quad (79)$$

Duan et al. [12] also studied a discrete Timoshenko beam model based on rigid links where the displacement fields are defined at the joint element. The scheme of their study slightly differs from the granular model considered in this chapter, essentially from the last term in the fourth-order difference equation of each model. The appearance of the difference operator δ_0 in this model in comparison with Duan et al. [12], stems from the enhanced shear interaction modeling of the granular elements which refers to the fundamental difference between the two microstructural models.

$$\left[\delta_2{}^2 + \omega^2\left(\frac{\rho}{E} + \frac{\rho}{K_sG}\right)\delta_2 - \omega^2\left(\frac{\rho A}{EI} - \frac{\rho^2\omega^2}{EK_sG}\right)\right]w_i = 0 \quad (80)$$

Eq. (79) and Eq. (80) are the governing deflection equations of two alternative discrete granular models for studying the beam vibration and its dynamic responses.

The fourth-order difference equation Eq. (11) is equivalent to the one of Challamel et al. [117] in the static range ($\omega = 0$). Considering infinite number of grains ($n \to \infty$) for the continuum beam, the fourth-order differential equation valid for a Bresse-Timoshenko beam on Winkler elastic foundation is given by Eq. (81) which also could be compared well by Wang and Stephens [64], Cheng and Pantelides [118] and Manevich [65].

$$\frac{d^4w}{dx^4} + \left(\frac{\rho\omega^2}{E}\left(1 + \frac{E}{k_sG}\right) - \frac{k}{k_sGA}\right)\frac{d^2w}{dx^2} - \left(\frac{\rho\omega^2}{E}\left(\frac{A}{I} + \frac{k}{k_sGA} - \frac{\rho\omega^2}{k_sG}\right) - \frac{k}{EI}\right)w = 0 \quad (81)$$

3. Resolution of The Difference Equation

In this section, the exact solution for the fourth-order linear difference eigenvalue problem of Eq. (11) will be established (see the books of Goldberg [119] or Elaydi [120] for the general solution of linear difference equations). This approach, as detailed for instance by Elishakoff and Santoro [121, [122], has been used to analyze the error in the finite difference based probabilistic dynamic problems. Eq. (11) and Eq. (78) restricted to the vibration terms, the linear fourth-order difference equation may be expanded as

$$\begin{aligned}&(\boldsymbol{w_{i+2}-4w_{i+1}+6w_i-4w_{i-1}+w_{i-2}})+\boldsymbol{a^2}\left(\frac{\boldsymbol{\rho I}}{\boldsymbol{EI}}\boldsymbol{\omega^2}-\frac{\boldsymbol{k}}{\boldsymbol{K_sGA}}+\frac{\boldsymbol{\rho A\omega^2}}{\boldsymbol{K_sGA}}\right)(\boldsymbol{w_{i+1}-2w_i}+\\&\boldsymbol{w_{i-1}})+\boldsymbol{a^4}\left(\frac{\boldsymbol{k}}{\boldsymbol{4EI}}-\frac{\boldsymbol{\rho A\omega^2}}{\boldsymbol{4EI}}\right)(\boldsymbol{w_{i+1}+2w_i+w_{i-1}})+\boldsymbol{a^4}(-\frac{\boldsymbol{k\rho I\omega^2}}{\boldsymbol{EIK_sGA}}+\frac{\boldsymbol{\rho^2IA\omega^4}}{\boldsymbol{EIK_sGA}})\boldsymbol{w_i}=\boldsymbol{0}\end{aligned} \tag{82}$$

$$\begin{aligned}&(\boldsymbol{\theta_{i+2}-4\theta_{i+1}+6\theta_i-4\theta_{i-1}+\theta_{i-2}})+\boldsymbol{a^2}\left(\frac{\boldsymbol{\rho I}}{\boldsymbol{EI}}\boldsymbol{\omega^2}-\frac{\boldsymbol{k}}{\boldsymbol{K_sGA}}+\frac{\boldsymbol{\rho A\omega^2}}{\boldsymbol{K_sGA}}\right)(\boldsymbol{\theta_{i+1}-2\theta_i}+\\&\boldsymbol{\theta_{i-1}})+\boldsymbol{a^4}\left(\frac{\boldsymbol{k}}{\boldsymbol{4EI}}-\frac{\boldsymbol{\rho A\omega^2}}{\boldsymbol{4EI}}\right)(\boldsymbol{\theta_{i+1}+2\theta_i+\theta_{i-1}})+\boldsymbol{a^4}(-\frac{\boldsymbol{k\rho I\omega^2}}{\boldsymbol{EIK_sGA}}+\frac{\boldsymbol{\rho^2IA\omega^4}}{\boldsymbol{EIK_sGA}})\boldsymbol{\theta_i}=\boldsymbol{0}\end{aligned} \tag{83}$$

As it was mentioned in the previous section these two equation systems are true for all grains except the two ends. For simply supported boundary conditions as shown in Figure 5 and with respect to Eq. (25), the four boundary conditions are formulated as:

$$\begin{cases}\boldsymbol{W_0=0}\\ \boldsymbol{W_n=0}\\ \boldsymbol{C(\Theta_1-\Theta_0)+\frac{a}{2}S(W_1-W_0)-\frac{a^2}{4}S(\Theta_1+\Theta_0)-I_{m_0}\ddot{\Theta}_0=0}\\ \boldsymbol{C(\Theta_n-\Theta_{n-1})+\frac{a}{2}S(W_n-W_{n-1})-\frac{a^2}{4}S(\Theta_n+\Theta_{n-1})+I_{m_n}\ddot{\Theta}_n=0}\end{cases} \tag{84}$$

The two last equations of Eq. (84) are actually second-newton laws for the boundary grains and could be rewritten in the compact form by

$$\begin{aligned}\boldsymbol{M_{1/2}+\frac{a}{2}V_{1/2}=I_{m_0}\ddot{\Theta}_0}\\ \boldsymbol{-M_{n-1/2}-\frac{a}{2}V_{n-1/2}=I_{m_n}\ddot{\Theta}_n}\end{aligned} \tag{85}$$

where

$$M_{1/2} = C(\Theta_1 - \Theta_0), \qquad V_{1/2} = \frac{a}{2} S\left(W_1 - W_0 - \frac{a}{2}(\Theta_1 + \Theta_0)\right);$$
$$M_{n-1/2} = C(\Theta_n - \Theta_{n-1}), \qquad V_{n-1/2} = \frac{a}{2} S(W_n - W_{n-1} - \frac{a}{2}(\Theta_n + \Theta_{n-1})) \tag{86}$$

On the other hand, Eq. (69) could be applied for the boundary grains by considering two fictitious grains (*i=-1* and *i=n+1*) connected to the system with fictitious springs. The equilibrium conditions of the boundary grains could be written by Eq. (87).

$$M_{1/2} - M_{-1/2} + \frac{a}{2}(V_{1/2} - V_{-1/2}) = \tilde{I}_{m_0} \ddot{\Theta}_0$$
$$M_{n-1/2} - M_{n+1/2} + \frac{a}{2}(V_{n-1/2} - V_{n+1/2}) = \tilde{I}_{m_n} \ddot{\Theta}_n \tag{87}$$

where

$$M_{-1/2} = C(\Theta_0 - \Theta_{-1}), \qquad V_{-1/2} = \frac{a}{2} S(W_0 - W_{-1} - \frac{a}{2}(\Theta_0 + \Theta_{-1}))$$
$$M_{n+1/2} = C(\Theta_{n+1} - \Theta_n), \qquad V_{n+1/2} = \frac{a}{2} S(W_{n+1} - W_n - \frac{a}{2}(\Theta_{n+1} + \Theta_0)) \tag{88}$$

The antisymmetric conditions lead to:

$$M_{-1/2} = -M_{1/2}, \qquad V_{-1/2} = V_{1/2}$$
$$M_{n+1/2} = -M_{n-1/2}, \qquad V_{n+1/2} = V_{n-1/2} \tag{89}$$

It can be concluded that

$$\Theta_1 = \Theta_{-1}, \qquad W_1 = -W_{-1}$$
$$\Theta_{n-1} = \Theta_{n+1}, \qquad W_{n-1} = -W_{n+1} \tag{90}$$

Using the recent conditions in Eq. (69) for *i=0* and *i=n*, leads to

$$C(\Theta_1 - \Theta_0) + \frac{a}{2} S(W_1 - W_{-1} - \frac{a}{2}(\Theta_1 + \Theta_0)) - \frac{\tilde{I}_{m_0}}{2} \ddot{\Theta}_0 = 0$$
$$C(\Theta_{n-1} - \Theta_n) + \frac{a}{2} S(W_{n+1} - W_{n-1} - \frac{a}{2}(\Theta_n + \Theta_{n-1})) - \frac{\tilde{I}_{m_n}}{2} \ddot{\Theta}_n = 0 \tag{91}$$

where $\tilde{I}_{m_0}$ and $\tilde{I}_{m_n}$ represent the second moment of inertia for the boundary grains with consideration of the fictitious elements (*i=-1* and *n+1*).

Comparing the two systems of equations Eq. (84) and Eq. (91) results that the fictitious system behaves the same as the real model with the associated boundary conditions as follows:

$$\begin{aligned} &\boldsymbol{At\ i=0:\quad w_0=0\,;\ w_1=-w_{-1}\rightarrow \delta_2 w_0=0} \\ &\boldsymbol{At\ i=n:\quad w_n=0\,;\ w_{n-1}=-w_{n+1}\rightarrow \delta_2 w_n=0} \end{aligned} \tag{92}$$

These boundary conditions have been used also by Hunt et al. [123] for the problem of static bifurcation of granular chains under axial load. The non-dimensional quantities may be introduced

$$\boldsymbol{\Omega^2=\frac{\omega^2\rho AL^4}{EI}\ ,\ \mu_s=\frac{E}{K_s G}\ ,r=\sqrt{\frac{I}{A}}\ ,\ r^*=\frac{r}{L}\ ,\ k^*=\frac{kL^4}{EI}} \tag{93}$$

Ω is a dimensionless frequency; μ_s is inversely proportional to the shear stiffness; and r^* is proportional to the rotatory inertia. The solution of the linear difference equation (Goldberg [119] and Elaydi [120]) is thought in the form

$$\boldsymbol{w_i=B\lambda^i} \tag{94}$$

where *B* is a constant. Therefore, the characteristic equation could be obtained by replacing Eq. (94) in Eq. (82) as

$$\boldsymbol{(\lambda+\frac{1}{\lambda})^2+\left(\lambda+\frac{1}{\lambda}\right)\epsilon+\tau=0} \tag{95}$$

where the parameters ϵ and τ can be defined as

$$\boldsymbol{\epsilon=\left[\frac{r^{*2}\Omega^2}{n^2}\left(1+\mu_s-\frac{1}{4r^{*2}n^2}\right)-\frac{r^{*2}k^*\mu_s}{n^2}+\frac{k^*}{4n^4}-4\right],} \tag{96}$$

$$\boldsymbol{\tau = \left[\frac{r^{*2}\Omega^2}{n^4}\left(-\mu_s r^{*2}k^* + \mu_s r^{*2}\Omega^2\right) + 2\left(\frac{k^*}{4n^4} - \frac{\Omega^2}{4n^4}\right) - 2\left(\frac{r^{*2}\Omega^2}{n^2}(1+\mu_s) - \frac{r^{*2}k^*\mu_s}{n^2}\right) + 4\right]}$$

Solving Eq. (95) leads to the equation obtained by Zhang et al. [124] which could be written

$$\boldsymbol{\lambda + \frac{1}{\lambda} = \frac{-\epsilon \pm \sqrt{\epsilon^2 - 4\tau}}{2}} \tag{97}$$

Eq. (97) admits four solutions written

$$\boldsymbol{\lambda_{1,2} = \frac{-\epsilon + \sqrt{\epsilon^2 - 4\tau}}{4} \pm \sqrt{\left(\frac{\epsilon - \sqrt{\epsilon^2 - 4\tau}}{4}\right)^2 - 1}} \tag{98}$$

$$\boldsymbol{\lambda_{3,4} = \frac{-\epsilon - \sqrt{\epsilon^2 - 4\tau}}{4} \pm j\sqrt{1 - \left(\frac{\epsilon + \sqrt{\epsilon^2 - 4\tau}}{4}\right)^2}} \tag{99}$$

where $j^2 = -1$. On the other hand, it is important to notice that according to Eq. (97) the results of $\lambda + \frac{1}{\lambda}$ are in the ranges of $(-\infty,\ -2]$ or $[2,\ +\infty)$.

The limited cases when $\lambda + \frac{1}{\lambda} = \pm 2$ would happen for $\lambda = \pm 1$ which refers to the critical frequencies. The critical frequencies of the system are inconsistent condition with Eq. (94) would be obtained by assuming:

$$\boldsymbol{\tau = \pm 2\epsilon - 4} \tag{100}$$

The critical frequencies of the system might be obtained with the substitution of τ and ϵ in the aforementioned equation by using Eq. (96):

$$\boldsymbol{\left(\frac{r^{*2}\Omega_{cr}^2}{n^2} - 4\right)\left(\frac{\mu_s r^{*2}}{n^2}(\Omega_{cr}^2 - k^*) - 4\right) = 0} \tag{101}$$

$$\boldsymbol{\frac{1}{n^4}\left((\Omega_{cr}^2 - k^*)(\mu_s\, r^{*4}\Omega_{cr}^2 - 1)\right) = 0} \tag{102}$$

Therefore, two branches of critical frequencies would be obtained as follows

$$\boldsymbol{\Omega_{cr_{1,1}} = \frac{2n}{r^*} \quad , \quad \Omega_{cr_{1,2}} = \sqrt{\frac{4n^2}{\mu_s r^{*2}} + k^*}} \tag{103}$$

$$\boldsymbol{\Omega_{cr_{2,1}} = \sqrt{k^*} \quad , \quad \Omega_{cr_{2,2}} = \sqrt{\frac{1}{\mu_s r^{*4}}}} \tag{104}$$

The critical frequencies of the first branch depend on the grain number (microstructure parameter), mechanical properties and beam geometry (macrostructure parameters) while the second critical frequencies branch are only defined as a function of the beam mechanical properties and geometry. On the other hand, comparing these critical values with those of the Timoshenko continuum beam resting on the Winkler foundations (see Wang and Stephens [64]), leads to the equivalency of the second branch critical values (Eq. (104)) to the Timoshenko continuum beam's. For an infinite number of grains, since the first branch critical frequencies ($\Omega_{cr_{1,1}}$ and $\Omega_{cr_{1,2}}$) leads to infinite values and consequently disappear, so only the second branch would remain. These critical values could be shown as follows

$$\boldsymbol{\omega_{cr_{2,1}} = \omega_{cr_{Timoshenko\,1}} = \sqrt{\frac{k}{\rho A}} \quad , \quad \omega_{cr_{2,2}} = \omega_{cr_{Timoshenko\,2}} = \sqrt{\frac{K_s\, GA}{\rho I}}} \tag{105}$$

The behavior of the beam deflection solution would be separated by the critical frequencies into different regimes and depending on the frequencies values, the results would be in a distinct manner.

For a finite number of grains, four regimes would occur, categorized as follows: when $0 < \Omega < \Omega_{cr_{2,2}}$ there are two exponential terms and two traveling waves since $\lambda_{1,2}$ are real and $\lambda_{3,4}$ are imaginary. In this case, the deflection equation form would be obtained from Eq. (116).

When $\Omega_{cr_{2,2}} < \Omega < \Omega_{cr_{1,2}}$, $\lambda_{1,2,3,4}$ are all imaginary and therefore all terms represent traveling waves and for this case, the deflection equation form would be obtained from Eq. (117).

For $\Omega_{cr_{1,2}} < \Omega < \Omega_{cr_{1,1}}$ again there are two exponential terms and two traveling waves since $\lambda_{1,2}$ are imaginary and $\lambda_{3,4}$ are real and the deflection equation form would be obtained from Eq. (118).

Finally, for $\Omega_{cr_{1,1}} < \Omega$, since all parameters of $\lambda_{1,2,3,4}$ are real, thus whole terms represent exponential terms which leads to the deflection equation form of Eq. (119).

For a specific value of grain number, $\Omega_{cr_{1,1}}$ and $\Omega_{cr_{2,2}}$ would be equal together. This leads to the reduction of the four regimes to three.

$$\boldsymbol{n = \frac{1}{2r^*\sqrt{\mu_s}} = \frac{L}{2}\sqrt{\frac{K_s\, GA}{EI}}} \tag{106}$$

The results are shown for a case study of 50 grains and the dimensionless parameters of $\mu_s = 4.28$, $r^* = 0.029$, $k^* = 15$ in Figure 6. In this example, the values of the critical frequencies are respectively $\Omega_{cr_{1,1}} = 3464.1$, $\Omega_{cr_{1,2}} = 1673.7$, $\Omega_{cr_{2,1}} = 3.87$ and $\Omega_{cr_{2,2}} = 579.8$.

(a)

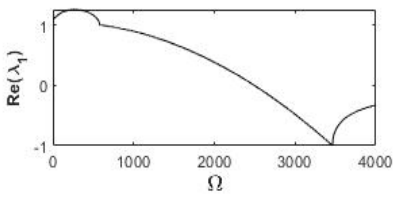

(b)

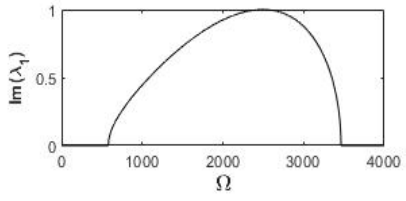

(c)

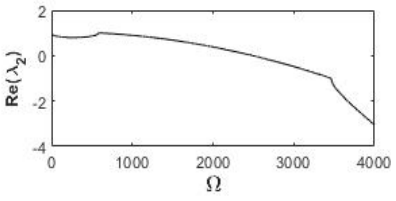

(d)

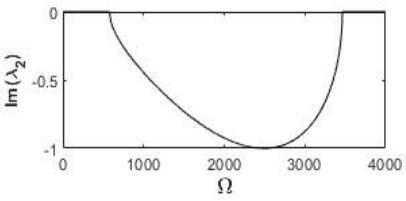

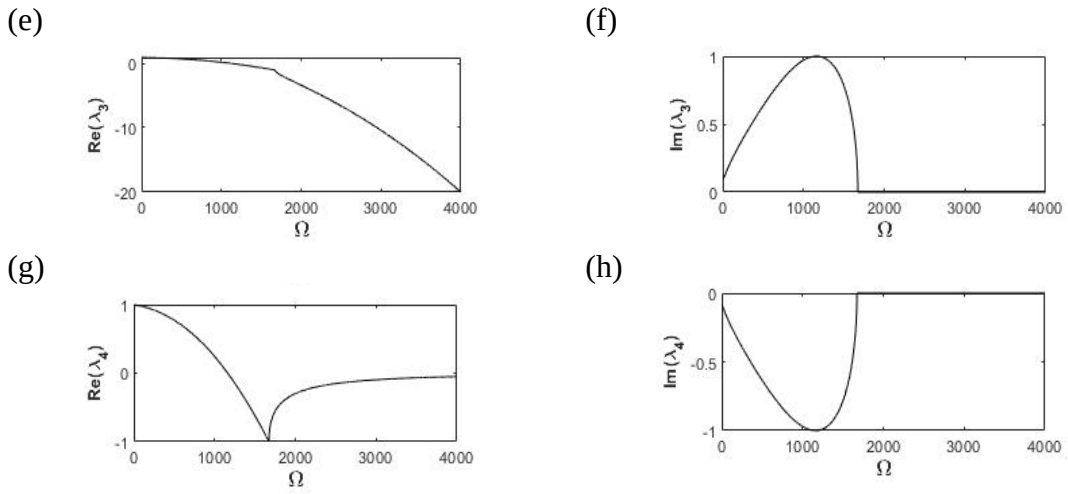

Figure 6. Schematic behavior of the wave vector regarding the eigenfrequencies for finite grain number (n=50). (a), (c), (e) and (g) correspond to the real part and (b), (d), (f) and (h) correspond to the imaginary part of the wave vector.

For an infinite number of grains, since the first two critical values converge to the infinite, so the previous different regimes reduce to two regimes (Elishakoff [67] and Traill-Nash and Collar [125]): when $0 < \Omega < \Omega_{cr_{2,2}}$ there are two exponential terms and two traveling waves as $\lambda_{1,2}$ are real and $\lambda_{3,4}$ are imaginary and thus the deflection equation form would be obtained from Eq. (116).

when $\Omega_{cr_{2,2}} < \Omega$, $\lambda_{1,2,3,4}$ are all imaginary and thus all terms represent traveling waves. This case leads to the deflection equation form of Eq. (117). These two regimes correspond to the ones obtained for the continuum beam of Timoshenko resting on Winkler foundations.

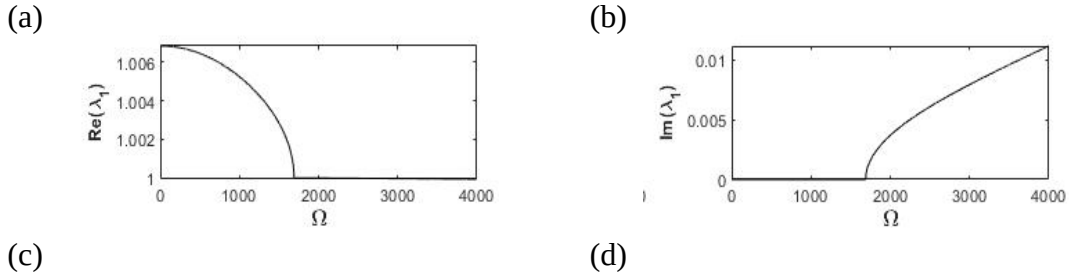

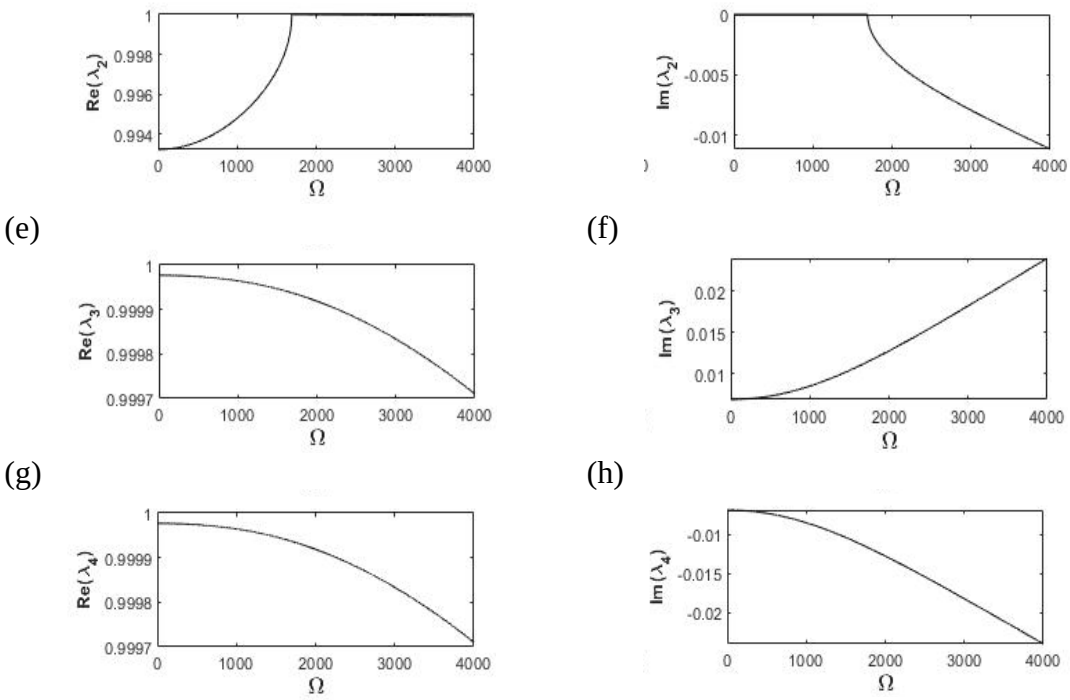

Figure 7. The effects of the eigenfrequencies on the wave behavior for a general discrete beam contains an infinite grain number ($\boldsymbol{n} \to \infty$). (a), (c), (e) and (g) correspond to the real part and (b), (d), (f) and (h) correspond to the imaginary part of the wave vector.

Therefore, $\lambda_{1,2}$ can be rewritten for $\Omega < \Omega_{cr_{2,2}}$ and $\Omega_{cr_{1,2}} < \Omega$ (see also Elishakoff and Santoro [122] for a similar presentation applied to the finite difference formulation of Euler-Bernoulli beams) as

$$\boldsymbol{\lambda_{1,2} = cosh\,\vartheta \pm sinh\,\vartheta} \tag{107}$$

where

$$\boldsymbol{cosh\,\vartheta = \frac{-\epsilon}{4} + \frac{1}{2}\sqrt{\left(\frac{-\epsilon}{2}\right)^2 - \tau} = \frac{-\epsilon}{2} - cos\varphi} \tag{108}$$

$$\boldsymbol{cos\,\varphi = \frac{-\epsilon}{4} - \frac{1}{2}\sqrt{\left(\frac{-\epsilon}{2}\right)^2 - \tau}} \tag{109}$$

while $\lambda_{1,2}$ would be obtained for $\Omega_{cr_{2,2}} < \Omega < \Omega_{cr_{1,2}}$

$$\boldsymbol{\lambda_{1,2} = cos\vartheta \pm jsin\vartheta} \tag{110}$$

where

$$\cos\vartheta = \frac{-\epsilon}{4} + \frac{1}{2}\sqrt{\left(\frac{-\epsilon}{2}\right)^2 - \tau} \tag{111}$$

On the other hand, $\lambda_{3,4}$ would be defined for $\Omega < \Omega_{cr_{1,1}}$ by

$$\lambda_{3,4} = \cos\varphi \pm j\sin\varphi \tag{112}$$

where

$$\varphi = \arccos\left(\frac{-\epsilon}{4} - \frac{1}{2}\sqrt{\left(\frac{-\epsilon}{2}\right)^2 - \tau}\right) \tag{113}$$

And for $\Omega_{cr_{1,1}} < \Omega$

$$\lambda_{3,4} = \cosh\varphi \pm \sinh\varphi \tag{114}$$

$$\varphi = \arccos h\left(\frac{-\epsilon}{4} - \frac{1}{2}\sqrt{\left(\frac{-\epsilon}{2}\right)^2 - \tau}\right) \tag{115}$$

In view of Eq. (108) and (109), there are three possible general solutions for w_i depending on the critical values of the frequencies which may be represented as

$$w_i = A_1 \cos i\varphi + A_2 \sin i\varphi + A_3 \cosh i\vartheta + A_4 \sinh i\vartheta \quad (\Omega < \Omega_{cr_{2,2}}) \tag{116}$$

$$w_i = B_1 \cos i\varphi + B_2 \sin i\varphi + B_3 \cos i\vartheta + B_4 \sin i\vartheta \quad (\Omega_{cr_{2,2}} < \Omega < \Omega_{cr_{1,2}}) \tag{117}$$

$$w_i = C_1 \cosh i\varphi + C_2 \sinh i\varphi + C_3 \cos i\vartheta + C_4 \sin i\vartheta \quad (\Omega_{cr_{1,2}} < \Omega < \Omega_{cr_{1,1}}) \tag{118}$$

$$w_i = D_1 \cosh i\varphi + D_2 \sinh i\varphi + D_3 \cosh i\vartheta + D_4 \sinh i\vartheta \quad (\Omega_{cr_{1,1}} < \Omega) \tag{119}$$

3.1. General Solution of The Difference Equation

The general solution for the coupled system of difference equation of Eq. (74) can be considered through the trigonometric and hyperbolic terms in the low frequency regime as follows:

$$w_i = A_1 a\cos i\varphi + A_2 a\sin i\varphi + A_3 a\cosh i\vartheta + A_4 a\sinh i\vartheta \tag{120}$$

$$\theta_i = B_1\cos i\varphi + B_2\sin i\varphi + B_3\cosh i\vartheta + B_4\sinh i\vartheta \tag{121}$$

Replacing the form of the solution of Eq. (120) and Eq. (121) in Eq. (69) by ignoring the Winkler elastic foundation terms *(k=0)* leads to the following matrix form equations

$$\begin{bmatrix} G_1 & 0 & 0 & 0 & 0 & -G_5 & 0 & 0 \\ 0 & G_1 & 0 & 0 & G_5 & 0 & 0 & 0 \\ 0 & 0 & G_2 & 0 & 0 & 0 & 0 & -G_6 \\ 0 & 0 & 0 & G_2 & 0 & 0 & -G_6 & 0 \\ 0 & a^2G_5 & 0 & 0 & G_3 & 0 & 0 & 0 \\ -a^2G_5 & 0 & 0 & 0 & 0 & G_3 & 0 & 0 \\ 0 & 0 & 0 & a^2G_6 & 0 & 0 & G_4 & 0 \\ 0 & 0 & a^2G_6 & 0 & 0 & 0 & 0 & G_4 \end{bmatrix} \begin{bmatrix} A_1 \\ A_2 \\ A_3 \\ A_4 \\ B_1 \\ B_2 \\ B_3 \\ B_4 \end{bmatrix} = \begin{bmatrix} 0 \\ 0 \\ 0 \\ 0 \\ 0 \\ 0 \\ 0 \\ 0 \end{bmatrix} \tag{122}$$

where the components of the coefficient matrix of *G* are expressed by

$$\begin{cases} G_1 = m_i\omega^2 - 2k_s + 2k_s cos(\varphi) \\ G_2 = m_i\omega^2 - 2k_s + 2k_s cosh(\vartheta) \\ G_3 = I_{m_i}\omega^2 - 2k_r - \dfrac{a^2k_s}{2} + 2k_r cos(\varphi) - \dfrac{a^2k_s cos(\varphi)}{2} \\ G_4 = I_{m_i}\omega^2 - 2k_r - \dfrac{a^2k_s}{2} + 2k_r cosh(\vartheta) - \dfrac{a^2k_s cosh(\vartheta)}{2} \\ G_5 = k_s sin(\varphi) \\ G_6 = k_s sinh(\vartheta) \end{cases} \tag{123}$$

Eq. (122) leads to

$$\begin{aligned} B_1 &= -A_2\frac{G_1}{G_5} = -A_2\frac{a^2G_5}{G_3}, \quad B_2 = A_1\frac{G_1}{G_5} = A_1\frac{a^2G_5}{G_3}; \\ B_3 &= A_4\frac{G_2}{G_6} = -A_4\frac{a^2G_6}{G_4}, \quad B_4 = A_3\frac{G_2}{G_6} = -A_3\frac{a^2G_6}{G_4} \end{aligned} \tag{124}$$

Thus, the following relations could be obtained

$$\frac{m_i\omega^2 - 2k_s + 2\,k_s cos(\varphi)}{k_s sin(\varphi)} = \frac{a^2 k_s sin(\varphi)}{I_{m_i}\omega^2 - 2k_r - \frac{a^2 k_s}{2} + 2k_r cos(\varphi) - \frac{a^2 k_s cos(\varphi)}{2}} \tag{125}$$

$$\frac{m_i\omega^2 - 2k_s + 2k_s cosh(\vartheta)}{k_s sinh(\vartheta)} = \frac{a^2 k_s sinh(\vartheta)}{I_{m_i}\omega^2 - 2k_r - \frac{a^2 k_s}{2} + 2k_r cosh(\vartheta) - \frac{a^2 k_s cosh(\vartheta)}{2}} \tag{126}$$

which leads to

$$4cos(\varphi)^2 + 2\epsilon cos(\varphi) + \tau = 0 \tag{127}$$

$$4cosh(\vartheta)^2 + 2\epsilon cosh(\vartheta) + \tau = 0 \tag{128}$$

The exact simply supported conditions might be assumed by Eq. (84). Replacing the form of the solution of Eq. (120) and Eq. (121) in Eq. (84) (with regards to the properties of Eq. Eq. (124) between the coefficients of A_i and B_i), the following transcendental equation could be obtained by prohibiting the zero solutions for the deformation

$$H(\omega) = f_1(\omega)\,\omega^8 + f_2(\omega)\,\omega^6 + f_3(\omega)\,\omega^4 + f_4(\omega)\,\omega^2 + f_5(\omega) = 0 \tag{129}$$

where the coefficients of $f(\omega)$ are expressed by

$$\begin{aligned} &f_1(\omega) \\ &= \Big(-4I_{m_0}I_{m_n}a^2 m_i^2\big(2sin(\varphi)sinh(\vartheta) - 2sin(n\varphi)sinh(n\vartheta) + sin(n\varphi)sinh(n\vartheta)(cos(\varphi)^2 \\ &+ cosh(\vartheta)^2) - 2cos(n\varphi)cosh(n\vartheta)sin(\varphi)sinh(\vartheta)\big)\Big)\,(k_s^2\sin^2(\varphi)\sinh^2(\vartheta))^{-1} \end{aligned} \tag{130}$$

$$\begin{aligned} &f_2(\omega) \\ &= -\Big(a^2\Big(m_i^2\big(I_{m_0}I_{m_n}\big)\big((4k_r + a^2k_s)(2\cos(2\varphi)\sin(n\varphi)\sinh(n\vartheta) + 2\cosh(2\vartheta)\sin(n\varphi)\sinh(n\vartheta) \\ &- 4\sin(n\varphi)\sinh(n\vartheta) + 8\sin(\varphi)\sinh(\vartheta) - 8\cos(n\varphi)\cosh(n\vartheta)\sin(\varphi)\sinh(\vartheta)) \\ &+ 2(4k_r - a^2k_s)(\sin(n\varphi)\sinh(n\vartheta)\cosh(\vartheta) - \sinh(2\vartheta)\sin(\varphi) - \sin(2\varphi)\sinh(\vartheta) \\ &+ \sinh(2\vartheta)\cos(n\varphi)\cosh(n\vartheta)\sin(\varphi) + \sin(2\varphi)\cos(n\varphi)\cosh(n\vartheta)\sinh(\vartheta) + \sin(n\varphi)\sinh(n\vartheta)\cos(\varphi) \\ &- \cos(2\varphi)\sin(n\varphi)\sinh(n\vartheta)\cosh(\vartheta) - \cosh(2\vartheta)\sin(n\varphi)\sinh(n\vartheta)\cos(\varphi))\big) \\ &+ 64I_{m_0}I_{m_n}k_s m_i(-\sin(2\varphi)\sinh(\vartheta) - \sinh(2\vartheta)\sin(\varphi) - 2\sin(n\varphi)\sinh(n\vartheta) + 4\sin(\varphi)\sinh(\vartheta) \\ &+ \sin(n\varphi)\sinh(n\vartheta)\cos(\varphi) + \sin(n\varphi)\sinh(n\vartheta)\cosh(\vartheta) + \cos(2\varphi)\sin(n\varphi)\sinh(n\vartheta) \\ &+ \cosh(2\vartheta)\sin(n\varphi)\sinh(n\vartheta) - \cos(2\varphi)\sin(n\varphi)\sinh(n\vartheta)\cosh(\vartheta) \\ &- \cosh(2\vartheta)\sin(n\varphi)\sinh(n\vartheta)\cos(\varphi) + \sin(2\varphi)\cos(n\varphi)\cosh(n\vartheta)\sinh(\vartheta) \\ &+ \sinh(2\vartheta)\cos(n\varphi)\cosh(n\vartheta)\sin(\varphi) - 4\cos(n\varphi)\cosh(n\vartheta)\sin(\varphi)\sinh(\vartheta))\Big)\Big)\Big({k_s}^2(\cos(2\varphi) \\ &- 1)(\cosh(2\vartheta) - 1)\Big)^{-1} \end{aligned}$$

$$
\begin{aligned}
&f_3(\omega)\\
&= -(a^2(\,16\big(I_{m_0}+I_{m_n}\big)k_r k_s m_i(2sin(2\varphi)sinh(\vartheta)+\,2sinh(2\vartheta)sin(\varphi)+\,2sin(2\varphi)sinh(\vartheta)\\
&+\,2sinh(2\vartheta)sin(\varphi)-\,sin(\varphi)sinh(\vartheta)^3+sin(\varphi)^3sinh(\vartheta)+\,4sin(n\varphi)sinh(n\vartheta)\\
&-\,0.5sin(2\varphi)sinh(2\vartheta)-\,6sin(\varphi)sinh(\vartheta)-4sin(n\varphi)sinh(n\vartheta)cos(\varphi)-\,4sin(n\varphi)sinh(n\vartheta)cosh(\vartheta)\\
&-sin(\varphi)sinh(\vartheta)^3-\,4sin(n\varphi)sinh(n\vartheta)cos(\varphi)^2cosh(\vartheta)^2-\,cos(n\varphi)sinh(n\vartheta)cos(\varphi)sin(\varphi)\\
&+\,4cos(n\varphi)cosh(n\vartheta)sin(\varphi)sinh(\vartheta)+cos(n\varphi)sinh(n\vartheta)cosh(\vartheta)sin(\varphi)\\
&+\,cosh(n\vartheta)sin(n\varphi)cos(\varphi)sinh(\vartheta)-\,cosh(n\vartheta)sin(n\varphi)cosh(\vartheta)sinh(\vartheta)\\
&+\,4sin(n\varphi)sinh(n\vartheta)cos(\varphi)cosh(\vartheta)^2+4sin(n\varphi)sinh(n\vartheta)cos(\varphi)^2cosh(\vartheta)\\
&-cos(n\varphi)sinh(n\vartheta)cosh(\vartheta)^3sin(\varphi)-\,cosh(n\vartheta)sin(n\varphi)cos(\varphi)^3sinh(\vartheta)\\
&+cos(n\varphi)cosh(n\vartheta)cos(\varphi)^2sin(\varphi)sinh(\vartheta)+cos(n\varphi)sinh(n\vartheta)cos(\varphi)cosh(\vartheta)^2sin(\varphi)\\
&+\,cos(n\varphi)cosh(n\vartheta)cosh(\vartheta)^2sin(\varphi)sinh(\vartheta)+\,cosh(n\vartheta)sin(n\varphi)cos(\varphi)^2cosh(\vartheta)sinh(\vartheta)\\
&-\,4cos(n\varphi)cosh(n\vartheta)cos(\varphi)sin(\varphi)sinh(\vartheta)-\,4cos(n\varphi)cosh(n\vartheta)cosh(\vartheta)sin(\varphi)sinh(\vartheta)\\
&+\,2cos(n\varphi)cosh(n\vartheta)cos(\varphi)cosh(\vartheta)sin(\varphi)sinh(\vartheta))\\
&+8a^2k_rk_s\big(k_rm_i^2+k_s\big(I_{m_0}+I_{m_n}\big)m_i\big)\big(0.25sin(2\varphi)sinh(2\vartheta)+sin(n\varphi)sinh(n\vartheta)-sin(\varphi)sinh(\vartheta)\\
&-sin(n\varphi)sinh(n\vartheta)cos(\varphi)^2-sin(n\varphi)sinh(n\vartheta)cosh(\vartheta)^2+sin(n\varphi)sinh(n\vartheta)cos(\varphi)^2cosh(\vartheta)^2\\
&-cos(n\varphi)cosh(n\vartheta)cos(\varphi)cosh(\vartheta)sin(\varphi)sinh(\vartheta)+cos(n\varphi)cosh(n\vartheta)sin(\varphi)sinh(\vartheta)\big)\\
&+\,16k_r^2m_i^2(-0.25sin(2\varphi)sinh(2\vartheta)+0.5sin(2\varphi)sinh(\vartheta)+0.5sinh(2\vartheta)sin(\varphi)+sin(n\varphi)sinh(n\vartheta)\\
&-sin(\varphi)sinh(\vartheta)-sin(n\varphi)sinh(n\vartheta)cos(\varphi)-sin(n\varphi)sinh(n\vartheta)cosh(\vartheta)\\
&+cos(n\varphi)cosh(n\vartheta)sin(\varphi)sinh(\vartheta)+sin(n\varphi)sinh(n\vartheta)cos(\varphi)cosh(\vartheta)^2\\
&+sin(n\varphi)sinh(n\vartheta)cos(\varphi)^2cosh(\vartheta)-sin(n\varphi)sinh(n\vartheta)cos(\varphi)^2cosh(\vartheta)^2\\
&-cos(n\varphi)cosh(n\vartheta)cos(\varphi)sin(\varphi)sinh(\vartheta)-cos(n\varphi)cosh(n\vartheta)cosh(\vartheta)sin(\varphi)sinh(\vartheta)\\
&+cos(n\varphi)cosh(n\vartheta)cos(\varphi)cosh(\vartheta)sin(\varphi)sinh(\vartheta))+a^4k_s^2m_i^2(-0.25sin(2\varphi)sinh(2\vartheta)\\
&-0.5sin(2\varphi)sinh(\vartheta)-0.5sinh(2\vartheta)sin(\varphi)-sin(n\varphi)sinh(n\vartheta)cos(\varphi)cosh(\vartheta)^2\\
&-sin(n\varphi)sinh(n\vartheta)cos(\varphi)^2cosh(\vartheta)+sin(n\varphi)sinh(n\vartheta)-sin(\varphi)sinh(\vartheta)+sin(n\varphi)sinh(n\vartheta)cos(\varphi)\\
&+sin(n\varphi)sinh(n\vartheta)cosh(\vartheta)-sin(n\varphi)sinh(n\vartheta)cos(\varphi)^2cosh(\vartheta)^2+cos(n\varphi)cosh(n\vartheta)sin(\varphi)sinh(\vartheta)\\
&+cos(n\varphi)cosh(n\vartheta)cos(\varphi)cosh(\vartheta)sin(\varphi)sinh(\vartheta)+cos(n\varphi)cosh(n\vartheta)cos(\varphi)sin(\varphi)sinh(\vartheta)\\
&+cos(n\varphi)cosh(n\vartheta)cosh(\vartheta)sin(\varphi)sinh(\vartheta))\\
&+64I_{m_0}I_{m_n}k_s^2\big(-0.25sin(2\varphi)sinh(2\vartheta)+0.5sin(2\varphi)sinh(\vartheta)+\,0.5sinh(2\vartheta)sin(\varphi)\\
&+sin(n\varphi)sinh(n\vartheta)-sin(\varphi)sinh(\vartheta)-sin(n\varphi)sinh(n\vartheta)cos(\vartheta)-sin(n\varphi)sinh(n\vartheta)cosh(\vartheta)\\
&-cos(n\varphi)cosh(n\vartheta)cos(\varphi)sin(\varphi)sinh(\vartheta)-cos(n\varphi)cosh(n\vartheta)cosh(\vartheta)sin(\varphi)sinh(\vartheta)\\
&+sin(n\varphi)sinh(n\vartheta)cos(\varphi)cosh(\vartheta)^2+cos(n\varphi)cosh(n\vartheta)cos(\varphi)cosh(\vartheta)sin(\varphi)sinh(\vartheta)\\
&+sin(n\varphi)sinh(n\vartheta)cos(\varphi)^2cosh(\vartheta)-sin(n\varphi)sinh(n\vartheta)cos(\varphi)^2cosh(\vartheta)^2\\
&+cos(n\varphi)cosh(n\vartheta)sin(\varphi)sinh(\vartheta)))\big)\big(k_s^2(\cos^2(\varphi)-\,1)(\cosh^2(\vartheta)-\,1)\big)^{-1}
\end{aligned}
$$

$$
\begin{aligned}
&f_4(\omega)\\
&= -(a^2(k_r k_s^2 m_i \big(10a^2 sin\big(\varphi(n-1)\big)sinh\big(\vartheta(n+1)\big) - 8a^2 sin\big(\varphi(n-1)\big)sinh\big(\vartheta(n-1)\big)\\
&+ 10a^2 sin\big(\varphi(n+1)\big)sinh\big(\vartheta(n-1)\big) - 12a^2 sin\big(\varphi(n+1)\big)sinh\big(\vartheta(n+1)\big)\\
&+ 2a^2 sin\big(\varphi(n-1)\big)sinh\big(\vartheta(n-2)\big) - 2a^2 sin\big(\varphi(n-1)\big)sinh\big(\vartheta(n+2)\big)\\
&- 2a^2 sin\big(\varphi(n+1)\big)sinh\big(\vartheta(n-2)\big) + 2a^2 sin\big(\varphi(n-2)\big)sinh\big(\vartheta(n-1)\big)\\
&- 2a^2 sin\big(\varphi(n-2)\big)sinh\big(\vartheta(n+1)\big) - 2a^2 sin\big(\varphi(n+2)\big)sinh\big(\vartheta(n-1)\big)\\
&- 2a^2 sin\big(\varphi(n-1)\big)sinh\big(\vartheta(n-3)\big) + 2a^2 sin\big(\varphi(n+1)\big)sinh\big(\vartheta(n-3)\big)\\
&+ 4a^2 sin\big(\varphi(n-2)\big)sinh\big(\vartheta(n-2)\big) - 6a^2 sin\big(\varphi(n-2)\big)sinh\big(\vartheta(n+2)\big)\\
&- 6a^2 sin\big(\varphi(n+2)\big)sinh\big(\vartheta(n-2)\big) - 2a^2 sin\big(\varphi(n-3)\big)sinh\big(\vartheta(n-1)\big)\\
&+ 2a^2 sin\big(\varphi(n-3)\big)sinh\big(\vartheta(n+1)\big) + 2a^2 sin\big(\varphi(n+2)\big)sinh\big(\vartheta(n-3)\big)\\
&+ 2a^2 sin\big(\varphi(n-3)\big)sinh\big(\vartheta(n+2)\big) - 6a^2 sin(2\varphi)sinh(\vartheta) - 6a^2 sinh(2\vartheta)sin(\varphi)\\
&+ 4a^2 sin(3\varphi)sinh(\vartheta) + 4a^2 sinh(3\vartheta)sin(\varphi) - 8a^2 sin(n\varphi)sinh(n\vartheta) - 16a^2 sin(2\varphi)sinh(2\vartheta)\\
&+ 2a^2 sin(2\varphi)sinh(3\vartheta) + 2a^2 sin(3\varphi)sinh(2\vartheta) + 2a^2 sin\big(\varphi(n+1)\big)sinh(n\vartheta)\\
&+ 2a^2 sinh\big(\vartheta(n+1)\big)sin(n\varphi) + 2a^2 sin\big(\varphi(n-2)\big)sinh(n\vartheta) + 6a^2 sin\big(\varphi(n+2)\big)sinh(n\vartheta)\\
&+ 2a^2 sinh\big(\vartheta(n-2)\big)sin(n\varphi) + 6a^2 sinh\big(\vartheta(n+2)\big)sin(n\varphi) - 2a^2 sin\big(\varphi(n-3)\big)sinh(n\vartheta)\\
&- 2a^2 sinh\big(\vartheta(n-3)\big)sin(n\varphi) + 40a^2 sin(\varphi)sinh(\vartheta)\big)\\
&k_r^2 k_s m_i \big(64sin\big(\varphi(n-1)\big)sinh(n\vartheta) + 56sin\big(\varphi(n+1)\big)sinh(n\vartheta) + 64sinh\big(\vartheta(n-1)\big)sin(n\varphi) +\\
&56sinh\big(\vartheta(n+1)\big)sin(n\varphi) + 8sin\big(\varphi(n-2)\big)sinh(n\vartheta) + 24sin\big(\varphi(n+2)\big)sinh(n\vartheta) +\\
&8sinh\big(\vartheta(n-2)\big)sin(n\varphi) + 24sinh\big(\vartheta(n+2)\big)sin(n\varphi) + 8sin\big(\varphi(n-3)\big)sinh(n\vartheta) +\\
&8sinh\big(\vartheta(n-3)\big)sin(n\varphi) + 160sin(\varphi)sinh(\vartheta) - 32sin\big(\varphi(n-1)\big)sinh\big(\vartheta(n-1)\big) +\\
&40sin\big(\varphi(n-1)\big)sinh\big(\vartheta(n+1)\big) + 40sin\big(\varphi(n+1)\big)sinh\big(\vartheta(n-1)\big) - 48sin\big(\varphi(n+\\
&1)\big)sinh\big(\vartheta(n+1)\big) - 8sin\big(\varphi(n-1)\big)sinh\big(\vartheta(n-2)\big) - 56sin\big(\varphi(n-1)\big)sinh\big(\vartheta(n+2)\big) -\\
&56sin\big(\varphi(n+1)\big)sinh\big(\vartheta(n-2)\big) - 8sin\big(\varphi(n-2)\big)sinh\big(\vartheta(n-1)\big) - 56sin\big(\varphi(n-\\
&2)\big)sinh\big(\vartheta(n+1)\big) - 56sin\big(\varphi(n+2)\big)sinh\big(\vartheta(n-1)\big) - 8sin\big(\varphi(n-1)\big)sinh\big(\vartheta(n-3)\big) +\\
&8sin\big(\varphi(n+1)\big)sinh\big(\vartheta(n-3)\big) + 16sin\big(\varphi(n-2)\big)sinh\big(\vartheta(n-2)\big) + 40sin\big(\varphi(n-\\
&2)\big)sinh\big(\vartheta(n+2)\big) + 40sin\big(\varphi(n+2)\big)sinh\big(\vartheta(n-2)\big) - 8sin\big(\varphi(n-3)\big)sinh\big(\vartheta(n-1)\big) +\\
&8sin\big(\varphi(n-3)\big)sinh\big(\vartheta(n+1)\big) - 8sin\big(\varphi(n+2)\big)sinh\big(\vartheta(n-3)\big) - 8sin\big(\varphi(n-\\
&3)\big)sinh\big(\vartheta(n+2)\big) - 104sin(2\varphi)sinh(\vartheta) - 104sinh(2\vartheta)sin(\varphi) + 16sin(3\varphi)sinh(\vartheta) +\\
&16sinh(3\vartheta)sin(\varphi) - 160sin(n\varphi)sinh(n\vartheta) + 64sin(2\varphi)sinh(2\vartheta) - 8sin(2\varphi)sinh(3\vartheta) -\\
&8sin(3\varphi)sinh(2\vartheta)\big)\mathrm{l}\\
&0.5\big(I_{m_0} + I_{m_n}\big)k_r k_s^2 \big(128sin\big(\varphi(n-1)\big)sinh(n\vartheta) + 112sin\big(\varphi(n+1)\big)sinh(n\vartheta)\\
&+ 128sinh\big(\vartheta(n-1)\big)sin(n\varphi) + 112sinh\big(\vartheta(n+1)\big)sin(n\varphi) + 16sin\big(\varphi(n-2)\big)sinh(n\vartheta)\\
&+ 48sin\big(\varphi(n+2)\big)sinh(n\vartheta) + 16sinh\big(\vartheta(n-2)\big)sin(n\varphi) + 48sinh\big(\vartheta(n+2)\big)sin(n\varphi)\\
&+ 16sin\big(\varphi(n-3)\big)sinh(n\vartheta) + 16sinh\big(\vartheta(n-3)\big)sin(n\varphi) + 320sin(\varphi)sinh(\vartheta)\\
&- 64sin\big(\varphi(n-1)\big)sinh\big(\vartheta(n-1)\big) + 80sin\big(\varphi(n-1)\big)sinh\big(\vartheta(n+1)\big)\\
&+ 80sin\big(\varphi(n+1)\big)sinh\big(\vartheta(n-1)\big) - 96sin\big(\varphi(n+1)\big)sinh\big(\vartheta(n+1)\big)\\
&- 16sin\big(\varphi(n-1)\big)sinh\big(\vartheta(n-2)\big) - 112sin\big(\varphi(n-1)\big)sinh\big(\vartheta(n+2)\big)\\
&- 112sin\big(\varphi(n+1)\big)sinh\big(\vartheta(n-2)\big) - 16sin\big(\varphi(n-2)\big)sinh\big(\vartheta(n-1)\big)\\
&- 112sin\big(\varphi(n-2)\big)sinh\big(\vartheta(n+1)\big) - 112sin\big(\varphi(n+2)\big)sinh\big(\vartheta(n-1)\big)\\
&- 16sin\big(\varphi(n-1)\big)sinh\big(\vartheta(n-3)\big) + 16sin\big(\varphi(n+1)\big)sinh\big(\vartheta(n-3)\big)\\
&+ 32sin\big(\varphi(n-2)\big)sinh\big(\vartheta(n-2)\big) + 80sin\big(\varphi(n-2)\big)sinh\big(\vartheta(n+2)\big)\\
&+ 80sin\big(\varphi(n+2)\big)sinh\big(\vartheta(n-2)\big) - 16sin\big(\varphi(n-3)\big)sinh\big(\vartheta(n-1)\big)\\
&+ 16sin\big(\varphi(n-3)\big)sinh\big(\vartheta(n+1)\big) - 16sin\big(\varphi(n+2)\big)sinh\big(\vartheta(n-3)\big)\\
&- 16sin\big(\varphi(n-3)\big)sinh\big(\vartheta(n+2)\big) - 208sin(2\varphi)sinh(\vartheta) - 208sinh(2\vartheta)sin(\varphi)\\
&+ 32sin(3\varphi)sinh(\vartheta) + 32sinh(3\vartheta)sin(\varphi) - 320sin(n\varphi)sinh(n\vartheta) + 128sin(2\varphi)sinh(2\vartheta)\\
&- 16sin(2\varphi)sinh(3\vartheta) - 16sin(3\varphi)sinh(2\vartheta)\big)\big)\big)\big(k_s^2(\cos(2\varphi)-1)(\cosh^2(\vartheta)-1)\big)^{-1}
\end{aligned}
$$

$$
\begin{aligned}
&f_5(\omega)\\
&= -\big(\,4a^2k_r^2(6\sin\big(\varphi(n\,-\,1)\big)\sinh(n\vartheta) + \,6\sinh\big(\vartheta(n\,-\,1)\big)\sin(n\varphi) - \,6\sin\big(\varphi(n\,-\,2)\big)\sinh(n\vartheta)\\
&- \,6\sinh\big(\vartheta(n\,-\,2)\big)\sin(n\varphi) + \,2\sin\big(\varphi(n\,-\,3)\big)\sinh(n\vartheta) + \,2\sinh\big(\vartheta(n\,-\,3)\big)\sin(n\varphi)\\
&+ \,8\sin(\varphi)\sinh(\vartheta) + \,10\sin\big(\varphi(n\,-\,1)\big)\sinh\big(\vartheta(n\,-\,1)\big) + \,9\sin\big(\varphi(n\,-\,1)\big)\sinh\big(\vartheta(n\,+\,1)\big)\\
&+ \,9\sin\big(\varphi(n\,+\,1)\big)\sinh\big(\vartheta(n\,-\,1)\big) - \,2\sin\big(\varphi(n\,-\,1)\big)\sinh\big(\vartheta(n\,-\,2)\big)\\
&- \,6\sin\big(\varphi(n\,+\,1)\big)\sinh\big(\vartheta(n\,-\,2)\big) - \,2\sin\big(\varphi(n\,-\,2)\big)\sinh\big(\vartheta(n\,-\,1)\big)\\
&- \,6\sin\big(\varphi(n\,-\,2)\big)\sinh\big(\vartheta(n\,+\,1)\big) + \sin\big(\varphi(n\,-\,1)\big)\sinh\big(\vartheta(n\,-\,3)\big)\\
&+ \sin\big(\varphi(n\,+\,1)\big)\sinh\big(\vartheta(n\,-\,3)\big) - \,2\sin\big(\varphi(n\,-\,2)\big)\sinh\big(\vartheta(n\,-\,2)\big)\\
&+ \sin\big(\varphi(n\,-\,3)\big)\sinh\big(\vartheta(n\,-\,1)\big) + \sin\big(\varphi(n\,-\,3)\big)\sinh\big(\vartheta(n\,+\,1)\big) - \,4\sin(2\varphi)\sinh(\vartheta)\\
&- \,4\sinh(2\vartheta)\sin(\varphi) - \,18\sin(n\varphi)\sinh(n\vartheta) + \,2\sin(2\varphi)\sinh(2\vartheta)\big)\big)\big((\cos(\varphi) + \,1)(\cosh(\vartheta) + \,1)\big)^{-1}
\end{aligned}
$$

3.2. Antisymmetric Boundary Conditions on Deflection

For the simply supported discrete system by substituting Eq. (92) in Eq. (116), (117), (118) and (119) the boundary conditions could be defined in matrix form, respectively

$$
\begin{bmatrix}
\mathbf{1} & \mathbf{0} & \mathbf{1} & \mathbf{0}\\
\boldsymbol{cos(n\varphi)} & \boldsymbol{sin(n\varphi)} & \boldsymbol{cosh(n\vartheta)} & \boldsymbol{sinh(n\vartheta)}\\
\mathbf{2}\,\boldsymbol{cos\,\varphi} & \mathbf{0} & \mathbf{2}\,\boldsymbol{cosh\,\vartheta} & \mathbf{0}\\
\mathbf{2}\boldsymbol{cos\,\varphi\,cos(n\varphi)} & \mathbf{2}\boldsymbol{cos\,\varphi\,sin(n\varphi)} & \mathbf{2}\,\boldsymbol{cosh\,\vartheta\,cosh(n\vartheta)} & \mathbf{2}\,\boldsymbol{cosh\,\vartheta\,sinh(n\vartheta)}
\end{bmatrix}
\begin{bmatrix}
\boldsymbol{A_1}\\ \boldsymbol{A_2}\\ \boldsymbol{A_3}\\ \boldsymbol{A_4}
\end{bmatrix} = \mathbf{0} \tag{131}
$$

$$
\begin{bmatrix}
\mathbf{1} & \mathbf{0} & \mathbf{1} & \mathbf{0}\\
\boldsymbol{cos(n\varphi)} & \boldsymbol{sin(n\varphi)} & \boldsymbol{cos(n\vartheta)} & \boldsymbol{sin(n\vartheta)}\\
\mathbf{2}\,\boldsymbol{cos\,\varphi} & \mathbf{0} & \mathbf{2}\,\boldsymbol{cos\,\vartheta} & \mathbf{0}\\
\mathbf{2}\boldsymbol{cos\,\varphi\,cos(n\varphi)} & \mathbf{2}\boldsymbol{cos\,\varphi\,sin(n\varphi)} & \mathbf{2}\,\boldsymbol{cos\,\vartheta\,cos(n\vartheta)} & \mathbf{2}\,\boldsymbol{cos\,\vartheta\,sin(n\vartheta)}
\end{bmatrix}
\begin{bmatrix}
\boldsymbol{B_1}\\ \boldsymbol{B_2}\\ \boldsymbol{B_3}\\ \boldsymbol{B_4}
\end{bmatrix} = \mathbf{0} \tag{132}
$$

$$
\begin{bmatrix}
\mathbf{1} & \mathbf{0} & \mathbf{1} & \mathbf{0}\\
\boldsymbol{cosh(n\varphi)} & \boldsymbol{sinh(n\varphi)} & \boldsymbol{cos(n\vartheta)} & \boldsymbol{sin(n\vartheta)}\\
\mathbf{2}\,\boldsymbol{cosh\,\varphi} & \mathbf{0} & \mathbf{2}\,\boldsymbol{cos\,\vartheta} & \mathbf{0}\\
\mathbf{2}\boldsymbol{cosh\,\varphi\,cos\,h(n\varphi)} & \mathbf{2}\boldsymbol{cosh\,\varphi\,sin\,h(n\varphi)} & \mathbf{2}\,\boldsymbol{cos\,\vartheta\,cos(n\vartheta)} & \mathbf{2}\,\boldsymbol{cos\,\vartheta\,sinh(n\vartheta)}
\end{bmatrix}
\begin{bmatrix}
\boldsymbol{C_1}\\ \boldsymbol{C_2}\\ \boldsymbol{C_3}\\ \boldsymbol{C_4}
\end{bmatrix} = \mathbf{0} \tag{133}
$$

$$
\begin{bmatrix}
\mathbf{1} & \mathbf{0} & \mathbf{1} & \mathbf{0}\\
\boldsymbol{cosh(n\varphi)} & \boldsymbol{sinh(n\varphi)} & \boldsymbol{cosh(n\vartheta)} & \boldsymbol{sinh(n\vartheta)}\\
\mathbf{2}\,\boldsymbol{cosh\,\varphi} & \mathbf{0} & \mathbf{2}\,\boldsymbol{cosh\,\vartheta} & \mathbf{0}\\
\mathbf{2}\boldsymbol{cosh\,\varphi\,cosh(n\varphi)} & \mathbf{2}\boldsymbol{cosh\,\varphi\,sinh(n\varphi)} & \mathbf{2}\,\boldsymbol{cosh\,\vartheta\,cosh(n\vartheta)} & \mathbf{2}\,\boldsymbol{cosh\,\vartheta\,sinh(n\vartheta)}
\end{bmatrix}
\begin{bmatrix}
\boldsymbol{D_1}\\ \boldsymbol{D_2}\\ \boldsymbol{D_3}\\ \boldsymbol{D_4}
\end{bmatrix} = \mathbf{0} \tag{134}
$$

Setting the determinant of the homogeneous coefficient matrix of Eq. (131), (132), (133) and (134) to zero would be simplified

$$
\mathbf{4}\,\boldsymbol{sin(n\varphi)\,sinh(n\vartheta)\,(cos\varphi - cosh\,\vartheta)^2} = \mathbf{0} \tag{135}
$$

$$\mathbf{4}\,\boldsymbol{sin}(\boldsymbol{n\varphi})\,\boldsymbol{sin}(\boldsymbol{n\vartheta})\,(\boldsymbol{cos\varphi}-\boldsymbol{cos}\,\boldsymbol{\vartheta})^{\mathbf{2}}=\mathbf{0} \tag{136}$$

$$\mathbf{4}\,\boldsymbol{sinh}(\boldsymbol{n\varphi})\,\boldsymbol{sin}(\boldsymbol{n\vartheta})\,(\boldsymbol{cosh\varphi}-\boldsymbol{cos}\,\boldsymbol{\vartheta})^{\mathbf{2}}=\mathbf{0} \tag{137}$$

$$\mathbf{4}\,\boldsymbol{sinh}(\boldsymbol{n\varphi})\,\boldsymbol{sinh}(\boldsymbol{n\vartheta})\,(\boldsymbol{cosh\varphi}-\boldsymbol{cosh}\,\boldsymbol{\vartheta})^{\mathbf{2}}=\mathbf{0} \tag{138}$$

It is found from Eq. (135), (136) and (137) that $\sin(n\varphi) = 0$ and or $\sin(n\vartheta) = 0$. Thus, the natural vibration modes are obtained from the trigonometric shape function $w_i = B\ sin(i\varphi)$ and or $w_i = B\ sin(i\vartheta)$ which lead to the fundamental natural vibration frequency, which are associated with the non-trivial condition:

$$\textbf{For i = n},\ \ \boldsymbol{w_i}=\mathbf{0}\Rightarrow\boldsymbol{sin}(\boldsymbol{n\Lambda})=\mathbf{0}\Rightarrow\boldsymbol{\Lambda}=\frac{\boldsymbol{p\pi}}{\boldsymbol{n}}\ ,\ \ \boldsymbol{\Lambda}=\boldsymbol{\varphi},\boldsymbol{\vartheta} \tag{139}$$

On the other hand, one would be obtained from Eq. (138) that $\varphi = \vartheta$ which leads to

$$\frac{-\boldsymbol{\epsilon}+\sqrt{\boldsymbol{\epsilon}^{\mathbf{2}}-\mathbf{4}\,\boldsymbol{\tau}}}{\mathbf{4}}=\frac{-\boldsymbol{\epsilon}-\sqrt{\boldsymbol{\epsilon}^{\mathbf{2}}-\mathbf{4}\,\boldsymbol{\tau}}}{\mathbf{4}}\Rightarrow\boldsymbol{\epsilon}^{\mathbf{2}}-\mathbf{4}\,\boldsymbol{\tau}=\mathbf{0} \tag{140}$$

The frequencies could be obtained from Eq. (140) as follows

$$\boldsymbol{\Omega}=\sqrt{\frac{\mathbf{32}\boldsymbol{n}^{\mathbf{4}}-\boldsymbol{k}^{*}+\mathbf{4}\boldsymbol{k}^{*}\boldsymbol{r}^{*^{\mathbf{2}}}\boldsymbol{n}^{\mathbf{2}}(\mathbf{1}+\mathbf{2}\boldsymbol{\mu_s}(\mathbf{1}+\mathbf{2}\boldsymbol{r}^{*^{\mathbf{2}}}\boldsymbol{n}^{\mathbf{2}}(\mathbf{1}-\boldsymbol{\mu_s})))\pm\boldsymbol{A}^{*}}{\boldsymbol{B}^{*}}} \tag{141}$$

where A^* and B^* are defined by

$$\boldsymbol{A}^{*}=\mathbf{16}\boldsymbol{n}^{\mathbf{3}}\sqrt{\boldsymbol{k}^{*}(\boldsymbol{k}^{*}\boldsymbol{\mu_s}\boldsymbol{r}^{*^{\mathbf{6}}}-\mathbf{16}\boldsymbol{\mu_s}^{\mathbf{3}}\boldsymbol{r}^{*^{\mathbf{6}}}\boldsymbol{n}^{\mathbf{4}}+\mathbf{32}\boldsymbol{\mu_s}^{\mathbf{2}}\boldsymbol{r}^{*^{\mathbf{6}}}\boldsymbol{n}^{\mathbf{4}}+\mathbf{8}\boldsymbol{\mu_s}^{\mathbf{2}}\boldsymbol{r}^{*^{\mathbf{4}}}\boldsymbol{n}^{\mathbf{2}}-\mathbf{16}\boldsymbol{\mu_s}\boldsymbol{r}^{*^{\mathbf{6}}}\boldsymbol{n}^{\mathbf{4}}+\mathbf{4}\boldsymbol{\mu_s}\boldsymbol{r}^{*^{\mathbf{4}}}\boldsymbol{n}^{\mathbf{2}}-\boldsymbol{\mu_s}\boldsymbol{r}^{*^{\mathbf{2}}}+\mathbf{4}\boldsymbol{r}^{*^{\mathbf{4}}}\boldsymbol{n}^{\mathbf{2}}-\boldsymbol{r}^{*^{\mathbf{2}}})+\mathbf{4}\boldsymbol{n}^{\mathbf{2}}} \tag{142}$$

$$\boldsymbol{B}^{*}=-\mathbf{16}\boldsymbol{\mu_s}^{\mathbf{2}}\boldsymbol{r}^{*^{\mathbf{4}}}\boldsymbol{n}^{\mathbf{4}}+\mathbf{32}\boldsymbol{\mu_s}\boldsymbol{r}^{*^{\mathbf{4}}}\boldsymbol{n}^{\mathbf{4}}+\mathbf{8}\boldsymbol{\mu_s}\boldsymbol{r}^{*^{\mathbf{2}}}\boldsymbol{n}^{\mathbf{2}}-\mathbf{16}\boldsymbol{r}^{*^{\mathbf{4}}}\boldsymbol{n}^{\mathbf{4}}+\mathbf{8}\boldsymbol{r}^{*^{\mathbf{2}}}\boldsymbol{n}^{\mathbf{2}}-\mathbf{1} \tag{143}$$

For a simplified case by neglecting the elastic foundation, the dimensionless eigen frequencies can be obtained as

$$\boldsymbol{\Omega}=\frac{\mathbf{8}\boldsymbol{n}^{\mathbf{2}}\sqrt{(\mathbf{4}\boldsymbol{r}^{*}\boldsymbol{n}+(\mathbf{4}\boldsymbol{r}^{*^{\mathbf{2}}}\boldsymbol{n}^{\mathbf{2}}(\boldsymbol{\mu_s}-\mathbf{1})-\mathbf{1}))(\mathbf{4}\boldsymbol{r}^{*}\boldsymbol{n}-(\mathbf{4}\boldsymbol{r}^{*^{\mathbf{2}}}\boldsymbol{n}^{\mathbf{2}}(\boldsymbol{\mu_s}-\mathbf{1})-\mathbf{1}))}}{\boldsymbol{B}^{*}} \tag{144}$$

the exact resolution of the dynamic analysis of the granular system that would be studied here is only true for the frequencies lower than $\Omega_{cr_{1,2}}$. Since $\Omega_{cr_{1,2}}$ is a function of grain number, the results could be compared well for an infinite number of grains with those correspond to the Timoshenko continuum beam.

Therefore, regarding to Eq. (139), the deflection and rotation angle of each grain could be obtained by the following equation while $\Omega < \Omega_{cr_{1,2}}$

$$\boldsymbol{w_i = \mathbf{B}\sin\left(\frac{ip\pi}{n}\right)} \tag{145}$$

where p is the mode number or natural number ($1 \leq p < n$ for w_i and $0 \leq p \leq n$ for θ_i) and i is the grain number ($0 \leq i \leq n$).

Substituting Eq. (139) in Eq. (109) leads to

$$\boldsymbol{cos\left(\frac{p\pi}{n}\right) = \frac{-\epsilon}{4} - \frac{1}{2}\sqrt{\left(\frac{-\epsilon}{2}\right)^2 - \tau}} \tag{146}$$

$$\boldsymbol{2\epsilon\, cos\left(\frac{p\pi}{n}\right) + \tau + 4(cos\left(\frac{p\pi}{n}\right))^2 = 0} \tag{147}$$

which is a quartic equation. Using non-dimensional eigenfrequency parameters

$$\begin{aligned}\boldsymbol{\left[\frac{\mu_s r^{*4}}{n^4}\right]\Omega^4 + \left[\frac{2r^{*2}}{n^2}\left(1+\mu_s - \frac{1}{4r^{*2}n^2}\right)cos\left(\frac{p\pi}{n}\right) - \frac{\mu_s r^{*4}k^*}{n^4} - \frac{1}{2n^4} - \right.}\\ \boldsymbol{\left.\frac{2r^{*2}}{n^2}(1+\mu_s)\right]\Omega^2 + \left[2(-\frac{r^{*2}k^*\mu_s}{n^2} + \frac{k^*}{4n^4} - 4)\,cos\left(\frac{p\pi}{n}\right) + \frac{k^*}{2n^4} + \frac{2r^{*2}k^*\mu_s}{n^2} + 4 + \right.}\\ \boldsymbol{\left. 4(cos\left(\frac{p\pi}{n}\right))^2\right] = 0}\end{aligned} \tag{148}$$

Neglecting the terms of Winkler elastic foundation *($k^* = 0$)*, Eq. (148) leads to

$$\boldsymbol{\left[\frac{\mu_s r^{*4}}{n^4}\right]\Omega^4 - \left[\frac{4r^{*2}}{n^2}(1+\mu_s)\,sin^2\left(\frac{p\pi}{2n}\right) + \frac{1}{n^4}cos^2\left(\frac{p\pi}{2n}\right)\right]\Omega^2 + \left[16\,sin^4\left(\frac{p\pi}{2n}\right)\right] = 0} \tag{149}$$

The last equation is different from the quartic equation of Duan et al. [12] that had been obtained as follows:

$$\left[\frac{\mu_s r^{*4}}{n^4}\right]\Omega^4 - \left[\frac{4r^{*2}}{n^2}(1+\mu_s)\,sin^2\left(\frac{p\pi}{2n}\right) + \frac{1}{n^4}\right]\Omega^2 + \left[16\,sin^4\left(\frac{p\pi}{2n}\right)\right] = 0 \tag{150}$$

Going back to Eq. (148), it could be written in the compact form

$$\Omega^4 - B\Omega^2 + C = 0 \tag{151}$$

in which the coefficients of *B* and *C* are defined

$$\begin{aligned} B &= -\frac{2n^2}{\mu_s r^{*2}}\left(1+\mu_s - \frac{1}{4r^{*2}n^2}\right)cos\left(\frac{p\pi}{n}\right) + k^* + \frac{1}{2\mu_s r^{*4}} + \frac{2n^2}{\mu_s r^{*2}}(1+\mu_s), \\ C &= \frac{2n^4}{\mu_s r^{*4}}\left(-\frac{r^{*2}k^*\mu_s}{n^2} + \frac{k^*}{4n^4} - 4\right)cos\left(\frac{p\pi}{n}\right) + \frac{k^*}{2\mu_s r^{*4}} + \frac{2n^2k^*}{r^{*2}} + \\ &\quad \frac{4n^4}{\mu_s r^{*4}}\left(1+cos\left(\frac{p\pi}{n}\right)\right)^2 \end{aligned} \tag{152}$$

Eq. (151) has two real positive roots

$$\Omega = \sqrt{\frac{B \pm \sqrt{B^2 - 4C}}{2}} \tag{153}$$

Eq. (153) shows that for a given mode number *(p)*, there are two valid positive roots that refer to the two eigenfrequency spectra, in the distinction of the results refer to the Euler-Bernoulli beam associated with a single positive root. The same phenomenon for the continuum Bresse-Timoshenko beam has been already investigated by Traill-Nash and Collar [125] and Manevich [65].

The natural frequencies of the granular chain represented in Figure 5 could be presented in a single form

$$\omega = \frac{\Omega}{L^2}\sqrt{\frac{EI}{\rho A}} \tag{154}$$

Substituting Eq. (153) in Eq. (154) gives the exact eigenfrequencies of the granular beam as a function of grain number *(n)* and for whatever mode numbers *(p)*.

The recent natural frequency was obtained by the assumption of $\Omega < \Omega_{cr_{1,2}}$ which means that it needs to be able to support both the low and high frequencies. Therefore, the maximum value of γ must be less than $\Omega_{cr_{1,2}}$. Here the validity of this hypothesis is checked by analyzing the behavior of Eq. (154). Since γ is an ascending function of mode number (*p*) and knowing the mode number values cannot exceed the grain number, thus the maximum value of γ could be obtained for *p=n* which leads to

$$\boldsymbol{\gamma_{max}} = \sqrt{\frac{k^*}{2} + \frac{2n^2}{\mu_s r^{*2}}(\mathbf{1} + \boldsymbol{\mu_s}) \pm \sqrt{(\frac{k^*}{2} + \frac{2n^2}{\mu_s r^{*2}}(\mathbf{1} + \boldsymbol{\mu_s}))^2 - \frac{n^4}{\mu_s r^{*4}}(+\frac{4r^{*2}k^*\mu_s}{n^2} + \mathbf{16})}} \tag{155}$$

According to the definition of $\Omega_{cr_{1,2}}$ Eq. (155) could be rewritten in the short form as follows

$$\boldsymbol{\gamma_{max}} = \sqrt{\frac{\Omega_{cr_{1,2}}{}^2}{2} + \frac{2n^2}{r^{*2}} \pm \sqrt{(\frac{\Omega_{cr_{1,2}}{}^2}{2} + \frac{2n^2}{r^{*2}})^2 - \frac{4n^2\Omega_{cr_{1,2}}{}^2}{r^{*2}}}} \tag{156}$$

Simplifying Eq. (156) leads to the two max frequency values (Eq. (157)) each referring to the one branch. Therefore, Eq. (154) could be verified well for the range of high-frequency values, the natural frequencies of the discrete system do not exceed their critical values and thus the general solution form of the beam deflection remains in the harmonic and trigonometric manner.

$$\boldsymbol{\gamma_{max,1}} = \boldsymbol{\Omega_{cr_{1,1}}} \quad , \quad \boldsymbol{\gamma_{max,2}} = \boldsymbol{\Omega_{cr_{1,2}}} \tag{157}$$

By considering low mode number (*p*<<*n*) and for the continuum case when $n \to \infty$, the assumption of $cos\left(\frac{p\pi}{n}\right) \sim 1 - \frac{1}{2}(\frac{p\pi}{n})^2$ could be applied to Eq. (148). This leads to

$$\left[\frac{\mu_s r^{*4}}{n^4}\right]\boldsymbol{\Omega^4} + \left[\frac{2r^{*2}}{n^2}\left(\mathbf{1}+\boldsymbol{\mu_s}-\frac{1}{4r^{*2}n^2}\right)\left(\mathbf{1}-\frac{1}{2}\left(\frac{p\pi}{n}\right)^2\right)-\frac{\mu_s r^{*4}k^*}{n^4}-\frac{1}{2n^4}-\right.$$
$$\left.\frac{2r^{*2}}{n^2}(\mathbf{1}+\boldsymbol{\mu_s})\right]\boldsymbol{\Omega^2} + \left[\mathbf{2}\left(-\frac{r^{*2}k^*\mu_s}{n^2}+\frac{k^*}{4n^4}-\mathbf{4}\right)\left(\mathbf{1}-\frac{1}{2}\left(\frac{p\pi}{n}\right)^2\right)+\frac{k^*}{2n^4}+\frac{2r^{*2}k^*\mu_s}{n^2}+\mathbf{4}+\right.$$
$$\left.\mathbf{4}\left(\mathbf{1}-\left(\frac{p\pi}{n}\right)^2+\frac{1}{4}\left(\frac{p\pi}{n}\right)^4\right)\right]=\mathbf{0} \tag{158}$$

Eq. (158) can be simplified

$$\boldsymbol{\Omega^4}-\left[\frac{p^2\pi^2}{\mu_s r^{*2}}(\mathbf{1}+\boldsymbol{\mu_s})+\boldsymbol{k^*}+\frac{1}{\mu_s r^{*4}}\right]\boldsymbol{\Omega^2}+\left[\left(\frac{k^*p^2\pi^2}{r^{*2}}+\frac{p^4\pi^4}{\mu_s r^{*4}}\right)+\frac{k^*}{\mu_s r^{*4}}\right]=\mathbf{0} \tag{159}$$

and in the compact form

$$\boldsymbol{\Omega^4}-\boldsymbol{B\Omega^2}+\boldsymbol{C}=\mathbf{0} \tag{160}$$

where the two coefficients of B and C are defined as:

$$\boldsymbol{B}=\frac{p^2\pi^2}{\mu_s r^{*2}}(\mathbf{1}+\boldsymbol{\mu_s})+\frac{1}{\mu_s r^{*2}}\left(\boldsymbol{\mu_s r^{*2}k^*}+\frac{1}{r^{*2}}\right),\quad \boldsymbol{C}=\frac{p^4\pi^4}{\mu_s r^{*4}}+\frac{k^*p^2\pi^2}{r^{*2}}+\frac{k^*}{\mu_s r^{*4}}, \tag{161}$$

Solving the quartic equation of (160) leads to the eigenfrequency values of the continuous beam that would be obtained again by Eq. (154) and with γ expressed as follows:

$$\boldsymbol{\gamma}=\sqrt{\frac{p^2\pi^2}{2\mu_s r^{*2}}(\mathbf{1}+\boldsymbol{\mu_s})+\frac{k^*}{2}+\frac{1}{2\mu_s r^{*4}}\pm\sqrt{\left(\frac{p^2\pi^2}{2\mu_s r^{*2}}(\mathbf{1}+\boldsymbol{\mu_s})+\frac{k^*}{2}+\frac{1}{2\mu_s r^{*4}}\right)^2-\left(\frac{k^*}{\mu_s r^{*4}}+\frac{k^*p^2\pi^2}{r^{*2}}+\frac{p^4\pi^4}{\mu_s r^{*4}}\right)}} \tag{162}$$

These results agree with those obtained by Wang and Stephens [64], Cheng and Pantelides [118] and Manevich [65]. Also with the negligence of the Winkler elastic foundation *($k^*=0$)*, it could be compared well to Timoshenko [17, [18].

3.3. Explicit Method: Granular Beam Composed of Three Grains

Let's consider a vibrating granular chain composed of three rigid grains with the negligence of the Winkler elastic foundation *($k^*=0$)* resting on simply supported boundary conditions. The equilibrium equations of such a system could be considered as follows:

For i = 0 :

$$W_0 = 0$$

$$k_r(\Theta_1 - \Theta_0) + \frac{a}{2}k_s(W_1 - W_0) - \frac{a^2}{4}k_s(\Theta_1 + \Theta_0) - I_{m_0}\ddot{\Theta}_0 = 0$$

For i = 1 :

$$k_s(W_2 + W_0 - 2W_1) - \frac{a}{2}k_s(\Theta_2 - \Theta_0) - m_1\ddot{W}_1 = 0 \tag{163}$$

$$k_r(\Theta_2 + \Theta_0 - 2\Theta_1) + \frac{a}{2}k_s(W_2 - W_0) - \frac{a^2}{4}k_s(\Theta_2 + \Theta_0 + 2\Theta_1) - I_{m_1}\ddot{\Theta}_1 = 0$$

For i = 2 :

$$W_2 = 0$$

$$-k_r(\Theta_2 - \Theta_1) + \frac{a}{2}k_s(W_2 - W_1) - \frac{a^2}{4}k_s(\Theta_2 + \Theta_1) - I_{m_2}\ddot{\Theta}_2 = 0$$

Assuming $I_{m_0} = I_{m_2}$, this equation could be simplified and eventually expressed in a matrix form as

$$k_s(-2W_1) - \frac{a}{2}k_s(\Theta_2 - \Theta_0) - m_1\ddot{W}_1 = 0$$

$$k_r(\Theta_1 - \Theta_0) + \frac{a}{2}k_s(W_1) - \frac{a^2}{4}k_s(\Theta_1 + \Theta_0) - I_{m_0}\ddot{\Theta}_0 = 0 \tag{164}$$

$$k_r(\Theta_2 + \Theta_0 - 2\Theta_1) - \frac{a^2}{4}k_s(\Theta_2 + \Theta_0 + 2\Theta_1) - I_{m_1}\ddot{\Theta}_1 = 0$$

$$-k_r(\Theta_2 - \Theta_1) + \frac{a}{2}k_s(-W_1) - \frac{a^2}{4}k_s(\Theta_2 + \Theta_1) - I_{m_0}\ddot{\Theta}_2 = 0$$

this equation could be rewritten in matrix form as

$$\begin{bmatrix} m_1 & 0 & 0 & 0 \\ 0 & I_{m_0} & 0 & 0 \\ 0 & 0 & I_{m_1} & 0 \\ 0 & 0 & 0 & I_{m_0} \end{bmatrix} \begin{bmatrix} \ddot{W}_1 \\ \ddot{\Theta}_0 \\ \ddot{\Theta}_1 \\ \ddot{\Theta}_2 \end{bmatrix} + \begin{bmatrix} 2k_s & -0.5ak_s & 0 & 0.5ak_s \\ -0.5ak_s & k_r + 0.25a^2k_s & -k_r + 0.25a^2k_s & 0 \\ 0 & -k_r + 0.25a^2k_s & 2k_r + 0.5a^2k_s & -k_r + 0.25a^2k_s \\ 0.5ak_s & 0 & -k_r + 0.25a^2k_s & k_r + 0.25a^2k_s \end{bmatrix} \begin{bmatrix} W_1 \\ \Theta_0 \\ \Theta_1 \\ \Theta_2 \end{bmatrix} = 0 \tag{165}$$

Assuming a harmonic motion $W_i = w_i e^{j\omega t}$ and $\Theta_i = \theta_i e^{j\omega t}$ with $j^2 = -1$,

$$\begin{bmatrix} 2k_s - m_1\omega^2 & -0.5ak_s & 0 & 0.5ak_s \\ -0.5ak_s & k_r + 0.25a^2k_s - I_{m_0}\omega^2 & -k_r + 0.25a^2k_s & 0 \\ 0 & -k_r + 0.25a^2k_s & 2k_r + 0.5a^2k_s - I_{m_1}\omega^2 & -k_r + 0.25a^2k_s \\ 0.5ak_s & 0 & -k_r + 0.25a^2k_s & k_r + 0.25a^2k_s - I_{m_0}\omega^2 \end{bmatrix} \begin{bmatrix} W_1 \\ \Theta_0 \\ \Theta_1 \\ \Theta_2 \end{bmatrix} = 0 \quad (166)$$

The natural frequencies of the system could be obtained by considering the determinant of the coefficient matrix equal to zero.

3.4. Continuum Solution

In the limit case for the continuum beam, the fourth-order differential equation including the Winkler elastic foundation could be considered in dimensionless form

$$\frac{d^4\bar{w}}{d\bar{x}^4} + \left[r^{*2}\Omega^2(1+\mu_s) - r^{*2}k^*\mu_s\right]\frac{d^2\bar{w}}{d\bar{x}^2} - \left[r^{*2}\Omega^2\left(\mu_s r^{*2}k^* + \frac{1}{r^{*2}} - \mu_s r^{*2}\Omega^2\right) - k^*\right]\bar{w} = 0 \quad (167)$$

Eq. (167) is obtained by Wang and Stephens [64] and the non-dimensional parameters can be introduced

$$\bar{x} = \frac{x}{L}\ ,\ \bar{w} = \frac{w}{L}\ , \frac{d^2\bar{w}}{dX^2} = L\frac{d^2w}{dx^2}\ ,\ \frac{d^4\bar{w}}{dX^4} = L^3\frac{d^4w}{dx^4} \quad (168)$$

For simply supported beam, the solution of Eq. (167) can be proposed by

$$\bar{w}(\bar{x}) = \sin(p\pi\bar{x}) \quad (169)$$

Substituting Eq. (169) in Eq. (167) leads to the following quartic frequency equation.

$$\left[\mu_s r^{*4}\right]\Omega^4 - \left[r^{*2}\left(\mu_s r^{*2}k^* + \frac{1}{r^*}\right) + r^{*2}p^2\pi^2(1+\mu_s)\right]\Omega^2 + \left[r^{*2}k^*\mu_s p^2\pi^2 + k^* + p^4\pi^4\right] = 0 \quad (170)$$

which can be considered in the compact form

$$\Omega^4 - B\Omega^2 + C = 0 \quad (171)$$

The two coefficients of *B* and *C* are defined as:

$$\boldsymbol{B} = \frac{\boldsymbol{p^2\pi^2}}{\boldsymbol{\mu_s r^{*2}}}(\boldsymbol{1}+\boldsymbol{\mu_s}) + \frac{\boldsymbol{1}}{\boldsymbol{\mu_s r^{*2}}}\left(\boldsymbol{\mu_s r^{*2} k^*} + \frac{\boldsymbol{1}}{\boldsymbol{r^{*2}}}\right), \quad \boldsymbol{C} = \frac{\boldsymbol{p^4\pi^4}}{\boldsymbol{\mu_s r^{*4}}} + \frac{\boldsymbol{k^* p^2\pi^2}}{\boldsymbol{r^{*2}}} + \frac{\boldsymbol{k^*}}{\boldsymbol{\mu_s r^{*4}}} \tag{172}$$

So, the natural frequencies of the continuous beam could be obtained from the quartic equation of Eq. (171). The results are in the same form as Eq. (154) with substitution of Eq. (162) and can be compared well to Wang and Stephens [64], Cheng and Pantelides [118] and Manevich [65]. If the elastic Winkler foundation is neglected ($k^*=0$) the eigenfrequency values will be similar to those obtained by Timoshenko [17, [18].

The sensitivity analysis is performed for the granular chain by assuming that the following set of dimensionless parameters for four grain number values *(n=5; n=20; n=35; n=50)*

$$\mu_s = 4.28 \text{ and } k^* \in \{1.875, 480, 4502, 18750\} \tag{173}$$

In Figure 8, the frequency results obtained by the exact solution of the discrete lattice model have been compared with those of Duan et al. [12]. In this asymptotic analysis, the length of the beam is considered constant for instance and by increasing the number of grains subsequently reducing the grain diameter (a) the natural frequencies of the system are obtained. Since the local continuum solution of the problem (mentioned in Eq. (172)) is independent of the grain number, the results do not change by varying the grain number. Each model leads to two branches of frequency.

Regarding to the first branch (lower frequencies), for each typical value of the grain number, the results of two discrete models, diverge from each other and also from the continuum ones by increasing the mode number, starting from two different values of mode number. While for the second branch these two results are close to each other (Figure 9).

(a) (b)

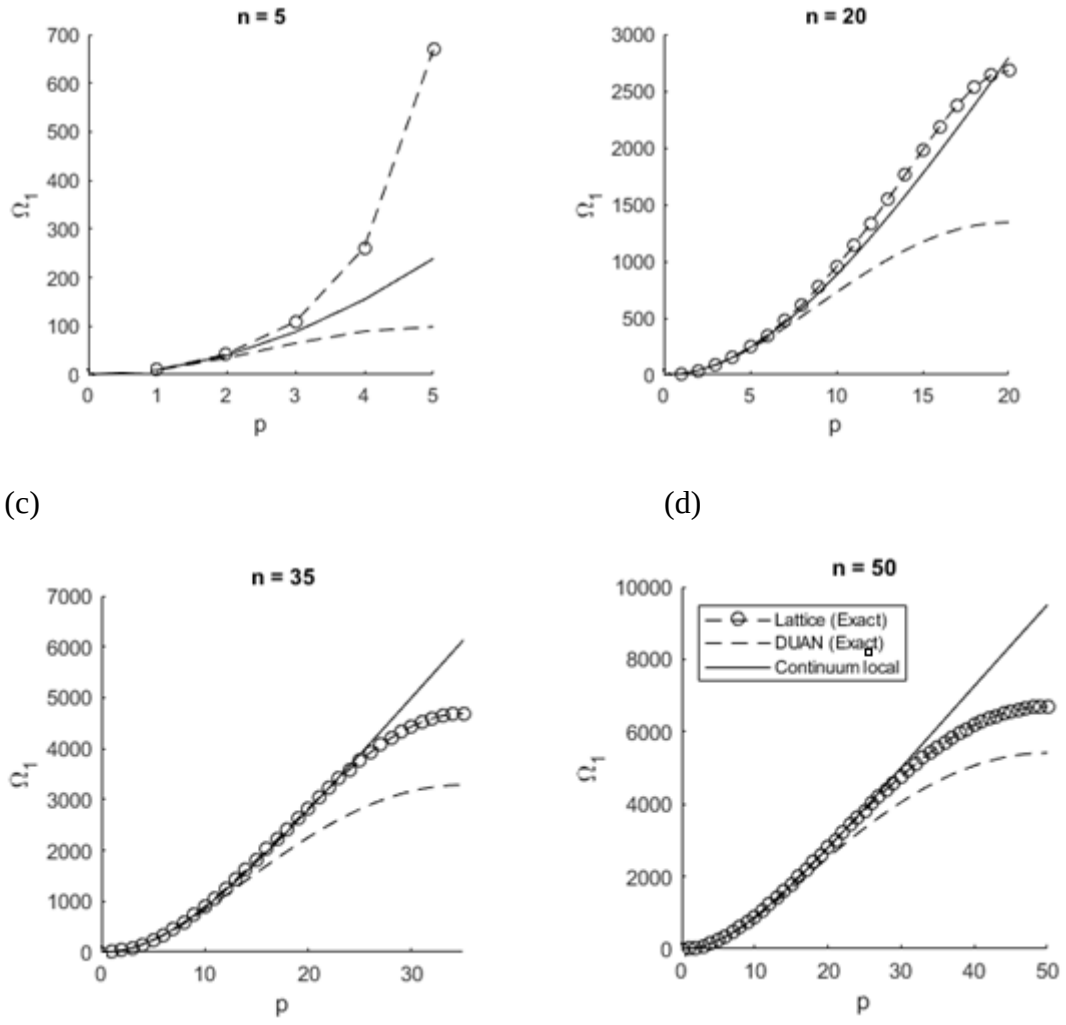

Figure 8. Comparison of the first branch natural frequencies for the discrete exact, Duan et al. [12] and continuum solutions with respect to the mode number (p) and grain number: (a) $\boldsymbol{n = 5}$, (b) $\boldsymbol{n = 20}$, (c) $\boldsymbol{n = 35}$ and (d) $\boldsymbol{n = 50}$ for $\boldsymbol{\mu_s = 4.28}$, $\boldsymbol{r^* = 0.007}$ and $\boldsymbol{k^* = 0}$.

The results for the second branches of eigenfrequencies have been shown in Figure 9 for the two discrete model and the equivalent continuum beam with respect to the mode number (p) and four grain number values (*n=5*; *n=20*; *n=35*; *n=50*). It can be concluded the exact solution of the discrete model always predicts lower frequencies than the continuum one. As it is expected, by increasing the ratio of *n/p*, the results of the two discrete models converge to the continuous ones. The coincidence of the results happens

for the second branch when the ratio of *n/p* is typically higher than the approximate value of *3*, while this approximate limit value is typically *2* for the first branch.

Furthermore, for the first branch or lower frequencies, the results of the discrete model developed in this study are closer to the continuum ones in comparison with those obtained by Duan et al. [12], for a typical value of the mode number. While this conclusion is opposite for the second branch which means for small values of the grain number Duan et al. [12] predict the dynamic response closer to the continuum results.

(a)

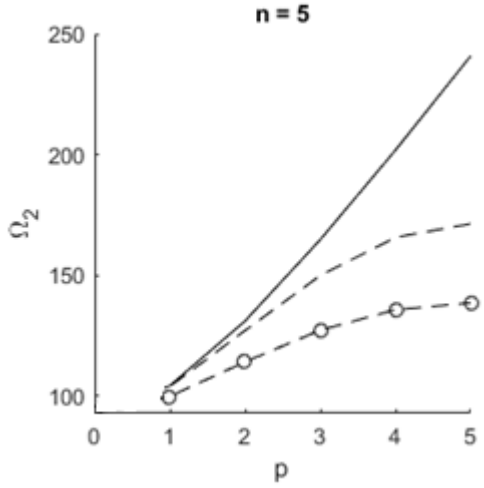

(b)

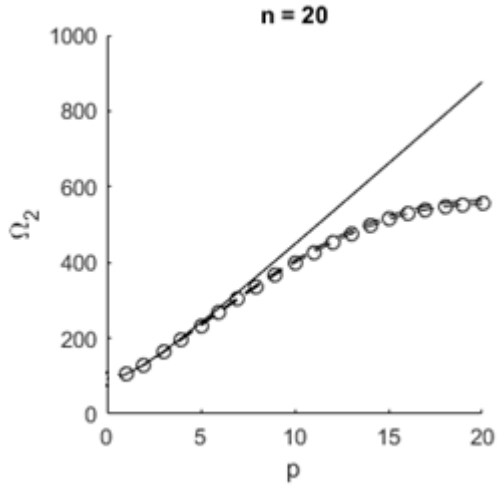

(c)

(d)

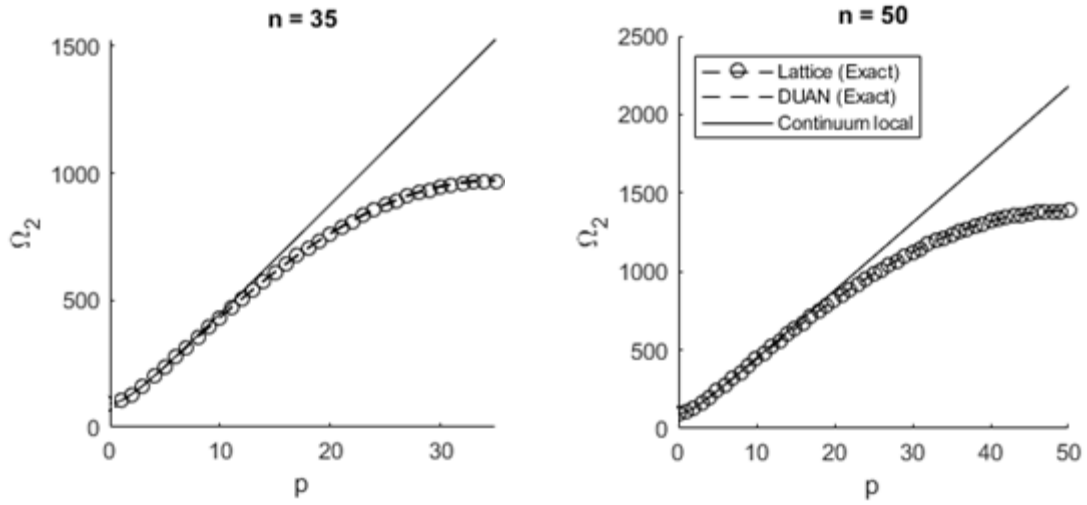

Figure 9. Comparison of the second branch natural frequencies for the discrete exact, Duan et al. [12] and continuum solutions with respect to the mode number (p) and grain number: (a) $\boldsymbol{n = 5}$, (b) $\boldsymbol{n = 20}$, (c) $\boldsymbol{n = 35}$ and (d) $\boldsymbol{n = 50}$ for $\boldsymbol{\mu_s = 4.28}$, $\boldsymbol{r^* = 0.07}$ and $\boldsymbol{k^* = 0}$.

Here, for a constant grain number and various geometric dimensionless parameters (r^*), the results have been compared and shown for the two branches respectively in Figure 10 and Figure 11. Increasing the values of the length ratio, the results obtained by discrete exact solution and Duan et al. [12] converge each other, for both the first and second branches. For the first branch, it can be understood that generally, the behavior of the exact discrete solution is closer to continuum one in comparison with Duan et al. [12], for low values of the mode number (p). On the other hand, for the second branch or higher frequencies, the behavior of the results obtained by the exact model introduced here is more sensitive to the length ratio.

(a) (b)

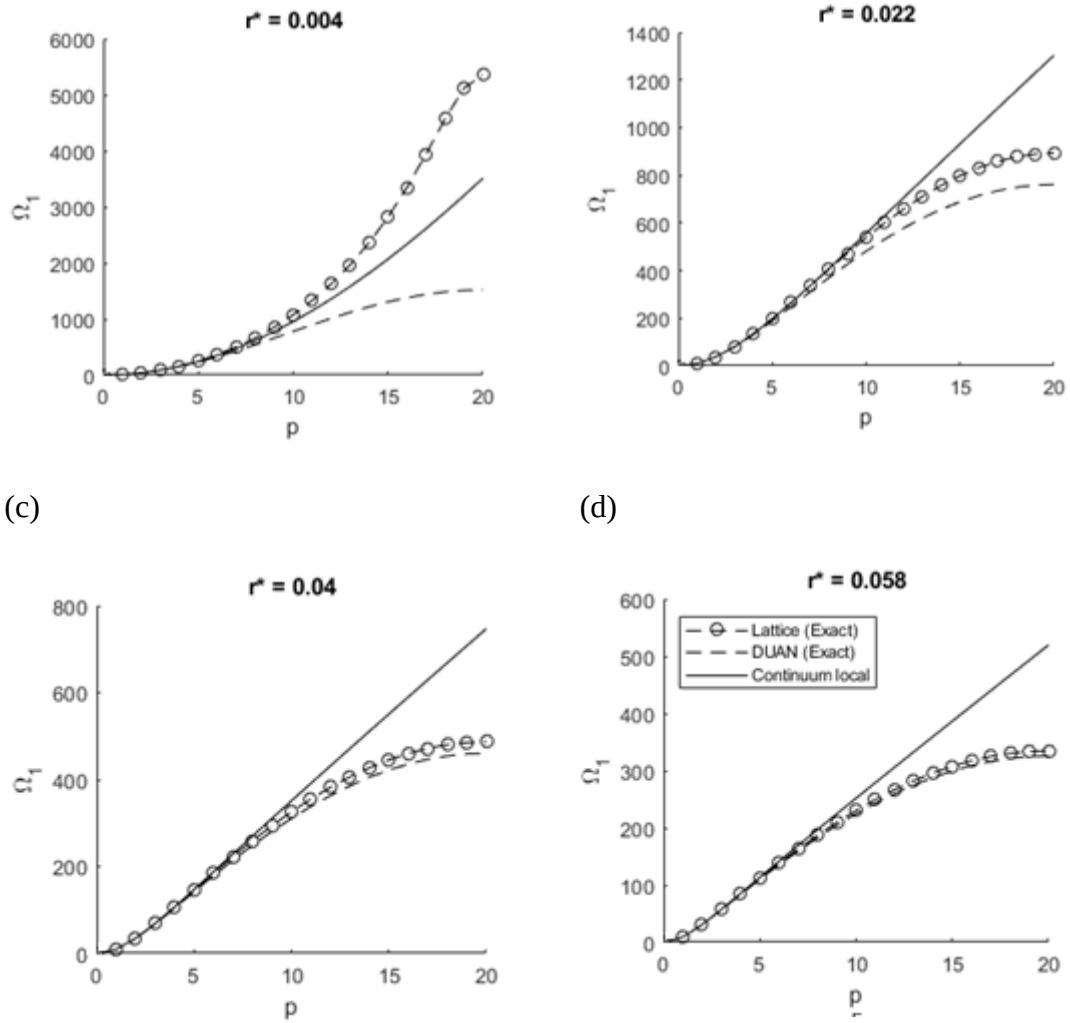

(c) (d)

Figure 10. Comparison of the first branch natural frequencies for the discrete exact, Duan et al. [12] and continuum solutions with respect to the mode number (p) and grain number: (a) $\boldsymbol{r^* = 0.004}$, (b) $\boldsymbol{r^* = 0.022}$, (c) $\boldsymbol{r^* = 0.04}$ and (d) $\boldsymbol{r^* = 0.058}$ for $\boldsymbol{n = 20}$, $\boldsymbol{\mu_s = 4.28}$ and $\boldsymbol{k^* = 0}$.

(a) (b)

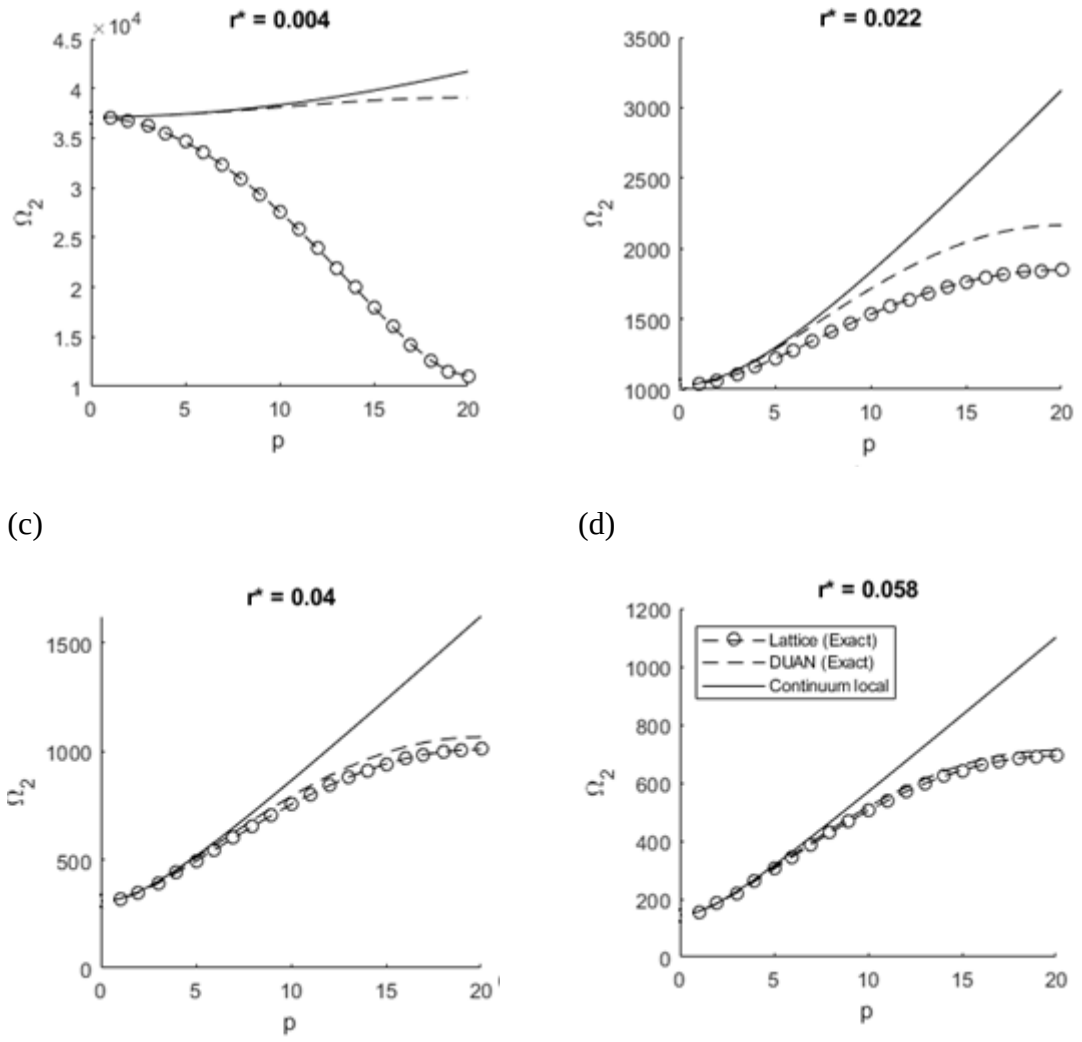

Figure 11. Comparison of the second branch natural frequencies for the discrete exact, Duan et al. [12] and continuum solutions with respect to the mode number (p) and grain number: (a) $\mathbf{r}^* = \mathbf{0.004}$, (b) $\mathbf{r}^* = \mathbf{0.022}$, (c) $\mathbf{r}^* = \mathbf{0.04}$ and (d) $\mathbf{r}^* = \mathbf{0.058}$ for $\mathbf{n = 20}$, $\boldsymbol{\mu}_s = \mathbf{4.28}$ and $\mathbf{k}^* = \mathbf{0}$.

In Figure 12, the effect of length ratio (beam thickness/beam length) regarding to the grain number has been studied for two typical mode numbers (p=1 and p=10). The minimum values of the required grain number (n*) have been also determined and reported when the difference between the discrete and continuum results start to be smaller than *1%*. It can be concluded generally that in order to achieve the continuum results from discrete solution, whether the length ratio decrease or the mode number increase, the grain number value needs to increase.

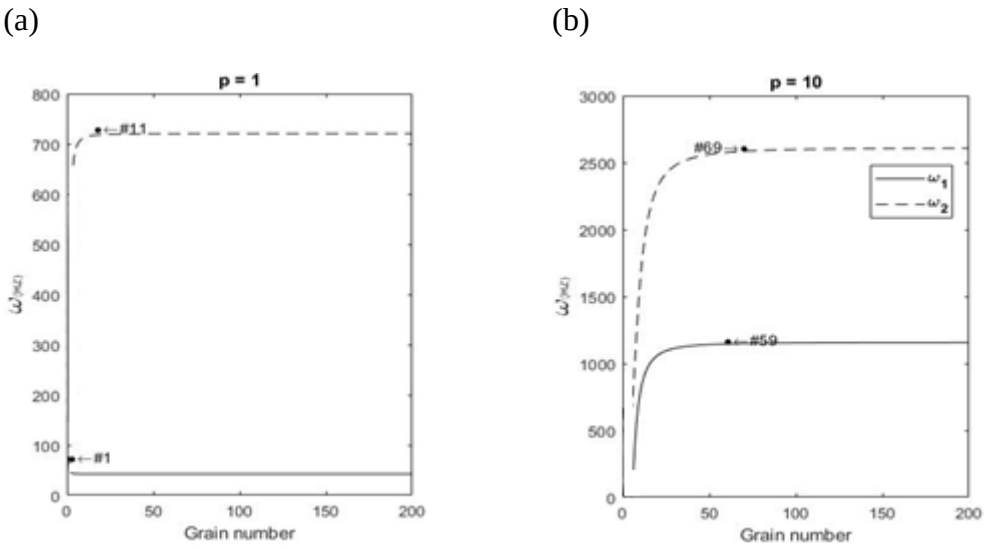

Figure 12. Analysis of the grain number effect on the frequencies (discrete exact solution) for the mode number (a) $\boldsymbol{p = 1}$ and (b) $\boldsymbol{p = 10}$ with respect to the length ratio ($\boldsymbol{r^* = 0.029}$) for $\boldsymbol{\mu_s = 4.28}$ and $\boldsymbol{k^* = 1.87}$.

4. Nonlocal Approximate Solutions - Continuous Approach

The fourth-order difference equations of Eq. (77) may be continualized in two general ways: the simplest approach is based on the polynomial expansions in which the finite differences operators are expanded with the Taylor approximation. This leads to a higher-order gradient Cosserat continuum theory. Another effective method considers a rational expansion based on the Padé approximation which could give a better homogenized solution compared to the Taylor series (see for instance Duan et al. [12] for the application of this technique to a similar discrete Bresse-Timoshenko system). The second strategy is based on homogenization of the equations by means of a discrete Fourier transformation. The result, in this case, is a Kunin-type non-local theory.

In the next section, the discrete nature of the granular beam structure which has been modeled utilizing the difference equation as Eq. (77) is continualized by applying the Taylor series and the Padé approximation.

4.1. Polynomial Expansion (Taylor Series Approximant)

The general solution for the granular beam will be investigated by a continualization transform based on exponential pseudo-differential operators. The following pseudo-differential operators are defined in order to introduce the relation between the discrete and the equivalent continuous system holds for a sufficiently smooth deflection function (Salvadori [126]):

$$w_i = w\,(x = ia)$$

$$w_{i+1} = \sum_{k=0}^{\infty} \frac{a^k D_x^k}{k!} w(x) = \left[1 + \frac{aD_x^1}{1!} + \frac{a^2 D_x^2}{2!} + \frac{a^3 D_x^3}{3!} + \cdots\right] w(x) = e^{aD_x} w(x);\ x = ia \tag{174}$$

Subsequently, the involved pseudo-differential equations ${\delta_2}^2 w(x)$, $\delta_2 w(x)$ and $\delta_0 w(x)$ may be defined as:

$$\begin{aligned} {\delta_2}^2 w(x) &= \left(\frac{e^{2aD_x} - 4e^{aD_x} + 6 - 4e^{-aD_x} + e^{-2aD_x}}{a^4}\right) w(x) \\ &= \left(1 + \frac{a^2 D_x^2}{6} + \frac{a^4 D_x^4}{80} + O\left(a^6 D_x^6\right)\right) D_x^4 w(x); \\ \delta_2 w(x) &= \left(\frac{e^{aD_x} - 2 + e^{-aD_x}}{a^2}\right) w(x) = \left(1 + \frac{a^2 D_x^2}{12} + \frac{a^4 D_x^4}{360} + O\left(a^6 D_x^6\right)\right) D_x^2 w(x); \\ \delta_0 w(x) &= \left(\frac{e^{aD_x} + 2 + e^{-aD_x}}{4}\right) w(x) = \left(1 + \frac{a^2 D_x^2}{4} + \frac{a^4 D_x^4}{48} + O\left(a^6 D_x^6\right)\right) w(x) \end{aligned} \tag{175}$$

Substitution of the fourth-order expansions of Eq. (175) for the pseudo-differential operators in Eq. (11) leads to

$$\begin{aligned} &[EI(1 + \frac{a^2 D_x^2}{6}) D_x^4 + \left(\rho I\omega^2 - \frac{kEI}{K_s GA} + \frac{EI\rho A\omega^2}{K_s GA}\right)(1 + \frac{a^2 D_x^2}{12}) D_x^2 + (k - \rho A\omega^2)(1 \\ &+ \frac{a^2 D_x^2}{4}) - \frac{k\rho I\omega^2}{K_s GA} + \frac{\rho^2 IA\omega^4}{K_s GA}] w(x) = 0 \end{aligned} \tag{176}$$

Next, a gradient-type differential equation could be obtained as follows with the multiplication of the last equation by $(1 - \frac{a^2 D_x^2}{3})$ and neglecting higher-order terms in a^4.

$$\left[EI\left(1-\frac{a^2D_x^2}{6}\right)D_x^4+\left(\rho I\omega^2-\frac{kEI}{K_sGA}+\frac{EI\rho A\omega^2}{K_sGA}\right)\left(1-\frac{a^2D_x^2}{4}\right)D_x^2\right.$$
$$\left.+\left(k-\rho A\omega^2\right)\left(1-\frac{a^2D_x^2}{12}\right)+\left(-\frac{k\rho I\omega^2}{K_sGA}+\frac{\rho^2IA\omega^4}{K_sGA}\right)\left(1-\frac{a^2D_x^2}{3}\right)\right]w(x)\ =0 \tag{177}$$

With ignorance of shear effects in the granular system ($K_sGA \to \infty$), Eq. (177) could be simplified

$$EI\left(1-\frac{a^2D_x^2}{6}\right)D_x^4w(x)+\left(\rho I\omega^2\right)\left(1-\frac{a^2D_x^2}{4}\right)D_x^2w(x)+\left(k-\rho A\omega^2\right)\left(1-\frac{a^2D_x^2}{12}\right)w(x) = 0 \tag{178}$$

which is equivalent to

$$EI\left(-\frac{a^2}{6}w^{(6)}+w^{(4)}\right)+k\left(w-\frac{a^2}{12}w''\right)-\rho A\omega^2\left(w-\frac{a^2}{12}w''\right)+\rho I\omega^2\left(w''-\frac{a^2}{4}w^{(4)}\right) = 0 \tag{179}$$

The last equation is formally the same as the gradient elasticity of Rayleigh beam equation under the Pasternak-type foundation. This differential equation can be obtained from the application of the Hamilton principle associated with some connected energy functions. The (definitive positive) potential energy and kinetic energy functions are respectively given by

$$W=\int_0^L\frac{1}{2}EI\left(w''^2+\frac{a^2}{6}w'''^2\right)dx+\int_0^L\frac{1}{2}k\left(w^2+\frac{a^2}{12}w'^2\right)dx\ =0 \tag{180}$$

$$T=\int_0^L\frac{1}{2}\rho A\left(\dot{w}^2+\frac{a^2}{12}\dot{w}'^2\right)dx+\int_0^L\frac{1}{2}\rho I\left(\dot{w}'^2+\frac{a^2}{4}\dot{w}''^2\right)dx\ =0 \tag{181}$$

Assuming static case ($\omega = 0$), Eq. (178) leads to an equivalent gradient elasticity of Euler-Bernoulli beam under Pasternak-type foundation

$$EI\left(-\frac{a^2}{6}w^{(6)}+w^{(4)}\right)+k\left(w-\frac{a^2}{12}w''\right)\ =0 \tag{182}$$

Going back to Eq. (176) which is an approximation of the discrete model, the higher-order differential equation could be rewritten

$$\left[\frac{EIa^2}{6}w^{(6)} + \left[EI + \left(\rho I\omega^2 - \frac{kEI}{K_sGA} + \frac{EI\rho A\omega^2}{K_sGA}\right)\frac{a^2}{12}\right]w^{(4)} + \left[\left(\rho I\omega^2 - \frac{kEI}{K_sGA} + \frac{EI\rho A\omega^2}{K_sGA}\right) + \left(k - \rho A\omega^2\right)\frac{a^2}{4}\right]w^{(2)} + \left[\left(k - \rho A\omega^2\right) - \frac{k\rho I\omega^2}{K_sGA} + \frac{\rho^2 IA\omega^4}{K_sGA}\right]\right]w = 0 \tag{183}$$

Eq. (183) has been obtained by Challamel et al. [117] in the static range ($\omega = 0$). For simply supported boundary conditions, the solution of Eq. (183) could be assumed in the following form:

$$w(x) = \sin\left(\frac{p\pi x}{L}\right) \tag{184}$$

So, by substituting this fundamental solution in Eq. (183), the natural frequencies of the granular chain may be obtained from solving the following equation:

$$\left[\frac{\rho^2 I}{k_sG}\right]\omega^4 + \left[\left(\rho I + \frac{EI\rho}{k_sG}\right)\frac{a^2}{12}\times\frac{p^4\pi^4}{L^4} - \left(\rho I + \frac{EI\rho}{k_sG} - \rho A\frac{a^2}{4}\right)\frac{p^2\pi^2}{L^2} - (\rho A + \frac{kI\rho}{k_sGA})\right]\omega^2 + \left[-EI\frac{a^2}{6}\times\frac{p^6\pi^6}{L^6} + EI\frac{p^4\pi^4}{L^4} - \frac{kEI}{k_sGA}\times\frac{a^2}{12}\times\frac{p^4\pi^4}{L^4} + \frac{kEI}{k_sGA}\times\frac{p^2\pi^2}{L^2} - k\frac{a^2}{4}\times\frac{p^2\pi^2}{L^2} + k\right] = 0 \tag{185}$$

or in non-dimensional form

$$\Omega^4 + \left[\left(\frac{1}{\mu_s r^{*2}} + \frac{1}{r^{*2}}\right)\frac{p^4\pi^4}{12n^2} - \left(\frac{1}{\mu_s r^{*2}} + \frac{1}{r^{*2}} - \frac{1}{4\mu_s r^{*4}n^2}\right)p^2\pi^2 - (\frac{1}{\mu_s r^{*4}} + k^*)\right]\Omega^2 + \left[\frac{p^6\pi^6}{6\mu_s r^{*4}n^2} + \frac{p^4\pi^4}{\mu_s r^{*4}} - \frac{k^*p^4\pi^4}{12r^{*2}n^2} + \frac{k^*p^2\pi^2}{r^{*2}} - \frac{k^*p^2\pi^2}{4\mu_s r^{*4}n^2} + \frac{k^*}{\mu_s r^{*4}}\right] = 0 \tag{186}$$

By solving Eq. (186) leads to the form of Eq. (153) with the parameters

$$B = \left(\frac{1}{\mu_s r^{*2}} + \frac{1}{r^{*2}}\right)\frac{p^4\pi^4}{12n^2} - \left(\frac{1}{\mu_s r^{*2}} + \frac{1}{r^{*2}} - \frac{1}{4\mu_s r^{*4}n^2}\right)p^2\pi^2 - \left(\frac{1}{\mu_s r^{*4}} + k^*\right),$$

$$C = \frac{1}{6\mu_s r^{*4}n^2}p^6\pi^6 + (\frac{1}{\mu_s r^{*4}} - \frac{k^*}{12r^{*2}n^2})p^4\pi^4 + (\frac{k^*}{r^{*2}} - \frac{k^*}{4\mu_s r^{*4}n^2})p^2\pi^2 + \frac{k^*}{\mu_s r^{*4}} \tag{187}$$

The natural frequencies could be calculated by substituting Eq. (153) in the following equation with respect to the parameters of Eq. (187).

$$\boldsymbol{\omega} = \frac{\Omega}{L^2}\sqrt{\frac{EI}{\rho A}} \tag{188}$$

For continuum modeling when $n \to \infty$, γ change to

$$\boldsymbol{\gamma} = \sqrt{\left(\frac{p^2\pi^2}{2\mu_s r^{*2}}(1+\mu_s)+\frac{k^*}{2}+\frac{1}{2\mu_s r^{*4}}\right) \pm \sqrt{\left(\frac{p^2\pi^2}{2\mu_s r^{*2}}(1+\mu_s)+\frac{k^*}{2}+\frac{1}{2\mu_s r^{*4}}\right)^2 - \left(\frac{k^*}{\mu_s r^{*4}}+\frac{k^* p^2\pi^2}{r^{*2}}+\frac{p^4\pi^4}{\mu_s r^{*4}}\right)}} \tag{189}$$

Eq. (189) coincides with Eq. (162), which also exactly agrees with the results of Wang and Stephens [64], Cheng and Pantelides [118] and Manevich [65].

In Figure 13, the natural frequencies of the discrete granular model obtained from the Taylor expansion of pseudo-differential (nonlocal approach) have been compared with the local continuum solution for the two spectra. The coincidence of the discrete and continuum eigenfrequencies occurs when the ratio of *n/p* is sufficiently large which can be quantified for the second branch typically *7* and for the first branch by a typical value of *5*. In comparison with the exact solution, it can be clarified that the Taylor approximation requires more discrete elements in order to converge to the continuum results.

It is important to note that by decreasing the *n/p* ratio, the imaginary term appears in the nonlocal results for the two branches. For these cases, the real parts of the two branches are equal together while the imaginary parts are equal in values but opposite in sign. Therefore, using the Taylor series for continualizing the difference equations of the granular beam implies imaginary eigenfrequencies. The length ratio and grain number effects on frequencies have been studied in Figure 14.

(a) (b)

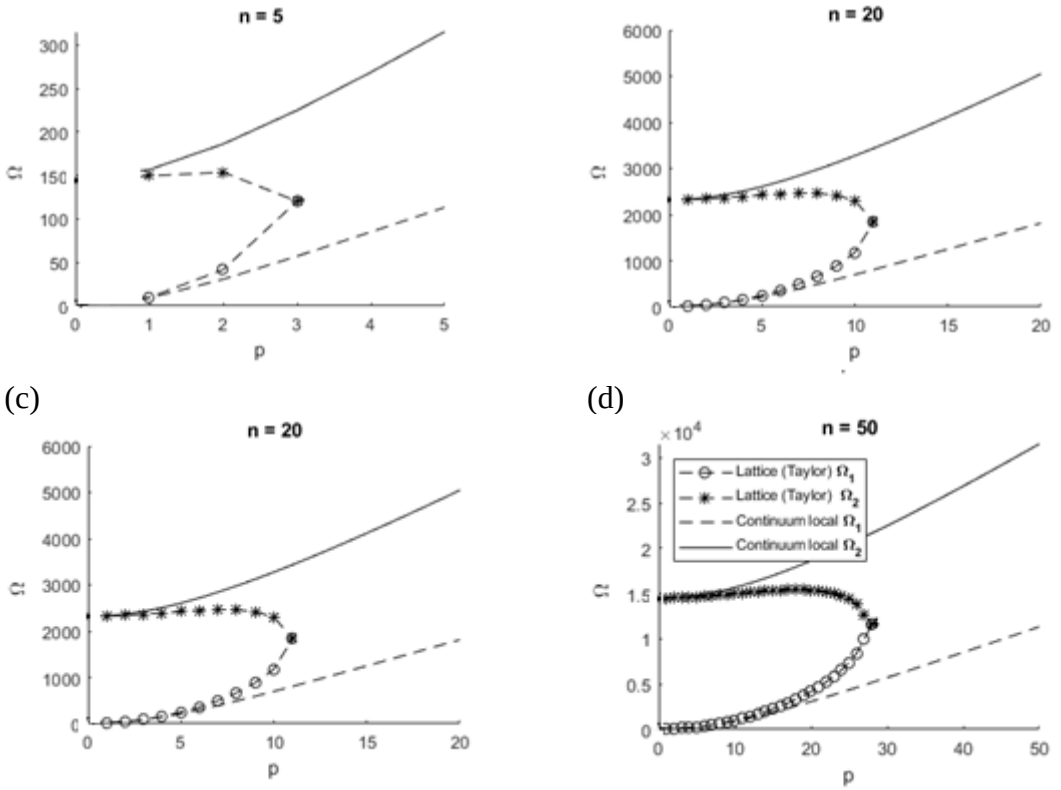

Figure 13. Comparison of the natural frequencies for the nonlocal Taylor and continuum solutions with respect to the mode number (p) and grain number: (a) $\boldsymbol{n = 5}$ and $\boldsymbol{r^* = 0.058}$, (b) $\boldsymbol{n = 20}$ and $\boldsymbol{r^* = 0.014}$, (c) $\boldsymbol{n = 35}$ and $\boldsymbol{r^* = 0.0082}$ and (d) $\boldsymbol{n = 50}$ and $\boldsymbol{r^* = 0.0058}$ for $\boldsymbol{\mu_s = 4.28}$.

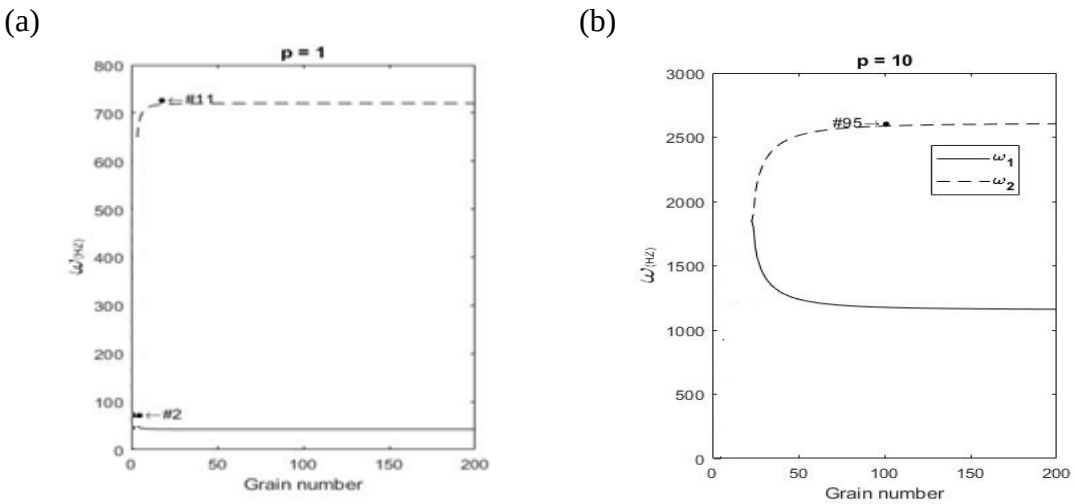

Figure 14. Analysis of the grain number effect on the frequencies (nonlocal Taylor) for the mode number (a) $\boldsymbol{p = 1}$ and (b) $\boldsymbol{p = 10}$ with respect to the length ratio for $\boldsymbol{\mu_s = 4.28}$ and $\boldsymbol{k^* = 1.87}$.

4.2. Rational Expansion (Padé Approximant)

In this section, the approximation of Padé has been used in the asymptotic expansion of the pseudo-differential operators. This method often gives a better

approximation of a function than its Taylor series counterpart (Baker and Graves-Morris [127]).

Applying the Padé approximant of *[1/4]*, *[1/2]* and *[1/2]* in Eq. (175) yields:

$$\begin{gathered}\boldsymbol{\delta_2}^2\boldsymbol{w(x)} \approx \left(\frac{\mathbf{1}}{\mathbf{1}-\frac{\boldsymbol{a^2D_x^2}}{\mathbf{6}}+\frac{\mathbf{11}\boldsymbol{a^4D_x^4}}{\mathbf{720}}}\right)\boldsymbol{D_x^4 w(x)} \approx \left(\frac{\mathbf{1}}{\left(\mathbf{1}-\frac{\boldsymbol{a^2D_x^2}}{\mathbf{12}}\right)^2}\right)\boldsymbol{D_x^4 w(x)};\\ \boldsymbol{\delta_2 w(x)} \approx \left(\frac{\mathbf{1}}{\mathbf{1}-\frac{\boldsymbol{a^2D_x^2}}{\mathbf{12}}}\right)\boldsymbol{D_x^2 w(x)};\\ \boldsymbol{\delta_0 w(x)} \approx [\mathbf{1}+\left(\frac{\mathbf{1}}{\mathbf{1}-\frac{\boldsymbol{a^2D_x^2}}{\mathbf{12}}}\right)\frac{\boldsymbol{a^2D_x^2}}{\mathbf{4}}]\boldsymbol{w(x)}\end{gathered} \tag{190}$$

Eq. (11) could be rewritten as a function of Eq. (175)

$$\begin{gathered}\left[\left(\frac{1}{\left(1-\frac{a^2D_x^2}{12}\right)^2}\right)D_x^4+\left(\frac{\rho I}{EI}\omega^2-\frac{k}{K_sGA}+\frac{\rho A\omega^2}{K_sGA}\right)\left(\frac{1}{1-\frac{a^2D_x^2}{12}}\right)D_x^2+\left(\frac{k}{EI}-\frac{\rho A\omega^2}{EI}\right)\left(1+\right.\right.\\ \left.\left.\left(\frac{1}{1-\frac{a^2D_x^2}{12}}\right)\frac{a^2D_x^2}{4}\right)+\left(-\frac{k\rho I\omega^2}{EIK_sGA}+\frac{\rho^2IA\omega^4}{EIK_sGA}\right)\right]w(x)=0\end{gathered} \tag{191}$$

Multiplication of Eq. (191) by $\left(1-\frac{a^2D_x^2}{12}\right)^2$ leads to the following compact form equation.

$$\begin{gathered}\left(D_x^4+\left[\frac{\rho\omega^2}{E}+\frac{\rho\omega^2}{K_sG}-\frac{\rho A\omega^2}{4EI}a^2-\frac{k}{K_sGA}+\frac{ka^2}{4EI}\right]\left(1-\frac{a^2D_x^2}{12}\right)D_x^2\right.\\ \left.+\left[\frac{\rho^2\omega^4}{EK_sG}-\frac{\rho A\omega^2}{EI}-\frac{k\rho\omega^2}{EK_sGA}+\frac{k}{EI}\right]\left(1-\frac{a^2D_x^2}{12}\right)^2\right)w_{(x)}=0\end{gathered} \tag{192}$$

Eq. (192) can be written in the dimensionless form

$$\left(L^4D_x^4+\alpha\left(1-\frac{a^2D_x^2}{12}\right)L^2D_x^2+\beta\left(1-\frac{a^2D_x^2}{6}+\frac{a^4D_x^4}{144}\right)\right)w(x)=0 \tag{193}$$

in which α and β are defined as:

$$\boldsymbol{\alpha} = \left[\boldsymbol{r^{*2}\Omega^2}\left(\mathbf{1}+\boldsymbol{\mu_s}-\frac{\mathbf{1}}{\mathbf{4}\boldsymbol{r^{*2}n^2}}\right)-\boldsymbol{r^{*2}k^*\mu_s}+\frac{\boldsymbol{k^*}}{\mathbf{4}\boldsymbol{n^2}}\right]; \qquad (194)$$

$$\boldsymbol{\beta} = -\left[\boldsymbol{r^{*2}\Omega^2}\left(\boldsymbol{\mu_s r^{*2}k^*}+\frac{\mathbf{1}}{\boldsymbol{r^{*2}}}-\boldsymbol{\mu_s r^{*2}\Omega^2}\right)-\boldsymbol{k^*}\right]$$

Using Eq. (190), the dimensionless differential equation can be presented in the following form:

$$\begin{aligned}&\left[\frac{\boldsymbol{r^{*2}\Omega^2}}{\mathbf{144}\boldsymbol{n^4}}\left(\boldsymbol{\mu_s r^{*2}\Omega^2}-\boldsymbol{\mu_s r^{*2}k^*}-\frac{\mathbf{1}}{\boldsymbol{r^{*2}}}\right)-\frac{\boldsymbol{r^{*2}\Omega^2}}{\mathbf{12}\boldsymbol{n^2}}\left(\mathbf{1}+\boldsymbol{\mu_s}-\frac{\mathbf{1}}{\mathbf{4}\boldsymbol{r^{*2}n^2}}\right)+\frac{\boldsymbol{r^{*2}k^*\mu_s}}{\mathbf{12}\boldsymbol{n^2}}-\frac{\boldsymbol{k^*}}{\mathbf{48}\boldsymbol{n^4}}\right.\\&\qquad\left.+\frac{\boldsymbol{k^*}}{\mathbf{144}\boldsymbol{n^4}}+\mathbf{1}\right]\frac{\boldsymbol{d^4\bar{w}}}{\boldsymbol{d\bar{x}^4}}\\&+\left[\boldsymbol{r^{*2}\Omega^2}\left(\mathbf{1}+\boldsymbol{\mu_s}-\frac{\mathbf{1}}{\mathbf{4}\boldsymbol{r^{*2}n^2}}\right)-\boldsymbol{r^{*2}k^*\mu_s}+\frac{\boldsymbol{k^*}}{\mathbf{4}\boldsymbol{n^2}}+\frac{\boldsymbol{r^{*2}\Omega^2}}{\mathbf{6}\boldsymbol{n^2}}\left(\boldsymbol{\mu_s r^{*2}k^*}+\frac{\mathbf{1}}{\boldsymbol{r^{*2}}}-\boldsymbol{\mu_s r^{*2}\Omega^2}\right)\right.\\&\qquad\left.-\frac{\boldsymbol{k^*}}{\mathbf{6}\boldsymbol{n^2}}\right]\frac{\boldsymbol{d^2\bar{w}}}{\boldsymbol{d\bar{x}^2}}+\left[\boldsymbol{r^{*2}\Omega^2}\left(\boldsymbol{\mu_s r^{*2}\Omega^2}-\boldsymbol{\mu_s r^{*2}k^*}-\frac{\mathbf{1}}{\boldsymbol{r^{*2}}}\right)+\boldsymbol{k^*}\right]\boldsymbol{\bar{w}}=\mathbf{0}\end{aligned} \qquad (195)$$

Ignoring Winkler foundation effect ($k^* = 0$), Eq. (195) leads to

$$\begin{aligned}&\left[\frac{\boldsymbol{r^{*2}\Omega^2}}{\mathbf{144}\boldsymbol{n^4}}\left(\boldsymbol{\mu_s r^{*2}\Omega^2}-\frac{\mathbf{1}}{\boldsymbol{r^{*2}}}\right)-\frac{\boldsymbol{r^{*2}\Omega^2}}{\mathbf{12}\boldsymbol{n^2}}\left(\mathbf{1}+\boldsymbol{\mu_s}-\frac{\mathbf{1}}{\mathbf{4}\boldsymbol{r^{*2}n^2}}\right)+\mathbf{1}\right]\frac{\boldsymbol{d^4\bar{w}}}{\boldsymbol{d\bar{x}^4}}\\&+\left[\boldsymbol{r^{*2}\Omega^2}\left(\mathbf{1}+\boldsymbol{\mu_s}-\frac{\mathbf{1}}{\mathbf{4}\boldsymbol{r^{*2}n^2}}\right)+\frac{\boldsymbol{r^{*2}\Omega^2}}{\mathbf{6}\boldsymbol{n^2}}\left(\frac{\mathbf{1}}{\boldsymbol{r^{*2}}}-\boldsymbol{\mu_s r^{*2}\Omega^2}\right)\right]\frac{\boldsymbol{d^2\bar{w}}}{\boldsymbol{d\bar{x}^2}}+\left[\boldsymbol{r^{*2}\Omega^2}\left(\boldsymbol{\mu_s r^{*2}\Omega^2}-\frac{\mathbf{1}}{\boldsymbol{r^{*2}}}\right)\right]\boldsymbol{\bar{w}}\\&=\mathbf{0}\end{aligned} \qquad (196)$$

If the pseudo-differential operator effect of $\delta_0 w(x)$ is neglected, Eq. (196) leads to the one of Duan et al. [12]. The dimensionless differential equation of Duan et al. [12] is given by

$$\begin{aligned}&\left[\frac{\boldsymbol{r^{*2}\Omega^2}}{\mathbf{144}\boldsymbol{n^4}}\left(\boldsymbol{\mu_s r^{*2}\Omega^2}-\frac{\mathbf{1}}{\boldsymbol{r^{*2}}}\right)-\frac{\boldsymbol{r^{*2}\Omega^2}}{\mathbf{12}\boldsymbol{n^2}}(\mathbf{1}+\boldsymbol{\mu_s})+\mathbf{1}\right]\frac{\boldsymbol{d^4\bar{w}}}{\boldsymbol{d\bar{x}^4}}\\&+\left[\boldsymbol{r^{*2}\Omega^2}(\mathbf{1}+\boldsymbol{\mu_s})+\frac{\boldsymbol{r^{*2}\Omega^2}}{\mathbf{6}\boldsymbol{n^2}}\left(\frac{\mathbf{1}}{\boldsymbol{r^{*2}}}-\boldsymbol{\mu_s r^{*2}\Omega^2}\right)\right]\frac{\boldsymbol{d^2\bar{w}}}{\boldsymbol{d\bar{x}^2}}+\left[\boldsymbol{r^{*2}\Omega^2}\left(\boldsymbol{\mu_s r^{*2}\Omega^2}-\frac{\mathbf{1}}{\boldsymbol{r^{*2}}}\right)\right]\boldsymbol{\bar{w}}\\&=\mathbf{0}\end{aligned} \qquad (197)$$

For the simply supported boundary conditions, the solution of the Eq. (195) can be considered again as the form of Eq. (169). Substitution of the Eq. (169) in Eq. (195) yields:

$$\left[\frac{\mu_s r^{*4} p^4 \pi^4}{144 n^4} + \frac{\mu_s r^{*4} p^2 \pi^2}{6 n^2} + \mu_s r^{*4}\right] \Omega^4$$

$$+ \left[\frac{r^{*2} p^4 \pi^4}{144 n^4}\left(-\mu_s r^{*2} k^* - \frac{1}{r^{*2}}\right) - \frac{r^{*2} p^4 \pi^4}{12 n^2}\left(1 + \mu_s - \frac{1}{4 r^{*2} n^2}\right)\right. \tag{198}$$

$$\left. - r^{*2} p^2 \pi^2 \left(1 + \mu_s - \frac{1}{4 r^{*2} n^2}\right) - \frac{r^{*2} p^2 \pi^2}{6 n^2}\left(r^{*2} \mu_s k^* + \frac{1}{r^{*2}}\right) + r^{*2}\left(-\mu_s r^{*2} k^* - \frac{1}{r^{*2}}\right)\right] \Omega^2$$

$$+ \left[\frac{r^{*2} k^* \mu_s p^4 \pi^4}{12 n^2} - \frac{k^* p^4 \pi^4}{48 n^4} + \frac{k^* p^4 \pi^4}{144 n^4} + p^4 \pi^4 + r^{*2} k^* \mu_s p^2 \pi^2 - \frac{k^* p^2 \pi^2}{4 n^2} + \frac{k^* p^2 \pi^2}{6 n^2} + k^*\right]$$

$$= 0$$

or in the compact form

$$A\Omega^4 - B\Omega^2 + C = 0 \tag{199}$$

A, *B* and *C* are defined as:

$$A = \frac{\mu_s r^{*4} p^4 \pi^4}{144 n^4} + \frac{\mu_s r^{*4} p^2 \pi^2}{6 n^2} + r^{*4} \mu_s;$$

$$B$$

$$= \frac{r^{*2} p^4 \pi^4}{144 n^4}\left(\mu_s r^{*2} k^* + \frac{1}{r^{*2}}\right) + \left(\frac{r^{*2} p^4 \pi^4}{12 n^2} + r^{*2} p^2 \pi^2\right)\left(1 + \mu_s - \frac{1}{4 r^{*2} n^2}\right)$$

$$+ \left(\frac{r^{*2} p^2 \pi^2}{6 n^2} + r^{*2}\right)\left(\mu_s r^{*2} k^* + \frac{1}{r^{*2}}\right); \tag{200}$$

$$C = \frac{k^* p^2 \pi^2}{12 n^2}\left(r^{*2} \mu_s p^2 \pi^2 - \frac{p^2 \pi^2}{6 n^2} - 1\right) + p^4 \pi^4 + r^{*2} k^* \mu_s p^2 \pi^2 + k^*$$

where *p* is the mode number (natural number). Ω would be obtained by

$$\Omega = \sqrt{\frac{B \pm \sqrt{B^2 - 4AC}}{2A}} \tag{201}$$

For continuum case when $n \to \infty$, Eq. (198) could be written in a quartic form

$$\Omega^4 - B\Omega^2 + C = 0 \tag{202}$$

B and *C* are defined as:

$$\boldsymbol{B}=\frac{\boldsymbol{p^2\pi^2}}{\boldsymbol{\mu_s r^{*2}}}(\boldsymbol{1}+\boldsymbol{\mu_s})+\frac{\boldsymbol{1}}{\boldsymbol{\mu_s r^{*2}}}\left(\boldsymbol{\mu_s r^{*2} k^*}+\frac{\boldsymbol{1}}{\boldsymbol{r^{*2}}}\right),\ \ \boldsymbol{C}=\frac{\boldsymbol{p^4\pi^4}}{\boldsymbol{\mu_s r^{*4}}}+\frac{\boldsymbol{k^* p^2\pi^2}}{\boldsymbol{r^{*2}}}+\frac{\boldsymbol{k^*}}{\boldsymbol{\mu_s r^{*4}}} \tag{203}$$

Thus, again the natural frequency could be obtained by Eq. (154) with γ expressed

$$\boldsymbol{\gamma}=\sqrt{\frac{\boldsymbol{p^2\pi^2}}{\boldsymbol{2\mu_s r^{*2}}}(\boldsymbol{1}+\boldsymbol{\mu_s})+\frac{\boldsymbol{k^*}}{\boldsymbol{2}}+\frac{\boldsymbol{1}}{\boldsymbol{2\mu_s r^{*4}}}\pm\sqrt{(\frac{\boldsymbol{p^2\pi^2}}{\boldsymbol{2\mu_s r^{*2}}}(\boldsymbol{1}+\boldsymbol{\mu_s})+\frac{\boldsymbol{k^*}}{\boldsymbol{2}}+\frac{\boldsymbol{1}}{\boldsymbol{2\mu_s r^{*4}}})^2-(\frac{\boldsymbol{k^*}}{\boldsymbol{\mu_s r^{*4}}}+\frac{\boldsymbol{k^* p^2\pi^2}}{\boldsymbol{r^{*2}}}+\frac{\boldsymbol{p^4\pi^4}}{\boldsymbol{\mu_s r^{*4}}})}} \tag{204}$$

The last equation is valid for the continuum case and agrees with the results of the Bresse-Timoshenko beam on elastic Winkler foundation, as treated by Wang and Stephens [64], Cheng and Pantelides [118] and Manevich [65].

The natural frequencies of the two existing branches regarding Eq. (204), have been shown in Figure 15. The frequencies obtained by the Padé approximants can be supposed equal to the continuum results when the ratio of *n/p* is large enough. For the second branch, this ratio needs to be typically higher than 5 while for the first branch this limit value is typically 3. These typical limit values are the same as those obtained by the exact solution. Figure 16 shows the length ratio (r^*) and grain number effects on frequencies. Increasing the length ratio (refers to beam thickness/beam length) causes an increase in the eigenfrequencies. The values of grain number limit (n^*) have been also reported for each case.

(a)

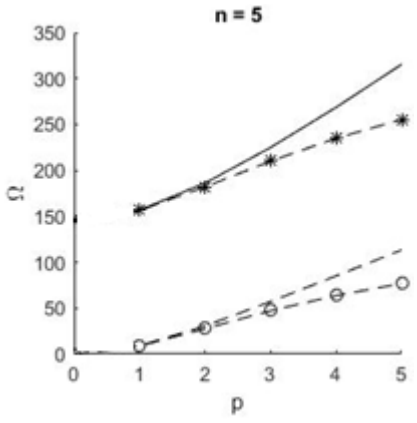

(b)

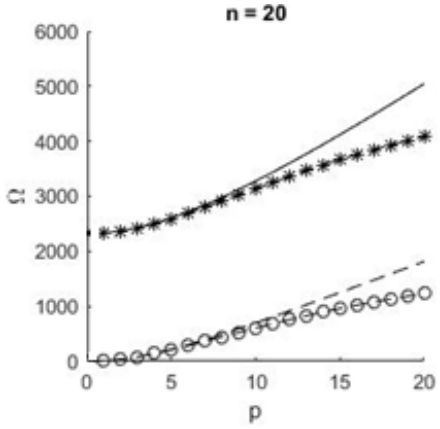

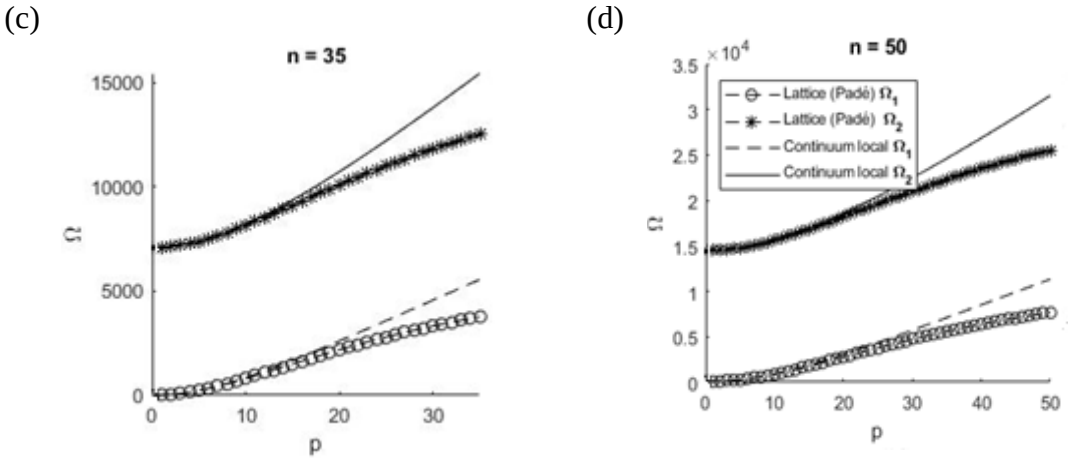

Figure 15. Comparison of the natural frequencies for the nonlocal Padé and continuum solutions with respect to the mode number (p) and grain number: (a) $\boldsymbol{n = 5}$ and $\boldsymbol{r^* = 0.058}$, (b) $\boldsymbol{n = 20}$ and $\boldsymbol{r^* = 0.014}$, (c) $\boldsymbol{n = 35}$ and $\boldsymbol{r^* = 0.0082}$ and (d) $\boldsymbol{n = 50}$ and $\boldsymbol{r^* = 0.0058}$ for $\boldsymbol{\mu_s = 4.28}$.

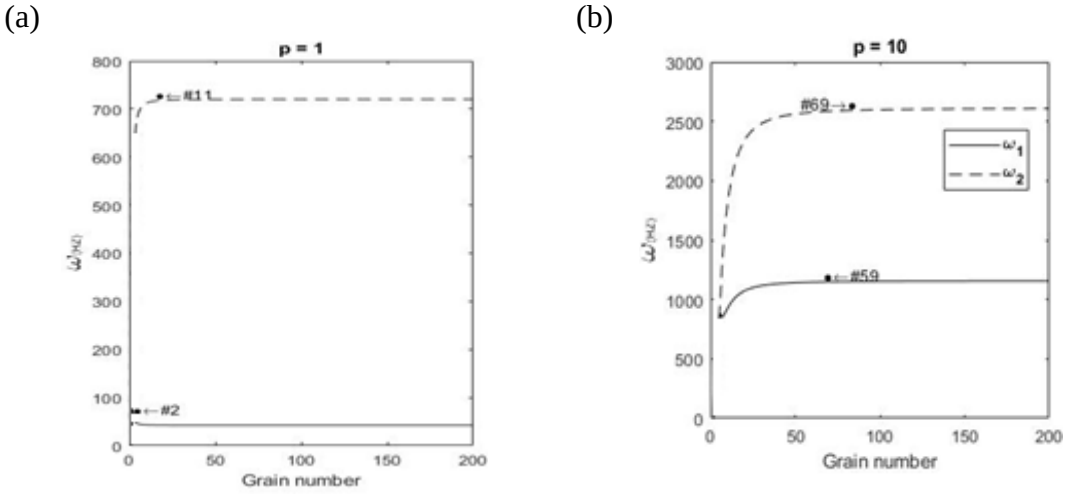

Figure 16. Analysis of the grain number effect on the frequencies (nonlocal Padé) with respect to the length ratio ($\boldsymbol{r^* = 0.029}$) for mode number: (a) $\boldsymbol{p = 1}$ and (b) $\boldsymbol{p = 10}$ $\boldsymbol{\mu_s = 4.28}$.

5. Discussion

The eigenfrequency results of the two branches are gathered together for all approaches (local, nonlocal and continuum models) in Figure 17 and Figure 18. The results are reported as a function of mode number (p) for four typical grain number values ($n \in \{5, 20, 35, 50\}$) and the dimensionless parameters of $r^* \in \{0.058, 0.014, 0.0082, 0.0058\}$ and $k^* \in \{1.875, 480, 4502, 18750\}$. It can be obtained from the figures that the results of the Padé approximation are closer to the results of exact resolution. Another point is that

the eigenfrequencies obtained by the Taylor series are imaginary when the ratio of *n/p* is less than the typical approximate value of 2. Furthermore, the results are investigated for the weak shear interaction ($K_sGA \to 0$) model in Figure 19 and Figure 20.

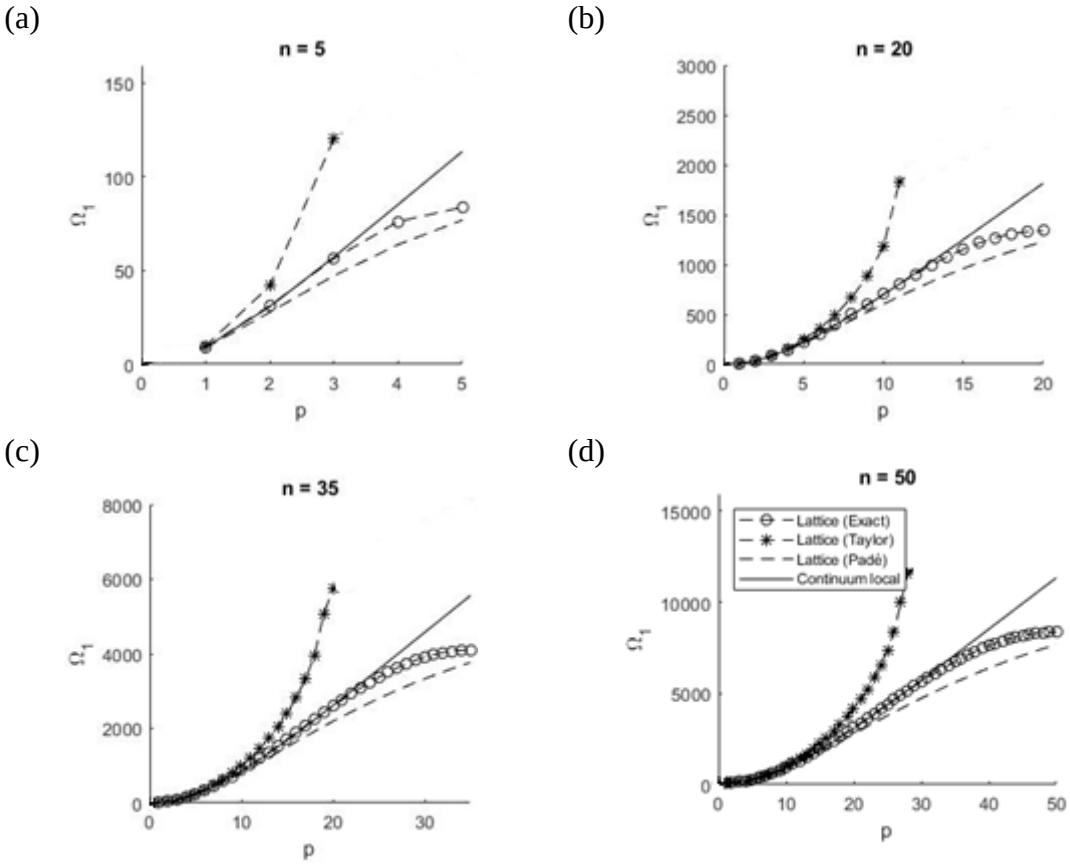

Figure 17. Comparison of the first branch natural frequencies for different approaches as a function of mode number (p) with respect to the grain number: (a) $\boldsymbol{n = 5}$, (b) $\boldsymbol{n = 20}$, (c) $\boldsymbol{n = 35}$ and (d) $\boldsymbol{n = 50}$ for $\boldsymbol{\mu_s = 4.28}$.

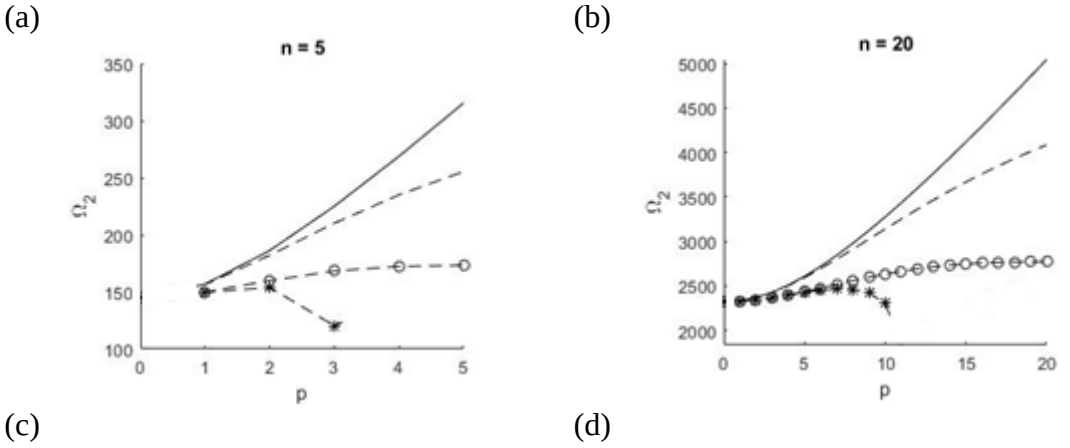

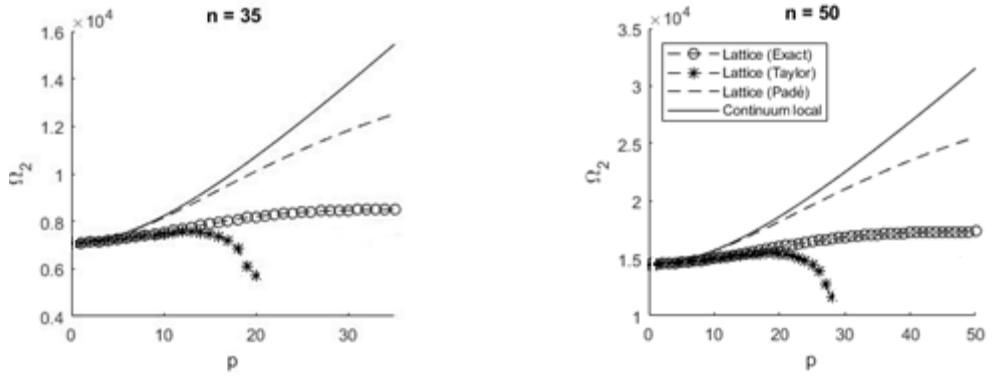

Figure 18. Comparison of the second branch natural frequencies for different approaches as a function of mode number (p) with respect to the grain number: (a) $\mathbf{n = 5}$ and $\mathbf{r^* = 0.058}$, (b) $\mathbf{n = 20}$ and $\mathbf{r^* = 0.014}$, (c) $\mathbf{n = 35}$ and $\mathbf{r^* = 0.0082}$ and (d) $\mathbf{n = 50}$ and $\mathbf{r^* = 0.0058}$ for $\boldsymbol{\mu_s = 4.28}$.

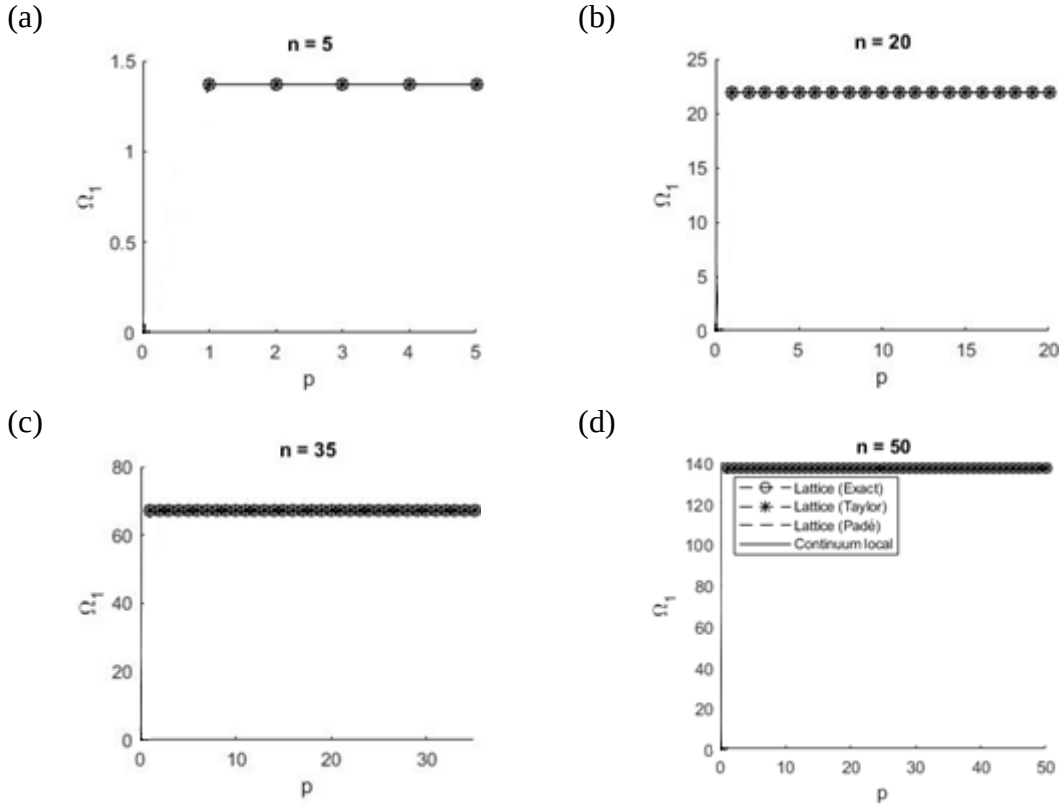

Figure 19. Comparison of the natural frequencies of the first branch for different approaches as a function of mode number (p) with respect to the grain number: (a) $\boldsymbol{n = 5}$ and $\boldsymbol{r^* = 0.058}$, (b) $\boldsymbol{n = 20}$ and $\boldsymbol{r^* = 0.014}$, (c) $\boldsymbol{n = 35}$ and $\boldsymbol{r^* = 0.0082}$ and (d) $\boldsymbol{n = 50}$ and $\boldsymbol{r^* = 0.0058}$ for $\boldsymbol{\mu_s \to \infty}$ (weak shear interaction).

(a) (b)

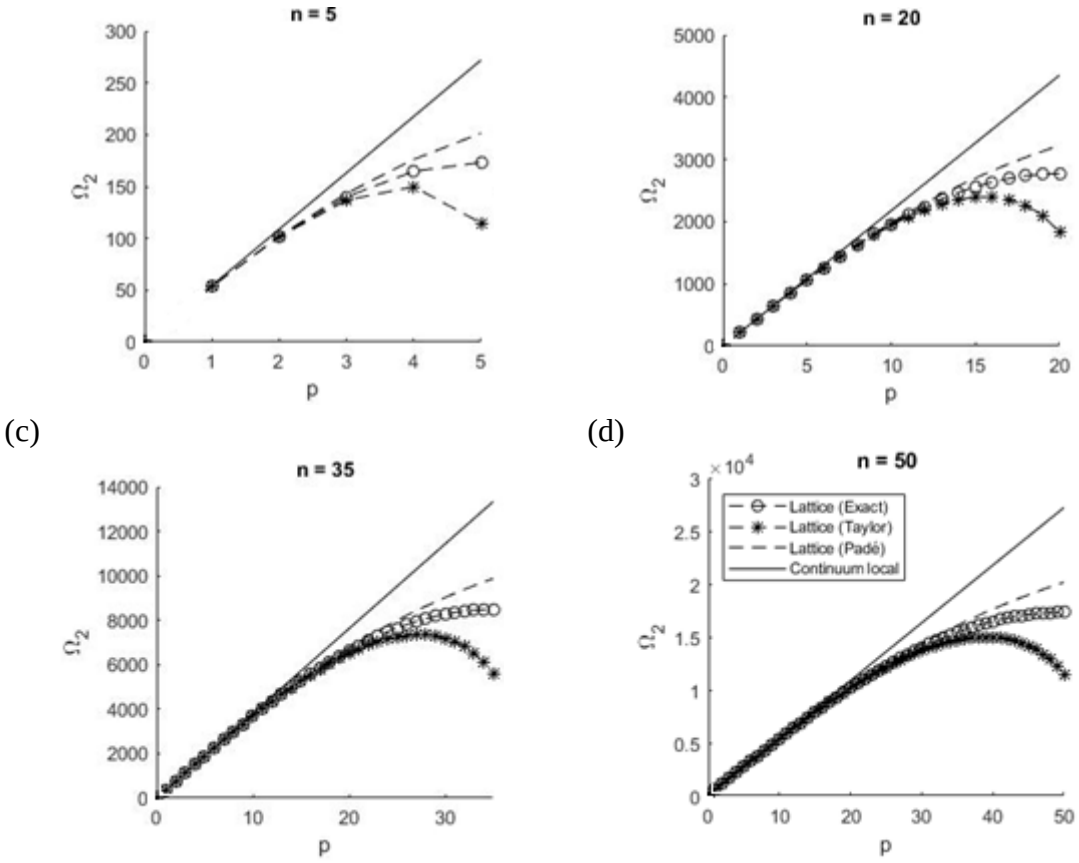

Figure 20. Comparison of the natural frequencies of the second branch for different approaches as a function of mode number (p) with respect to the grain number: (a) $\boldsymbol{n = 5}$ and $\boldsymbol{r^* = 0.058}$, (b) $\boldsymbol{n = 20}$ and $\boldsymbol{r^* = 0.014}$, (c) $\boldsymbol{n = 35}$ and $\boldsymbol{r^* = 0.0082}$ and (d) $\boldsymbol{n = 50}$ and $\boldsymbol{r^* = 0.0058}$ for $\boldsymbol{\mu_s \to \infty}$ (weak shear interaction).

The results of Ω_{10}/Ω_0 on a Winkler type foundation for the first five modes, with length ratio (r^*) varying from *0* to *0.1* are plotted in Figure 21.

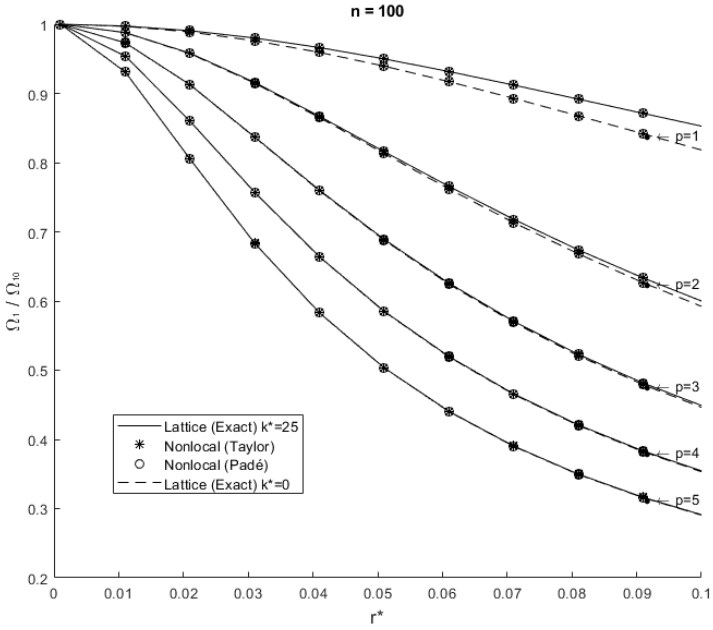

Figure 21. Correction in the first branch natural frequencies regarding Winkler foundation effect.

6. Conclusion

This chapter investigates the macroscopic free vibration behavior of a discrete granular system resting on a Winkler elastic foundation. This microstructured system consists of uniform grains elastically connected by shear and rotation springs. It is shown that the discrete deflection equation of this granular system (Cosserat chain) is mathematically equivalent to the finite difference formulation of a shear deformable Bresse-Timoshenko beam resting on Winkler foundation. Next, the natural frequencies of such a granular model with simply supported ends are first analytically investigated, whatever considered modes through the resolution of a linear difference equation.

The model is continualized to its equivalent continuous system by using two approximate methods based on the Taylor series and Padé approximants (nonlocal continuum). The eigenfrequencies obtained from the continualized beam using the Padé approximation have shown a good performance if compared to the corresponding responses of the Taylor

approximation. Nevertheless, it has been shown that in some cases the approach based on the Taylor approximant provides imaginary values for the two eigenfrequencies branches without a physical sense for the homogenized continuum.

The dependency of the beam dynamic responses to its length ratio is clarified and the equations of the eigenfrequencies are obtained regarding the discrete Cosserat model, local and nonlocal continuous models. Finally, the results of the exact approach for the discrete Cosserat model are compared with those of the nonlocal continuous approach. It is found that the shear stiffness (represented by shear springs) has a significant effect on the vibration frequencies. Furthermore, the scale effects of the granular chain are captured by the continuous gradient elasticity model. This scale effect is related to the grain size with respect to the total length of the Cosserat chain.

CHAPTER 4

Wave Dispersion Analysis of Granular Beam

1. Introduction

The current study focuses on the analysis of wave propagation and the dispersive behavior of mechanical waves in discrete granular media resting on elastic foundations. Misra and Nejadsadeghi [82] studied the dispersive behavior of granular materials in response to elastic deformation waves using the granular micromechanics approach proposed by Misra and Poorsolhjouy [107]. This study can be considered also as the discrete study of the continuous Bresse-Timoshenko beam on the continuous linear elastic foundation (Winkler foundation). Assuming an infinite number of grains, the results lead to the response of a continuous Bresse-Timoshenko beam on an elastic foundation, studied for instance by Wang and Stephens [64], Cheng and Pantelides [118] or Manevich [65]. In particular, the dispersive behavior of continuous Bresse-Timoshenko beam resting on elastic foundation has been specifically addressed by Manevich [65]. The Bresse-Timoshenko continuum limit may be also understood as the long-wave limit of the discrete granular model. The granular chain composed of rigid grains is assumed to interact with a Winkler elastic foundation (Winkler [128]). The wave dispersion of this granular system is derived from the uncoupled equation of motion using a discrete Cosserat theory, based on both rotational and translational degrees of freedom for each grain. For the long-wave limit, the dispersion equation converges towards the continuum model of the Bresse-Timoshenko beam on the Winkler foundation, as treated by Manevich [20]. Also, the results valid for the discrete granular beam could be well compared to those of Pasternak and Mühlhaus [11] and Pichard et al. [60], neglecting the foundation contribution (k=0).

Next, the nonlocal dispersion results are obtained through the homogenization of the fourth-order difference equation of the system by applying the Taylor series and Padé approximation. Finally, a comparison between the discrete and the enriched continuous model will be discussed and conclusions sections are presented. A comprehensive dispersion analysis is done regarding the local and nonlocal deflection equations of this 1D granular chain. Based on the presented parametric study, the wave dispersion curves for the discrete lattice models are compared to the corresponding continuum models (Bresse-Timoshenko). The results also compared to molecular dynamics of the flexural behavior in carbon nanotubes with acceptable coincidence. The results of this study is a generalization for the outcome of Pasternak and Mühlhaus [11] and Pichard et al. [60] valid for the wave propagation of elastic chain without elastic foundation.

2. Discrete Approach via Exact Solution

Dispersion of propagation waves would influence the media if the wavelength is of the same magnitude order as the characteristic spacing of the dominant source of heterogeneity. In order to capture wave dispersion, continuum models need to be equipped with appreciate terms that capture the lower scale behavior (Domenico and Askes [129]).

Recalling, the dynamic equation for the deflection of the granular chain resting on Winkler elastic foundation (granular lattice model)

$$[EI\delta_2{}^2 - \left(\rho I\partial_t{}^2 + \frac{kEI}{K_sGA} + \frac{EI\rho\partial_t{}^2}{K_sG}\right)\delta_2 + \left(k + \rho A\partial_t{}^2\right)\delta_0 + \frac{k\rho I\partial_t{}^2}{K_sGA} + \frac{\rho^2 I\partial_t{}^4}{K_sG}]w_i = 0 \tag{205}$$

To satisfy this fourth-order mixed difference-differential equation, a fundamental solution in the harmonic form could be considered as follow:

$$\boldsymbol{w_i = \beta e^{j(\omega t - k_w x_i)}} \tag{206}$$

Substitution of the expression Eq. (206) into Eq. (205) provides the algebraic equation as:

$$\begin{aligned}\boldsymbol{\beta e^{j(\omega t - k_w x_i)}} &\left[\left(e^{2ak_wj} - 4e^{ak_wj} + 6 - 4e^{-ak_wj} + e^{-2ak_wj}\right)\right. \\ + a^2\left(\frac{\rho\omega^2}{E} - \frac{k}{K_sGA} + \frac{\rho\omega^2}{K_sG}\right)&\left(e^{ak_wj} - 2 + e^{-ak_wj}\right) + a^4\left(\frac{k}{4EI} - \frac{\rho A\omega^2}{4EI}\right)\left(e^{ak_wj} + 2 + e^{-ak_wj}\right) \\ &\left. + a^4\left(-\frac{k\rho\omega^2}{EK_sGA} + \frac{\rho^2\omega^4}{EK_sG}\right)\right] = 0\end{aligned} \tag{207}$$

The following biquadratic equation expressed by the angular frequency could be obtained from Eq. (207):

$$\begin{aligned}[\rho a^2]\omega^4 - 4&\left[(K_sG + E)\sin^2\left(\frac{ak_w}{2}\right) + \frac{Aa^2K_sG}{4I}\cos^2\left(\frac{ak_w}{2}\right) + \frac{ka^2}{4A}\right]\omega^2 \\ + &\left[16\frac{EK_sG}{\rho a^2}\sin^4\left(\frac{ak_w}{2}\right) + k\left(\frac{4E}{\rho A}\sin^2\left(\frac{ak_w}{2}\right) + \frac{a^2K_sG}{\rho I}\cos^2\left(\frac{ak_w}{2}\right)\right)\right] = 0\end{aligned} \tag{208}$$

Neglecting the Winkler foundation ($k = 0$), the aforementioned equation leads to the results obtained by Pasternak and Mühlhaus [11] (Eq. (209)).

$$[MN]\omega^4 - 4\left[(NS + MC)\sin^2\left(\frac{ak_w}{2}\right) + \frac{MSa^2}{4}\cos^2\left(\frac{ak_w}{2}\right)\right]\omega^2 + \left[16SC\sin^4\left(\frac{ak_w}{2}\right)\right] = 0 \tag{209}$$

with $M = \rho Aa$ and $N = I_m = \rho Ia$. Two asymptotic cases for a granular chain could be obtained from Eq. (208) supposing pure shear and or pure bending. Assuming only shear interaction ($E = 0$)

$$[\rho a^2]\omega^4 - 4\left[K_sG\sin^2\left(\frac{ak_w}{2}\right) + \frac{Aa^2K_sG}{4I}\cos^2\left(\frac{ak_w}{2}\right) + \frac{ka^2}{4A}\right]\omega^2 + \left[\frac{a^2K_sGk}{\rho I}\cos^2\left(\frac{ak_w}{2}\right)\right] = 0 \tag{210}$$

This equation leads to the following quadratic equation of Schwartz et al. [59] with respect to the angular frequency by omitting Winkler foundation ($k = 0$):

$$\left[\boldsymbol{\omega^2 - \omega_0^2\left(sin^2\left(\frac{ak_w}{2}\right) + \alpha\, cos^2\left(\frac{ak_w}{2}\right)\right)}\right]\boldsymbol{\omega^2 = 0} \tag{211}$$

in which $\omega_0^2 = \frac{4S}{M}$ and $\alpha = \frac{Mr^2}{I_m}$. On the other hand, considering only the rotational effect ($G = 0$) in Eq. (208) leads to

$$[\boldsymbol{\rho a^2}]\boldsymbol{\omega^4} - \mathbf{4}\left[\boldsymbol{E\, sin^2\left(\frac{ak_w}{2}\right) + \frac{ka^2}{4A}}\right]\boldsymbol{\omega^2} + \left[\boldsymbol{\frac{4Ek}{\rho A}\, sin^2\left(\frac{ak_w}{2}\right)}\right] = \mathbf{0} \tag{212}$$

For the continuum case by assuming an infinite number of grains Eq. (208) leads to the quartic equation obtained by Manevich [65] as follows

$$[\boldsymbol{\mathcal{X}}]\boldsymbol{\varpi^4} - [\mathbf{1} + (\mathbf{1} + \boldsymbol{\mathcal{X}})\boldsymbol{\hbar^2} + \boldsymbol{w_1\mathcal{X}}]\boldsymbol{\varpi^2} + [\boldsymbol{w_1}(\mathbf{1} + \boldsymbol{\mathcal{X}\hbar^2}) + \boldsymbol{\hbar^4}] = \mathbf{0} \tag{213}$$

in which $w_1 = \frac{I}{EA^2}k$, $\mathcal{X} = \frac{E}{K_S G}$, $\varpi^2 = \frac{I\rho}{EA}\omega^2$ and $\hbar^2 = \frac{I}{A}{k_w}^2$. Introducing the non-dimensional quantities as follows:

$$\boldsymbol{\Omega_{b,s} = \frac{a}{c_{b,s}}\omega} \;,\; \boldsymbol{\mu_s = \frac{E}{K_s\, G}} \;,\; \boldsymbol{r^* = \frac{1}{a}\sqrt{\frac{I}{A}}} \;,\; \boldsymbol{k^* = \frac{ka^4}{EI}} \tag{214}$$

where c_0 is the one-dimensional wave velocity and could be defined by either shear or bending beam parameters as $c_{bending} = \sqrt{\frac{EI}{\rho A a^2}}$ and $c_{shear} = \sqrt{\frac{K_s\, G}{\rho}}$. Eq. (208) could be rewritten in the following form

$$\begin{aligned}\boldsymbol{\Omega_b{}^4} - \left[\left(\frac{\mathbf{4}}{\boldsymbol{\mu_s r^{*2}}} + \frac{\mathbf{4}}{\boldsymbol{r^{*2}}}\right)\boldsymbol{sin^2\left(\frac{ak_w}{2}\right)} + \frac{\mathbf{1}}{\boldsymbol{\mu_s r^{*4}}}\boldsymbol{cos^2\left(\frac{ak_w}{2}\right)} + \boldsymbol{k^*}\right]\boldsymbol{\Omega_b{}^2} \\ + \left[\mathbf{16}\frac{\mathbf{1}}{\boldsymbol{\mu_s r^{*4}}}\boldsymbol{sin^4\left(\frac{ak_w}{2}\right)} + \boldsymbol{k^*}\left(\frac{\mathbf{4}}{\boldsymbol{r^{*2}}}\boldsymbol{sin^2\left(\frac{ak_w}{2}\right)} + \frac{\mathbf{1}}{\boldsymbol{\mu_s r^{*4}}}\boldsymbol{cos^2\left(\frac{ak_w}{2}\right)}\right)\right] = \mathbf{0}\end{aligned} \tag{215}$$

or through the shear wave velocity definition

$$\Omega_s{}^4 - \left[(4+4\mu_s)\sin^2\left(\frac{ak_w}{2}\right) + \frac{1}{r^{*2}}\cos^2\left(\frac{ak_w}{2}\right) + k^*\mu_s r^{*2}\right]\Omega_s{}^2 + \left[16\,\mu_s \sin^4\left(\frac{ak_w}{2}\right) + k^*\mu_s\left(4\mu_s r^{*2}\sin^2\left(\frac{ak_w}{2}\right) + \cos^2\left(\frac{ak_w}{2}\right)\right)\right] = 0 \tag{216}$$

In order to know the nature of the results for Eq. (208), the sign of the coefficients in the characteristic equation need to be clarified.

$\forall\, E, G, k, I, A, K_s, a, k_w$:

$$\rho a^2 > 0,$$

$$-4\left((K_sG+E)\sin^2\left(\frac{ak_w}{2}\right) + \frac{Aa^2K_sG}{4I}\cos^2\left(\frac{ak_w}{2}\right) + \frac{ka^2}{4A}\right) < 0, \tag{217}$$

$$16\frac{EK_sG}{\rho a^2}\sin^4\left(\frac{ak_w}{2}\right) + k\left(\frac{4E}{\rho A}\sin^2\left(\frac{ak_w}{2}\right) + \frac{a^2K_sG}{\rho I}\cos^2\left(\frac{ak_w}{2}\right)\right) > 0$$

The discriminant (Δ) of Eq. (208) would be obtained as follows

$$\begin{aligned}\Delta_1 = {} & \left[(K_sG-E)\sin^2\left(\frac{ak_w}{2}\right)\right]^2 + \left[\frac{Aa^2K_sG}{4I}\cos^2\left(\frac{ak_w}{2}\right) - \frac{ka^2}{4A}\right]^2 \\ & + \left[2E\sin^2\left(\frac{ak_w}{2}\right)\right]\left[\frac{Aa^2K_sG}{4I}\cos^2\left(\frac{ak_w}{2}\right) - \frac{ka^2}{4A}\right] \\ & + \left[2K_sG\sin^2\left(\frac{ak_w}{2}\right)\right]\left[\frac{Aa^2K_sG}{4I}\cos^2\left(\frac{ak_w}{2}\right) + \frac{ka^2}{4A}\right]\end{aligned} \tag{218}$$

Considering Eq. (218) as a function of Winkler elastic foundation leads to the following parabolic equation

$$\begin{aligned}f(k) = {} & \left(\left[\frac{a^2}{4A}\right]^2\right)k^2 - \left(\frac{a^4K_sG}{8I}\cos^2\left(\frac{ak_w}{2}\right) + (E-K_sG)\left(\frac{a^2}{2A}\right)\sin^2\left(\frac{ak_w}{2}\right)\right)k \\ & + \left(\left(\frac{Aa^2K_sG}{4I}\cos^2\left(\frac{ak_w}{2}\right)\right)\left(\frac{Aa^2K_sG}{4I}\cos^2\left(\frac{ak_w}{2}\right) + 2(E+K_sG)\sin^2\left(\frac{ak_w}{2}\right)\right)\right. \\ & \left. + \left[(K_sG-E)\sin^2\left(\frac{ak_w}{2}\right)\right]^2\right)\end{aligned} \tag{219}$$

$f(0)$ leads to the result obtained by Pasternak and Mühlhaus [11]. Here an attempt is made to identify the effect of adding elastic foundation to the model, for the dynamic response of the system.

$\forall\, \boldsymbol{E, G, I, A, K_s, a, k_w}$:

$$\left[\frac{a^2}{4A}\right]^2 > 0\,,\ \Delta_2 = -\frac{\left(a^3 K_s G\right)^2}{16AI} sin^2(ak_w) < 0 \tag{220}$$

It can be concluded that the parabolic equation of Eq. (219) is upward with the minimum positive value of $\frac{-4A^2\Delta_2}{a^4}$. On the other hand, the behavior of Eq. (218) depending on k_w is studied for any physical parameters of the system. All terms of the discriminant (Δ_1) are positive except the third one. Therefore, the discriminant of Eq. (208) (Δ_1) is always positive for any values of Winkler elastic foundation and mode number. This fact with regard to Eq. (217) leads to two real positive solutions for Eq. (208) expressed by natural frequency.

Here the nature of the wave is tried to be clarified. Substituting the exponential form of Eq. (206) for θ_i and w_i by $\theta_i = \alpha e^{j(\omega t - k_w x_i)}$ and $w_i = \beta e^{j(\omega t - k_w x_i)}$ in the equilibrium equation system of Eq. (69) while assuming $\omega = k_w v_p$, leads to:

$$\begin{aligned} -4\beta S \sin\left(\frac{ak_w}{2}\right)^2 - a\alpha Sj \sin(ak_w) - a\beta k + \beta m {k_w}^2 {v_p}^2 = 0, \\ -4\alpha C \sin\left(\frac{ak_w}{2}\right)^2 + a\beta Sj \sin(ak_w) - a^2 \alpha S \cos\left(\frac{ak_w}{2}\right)^2 - \alpha I_m {k_w}^2 {v_p}^2 = 0 \end{aligned} \tag{221}$$

in which v_p is the phase velocity. The dynamic response of this coupled system of the equation can be obtained in the following form

$$\omega^2 = \frac{\sigma \pm \sqrt{\sigma^2 - 4\tau}}{2} \tag{222}$$

where σ and τ are represented by

$$\boldsymbol{\sigma = \frac{4}{\rho a^2}(K_s G + E)\, sin^2\left(\frac{ak_w}{2}\right) + \frac{AK_s G}{\rho I} cos^2\left(\frac{ak_w}{2}\right) + \frac{k}{\rho A}}\ ;$$
$$\boldsymbol{\tau = 16\frac{EK_s G}{\rho^2 a^4} sin^4\left(\frac{ak_w}{2}\right) + \frac{k}{\rho a^2}\left(\frac{4E}{\rho A} sin^2\left(\frac{ak_w}{2}\right) + \frac{a^2 K_s G}{\rho I} cos^2\left(\frac{ak_w}{2}\right)\right)} \quad (223)$$

Regarding the two positive responses of Eq. (153), the phase velocity could be obtained for $k_w \rightarrow 0$ as follows

$$\boldsymbol{v_p = \sqrt{\frac{\sigma \pm \sqrt{\sigma^2 - 4\tau}}{2{k_w}^2}} \xrightarrow{k_w \to 0} v_p \approx \sqrt{\frac{\left(\frac{AK_s G}{\rho I} + \frac{k}{\rho A}\right) \pm \left|\frac{AK_s G}{\rho I} - \frac{k}{\rho A}\right|}{2{k_w}^2}}} \quad (224)$$

The ratio of the amplitudes (α/β) can be found from Eq. (221). The first relation leads to

$$\boldsymbol{\frac{\alpha}{\beta} = j\frac{4S \sin\left(\frac{ak_w}{2}\right)^2 + ak - m{k_w}^2 {v_p}^2}{aS \sin(ak_w)}} \quad (225)$$

Supposing $k = 0$, Eq. (225) leads to the result obtained by Pasternak and Mühlhaus [11]. According to Eq. (224) and the positive root of Eq. (225) for the low value of mode number (long-wave limit), only the rotational wave could propagate in the system.

$$\boldsymbol{k_w \to 0}: \quad \boldsymbol{\frac{\alpha}{\beta} \approx j\frac{ak - \frac{aA^2 K_s G}{I}}{aS\, sin(ak_w)} \approx \infty} \text{ (Rotational wave)} \quad (226)$$

While regarding the other branch (the negative root), the shear term of the wave appears as follows

$$\boldsymbol{k_w \to 0}: \quad \boldsymbol{\frac{\alpha}{\beta} \approx j\frac{2}{a} tan\left(\frac{ak_w}{2}\right) \approx 0} \text{ (Shear wave)} \quad (227)$$

The oscillations here are the displacement of the grains in directions perpendicular to the propagation of the wave. Therefore, with the foundation, the wave nature is mixed of both types that one is dominant to the other and it can be considered as a shear-rotational wave.

The mode number cannot exceed the grain number value or in the other words, the wave length cannot be shorter than the grain size. Thus, the assumption of $k_w \to \infty$ can be true only for an infinite number of grains or continuum beams.

On the other hand, by neglecting the Winkler foundation, the phase velocity for a small value of mode number leads to

$$\boldsymbol{v_{p1}} = \sqrt{\frac{\boldsymbol{\sigma - \sqrt{\sigma^2 - 4\,\tau}}}{\boldsymbol{2{k_w}^2}}} \xrightarrow{k_w \to 0} \boldsymbol{v_p \propto k_w};$$

$$\boldsymbol{v_{p2}} = \sqrt{\frac{\boldsymbol{\sigma + \sqrt{\sigma^2 - 4\,\tau}}}{\boldsymbol{2{k_w}^2}}} \xrightarrow{k_w \to 0} \boldsymbol{v_p \propto \frac{1}{k_w}} \tag{228}$$

Using again the coefficient ratio of Eq. (225) for the long waves and $k = 0$ leads to the dominancy of the shear component when taking into account the first spectrum of the results of Eq. (227) as follows:

$$\boldsymbol{k_w \to 0}\text{: } \boldsymbol{\frac{\alpha}{\beta} \approx 0} \quad \text{(Shear wave)} \tag{229}$$

While for the second spectrum or the higher frequency branch, the rotational wave is dominated by the system.

$$\boldsymbol{k_w \to 0}\text{: } \boldsymbol{\frac{\alpha}{\beta} \approx \infty} \quad \text{(Rotational wave)} \tag{230}$$

Thus, without the Winkler elastic foundation, the wave nature is also combined of both types (Pasternak and Mühlhaus [11]).

On the other hand, the mixed differential-difference equation for a Hencky beam problem or discrete Euler-Bernoulli beam theory has been obtained as

$$\boldsymbol{\left[EI{\delta_2}^2 + \rho A{\partial_t}^2\right]w_i = 0} \tag{231}$$

Regarding the properties of Eq. (6), Eq. (231) leads to

$$\boldsymbol{EI}\left(\boldsymbol{e}^{2\boldsymbol{ak}_{\boldsymbol{wj}}}-\boldsymbol{4e}^{\boldsymbol{ak}_{\boldsymbol{wj}}}+\boldsymbol{6}-\boldsymbol{4e}^{-\boldsymbol{ak}_{\boldsymbol{wj}}}+\boldsymbol{e}^{-2\boldsymbol{ak}_{\boldsymbol{wj}}}\right)-\boldsymbol{\rho Aa}^{\boldsymbol{4}}\boldsymbol{\omega}^{\boldsymbol{2}}=\boldsymbol{0} \tag{232}$$

This equation can be simplified as

$$\frac{\boldsymbol{I}}{\boldsymbol{a}^{\boldsymbol{4}}}(\boldsymbol{2}\cos(\boldsymbol{2ak}_{\boldsymbol{w}})-\boldsymbol{8}\cos(\boldsymbol{ak}_{\boldsymbol{w}})+\boldsymbol{6})-\frac{\boldsymbol{\rho A}}{\boldsymbol{E}}\boldsymbol{\omega}^{\boldsymbol{2}}=\boldsymbol{0} \tag{233}$$

the quadratic wave dispersive equation would be obtained as follows in a dimensionless form with respect to the angular frequency of the granular chain with pure bending interactions:

$$\boldsymbol{\Omega_b}^{\boldsymbol{2}}=\boldsymbol{16}\,\boldsymbol{sin}^{\boldsymbol{4}}\left(\frac{\boldsymbol{ak}_{\boldsymbol{w}}}{\boldsymbol{2}}\right) \tag{234}$$

This equation associated with the discrete granular chain may be efficiently approximated by a nonlocal equation associated with the wave propagation in a nonlocal continuous beam.

On the other hand, let's consider the case of a granular chain with predominant bending interactions ($S \to \infty$) and neglecting the Winkler foundation ($k = 0$). In this case, the wave propagation equation expressed by transverse deflection for the granular system (Eq. (205)) leads to

$$[\boldsymbol{EI\delta_2}^{\boldsymbol{2}}+\boldsymbol{\partial_t}^{\boldsymbol{2}}(\boldsymbol{\rho A\delta_0}-\boldsymbol{\rho I\delta_2})]\boldsymbol{w_i}=\boldsymbol{0} \tag{235}$$

This equation leads to the following relation by using the definitions of Eq. (**6**)

$$\begin{aligned}&\boldsymbol{\beta e}^{\boldsymbol{j}(\boldsymbol{\omega t}-\boldsymbol{k}_{\boldsymbol{w}}\boldsymbol{x}_{\boldsymbol{i}})}[\left(\boldsymbol{e}^{\boldsymbol{2ak}_{\boldsymbol{wj}}}-\boldsymbol{4e}^{\boldsymbol{ak}_{\boldsymbol{wj}}}+\boldsymbol{6}-\boldsymbol{4e}^{-\boldsymbol{ak}_{\boldsymbol{wj}}}+\boldsymbol{e}^{-\boldsymbol{2ak}_{\boldsymbol{wj}}}\right)\\&+\boldsymbol{a}^{\boldsymbol{2}}\left(\frac{\boldsymbol{\rho\omega}^{\boldsymbol{2}}}{\boldsymbol{E}}\right)\left(\boldsymbol{e}^{\boldsymbol{ak}_{\boldsymbol{wj}}}-\boldsymbol{2}+\boldsymbol{e}^{-\boldsymbol{ak}_{\boldsymbol{wj}}}\right)+\boldsymbol{a}^{\boldsymbol{4}}\left(-\frac{\boldsymbol{\rho A\omega}^{\boldsymbol{2}}}{\boldsymbol{4EI}}\right)\left(\boldsymbol{e}^{\boldsymbol{ak}_{\boldsymbol{wj}}}+\boldsymbol{2}+\boldsymbol{e}^{-\boldsymbol{ak}_{\boldsymbol{wj}}}\right)]=\boldsymbol{0}\end{aligned} \tag{236}$$

Which can be simplified as

$$\boldsymbol{16}\,\boldsymbol{sin}^{\boldsymbol{4}}\left(\frac{\boldsymbol{ak}_{\boldsymbol{w}}}{\boldsymbol{2}}\right)+\frac{\boldsymbol{a}^{\boldsymbol{2}}}{\boldsymbol{A}}\left(\frac{\boldsymbol{\rho A\omega}^{\boldsymbol{2}}}{\boldsymbol{E}}\right)\left(\boldsymbol{4}\,\boldsymbol{sin}^{\boldsymbol{2}}\left(\frac{\boldsymbol{ak}_{\boldsymbol{w}}}{\boldsymbol{2}}\right)\right)-\frac{\boldsymbol{a}^{\boldsymbol{4}}}{\boldsymbol{I}}\left(\frac{\boldsymbol{\rho A\omega}^{\boldsymbol{2}}}{\boldsymbol{E}}\right)\left(\boldsymbol{cos}^{\boldsymbol{2}}\left(\frac{\boldsymbol{ak}_{\boldsymbol{w}}}{\boldsymbol{2}}\right)\right)=\boldsymbol{0} \tag{237}$$

Using Eq. (214) for the non-dimensional frequency with $c_{bending}$, leads to

$$\boldsymbol{\Omega_b}^2 = \frac{\mathbf{16}\,\boldsymbol{sin}^4\left(\frac{\boldsymbol{ak_w}}{\mathbf{2}}\right)}{\boldsymbol{cos}^2\left(\frac{\boldsymbol{ak_w}}{\mathbf{2}}\right) - \mathbf{4}\boldsymbol{r}^{*2}\,\boldsymbol{sin}^2\left(\frac{\boldsymbol{ak_w}}{\mathbf{2}}\right)} \tag{238}$$

Neglecting the rotational inertia terms leads to the following equation which is slightly different from Eq. (234).

$$\boldsymbol{\Omega_b}^2 = \mathbf{16}\,\boldsymbol{sin}^2\left(\frac{\boldsymbol{ak_w}}{\mathbf{2}}\right)\boldsymbol{tan}^2\left(\frac{\boldsymbol{ak_w}}{\mathbf{2}}\right) \tag{239}$$

For an infinite number of grains, the granular chain asymptotically behaves as a gradient elasticity Rayleigh model (where the bending interactions are predominant). Eq. (235) with terms of translation and rotation inertia leads to

$$[\boldsymbol{EI\partial_x^4} - \boldsymbol{\rho I\partial_t^2\partial_x^2} + \boldsymbol{\rho A\partial_t^2}]\boldsymbol{w} = \mathbf{0} \tag{240}$$

Lu et al. [130] investigated the wave propagation properties in a nonlocal Euler-Bernoulli beam (Eq. (241)), based on a differential nonlocal model introduced by Eringen [71] for one-dimensional media. Eq. (240) could be compared well by Lu et al. [130] which obtained in their study as follows

$$\left[\boldsymbol{EI\partial_x^4} - \boldsymbol{\rho A\partial_t}^2((\boldsymbol{e_0 d_0})^2\boldsymbol{\partial_x^2} - \mathbf{1})\right]\boldsymbol{w} = \mathbf{0} \tag{241}$$

e_0 is the nondimensional calibration parameter of the Eringen nonlocal approach. This parameter adjusts in order to achieve a good dispersive curve at the end of the Brillouin zone and d_0 is an internal characteristic length. Eq. (241) is equivalent to considering an Eringen's based nonlocal model by

$$\boldsymbol{M} - \boldsymbol{l_c^2 M''} = \boldsymbol{EIw''} \quad ; \quad \boldsymbol{M''} = -\boldsymbol{\rho A\ddot{w}} \tag{242}$$

Here l_c is the characteristic length of the nonlocal model. Regarding the fourth-order differential equation of the nonlocal beam (Eq. (241)) and considering the solution of the deflection in a harmonic form, the substitution of Eq. (206) in Eq. (242) gives

$$\boldsymbol{EIk_w^4 - \rho A\omega^2(1 + (ae_0k_w)^2) = 0} \tag{243}$$

in which e_0 could be defined by $e_0 = l_c/a$. The approximate angular frequencies calculated from Eringen's nonlocal beam approach could be obtained by:

$$\boldsymbol{\Omega_b^2 = \frac{(ak_w)^4}{1 + (ak_w)^2 e_0^2}} \tag{244}$$

where $\boldsymbol{\Omega_b}$ is the dimensionless parameter of frequency regarding the bending wave velocity definition. Comparing Eq. (244) with the one issued of Eringen's model (Eringen [71]) applied to beam mechanics, (Eq. (234)) leads to the two fundamental values that differ for the low and high natural frequencies. These two values are obtained as follows

$$\textbf{for } \boldsymbol{ak_w \to 0}: \quad \boldsymbol{(ak_w)^4\left(1 - \frac{(ak_w)^2}{24}\right)^4 = \frac{(ak_w)^4}{1 + (ak_w)^2 e_0^2} \Rightarrow e_0 = \sqrt{\frac{1}{6}} \approx 0.408} \tag{245}$$

$$\textbf{for } \boldsymbol{ak_w = \pi}: \quad \boldsymbol{16 = \frac{\pi^4}{1 + (\pi)^2 (e_0)^2} \Rightarrow e_0 = \sqrt{\frac{\pi^2}{16} - \frac{1}{\pi^2}} \approx 0.718} \tag{246}$$

The specific values of e_0 =0.408 and e_0 =0.718 obtained in Eq. (245) and (246) could be verified well also by Challamel et al. [131].

Assuming only shear effects (pure bending beam) ($\frac{EI}{K_s GAL^2} \to 0$) by considering $EI \to 0$ and neglecting the Winkler elastic foundation ($k = 0$), Eq. (205) leads to

$$\left[(A\delta_0 - I\delta_2)\partial_t^2 + \frac{\rho I \partial_t^4}{K_s G}\right] w_i = 0 \tag{247}$$

This equation leads to the following relation by using Eq. (6)

$$\boldsymbol{\beta e^{j(\omega t-k_w x_i)}\left[I\left(e^{ak_w j}-2+e^{-ak_w j}\right)-\frac{Aa^2}{4}\left(e^{ak_w j}+2+e^{-ak_w j}\right)+\frac{\rho I a^2}{K_s G}\omega^2\right]=0} \tag{248}$$

Which can be simplified as

$$\boldsymbol{4\,sin^2\left(\frac{ak_w}{2}\right)+\frac{Aa^2}{I}cos^2\left(\frac{ak_w}{2}\right)-\frac{\rho a^2}{K_s G}\omega^2=0} \tag{249}$$

Using Eq. (214) for the non-dimensional frequency with c_{shear}, one could be found as follows

$$\boldsymbol{\Omega_s{}^2=4\,sin^2\left(\frac{ak_w}{2}\right)+\frac{1}{r^{*2}}cos^2\left(\frac{ak_w}{2}\right)} \tag{250}$$

3. Continuous Approach

3.1. Exact Solution

From the continuum model, the wave propagation equation regarding the local Bresse-Timoshenko could be obtained as:

$$\boldsymbol{\left[EI\partial_x{}^4+\left(-\rho I\partial_t{}^2-\frac{kEI}{K_sGA}-\frac{EI\rho\partial_t{}^2}{K_sG}\right)\partial_x{}^2+\left(k+\rho A\partial_t{}^2\right)+\frac{k\rho I\partial_t{}^2}{K_sGA}+\frac{\rho^2 I\partial_t{}^4}{K_sG}\right]w=0} \tag{251}$$

Substituting the fundamental solution of $w=We^{j(\omega t-k_w x)}$ (the wave propagation equation in the harmonic form for the continuum beam model) in Eq. (251) leads to:

$$\boldsymbol{\left(\frac{\rho^2}{EK_sG}\right)\omega^4-\left(\left(\frac{\rho}{E}+\frac{\rho}{K_sG}\right)\left(k_w{}^2\right)+\frac{\rho A}{EI}+\frac{k\rho}{EK_sGA}\right)\omega^2+\left(k_w{}^4+\frac{k}{K_sGA}\left(k_w{}^2\right)+\frac{k}{EI}\right)=0} \tag{252}$$

On the other hand, for an infinite number of grains assuming $a\to 0$, the discrete dispersive relation of Eq. (208) leads to the biquadratic equation of Eq. (252). This dispersion equation for the continuum beam can be compared well also by the one obtained by Manevich [65] on Winkler elastic foundations (Eq. (213)).

3.2. Approximate Solution via Polynomial Expansion

In this section, the continualization of the difference equation of Eq. (205) is investigated using polynomial expansions. The finite difference terms are replaced by the corresponding Taylor series and lead to a Cosserat continuum theory.

Using this nonlocal solution allows to obtain the continuous approximate model of the discrete equations holds for a sufficiently smooth deflection function (Salvadori [126])(see for instance the application of this method for nonlinear lattices by Kruskal and Zabusky [132]):

$$w_i = w(x = ia);$$
$$w_{i+1} = \sum_{k=0}^{\infty} \frac{a^k \partial_x^k}{k!} w(x) = \left[1 + \frac{a\partial_x^1}{1!} + \frac{a^2\partial_x^2}{2!} + \frac{a^3\partial_x^3}{3!} + \cdots\right] w(x) = e^{a\partial_x} w(x);\ \mathbf{x = ia} \tag{253}$$

The pseudodifferential operators ${\delta_2}^2, \delta_2$ and δ_0 could be expanded as:

$$\begin{aligned} {\delta_2}^2 w &= \left(\frac{e^{2a\partial_x} - 4e^{a\partial_x} + 6 - 4e^{-a\partial_x} + e^{-2a\partial_x}}{a^4}\right) w \\ &= \left(1 + \frac{a^2\partial_x^2}{6} + \frac{a^4\partial_x^4}{80} + \frac{17a^6\partial_x^6}{30240} + O\left(a^8\partial_x^8\right)\right)\partial_x^4 w; \\ \delta_2 w &= \left(\frac{e^{a\partial_x} - 2 + e^{-a\partial_x}}{a^2}\right) w = \left(1 + \frac{a^2\partial_x^2}{12} + \frac{a^4\partial_x^4}{360} + \frac{a^6\partial_x^6}{20160} + O\left(a^8\partial_x^8\right)\right)\partial_x^2 w; \\ \delta_0 w &= \left(\frac{e^{a\partial_x} + 2 + e^{-a\partial_x}}{4}\right) w = \left(1 + \frac{a^2\partial_x^2}{4} + \frac{a^4\partial_x^4}{48} + \frac{a^6\partial_x^6}{1440} + O\left(a^8\partial_x^8\right)\right) w \end{aligned} \tag{254}$$

A continualization procedure up to the order a^6 from the mixed difference-differential equation of Eq. (205) through the substitution of the expansion series of Eq. (175) leads to the following higher-order gradient system:

$$\left[EI\left(1+\frac{a^2}{6}\partial_x^2+\frac{a^4}{80}\partial_x^4+\frac{17a^6\partial_x^6}{30240}\right)\partial_x^4\right.$$
$$-\left(\rho I{\partial_t}^2+\frac{kEI}{K_sGA}+\frac{EI\rho}{K_sG}{\partial_t}^2\right)\left(1+\frac{a^2}{12}\partial_x^2+\frac{a^4}{360}\partial_x^4+\frac{a^6\partial_x^6}{20160}\right)\partial_x^2$$
$$\left.+\left(k+\rho A{\partial_t}^2\right)\left(1+\frac{a^2}{4}\partial_x^2+\frac{a^4\partial_x^4}{48}+\frac{a^6\partial_x^6}{1440}\right)+\left(\frac{k\rho I}{K_sGA}{\partial_t}^2+\frac{\rho^2 I}{K_sG}{\partial_t}^4\right)\right]w=0 \quad (255)$$

which leads to the following nonlocal dispersion equation:

$$\left[\frac{17EIa^6}{30240}\right]w^{(10)}+\left[\frac{EIa^4}{80}-\left(\rho I{\partial_t}^2+\frac{kEI}{K_sGA}+\frac{EI\rho}{K_sG}{\partial_t}^2\right)\frac{a^6}{20160}\right]w^{(8)}$$
$$+\left[\frac{EIa^2}{6}-\left(\rho I{\partial_t}^2+\frac{kEI}{K_sGA}+\frac{EI\rho}{K_sG}{\partial_t}^2\right)\frac{a^4}{360}+\left(k+\rho A{\partial_t}^2\right)\frac{a^6}{1440}\right]w^{(6)}$$
$$+\left[EI-\left(\rho I{\partial_t}^2+\frac{kEI}{K_sGA}+\frac{EI\rho}{K_sG}{\partial_t}^2\right)\frac{a^2}{12}+\left(k+\rho A{\partial_t}^2\right)\frac{a^4}{48}\right]w^{(4)} \quad (256)$$
$$+\left[-\left(\rho I{\partial_t}^2+\frac{kEI}{K_sGA}+\frac{EI\rho}{K_sG}{\partial_t}^2\right)+\left(k+\rho A{\partial_t}^2\right)\frac{a^2}{4}\right]w^{(2)}$$
$$+\left[\left(k+\rho A{\partial_t}^2\right)+\frac{k\rho I}{K_sGA}{\partial_t}^2+\frac{\rho^2 I}{K_sG}{\partial_t}^4\right]w=0$$

To satisfy this eighth-order differential equation, a wave equation in a harmonic type is chosen again as Eq. (206). One would be obtained as:

$$\left[\frac{\rho^2}{EK_sG}\right]\omega^4$$
$$-\left[-\left(\frac{\rho}{E}+\frac{\rho}{K_sG}\right)\left(\frac{a^6}{20160}\right){k_w}^8\right.$$
$$+\left(\left(\frac{\rho}{E}+\frac{\rho}{K_sG}\right)-\left(\frac{\rho A}{EI}\right)\left(\frac{a^2}{4}\right)\right)\left(\left(\frac{a^4}{360}\right){k_w}^6-\left(\frac{a^2}{12}\right){k_w}^4+{k_w}^2\right)+\left(\frac{\rho A}{EI}+\frac{k\rho}{EK_sGA}\right)\left.\right]\omega^2$$
$$+\left[-\left(\frac{17a^6}{30240}\right){k_w}^{10}+\left(\frac{a^4}{80}-\frac{ka^6}{20160K_sGA}\right){k_w}^8+\left(-\frac{ka^6}{1440EI}+\frac{ka^4}{360K_sGA}-\frac{a^2}{6}\right){k_w}^6\right. \quad (257)$$
$$\left.+\left(1-\frac{ka^2}{12K_sGA}+\frac{ka^4}{48EI}\right){k_w}^4+\left(\frac{k}{K_sGA}-\frac{ka^2}{4EI}\right){k_w}^2+\frac{k}{EI}\right]=0$$

which could be rewritten through the dimensionless parameters of Eq. (214) as follows:

$$\begin{aligned}
&\boldsymbol{\Omega_b}^4 \\
&-\left[\left(\frac{1}{\mu_s r^{*2}}+\frac{1}{r^{*2}}\right)\left(-\frac{(ak_w)^8}{20160}+\frac{(ak_w)^6}{360}-\frac{(ak_w)^4}{12}+(ak_w)^2\right)\right. \\
&+\left(\frac{1}{\mu_s r^{*4}}\right)\left(-\frac{(ak_w)^6}{1440}+\frac{(ak_w)^4}{48}-\frac{(ak_w)^2}{4}+1\right)+k^*\Big]\boldsymbol{\Omega_b}^2 \\
&+\left[\left(\frac{1}{\mu_s r^{*4}}\right)\left(-\frac{17(ak_w)^{10}}{30240}+\frac{(ak_w)^8}{80}-\frac{(ak_w)^6}{6}+(ak_w)^4\right)\right. \\
&+\left(\frac{k^*}{r^{*2}}\right)\left(-\frac{(ak_w)^8}{20160}+\frac{(ak_w)^6}{360}-\frac{(ak_w)^4}{12}+(ak_w)^2\right) \\
&\left.+\left(\frac{k^*}{\mu_s r^{*4}}\right)\left(-\frac{(ak_w)^6}{1440}+\frac{(ak_w)^4}{48}-\frac{(ak_w)^2}{4}+1\right)\right]=0
\end{aligned} \tag{258}$$

While for the fourth-order continualization, neglecting the terms of $\boldsymbol{a^6}$, Eq. (257) could be simplified to the following quartic equation:

$$\begin{aligned}
&\left[\frac{\rho^2}{EK_sG}\right]\omega^4 \\
&-\left[\left(\frac{\rho}{E}+\frac{\rho}{K_sG}\right)\left(\left(\frac{a^4}{360}\right){k_w}^6-\left(\frac{a^2}{12}\right){k_w}^4+{k_w}^2\right)+\left(\frac{\rho A}{EI}\right)\left(\left(\frac{a^4}{48}\right){k_w}^4-\left(\frac{a^2}{4}\right){k_w}^2+1\right)+\left(\frac{k\rho}{EK_sGA}\right)\right]\omega^2 \\
&+\left[\left(\frac{a^4}{80}\right){k_w}^8+\left(\frac{ka^4}{360K_sGA}-\frac{a^2}{6}\right){k_w}^6+\left(1-\frac{ka^2}{12K_sGA}+\frac{ka^4}{48EI}\right){k_w}^4+\left(\frac{k}{K_sGA}-\frac{ka^2}{4EI}\right){k_w}^2+\frac{k}{EI}\right]=0
\end{aligned} \tag{259}$$

Using the dimensionless parameters of Eq. (214) leads to:

$$\begin{aligned}
&\boldsymbol{\Omega_b}^4 \\
&-\left[\left(\frac{1}{\mu_s r^{*2}}+\frac{1}{r^{*2}}\right)\left(\frac{(ak_w)^6}{360}-\frac{(ak_w)^4}{12}+(ak_w)^2\right)+\left(\frac{1}{\mu_s r^{*4}}\right)\left(\frac{(ak_w)^4}{48}-\frac{(ak_w)^2}{4}+1\right)\right. \\
&\left.+k^*\right]\boldsymbol{\Omega_b}^2 \\
&+\left[\left(\frac{1}{\mu_s r^{*4}}\right)\left(\frac{(ak_w)^8}{80}-\frac{(ak_w)^6}{6}+(ak_w)^4\right)+\left(\frac{k^*}{r^{*2}}\right)\left(\frac{(ak_w)^6}{360}-\frac{(ak_w)^4}{12}+(ak_w)^2\right)\right. \\
&\left.+\left(\frac{k^*}{\mu_s r^{*4}}\right)\left(\frac{(ak_w)^4}{48}-\frac{(ak_w)^2}{4}+1\right)\right]=0
\end{aligned} \tag{260}$$

Using the second-order $\boldsymbol{a^2}$ of the continualization of the Taylor expansion series of Eq. (175), Eq. (205) leads to the following higher-order gradient system:

$$\left[EI\left(1+\frac{a^2}{6}\partial_x^2\right)\partial_x^4-\left(\rho I{\partial_t}^2+\frac{kEI}{K_sGA}+\frac{EI\rho}{K_sG}{\partial_t}^2\right)\left(1+\frac{a^2}{12}\partial_x^2\right)\partial_x^2 + \left(k+\rho A{\partial_t}^2\right)\left(1+\frac{a^2}{4}\partial_x^2\right)+\left(\frac{k\rho I}{K_sGA}{\partial_t}^2+\frac{\rho^2 I}{K_sG}{\partial_t}^4\right)\right]w=0 \quad (261)$$

For the static range, this equation leads to the one obtained by Challamel et al. [13]. Using the dimensionless parameters introduced in Eq. (214), the comparable deflection equation of the continuous approximate for the static condition would be obtained as follows

$$\left[\left(1+\frac{a^2}{6}\partial_x^2\right)\partial_x^4-k^*\mu_s{r^*}^2\left(1+\frac{a^2}{12}\partial_x^2\right)\partial_x^2+k^*\left(1+\frac{a^2}{4}\partial_x^2\right)\right]\bar{w}=0 \quad (262)$$

where $w=\frac{\bar{w}}{a}$. Let's consider the case of a granular chain with predominant bending interactions ($S\to\infty$). Thus, Eq. (261) leads to

$$\left[EI\left(1+\frac{a^2}{6}\partial_x^2\right)\partial_x^4-\left(\rho I{\partial_t}^2\right)\left(1+\frac{a^2}{12}\partial_x^2\right)\partial_x^2+\left(k+\rho A{\partial_t}^2\right)\left(1+\frac{a^2}{4}\partial_x^2\right)\right]w=0 \quad (263)$$

This gradient elasticity Rayleigh model (pure bending) under a gradient Winkler elastic foundation is associated with a non-positive definite energy function. After integration by part, one obtains the following energy functional:

$$\Pi = \int\frac{1}{2}EI\left(w''^2-\frac{a^2}{6}w'''^2\right)dx+\int\frac{1}{2}\rho I{\partial_t}^2\left(w'^2-\frac{a^2}{12}w''^2\right)dx + \int\frac{1}{2}\left(k+\rho A{\partial_t}^2\right)\left(w^2-\frac{a^2}{4}w'^2\right)dx. \quad (264)$$

The wave propagation equation could be obtained as the following sixth-order differential equation from Eq. (261):

$$\left[\frac{EIa^2}{6}\right]w^{(6)}+\left[EI-\left(\rho I\partial_t{}^2+\frac{kEI}{K_sGA}+\frac{EI\rho}{K_sG}\partial_t{}^2\right)\frac{a^2}{12}\right]w^{(4)}$$
$$+\left[-\left(\rho I\partial_t{}^2+\frac{kEI}{K_sGA}+\frac{EI\rho}{K_sG}\partial_t{}^2\right)+\left(k+\rho A\partial_t{}^2\right)\frac{a^2}{4}\right]w^{(2)}$$
$$+\left[\left(k+\rho A\partial_t{}^2\right)+\frac{k\rho I}{K_sGA}\partial_t{}^2+\frac{\rho^2 I}{K_sG}\partial_t{}^4\right]w=0 \tag{265}$$

Again, using a wave equation in a harmonic type like Eq. (206) leads to:

$$\left[\frac{\rho^2}{EK_sG}\right]\omega^4+\left[\left(\frac{\rho}{E}+\frac{\rho}{K_sG}\right)\left(\frac{a^2}{12}\right)k_w{}^4+\left(\frac{\rho Aa^2}{4EI}-\frac{\rho}{E}-\frac{\rho}{K_sG}\right)k_w{}^2-\left(\frac{\rho A}{EI}+\frac{k\rho}{EK_sGA}\right)\right]\omega^2$$
$$+\left[-\left(\frac{a^2}{6}\right)k_w{}^6+\left(1-\frac{ka^2}{12K_sGA}\right)k_w{}^4+\left(\frac{k}{K_sGA}-\frac{ka^2}{4EI}\right)k_w{}^2+\frac{k}{EI}\right]=0 \tag{266}$$

and in the nondimensional form as:

$$\Omega_b{}^4+\left[\left(\frac{1}{\mu_s r^{*2}}+\frac{1}{r^{*2}}\right)\frac{(ak_w)^4}{12}+\left(\frac{1}{4\mu_s r^{*4}}-\frac{1}{\mu_s r^{*2}}-\frac{1}{r^{*2}}\right)(ak_w)^2-\left(\frac{1}{\mu_s r^{*4}}+k^*\right)\right]\Omega_b{}^2$$
$$+\left[-\left(\frac{1}{\mu_s r^{*4}}\right)\frac{(ak_w)^6}{6}+\left(\frac{1}{\mu_s r^{*4}}-\frac{k^*}{12r^{*2}}\right)(ak_w)^4+\left(\frac{k^*}{r^{*2}}-\frac{k^*}{4\mu_s r^{*4}}\right)(ak_w)^2+\frac{k^*}{\mu_s r^{*4}}\right]=0 \tag{267}$$

The dispersive analysis of the granular chain with regards to the dimensionless parameter of bending frequency is done for the two branches. The results are plotted in Figure 22 asymptotically for a numeral example characterized in Eq. (268) through the equations obtained for discrete exact, local continuum and nonlocal Taylor approaches (Eq. (208), (257), (259), (252) and (266)). For instance, in order to investigate a sensitive numerical analysis of the abovementioned model, we consider the following parameters (steel is assumed for the material parameter). Let's assume the mechanical parameters of steel with an elastic foundation as follows

$$E=200\ GPa,\ G=70\ GPa,\ K_s=0.667,\ \rho=8000\ \frac{kg}{m^3},\ k=50\ MPa. \tag{268}$$

(a) (b)

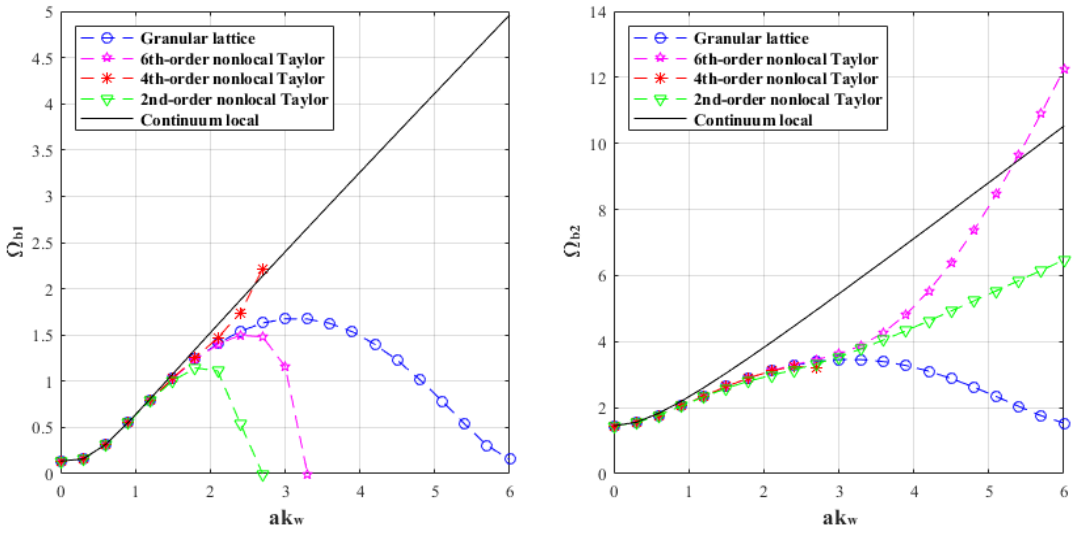

Figure 22. Dispersive curves for one-dimensional compression wave of (a) the first branch and (b) the second branch according to bending nondimensional parameter for $\boldsymbol{\mu_s = 4.28}$, $\boldsymbol{r^* = 0.289}$ and $\boldsymbol{k^* = 0.02}$.

Due to the quartic equation of Eq. (257), depending on the discriminant value of this equation for the sixth, the fourth and the second-order expansion of the Taylor series, the dynamic results could take complex values.

For analyzing the behavior of the nonlocal approach using the Taylor development precisely, here an asymptotic study of the frequency has been done. Regarding Eq. (258),one could be obtained for the dimensionless parameter of bending frequency as follows:

$$\boldsymbol{\Omega_b = \sqrt{\varepsilon \pm \sqrt{\varepsilon^2 - \gamma}}} \tag{269}$$

where ε and γ would be considered as

$$\boldsymbol{\varepsilon} = \frac{\mathbf{1}}{\mathbf{2}}\left[\left(\frac{\mathbf{1}}{\boldsymbol{\mu_s r^{*2}}} + \frac{\mathbf{1}}{\boldsymbol{r^{*2}}}\right)\left(-\frac{\boldsymbol{(ak_w)^8}}{\mathbf{20160}} + \frac{\boldsymbol{(ak_w)^6}}{\mathbf{360}} - \frac{\boldsymbol{(ak_w)^4}}{\mathbf{12}} + \boldsymbol{(ak_w)^2}\right) + \left(\frac{\mathbf{1}}{\boldsymbol{\mu_s r^{*4}}}\right)\left(-\frac{\boldsymbol{(ak_w)^6}}{\mathbf{1440}} + \frac{\boldsymbol{(ak_w)^4}}{\mathbf{48}} - \frac{\boldsymbol{(ak_w)^2}}{\mathbf{4}} + \mathbf{1}\right) + \boldsymbol{k^*}\right]; \tag{270}$$

$$\gamma = \left(\frac{1}{\mu_s r^{*4}}\right)\left(-\frac{17(ak_w)^{10}}{30240}+\frac{(ak_w)^8}{80}-\frac{(ak_w)^6}{6}+(ak_w)^4\right) + \left(\frac{k^*}{r^{*2}}\right)\left(-\frac{(ak_w)^8}{20160}+\frac{(ak_w)^6}{360}-\frac{(ak_w)^4}{12}+(ak_w)^2\right) + \left(\frac{k^*}{\mu_s r^{*4}}\right)\left(-\frac{(ak_w)^6}{1440}+\frac{(ak_w)^4}{48}-\frac{(ak_w)^2}{4}+1\right)$$

Due to the discriminant of Eq. (269) and the typical values for the mechanical and geometrical parameters of the system (Eq. (268)) the results contain the imaginary part. Figure 23 clarifies this evidence as follows

(a) (b)

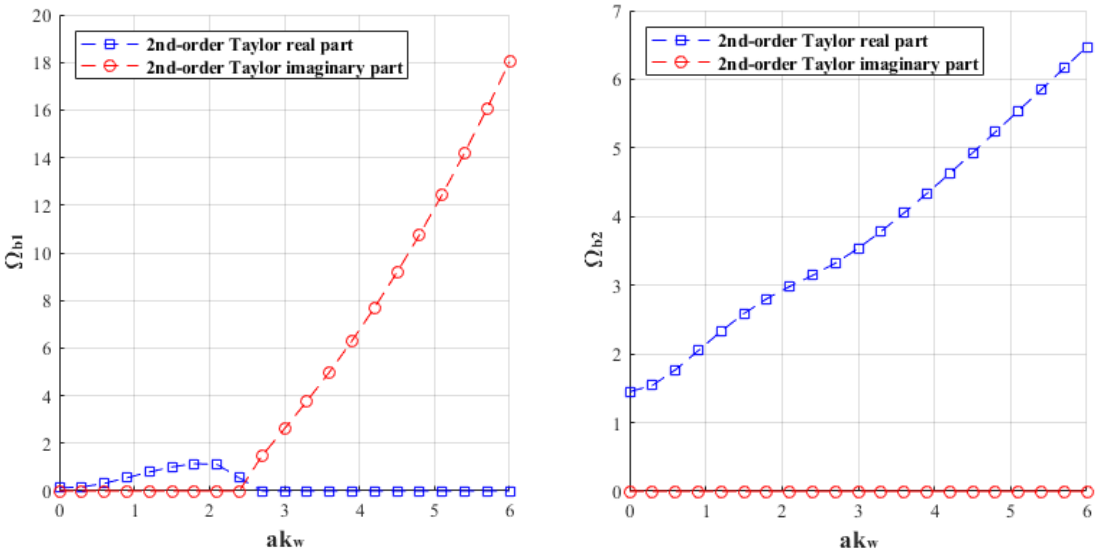

(c) (d)

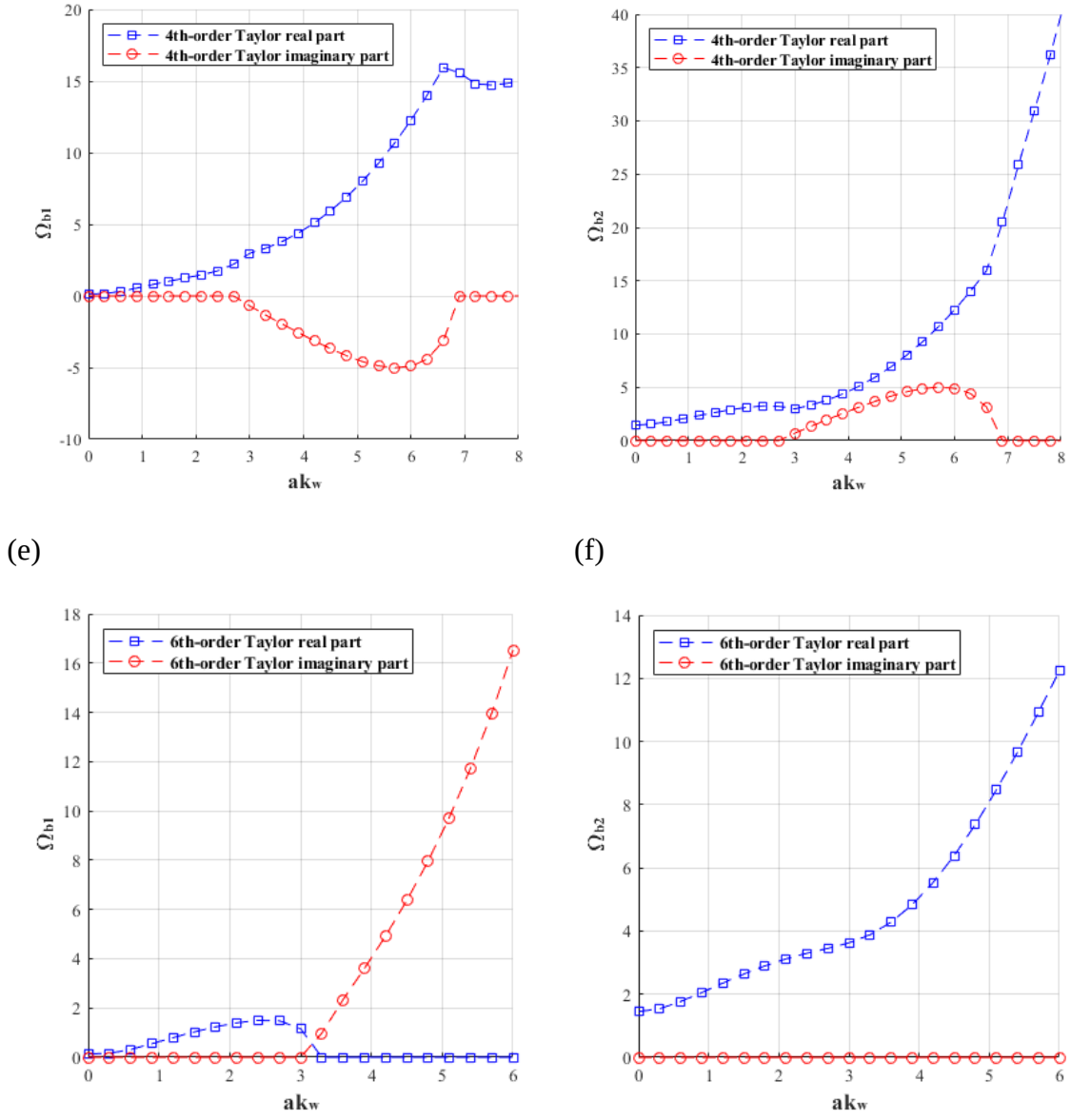

Figure 23. The complex results of nonlocal Taylor development (a) 2nd-order first branch, (b) 2nd-order second branch, (c) 4th-order first branch, (d) 4th-order second branch, (e) 6th-order first branch and (f) 6th -order second branch according to bending nondimensional parameter for $\boldsymbol{\mu_s = 4.28}$, $\boldsymbol{r^* = 0.289}$ and $\boldsymbol{k^* = 0.02}$.

3.3. Approximate Solution via Rational Expansion

Another nonlocal approximation is based on a rational expansion (Padé approximants) instead of the polynomial approximation, which may lead to a better-homogenized solution in comparison to the Taylor series (Duan et al. [12]). With the

application of Padé approximant of order in $\boldsymbol{a^4}$ subsequently for the pseudo-differential operators of Eq. (175), ones would be obtained as:

$$\begin{aligned}
\boldsymbol{\delta_2{}^2 w} &\approx \left(\mathbf{1}-\frac{\boldsymbol{a^2\partial_x^2}}{\mathbf{6}}+\frac{\mathbf{11}\boldsymbol{a^4\partial_x^4}}{\mathbf{720}}\right)^{-1}\boldsymbol{\partial_x^4 w};\\
\boldsymbol{\delta_2 w(x)} &\approx \left(\mathbf{1}-\frac{\boldsymbol{a^2\partial_x^2}}{\mathbf{12}}+\frac{\boldsymbol{a^4\partial_x^4}}{\mathbf{240}}\right)\left(\mathbf{1}-\frac{\boldsymbol{a^2\partial_x^2}}{\mathbf{6}}+\frac{\mathbf{11}\boldsymbol{a^4\partial_x^4}}{\mathbf{720}}\right)^{-1}\boldsymbol{\partial_x^2 w};\\
\boldsymbol{\delta_0 w} &\approx \left(\mathbf{1}+\frac{\boldsymbol{a^2\partial_x^2}}{\mathbf{12}}-\frac{\boldsymbol{a^4\partial_x^4}}{\mathbf{180}}\right)\left(\mathbf{1}-\frac{\boldsymbol{a^2\partial_x^2}}{\mathbf{6}}+\frac{\mathbf{11}\boldsymbol{a^4\partial_x^4}}{\mathbf{720}}\right)^{-1}\boldsymbol{w}
\end{aligned} \tag{271}$$

Thus, the deflection equation of Eq. (205) for a discrete system could be written for a continuous system using Eq. (190) as:

$$\begin{aligned}
&\left[\frac{\mathbf{1}}{\mathbf{1}-\frac{\boldsymbol{a^2\partial_x^2}}{\mathbf{6}}+\frac{\mathbf{11}\boldsymbol{a^4\partial_x^4}}{\mathbf{720}}}\boldsymbol{\partial_x^4}-\left(\left(\frac{\boldsymbol{\rho}}{\boldsymbol{E}}+\frac{\boldsymbol{\rho}}{\boldsymbol{K_sG}}\right)\boldsymbol{\partial_t}^2+\frac{\boldsymbol{k}}{\boldsymbol{K_sGA}}\right)\frac{\mathbf{1}-\frac{\boldsymbol{a^2\partial_x^2}}{\mathbf{12}}+\frac{\boldsymbol{a^4\partial_x^4}}{\mathbf{240}}}{\mathbf{1}-\frac{\boldsymbol{a^2\partial_x^2}}{\mathbf{6}}+\frac{\mathbf{11}\boldsymbol{a^4\partial_x^4}}{\mathbf{720}}}\boldsymbol{\partial_x^2}\right.\\
&\left.+\left(\frac{\boldsymbol{k}}{\boldsymbol{EI}}+\frac{\boldsymbol{\rho A}}{\boldsymbol{EI}}\boldsymbol{\partial_t}^2\right)\frac{\mathbf{1}+\frac{\boldsymbol{a^2\partial_x^2}}{\mathbf{12}}-\frac{\boldsymbol{a^4\partial_x^4}}{\mathbf{180}}}{\mathbf{1}-\frac{\boldsymbol{a^2\partial_x^2}}{\mathbf{6}}+\frac{\mathbf{11}\boldsymbol{a^4\partial_x^4}}{\mathbf{720}}}+\left(\frac{\boldsymbol{k\rho}}{\boldsymbol{EK_sGA}}\boldsymbol{\partial_t}^2+\frac{\boldsymbol{\rho^2}}{\boldsymbol{EK_sG}}\boldsymbol{\partial_t}^4\right)\right]\boldsymbol{w}=\mathbf{0}
\end{aligned} \tag{272}$$

Multiplying Eq. (191) by $(1-\frac{a^2\partial_x^2}{6}+\frac{11a^4\partial_x^4}{720})$ leads to the following compact form equation:

$$\begin{aligned}
&\left[\boldsymbol{\partial_x^4}-\left(\left(\frac{\boldsymbol{\rho}}{\boldsymbol{E}}+\frac{\boldsymbol{\rho}}{\boldsymbol{K_sG}}\right)\boldsymbol{\partial_t}^2+\frac{\boldsymbol{k}}{\boldsymbol{K_sGA}}\right)\left(\mathbf{1}-\frac{\boldsymbol{a^2\partial_x^2}}{\mathbf{12}}+\frac{\boldsymbol{a^4\partial_x^4}}{\mathbf{240}}\right)\boldsymbol{\partial_x^2}\right.\\
&\qquad+\left(\frac{\boldsymbol{k}}{\boldsymbol{EI}}+\frac{\boldsymbol{\rho A}}{\boldsymbol{EI}}\boldsymbol{\partial_t}^2\right)\left(\mathbf{1}+\frac{\boldsymbol{a^2\partial_x^2}}{\mathbf{12}}-\frac{\boldsymbol{a^4\partial_x^4}}{\mathbf{180}}\right)\\
&\left.+\left(\frac{\boldsymbol{k\rho}}{\boldsymbol{EK_sGA}}\boldsymbol{\partial_t}^2+\frac{\boldsymbol{\rho^2}}{\boldsymbol{EK_sG}}\boldsymbol{\partial_t}^4\right)\left(\mathbf{1}-\frac{\boldsymbol{a^2\partial_x^2}}{\mathbf{6}}+\frac{\mathbf{11}\boldsymbol{a^4\partial_x^4}}{\mathbf{720}}\right)\right]\boldsymbol{w}=\mathbf{0}
\end{aligned} \tag{273}$$

The wave propagation equation can be obtained by:

$$\left[-\left(\left(\frac{\rho}{E}+\frac{\rho}{K_sG}\right)\partial_t{}^2+\frac{k}{K_sGA}\right)\left(\frac{a^4}{240}\right)\right]\partial_x^6 w$$
$$+\left[1+\left(\left(\frac{\rho}{E}+\frac{\rho}{K_sG}\right)\partial_t{}^2+\frac{k}{K_sGA}\right)\left(\frac{a^2}{12}\right)-\left(\frac{k}{EI}+\frac{\rho A}{EI}\partial_t{}^2\right)\left(\frac{a^4}{180}\right)\right.$$
$$\left.+\left(\frac{k\rho}{EK_sGA}\partial_t{}^2+\frac{\rho^2}{EK_sG}\partial_t{}^4\right)\left(\frac{11a^4}{720}\right)\right]\partial_x^4 w$$
$$-\left[\left(\left(\frac{\rho}{E}+\frac{\rho}{K_sG}\right)\partial_t{}^2+\frac{k}{K_sGA}\right)-\left(\frac{k}{EI}+\frac{\rho A}{EI}\partial_t{}^2\right)\left(\frac{a^2}{12}\right)+\left(\frac{k\rho}{EK_sGA}\partial_t{}^2+\frac{\rho^2}{EK_sG}\partial_t{}^4\right)\left(\frac{a^2}{6}\right)\right]\partial_x^2 w$$
$$+\left[\left(\frac{k}{EI}+\frac{\rho A}{EI}\partial_t{}^2\right)+\left(\frac{k\rho}{EK_sGA}\partial_t{}^2+\frac{\rho^2}{EK_sG}\partial_t{}^4\right)\right]w=0 \tag{274}$$

Applying the fundamental solution of Eq. (206), the characteristic equation of the nonlocal continued model (nonlocal model Padé 1) is obtained as follows

$$\left[\frac{\rho^2}{EK_sG}\left(\frac{11a^4}{720}k_w{}^4+\frac{a^2}{6}k_w{}^2+1\right)\right]\omega^4$$
$$-\left[\left(\left(\frac{\rho}{E}+\frac{\rho}{K_sG}\right)\frac{a^4}{240}\right)k_w{}^6+\left(\left(\frac{\rho}{E}+\frac{\rho}{K_sG}\right)\frac{a^2}{12}+\left(\frac{k\rho}{EK_sGA}-\frac{4\rho A}{11EI}\right)\frac{11a^4}{720}\right)k_w{}^4\right.$$
$$\left.+\left(\frac{\rho}{E}+\frac{\rho}{K_sG}+\left(\frac{k\rho}{EK_sGA}-\frac{\rho A}{2EI}\right)\frac{a^2}{6}\right)k_w{}^2+\left(\frac{\rho A}{EI}+\frac{k\rho}{EK_sGA}\right)\right]\omega^2$$
$$+\left[\left(\left(\frac{k}{K_sGA}\right)\frac{a^4}{240}\right)k_w{}^6+\left(1+\left(\frac{k}{K_sGA}\right)\frac{a^2}{12}-\left(\frac{k}{EI}\right)\frac{a^4}{180}\right)k_w{}^4+\left(\frac{k}{K_sGA}-\left(\frac{k}{EI}\right)\frac{a^2}{12}\right)k_w{}^2+\frac{k}{EI}\right]=0 \tag{275}$$

The dimensionless form of this equation would be obtained through the dimensionless parameters of Eq. (214) as follows:

$$\left[\left(\frac{11(ak_w)^4}{720}+\frac{(ak_w)^2}{6}+1\right)\right]\Omega_b{}^4$$
$$-\left[\left(\frac{1}{\mu_s r^{*2}}+\frac{1}{r^{*2}}\right)\frac{(ak_w)^6}{240}+\left(\left(\frac{1}{\mu_s r^{*2}}+\frac{1}{r^{*2}}\right)\frac{1}{12}+\left(k^*-\frac{4}{11\mu_s r^{*4}}\right)\frac{11}{720}\right)(ak_w)^4\right.$$
$$\left.+\left(\frac{1}{\mu_s r^{*2}}+\frac{1}{r^{*2}}+\left(k^*-\frac{1}{2\mu_s r^{*4}}\right)\frac{1}{6}\right)(ak_w)^2+\left(\frac{1}{\mu_s r^{*4}}+k^*\right)\right]\Omega_b{}^2$$
$$+\left[\left(\frac{k^*}{240r^{*2}}\right)(ak_w)^6+\left(\frac{1}{\mu_s r^{*4}}+\frac{k^*}{12r^{*2}}-\frac{k^*}{180\mu_s r^{*4}}\right)(ak_w)^4+\left(\frac{k^*}{r^{*2}}-\frac{k^*}{12\mu_s r^{*4}}\right)(ak_w)^2+\frac{k^*}{\mu_s r^{*4}}\right]=0 \tag{276}$$

On the other hand, regarding the work of Bacigalupo and Gambarotta [115] or Bacigalupo and Gambarotta [50] by using the approach of enhanced continualization via the first-order regularization, the derivatives of the continuum fields could be expressed by

$$\boldsymbol{\partial_x \widetilde{w}_i = \frac{e^{a\partial_x} - e^{-a\partial_x}}{2a} w_i} \tag{277}$$

And the down-scaling law for each node defined by

$$\boldsymbol{w_i = \frac{2a\partial_x}{e^{a\partial_x} - e^{-a\partial_x}} \widetilde{w}_i} \tag{278}$$

Substituting Eq. (278) in Eq. (69) leads to

$$\begin{gathered}\left(2S\frac{(e^{a\partial_x} - (2 + ka/s) + e^{-a\partial_x})}{e^{a\partial_x} - e^{-a\partial_x}} a\partial_x\right)\widetilde{w}_i - a^2 S\partial_x\widetilde{\theta}_i - \left(\frac{2m}{e^{a\partial_x} - e^{-aD_x}} a\partial_x\right)\ddot{\widetilde{w}}_\iota = 0; \\ \left((C\frac{(e^{a\partial_x} - 2 + e^{-a\partial_x})}{e^{a\partial_x} - e^{-a\partial_x}} - \frac{a^2}{4}S\frac{(e^{a\partial_x} + 2 + e^{-a\partial_x})}{e^{a\partial_x} - e^{-a\partial_x}})2a\partial_x\right)\widetilde{\theta}_i + a^2 S\partial_x\widetilde{w}_i - \left(\frac{2I_m}{e^{a\partial_x} - e^{-a\partial_x}} a\partial_x\right)\ddot{\widetilde{\theta}}_\iota = 0\end{gathered} \tag{279}$$

Here, the differential equations of the equivalent homogenized continuum are obtained by applying the fourth-order terms of the Taylor series:

$$\begin{gathered}-kaw_i + \left(s + \frac{1}{6}ka\right)a^2\frac{\partial^2 w}{\partial x^2} - \left(\frac{s}{12} + \frac{7}{360}ka\right)a^4\frac{\partial^4 w}{\partial x^4} - aS\frac{\partial\theta}{\partial x} - m\left(\ddot{w} - \frac{a^2}{6}\frac{\partial^2\ddot{w}}{\partial x^2} + \frac{7a^4}{360}\frac{\partial^4\ddot{w}}{\partial x^4}\right) = 0; \\ -a^2 Sw_i + \left(C - \frac{a^2}{12}S\right)a^2\frac{\partial^2\theta_i}{\partial x^2} - \left(\frac{C}{12} + \frac{a^2}{144}S\right)a^4\frac{\partial^4\theta_i}{\partial x^4} + aS\frac{\partial w}{\partial x} - I_m\left(\ddot{\theta} - \frac{a^2}{6}\frac{\partial^2\ddot{\theta}}{\partial x^2} + \frac{7a^4}{360}\frac{\partial^4\ddot{\theta}}{\partial x^4}\right) = 0\end{gathered} \tag{280}$$

Regarding Eq. (278), the difference operators of Eq. (6) actually could be expressed in the following form

$$\begin{gathered}\boldsymbol{\delta_2{}^2 w} = \left(\frac{2a\partial_x}{e^{a\partial_x} - e^{-a\partial_x}}\right)\left(\frac{e^{2a\partial_x} - 4e^{a\partial_x} + 6 - 4e^{-a\partial_x} + e^{-2a\partial_x}}{a^4}\right)\widetilde{w} \\ = \left(1 + \frac{a^4\partial_x^4}{240} + O(a^6\partial_x^6)\right)\partial_x^4\widetilde{w}, \\ \boldsymbol{\delta_2 w} = \left(\frac{2a\partial_x}{e^{a\partial_x} - e^{-a\partial_x}}\right)\left(\frac{e^{a\partial_x} - 2 + e^{-a\partial_x}}{a^2}\right)\widetilde{w} = \left(1 - \frac{a^2\partial_x^2}{12} + \frac{a^4\partial_x^4}{120} + O(a^6\partial_x^6)\right)\partial_x^2\widetilde{w}, \\ \boldsymbol{\delta_1 w} = \left(\frac{2a\partial_x}{e^{a\partial_x} - e^{-a\partial_x}}\right)\left(\frac{e^{a\partial_x} - e^{-a\partial_x}}{2a}\right)\widetilde{w} = \partial_x\widetilde{w},\end{gathered} \tag{281}$$

$$\delta_0 w = \left(\frac{2a\partial_x}{e^{a\partial_x} - e^{-a\partial_x}}\right)\left(\frac{e^{a\partial_x} + 2 + e^{-a\partial_x}}{4}\right)\widetilde{w} = \left(1 + \frac{a^2\partial_x^2}{12} - \frac{a^4\partial_x^4}{720} + O(a^6\partial_x^6)\right)\widetilde{w}$$

Continualizing Eq. (205) through the application of the series of Eq. (281) and neglecting higher-order terms in a^4 leads to the following extended deflection equation

$$\left[EI\partial_x^4 - \left(\rho I{\partial_t}^2 + \frac{kEI}{K_sGA} + \frac{EI\rho}{K_sG}{\partial_t}^2\right)\left(1 - \frac{a^2\partial_x^2}{12}\right)\partial_x^2 + \left(k + \rho A{\partial_t}^2\right)\left(1 + \frac{a^2\partial_x^2}{12}\right) + \left(\frac{k\rho I{\partial_t}^2}{K_sGA} + \frac{\rho^2 I{\partial_t}^4}{K_sG}\right)\left(1 - \frac{a^2\partial_x^2}{6}\right)\right]\widetilde{w} = 0 \quad (282)$$

This equation (nonlocal model Padé 1) could be obtained also from Eq. (274) neglecting the higher-order terms in a^4. An alternative strategy to obtain Eq. (282) is through the multiplication of $\left(1 - \frac{a^2\partial_x^2}{6}\right)$ to Eq. (261). Eq. (282) would be simplified as:

$$\left[EI + \left(\rho I{\partial_t}^2 + \frac{kEI}{K_sGA} + \frac{EI\rho}{K_sG}{\partial_t}^2\right)\frac{a^2}{12}\right]\widetilde{w}^{(4)} - \left[\left(\rho I{\partial_t}^2 + \frac{kEI}{K_sGA} + \frac{EI\rho}{K_sG}{\partial_t}^2\right) - \left(k + \rho A{\partial_t}^2\right)\frac{a^2}{12} + \left(\frac{k\rho I{\partial_t}^2}{K_sGA} + \frac{\rho^2 I{\partial_t}^4}{K_sG}\right)\frac{a^2}{6}\right]\widetilde{w}^{(2)} + \left[k + \left(\rho A + \frac{k\rho I}{K_sGA} + \frac{\rho^2 I}{K_sG}{\partial_t}^2\right){\partial_t}^2\right]\widetilde{w} = 0 \quad (283)$$

Choosing again a wave equation in a harmonic type as Eq. (206), one would be obtained:

$$\left[\frac{\rho^2}{EK_sG}\left(1 + \frac{a^2}{6}{k_w}^2\right)\right]\omega^4 - \left[\left(\frac{\rho}{E} + \frac{\rho}{K_sG}\right)\left(\frac{a^2}{12}\right){k_w}^4 + \left(\frac{\rho}{E} + \frac{\rho}{K_sG} + \left(\frac{k\rho}{EK_sGA} - \frac{\rho A}{2EI}\right)\frac{a^2}{6}\right){k_w}^2 + \left(\frac{\rho A}{EI} + \frac{k\rho}{EK_sGA}\right)\right]\omega^2 + \left[\left(1 + \frac{ka^2}{12K_sGA}\right){k_w}^4 + \left(\frac{k}{K_sGA} - \frac{ka^2}{12EI}\right){k_w}^2 + \frac{k}{EI}\right] = 0 \quad (284)$$

Using Eq. (214), the following non-dimensional equation would be obtained through the bending wave velocity definition.

$$\left[\left(\frac{(ak_w)^2}{6}+1\right)\right]\Omega_b{}^4$$
$$-\left[\left(\frac{1}{\mu_s r^{*2}}+\frac{1}{r^{*2}}\right)\frac{(ak_w)^4}{12}+\left(\frac{1}{\mu_s r^{*2}}+\frac{1}{r^{*2}}+\left(k^*-\frac{1}{2\mu_s r^{*4}}\right)\frac{1}{6}\right)(ak_w)^2+\left(\frac{1}{\mu_s r^{*4}}+k^*\right)\right]\Omega_b{}^2$$
$$+\left[\left(\frac{1}{\mu_s r^{*4}}+\frac{k^*}{12r^{*2}}\right)(ak_w)^4+\left(\frac{k^*}{r^{*2}}-\frac{k^*}{12\mu_s r^{*4}}\right)(ak_w)^2+\frac{k^*}{\mu_s r^{*4}}\right]=0 \quad (285)$$

An alternative continuous approach could be obtained by multiplying the terms $\left(1-\frac{a^2\partial_x^2}{3}\right)$ to Eq. (261) and neglect higher-order terms in a^4. This leads to the following extended governed equation (nonlocal model Padé 2):

$$\left[EI\left(1-\frac{a^2}{6}\partial_x^2\right)\partial_x^4-\left(\rho I\partial_t{}^2+\frac{kEI}{K_sGA}+\frac{EI\rho}{K_sG}\partial_t{}^2\right)\left(1-\frac{a^2}{4}\partial_x^2\right)\partial_x^2+\left(k+\rho A\partial_t{}^2\right)\left(1-\frac{a^2}{12}\partial_x^2\right)\right.$$
$$\left.+\left(\frac{k\rho I}{K_sGA}\partial_t{}^2+\frac{\rho^2 I}{K_sG}\partial_t{}^4\right)\left(1-\frac{a^2}{3}\partial_x^2\right)\right]w=0 \quad (286)$$

Here, the gradient elasticity for a granular chain with predominant bending interactions are associated with positive definite energy function as follows:

$$\Pi = \int\frac{1}{2}EI\left(w''^2+\frac{a^2}{6}w''''^2\right)dx+\int\frac{1}{2}\rho I\partial_t{}^2\left(w'^2+\frac{a^2}{4}w''^2\right)dx+\int\frac{1}{2}\left(k+\rho A\partial_t{}^2\right)\left(w^2+\frac{a^2}{12}w'^2\right)dx. \quad (287)$$

For the static analysis, the comparable deflection equation of the continuous approximate again leads to the one investigated by Challamel et al. [13] neglecting the compressional buckling force as follows

$$\left[\left(1-\frac{a^2}{6}D_x^2\right)D_x^4-k^*\mu_s r^{*2}\left(1-\frac{a^2}{4}D_x^2\right)D_x^2+k^*\left(1-\frac{a^2}{12}D_x^2\right)\right]\bar{w}=0 \quad (288)$$

Going back to the continuous approximate model expressed by the enriched differential equation (Eq. (286)), the wave propagation equation could be obtained as:

$$\left[\frac{EIa^2}{6}\right]w^{(6)} - \left[EI + \left(\rho I\partial_t{}^2 + \frac{kEI}{K_sGA} + \frac{EI\rho}{K_sG}\partial_t{}^2\right)\frac{a^2}{4}\right]w^{(4)} + \left[\left(\rho I\partial_t{}^2 + \frac{kEI}{K_sGA} + \frac{EI\rho}{K_sG}\partial_t{}^2\right) + \left(k + \rho A\partial_t{}^2\right)\frac{a^2}{12} + \left(\frac{k\rho I}{K_sGA}\partial_t{}^2 + \frac{\rho^2 I}{K_sG}\partial_t{}^4\right)\frac{a^2}{3}\right]w^{(2)} - \left[\left(k + \rho A\partial_t{}^2\right) + \frac{k\rho I}{K_sGA}\partial_t{}^2 + \frac{\rho^2 I}{K_sG}\partial_t{}^4\right]w = 0 \quad (289)$$

Supposing a harmonic wave equation in the form of Eq. (206) leads to

$$\left[\frac{\rho^2}{EK_sG}\left(1 + \frac{a^2}{3}k_w{}^2\right)\right]\omega^4 - \left[\left(\frac{\rho}{E} + \frac{\rho}{K_sG}\right)\left(\frac{a^2}{4}\right)k_w{}^4 + \left(\frac{\rho}{E} + \frac{\rho}{K_sG} + \left(\frac{k\rho}{EK_sGA} + \frac{\rho A}{4EI}\right)\frac{a^2}{3}\right)k_w{}^2 + \left(\frac{\rho A}{EI} + \frac{k\rho}{EK_sGA}\right)\right]\omega^2 + \left[\left(\frac{a^2}{6}\right)k_w{}^6 + \left(1 + \frac{ka^2}{4K_sGA}\right)k_w{}^4 + \left(\frac{k}{K_sGA} + \frac{ka^2}{12EI}\right)k_w{}^2 + \frac{k}{EI}\right] = 0 \quad (290)$$

The non-dimensional equation of this approach could be obtained using Eq. (214) with respect to the bending wave velocity definition as follows:

$$\left[\left(\frac{(ak_w)^2}{3} + 1\right)\right]\Omega_b{}^4 - \left[\left(\frac{1}{\mu_s r^{*2}} + \frac{1}{r^{*2}}\right)\frac{(ak_w)^4}{4} + \left(\frac{1}{\mu_s r^{*2}} + \frac{1}{r^{*2}} + \left(k^* + \frac{1}{4\mu_s r^{*4}}\right)\frac{1}{3}\right)(ak_w)^2 + \left(\frac{1}{\mu_s r^{*4}} + k^*\right)\right]\Omega_b{}^2 + \left[\left(\frac{1}{\mu_s r^{*4}}\right)\frac{(ak_w)^6}{6} + \left(\frac{1}{\mu_s r^{*4}} + \frac{k^*}{4r^{*2}}\right)(ak_w)^4 + \left(\frac{k^*}{r^{*2}} + \frac{k^*}{12\mu_s r^{*4}}\right)(ak_w)^2 + \frac{k^*}{\mu_s r^{*4}}\right] = 0 \quad (291)$$

The dimensionless bending frequency results obtained through the Padé polynomial expansions are plotted in

(a) (b)

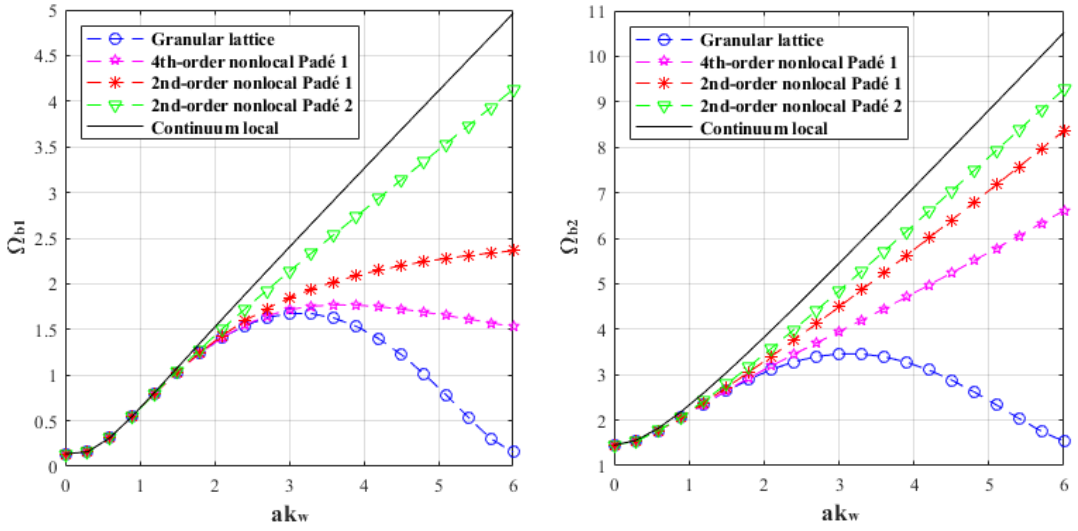

Figure **24** for the two branches. Again, for a numeral example defined in Eq. (268) and with respect to the equations presented by Eq. (208), (252), (275), (284) and (290), the calculations are done.

(a) (b)

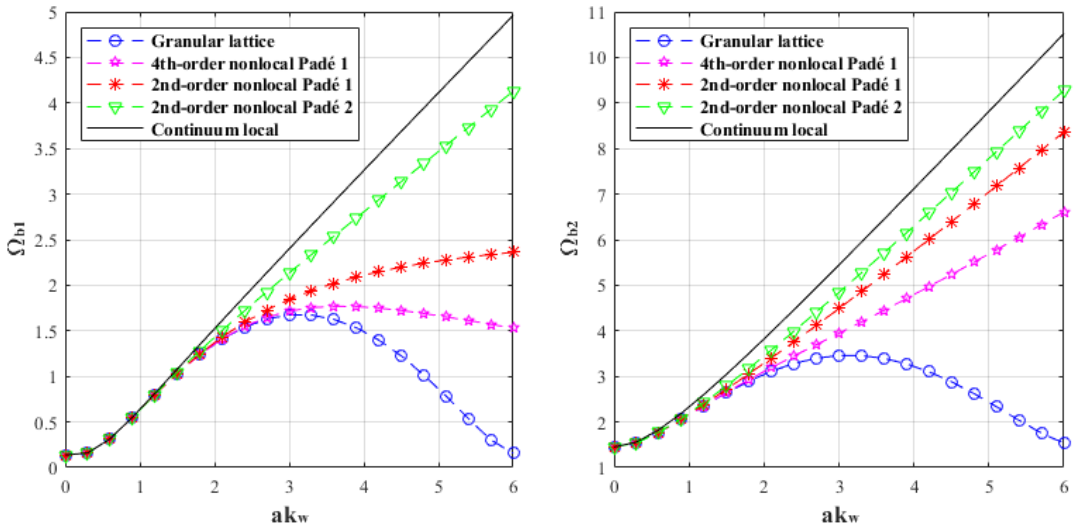

Figure 24. Dispersive curves for one-dimensional compression wave of (a) the first branch and (b) the second branch according to bending nondimensional parameter for $\boldsymbol{\mu_s = 4.28}$, $\boldsymbol{r^* = 0.289}$ and $\boldsymbol{k^* = 0.02}$.

4. Discussion

The dispersive results using Eq. (208), (252), (257), (259), (266), (275), (284) and (290) are plotted for shear dimensionless frequency in Figure 25. There exist two solutions leading to the two branches of the dynamic response of the system each refers to low and high frequencies. The lower branch refers to the acoustic mode and the higher one is the optical mode.

Reminding that the mechanical parameters were considered as $E= 200GPa$, $G= 70GPa$, $K_s= 0.667$, $\rho =8000kg/m^3$ and $k=50MPa$. For the long-wave limit ($ak_w \rightarrow 0$), the dispersive results obtained from the discrete and continuous model must be equivalent. So, the velocity at the infinite wavelength of the discrete model could be considered equal to the compression wave velocity of the classical elastic continuum. The divergence of the discrete and continuum frequencies for the wave number increase is obvious. Thus, the inhomogeneous effect by the particle size becomes more prominent or in the other words, the granular models behave more dispersive.

According to the sinusoidal dispersive curve of the exact results, when the curve meets the horizontal axis ($\omega = 0$), it continues periodically. Therefore, it can be concluded that for the exact discrete approach, the responses are always stable. Likewise, the dispersive curves of the Padé approximants could be considered stable as they increase continually from zero without any imaginary part. The unstable harmonic responses appear when the downward branch of the Taylor dispersive curve encounters axis $\omega = 0$.

(a) (b)

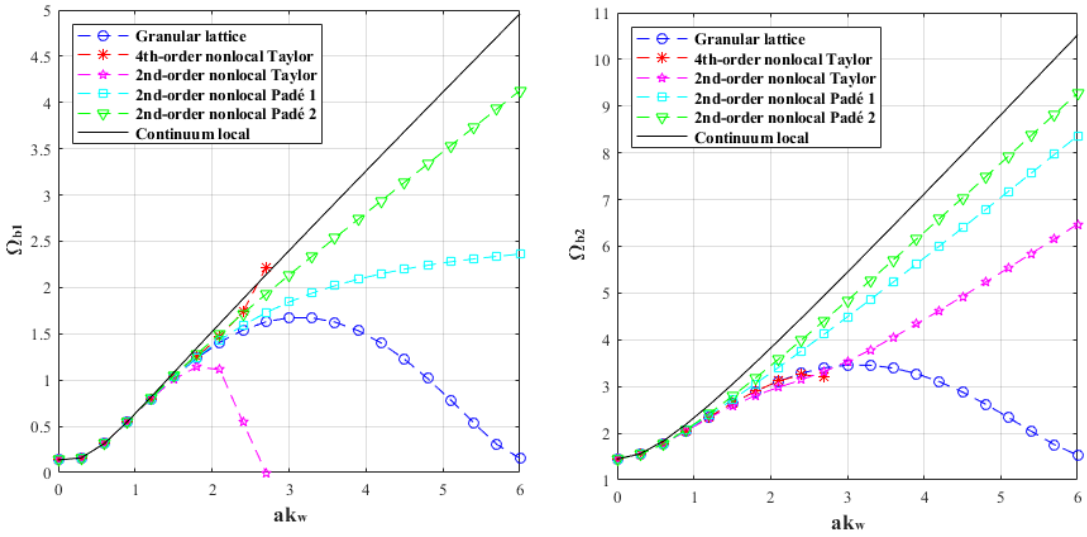

Figure 25. Dispersive curves for one-dimensional compression wave of (a) first branch or the acoustic mode and (b)second branch or the optical mode according to shear nondimensional parameter- various approaches for $\boldsymbol{\mu_s = 4.28}$, $\boldsymbol{r^* = 0.289}$ and $\boldsymbol{k^* = 1.03}$.

The derivation of $\frac{\partial \omega}{\partial k_w}$ represent the wave propagation speed in the system. The existence of the maximum point in the exact and Taylor dispersive results where $\frac{\partial \omega}{\partial k_w} = 0$, the wave energy can't propagate and it represents a standing wave. The dispersive results for the Taylor approach of the pair order and exact discrete solution show the same behavior in which both proceed into a downward trend after passing from a maximum frequency.

Since all the frequencies are in the limited domain, the transition of only low frequencies is possible and consequently, it can be supposed that the media act as a granular filter. This is in contrast to the Padé results and continuum curve since the dispersive curve increases continuously and so all ranges of frequencies can be transmitted.

Here, parametric studies are carried out in order to figure out how intergranular stiffness contributes to the dispersive behavior of the material. To this aim, the influence of the Young modulus on the wave velocity (c_0) and μ_s has been studied in Figure 15 and

Figure 27. The dispersive curves of the first branch frequency for the granular chain are plotted for different approaches.

(a) (b)

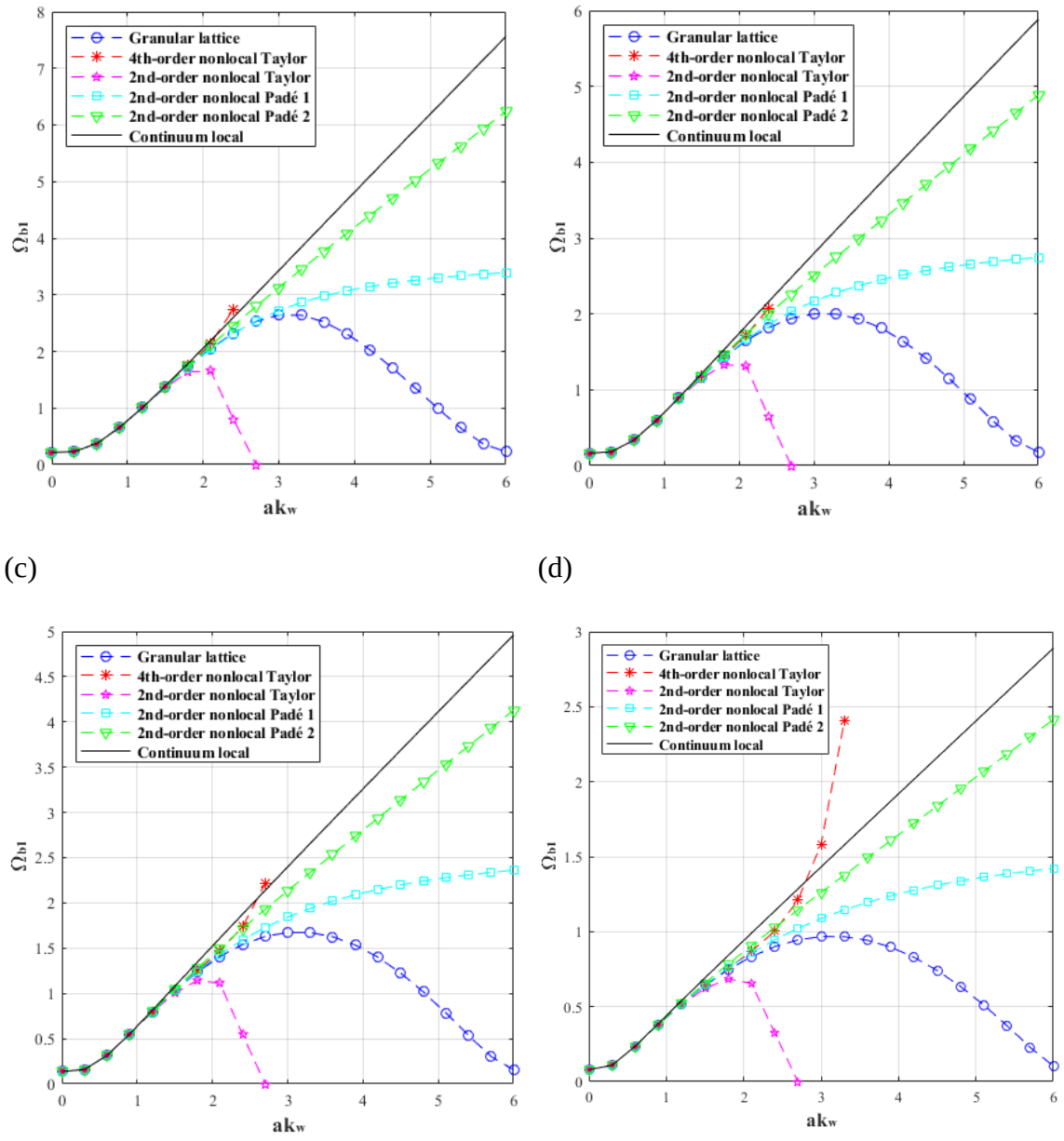

(c) (d)

Figure 26. Comparison of the first branch of natural frequency for the different values of Young modulus in 1D media: (a) $\boldsymbol{c_0 = 3162}$ m/s^2 and $\boldsymbol{\mu_s = 1.71}$, (b) $\boldsymbol{c_0 = 4183}$ m/s^2 and $\boldsymbol{\mu_s = 2.99}$, (c) $\boldsymbol{c_0 = 5000}$ m/s^2 and $\boldsymbol{\mu_s = 4.28}$ and (d) $\boldsymbol{c_0 = 8660}$ m/s^2 and $\boldsymbol{\mu_s = 12.85}$ for $\boldsymbol{r^* = 0.289}$ and $\boldsymbol{k^* = 0}$.

(a) (b)

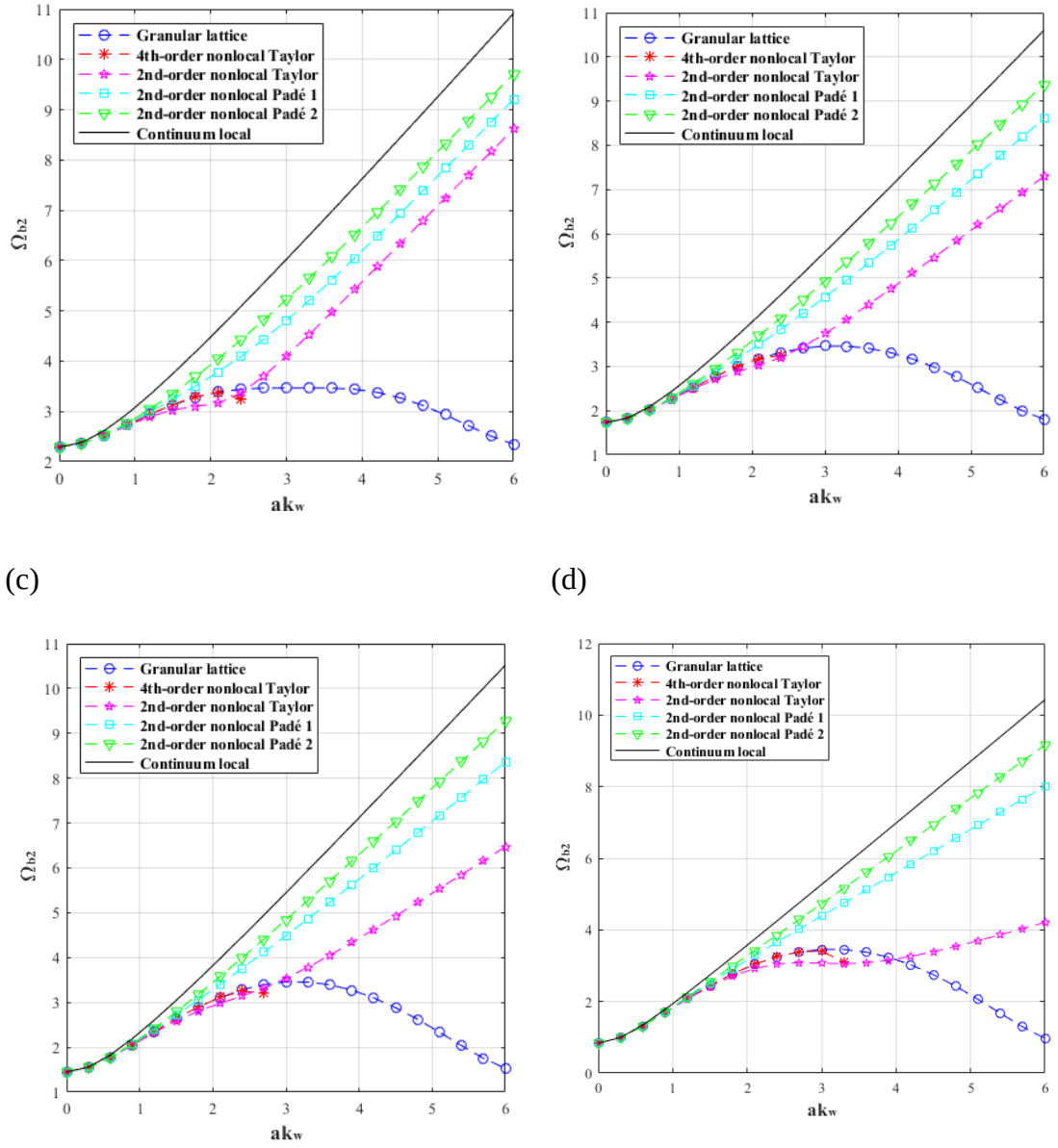

Figure 27. Comparison of the second branch of natural frequency for the different values of Young modulus in 1D media: (a) $\boldsymbol{c_0 = 3160\ m/s2}$ and $\boldsymbol{\mu_s = 1.71}$, (b) $\boldsymbol{c_0 = 4183\ m/s2}$ and $\boldsymbol{\mu_s = 2.99}$, (c) $\boldsymbol{c_0 = 5000}$ m/s^2 and $\boldsymbol{\mu_s = 4.28}$ and (d) $\boldsymbol{c_0 = 8660\ m/s2}$ and $\boldsymbol{\mu_s = 12.85}$ for $\boldsymbol{r^* = 0.289}$ and $\boldsymbol{k^* = 0}$.

The bending behavior of Carbon Nanotubes (CNTs) could be modeled quite well by the Timoshenko beam theory. In this study for short tubes, the short wavelengths or high frequencies are investigated and the results are compared by the molecular dynamics results of Wang and Hu [133] a different gradient enrichment of the Timoshenko beam theory for (5,5) and (10,10) armchair CNTs.

In this article, the effective parameters reported as K_s= *0.5*, $\rho = 2237 kg/m^3$, *k=0MPa*, *E= 460GPa* and *G= 188.5GPa* for (5,5) CNT and *E= 470GPa* and *G= 195.8GPa* for (10,10) CNT. The cross-section area and the second moment of inertia could be calculated subsequently by $A = 2\pi rt$ and $I = \pi(R^3 t + 0.25 t^3 R)$, where R is the radius of the CNT and t is the wall thickness. According to Domenico and Askes [129] for C-C bond length of $l = 0.142nm$ the closest longitudinal distance between two rings of atoms in an armchair CNT given by $L = \sqrt{3}l$ and R the radius of the CNT would be found by $R = \frac{3nl}{2\pi}$ (for $n = 5, 10$). The thickness of the tube wall is supposed $t = 0.0617\, nm$ (Vodenitcharova and Zhang [134]).

(a) (b)

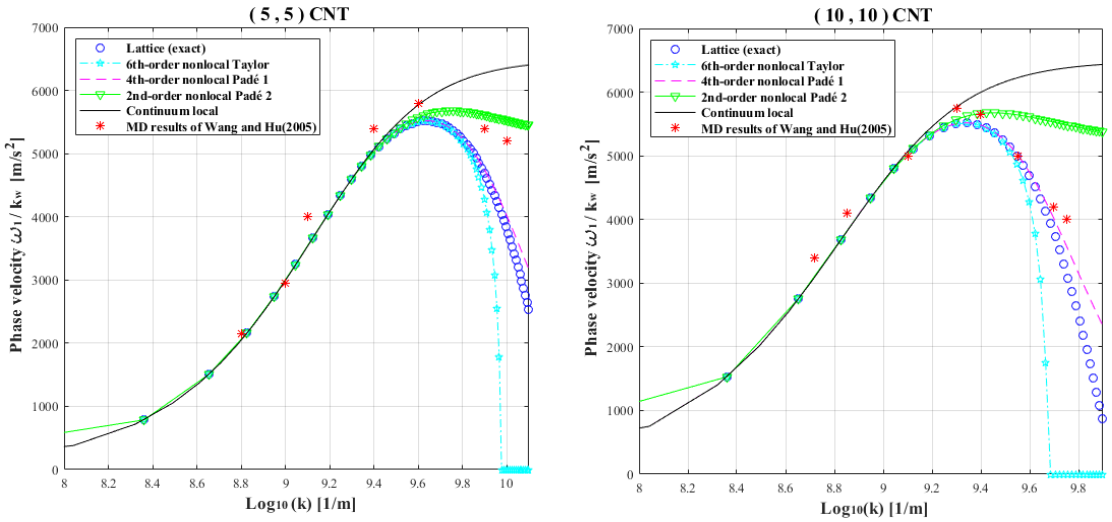

Figure 28. Comparison of the different approaches with the molecular dynamics results of Wang and Hu [133]: (a) (5,5) and (b) (10,10) armchair CNT - various approaches

5. Conclusions

Wave dispersion occurs in granular systems when the characteristic length scale of the discrete model is of the same order as the wavelength of the waves propagating through the equivalent continuous media. In order to capture this effect, a discrete Cosserat theory

has been used to analyze the wave propagation in discrete granular chains. First, the exact dispersive equation of the system has been obtained from the uncoupled equation of motion of the discrete granular chain resting on Winkler foundations. Using the exact resolution of the difference equation of the discrete system, it has been clarified that the two branches of eigenfrequencies exist for the granular model which leads to the ones obtained in the literature, namely by Bresse and Timoshenko for an infinite number of grains. Next, the model has been homogenized using non-local gradient terms by two approaches based on the Taylor series and Padé approximations. It has been shown that the dispersion behavior of higher-order continuous models is improved by considering additional gradient enrichments terms, as compared to the initial discrete one. It can be also concluded that, as observed for the dispersion curves of the discrete granular chain, the continuous approximation issued of a Padé approximant is always stable.

CHAPTER 5

Two-Dimensional Plane: Discrete and Continuum Modelling

1. Introduction

In this chapter, we investigate a novel micropolar model which is consistent with the non-linear first gradient formulation. The enriched model is obtained for isotropic plates. The new approach is based on introducing three measures of deformation namely the Cauchy-Green strain tensor, the wryness tensor in addition to a new relative rotation tensor. Instead of the Euler angles (Bojanczyk and Lutoborski [135]), the microrotation of the system is introduced by a tensor Q to describe the local rigid rotations. This orthogonal tensor consists of four independent components for 2D problems which admits four constraints: the latter correspond to the orthogonal property of the microrotation tensor and to its determinant which needs to be equal to one.

The present study is organized as follows. First, we try to investigate the generalization of discrete plane media. To this aim, for the kinematically constrained condition of a discrete Cosserat media, the Born-Karman media would be found. The model must converge asymptotically towards a linear elastic continuous media with two parameters (for example Young modulus and Poisson's ratio), and towards a continuous isotropic Cosserat media with 6 parameters (2 classical elastic parameters and 4 additional parameters - see for example Eremeyev et al. [136]). Next, the governing formulations of the nonlinear micropolar model and the deformation energy equations are obtained for isotropic materials. Finally, several numerical simulations have been performed with a finite element method using variational formulations to underline the main features of the proposed model. The finite element method which is based on the variations principle

minimizes the action functional of the physical problem in exam (dell'Isola and Gavrilyuk [137], Steinmann and Stein [138], Nistor [139] and Hashin and Shtrikman [140]).

2. In-Plane Granular Model

Let's consider a two-dimensional granular system of dimension $L_1 \times L_2$ that is modeled by a lattice granular structure. Such a system could be presented by microstructured granular chain comprising $n+1 \times m+1$ rigid grains with diameter a ($a=L_1/n=L_2/m$) that are connected elastically by n+m normal, shear and rotational springs as shown in Figure 29. Each grain has three degrees of freedom in-plane which are represented by $U_{i,j}$, $V_{i,j}$ and $\Theta_{i,j}$ for grain number i and j. The objective is finding the vibration equation governing the model and then trying to obtain the natural frequencies.

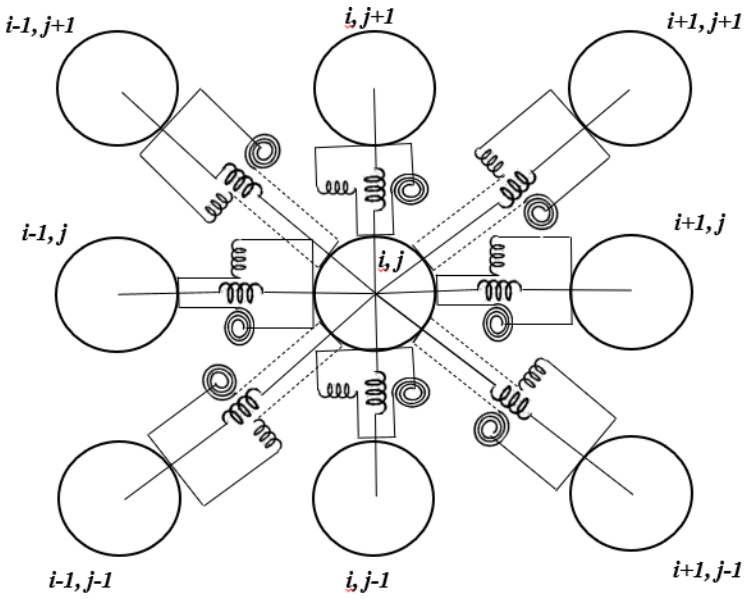

Figure 29. A discrete shear granular plane of dimension $\boldsymbol{L_1 \times L_2}$ composed of $(\boldsymbol{n+1}) \times (\boldsymbol{m+1})$ grains of diameter a and mass m

The strain energy function due to deformed normal springs is given by:

$$\begin{aligned} \boldsymbol{U_N} \\ = \frac{\mathbf{1}}{\mathbf{2}} \sum_{\boldsymbol{j=0}}^{\boldsymbol{m-1}} \sum_{\boldsymbol{i=0}}^{\boldsymbol{n-1}} \Big[\boldsymbol{k_n} \big(\boldsymbol{U_{i+1,j}} - \boldsymbol{U_{i,j}}\big)^{\mathbf{2}} + \boldsymbol{k_n} \big(\boldsymbol{V_{i,j+1}} - \boldsymbol{V_{i,j}}\big)^{\mathbf{2}} \\ + \boldsymbol{k_{nd}} \Big(\big(\boldsymbol{U_{i+1,j+1}} - \boldsymbol{U_{i,j}}\big) + \big(\boldsymbol{V_{i+1,j+1}} - \boldsymbol{V_{i,j}}\big) \Big)^{\mathbf{2}} + \boldsymbol{k_{nd}} \Big(\big(\boldsymbol{U_{i,j}} - \boldsymbol{U_{i-1,j+1}}\big) + \big(\boldsymbol{V_{i-1,j+1}} - \boldsymbol{V_{i,j}}\big) \Big)^{\mathbf{2}} \Big] \end{aligned} \tag{292}$$

One could define for the relative diagonal displacement as follows:

$$\begin{aligned} & \frac{\mathbf{1}}{\sqrt{\mathbf{2}}} \big[\big(U_{i+1,j+1} - \boldsymbol{U_{i,j}}\big) + \big(V_{i+1,j+1} - V_{i,j}\big) \big] \\ & = \frac{\mathbf{1}}{\sqrt{\mathbf{2}}} \big[\big(U_{i+1,j} - \boldsymbol{U_{i,j}}\big) + \big(U_{i,j+1} - \boldsymbol{U_{i,j}}\big) + \big(\boldsymbol{V_{i+1,j}} - V_{i,j}\big) + \big(\boldsymbol{V_{i,j+1}} - V_{i,j}\big) \big] \\ & = \frac{\mathbf{1}}{\sqrt{\mathbf{2}}} \big[\Delta U_i + \Delta \boldsymbol{U_j} + \Delta V_i + \Delta \boldsymbol{V_j} \big]; \\ & \frac{\mathbf{1}}{\sqrt{\mathbf{2}}} \big[\big(\boldsymbol{U_{i,j}} - U_{i-1,j+1}\big) + \big(V_{i-1,j+1} - V_{i,j}\big) \big] \\ & = \frac{\mathbf{1}}{\sqrt{\mathbf{2}}} \big[\big(\boldsymbol{U_{i,j}} - U_{i-1,j}\big) - \big(U_{i,j+1} - \boldsymbol{U_{i,j}}\big) - \big(V_{i,j} - \boldsymbol{V_{i-1,j}}\big) + \big(\boldsymbol{V_{i,j+1}} - V_{i,j}\big) \big] \\ & = \frac{\mathbf{1}}{\sqrt{\mathbf{2}}} \big[\Delta U_i - \Delta \boldsymbol{U_j} - \Delta V_i + \Delta \boldsymbol{V_j} \big] \end{aligned} \tag{293}$$

where k_n and k_{nd} are respectively the normal and diagonal rigidity characterize force interactions of the granules of extension/compression and the Poisson's ratio effect which can be expressed with respect to the normal stiffness EA of the equivalent material. These two parameters would be defined as $k_n = \frac{EA}{a} = \frac{nEA}{L_1} = \frac{mEA}{L_2}$ and $k_{nd} = \frac{EA}{\sqrt{2}a}$ in which E and A are Young's modulus and the cross-section area of the plate.

The strain energy function due to deformed shear springs (shear term) is given by:

$$
\begin{aligned}
&U_t \\
&= \frac{1}{2}\sum_{j=0}^{m-1}\sum_{i=0}^{n-1}\left(k_t\left(U_{i,j+1} - U_{i,j} + a\frac{\Theta_{i,j+1}+\Theta_{i,j}}{2}\right)^2 + k_t\left(V_{i+1,j} - V_{i,j} - a\frac{\Theta_{i+1,j}+\Theta_{i,j}}{2}\right)^2\right. \\
&+ k_{td}\left(U_{i+1,j+1} - U_{i,j} - V_{i+1,j+1} + V_{i,j} + a\frac{\Theta_{i+1,j+1}+\Theta_{i,j}}{2}\right)^2 \\
&\left.+ k_{td}\left(U_{i,j} - U_{i-1,j+1} + V_{i,j} - V_{i-1,j+1} + a\frac{\Theta_{i-1,j+1}+\Theta_{i,j}}{2}\right)^2\right)
\end{aligned} \tag{294}
$$

where k_t and k_{td} are the shear stiffness and can be expressed with respect to the shear stiffness s_0GA of the equivalent beam which would be defined as $k_t = \frac{s_0GA}{a} = \frac{ns_0GA}{L_1} = \frac{ms_0GA}{L_2}$ and $k_{td} = \frac{s_0GA}{\sqrt{2}a}$ in which G is the shear modulus, *A* is the cross-sectional area of the beam and s_0 the shear correction coefficient to compensate for the error in assuming a constant shear strain/stress.

The strain energy function due to deformed rotational springs is given as:

$$
\begin{aligned}
&\boldsymbol{U_b} \\
&= \frac{\mathbf{1}}{\mathbf{2}}\sum_{j=0}^{m-1}\sum_{i=0}^{n-1}\left(\boldsymbol{k_o}\left(\boldsymbol{\Theta_{i+1,j}} - \boldsymbol{\Theta_{i,j}}\right)^2\right. \\
&\left.+ \boldsymbol{k_o}\left(\boldsymbol{\Theta_{i,j+1}} - \boldsymbol{\Theta_{i,j}}\right)^2 + \boldsymbol{k_{od}}\left(\boldsymbol{\Theta_{i+1,j+1}} - \boldsymbol{\Theta_{i,j}}\right)^2 + \boldsymbol{k_{od}}\left(\boldsymbol{\Theta_{i+1,j-1}} - \boldsymbol{\Theta_{i,j}}\right)^2\right)
\end{aligned} \tag{295}
$$

where k_o and k_{od} are the rotational stiffness and are located between the neighbor grains whereas they transmit moments to particle rotation. This discrete stiffness can be expressed with respect to the bending stiffness *EI* of the equivalent beam and thus would be defined as $k_o = \frac{EI}{a} = \frac{nEI}{L_1} = \frac{mEI}{L_2}$ and $k_{od} = \frac{EI}{\sqrt{2}a}$where *E* and *I* are Young's modulus and the second moment of area.

The total kinetic energy *T* is given by:

$$
\boldsymbol{T} = \frac{\mathbf{1}}{\mathbf{2}}\sum_{\boldsymbol{j=1}}^{\boldsymbol{m}}\sum_{\boldsymbol{i=1}}^{\boldsymbol{n}}\left(\boldsymbol{m}\dot{\boldsymbol{U}}_{\boldsymbol{i,j}}{}^2 + \boldsymbol{I_m}\dot{\boldsymbol{\theta}}_{\boldsymbol{i,j}}^2 + \boldsymbol{m}\dot{\boldsymbol{V}}_{\boldsymbol{i,j}}{}^2\right) \tag{296}
$$

where $I_m = \frac{\rho IL}{n} = \rho Ia$ is the second moment of inertia of the beam segment.

Therefore, the Lagrangian equation of the granular system is defined as $L = T - (U_N + U_s + U_b)$ and can be expressed for the linear elastic isotropic granular system as

$$\begin{aligned}
\boldsymbol{L} &= \frac{\mathbf{1}}{\mathbf{2}}\sum_{j=1}^{m}\sum_{i=1}^{n}\left(\boldsymbol{m}\dot{\boldsymbol{U}}_{i,j}{}^{2} + \boldsymbol{I_m}\dot{\boldsymbol{\theta}}_{i,j}^{2} + \boldsymbol{m}\dot{\boldsymbol{V}}_{i,j}{}^{2}\right) \\
&- \left[\frac{\mathbf{1}}{\mathbf{2}}\sum_{j=0}^{m-1}\sum_{i=0}^{n-1}\left(\boldsymbol{k_n}\left(\boldsymbol{U}_{i+1,j} - \boldsymbol{U}_{i,j}\right)^{2} + \boldsymbol{k_n}\left(\boldsymbol{V}_{i,j+1} - \boldsymbol{V}_{i,j}\right)^{2}\right.\right. \\
&+ \boldsymbol{k_{nd}}\left(\left(\boldsymbol{U}_{i+1,j} - \boldsymbol{U}_{i,j}\right)^{2} + \left(\boldsymbol{U}_{i,j+1} - \boldsymbol{U}_{i,j}\right)^{2} + \left(\boldsymbol{V}_{i+1,j} - \boldsymbol{V}_{i,j}\right)^{2} + \left(\boldsymbol{V}_{i,j+1} - \boldsymbol{V}_{i,j}\right)^{2}\right. \\
&\left.\left.\left. + \mathbf{2}\left(\boldsymbol{U}_{i+1,j} - \boldsymbol{U}_{i,j}\right)\left(\boldsymbol{V}_{i,j+1} - \boldsymbol{V}_{i,j}\right) + \mathbf{2}\left(\boldsymbol{U}_{i,j+1} - \boldsymbol{U}_{i,j}\right)\left(\boldsymbol{V}_{i+1,j} - \boldsymbol{V}_{i,j}\right)\right)\right)\right. \\
&+ \frac{\mathbf{1}}{\mathbf{2}}\sum_{j=1}^{m}\sum_{i=1}^{n}\left(\boldsymbol{k_t}\left(\boldsymbol{U}_{i,j+1} - \boldsymbol{U}_{i,j} + \boldsymbol{a}\frac{\boldsymbol{\Theta}_{i,j+1} + \boldsymbol{\Theta}_{i,j}}{\mathbf{2}}\right)^{2} + \boldsymbol{k_t}\left(\boldsymbol{V}_{i+1,j} - \boldsymbol{V}_{i,j} - \boldsymbol{a}\frac{\boldsymbol{\Theta}_{i+1,j} + \boldsymbol{\Theta}_{i,j}}{\mathbf{2}}\right)^{2}\right. \\
&+ \boldsymbol{k_{td}}\left(\boldsymbol{U}_{i+1,j+1} - \boldsymbol{U}_{i,j} - \boldsymbol{V}_{i+1,j+1} + \boldsymbol{V}_{i,j} + \boldsymbol{a}\frac{\boldsymbol{\Theta}_{i+1,j+1} + \boldsymbol{\Theta}_{i,j}}{\mathbf{2}}\right)^{2} \\
&\left.\left. + \boldsymbol{k_{td}}\left(\boldsymbol{U}_{i,j} - \boldsymbol{U}_{i-1,j+1} + \boldsymbol{V}_{i,j} - \boldsymbol{V}_{i-1,j+1} + \boldsymbol{a}\frac{\boldsymbol{\Theta}_{i-1,j+1} + \boldsymbol{\Theta}_{i,j}}{\mathbf{2}}\right)^{2}\right)\right. \\
&\left. + \frac{\mathbf{1}}{\mathbf{2}}\sum_{j=0}^{m-1}\sum_{i=0}^{n-1}\left(\boldsymbol{k_o}\left(\boldsymbol{\Theta}_{i+1,j} - \boldsymbol{\Theta}_{i,j}\right)^{2} + \boldsymbol{k_o}\left(\boldsymbol{\Theta}_{i,j+1} - \boldsymbol{\Theta}_{i,j}\right)^{2} + \boldsymbol{k_{od}}\left(\boldsymbol{\Theta}_{i+1,j+1} - \boldsymbol{\Theta}_{i,j}\right)^{2} + \boldsymbol{k_{od}}\left(\boldsymbol{\Theta}_{i+1,j-1} - \boldsymbol{\Theta}_{i,j}\right)^{2}\right)\right]
\end{aligned} \tag{297}$$

The Euler-Lagrange equations are given by:

$$\frac{\partial L}{\partial U_{i,j}} = \frac{d}{dt}\left(\frac{\partial L}{\partial \dot{U}_{i,j}}\right);\ \frac{\partial L}{\partial V_{i,j}} = \frac{d}{dt}\left(\frac{\partial L}{\partial \dot{V}_{i,j}}\right);\ \frac{\partial L}{\partial \Theta_{i,j}} = \frac{d}{dt}\left(\frac{\partial L}{\partial \dot{\Theta}_{i,j}}\right) \tag{298}$$

The Euler-Lagrange equations based on the energy function of Eq. (297) are obtained as follows:

$$\begin{aligned}
&(\mathrm{k}_n + \mathrm{k}_{nd} + \mathrm{k}_{td})\left(U_{i+1,j} + U_{i-1,j} - 2U_{i,j}\right) + (\mathrm{k}_t + \mathrm{k}_{nd} + \mathrm{k}_{td})\left(U_{i,j+1} + U_{i,j-1} - 2U_{i,j}\right) \\
&+ \frac{a}{2}(\mathrm{k}_t + 2\mathrm{k}_{td})\left(\Theta_{i+1,j} + \Theta_{i-1,j} + \Theta_{i,j+1} + \Theta_{i,j-1} - 4\Theta_{i,j}\right) \\
&+ (\mathrm{k}_{nd} + \mathrm{k}_{td})\left(V_{i+1,j} + V_{i-1,j} + V_{i,j+1} + V_{i,j-1} - 4V_{i,j}\right) - m\ddot{U}_{i,j} = 0
\end{aligned} \tag{299}$$

$$(\mathrm{k}_n + \mathrm{k}_{nd} + \mathrm{k}_{td})\big(V_{i,j+1} + V_{i,j-1} - 2V_{i,j}\big) + (\mathrm{k}_t + \mathrm{k}_{nd} + \mathrm{k}_{td})\big(V_{i+1,j} + V_{i-1,j} - 2V_{i,j}\big) \tag{300}$$
$$-\frac{a}{2}(\mathrm{k}_t + 2\mathrm{k}_{td})\big(\Theta_{i+1,j} - \Theta_{i-1,j}\big) + (\mathrm{k}_{nd} + \mathrm{k}_{td})\big(U_{i+1,j} + U_{i-1,j} + U_{i,j+1} + U_{i,j-1} - 4U_{i,j}\big)$$
$$- m\ddot{V}_{i,j} = 0$$

$$(\mathrm{k}_o + 2\mathrm{k}_{od})\big[\big(\Theta_{i+1,j} + \Theta_{i-1,j} - 2\Theta_{i,j}\big) + \big(\Theta_{i,j+1} + \Theta_{i,j-1} - 2\Theta_{i,j}\big)\big] \tag{301}$$
$$+ 2\mathrm{k}_{od}\big[\Theta_{i+1,j} + \Theta_{i-1,j} + \Theta_{i,j+1} + \Theta_{i,j-1} - 4\Theta_{i,j}\big]$$
$$-\frac{a}{2}(\mathrm{k}_t + 2\mathrm{k}_{td})\big[\big(U_{i,j+1} - U_{i,j-1}\big) - \big(V_{i+1,j} - V_{i-1,j}\big)\big]$$
$$-\frac{a^2}{4}(\mathrm{k}_t + 2\mathrm{k}_{td})\big[\big(\Theta_{i+1,j} + \Theta_{i-1,j} + 2\Theta_{i,j}\big) + \big(\Theta_{i,j+1} + \Theta_{i,j-1} + 2\Theta_{i,j}\big)\big] - I_m\ddot{\Theta}_{i,j} = 0$$

In order to shorten the equations, the following difference operators can be defined:

$$\delta_{0j}\chi = \frac{\chi_{i+1,j} + 2\chi_{i,j} + \chi_{i-1,j}}{4}, \delta_{1j}\chi = \frac{\chi_{i+1,j} - \chi_{i-1,j}}{2a}, \delta_{2j}\chi = \frac{\chi_{i+1,j} - 2\chi_{i,j} + \chi_{i-1,j}}{a^2}$$
$$\delta_{i0}\chi = \frac{\chi_{i,j+1} + 2\chi_{i,j} + \chi_{i,j-1}}{4}, \delta_{i1}\chi = \frac{\chi_{i,j+1} - \chi_{i,j-1}}{2a}, \delta_{i2}\chi = \frac{\chi_{i,j+1} - 2\chi_{i,j} + \chi_{i,j-1}}{a^2}$$
$$\delta_{11}\chi = \frac{\chi_{i+1,j+1} + \chi_{i-1,j-1} - \chi_{i-1,j+1} - \chi_{i+1,j-1}}{a^2} = \frac{\chi_{i+1,j} + \chi_{i,j+1} + \chi_{i-1,j} + \chi_{i,j-1} - 4\chi_{i,j}}{2a^2} \tag{302}$$

Therefore Eq. (299), (300) and (301) could be rewritten compactly as:

$$(\mathrm{k}_n + \mathrm{k}_{nd} + \mathrm{k}_{td})\delta_{2j}U + (\mathrm{k}_t + \mathrm{k}_{nd} + \mathrm{k}_{td})\delta_{i2}U + (\mathrm{k}_t + 2\mathrm{k}_{td})\delta_{i1}\Theta$$
$$+ 2(\mathrm{k}_{nd} + \mathrm{k}_{td})\delta_{11}V - \rho A\ddot{U}_{i,j} = 0$$
$$(\mathrm{k}_n + \mathrm{k}_{nd} + \mathrm{k}_{td})\delta_{i2}V + (\mathrm{k}_t + \mathrm{k}_{nd} + \mathrm{k}_{td})\delta_{2j}V - (\mathrm{k}_t + 2\mathrm{k}_{td})\delta_{1j}\Theta$$
$$+ 2(\mathrm{k}_{nd} + \mathrm{k}_{td})\delta_{11}U - \rho A\ddot{V}_{i,j} = 0$$
$$(\mathrm{k}_o + 2\mathrm{k}_{od})\big(\delta_{2j} + \delta_{i2}\big)\Theta + 4\mathrm{k}_{od}\delta_{11}\Theta - (\mathrm{k}_t + 2\mathrm{k}_{td})\big(\delta_{i1}U - \delta_{1j}V\big) \tag{303}$$
$$- (\mathrm{k}_t + 2\mathrm{k}_{td})\big(\delta_{0j} + \delta_{i0}\big)\Theta - \rho I\ddot{\Theta}_{i,j} = 0$$

Considering only two degrees of freedom (U and V), these equations of motion leads to the ones obtained by Suiker et al. [141] neglecting the effects of rotation angle and rotational springs ($\mathrm{k}_o = 0$ and $\mathrm{k}_{od} = 0$) as follows

$$
\begin{aligned}
&(\mathrm{k}_n)\big(\delta_{2j}U\big) + (\mathrm{k}_{nd})\big(\delta_{2j}U + \delta_{i2}U + 2\delta_{11}V\big) + (\mathrm{k}_t)(\delta_{i2}U) \\
&\quad + (\mathrm{k}_{td})\big(\delta_{2j}U + \delta_{i2}U + 2\delta_{11}V\big) - \rho A\ddot{U}_{i,j} = 0 \\
&(\mathrm{k}_n)(\delta_{i2}V) + (\mathrm{k}_{nd})\big(\delta_{i2}V + \delta_{2j}V + 2\delta_{11}U\big) + (\mathrm{k}_t)\big(\delta_{2j}V\big) \\
&\quad + (\mathrm{k}_{td})\big(\delta_{i2}V + \delta_{2j}V + 2\delta_{11}U\big) - \rho A\ddot{V}_{i,j} = 0
\end{aligned}
\tag{304}
$$

Assuming a harmonic motion leads to the consideration of displacement and rotation in a general form as $U_{i,j} = u_{i,j}e^{i\omega t}$, $V_{i,j} = v_{i,j}e^{i\omega t}$ and $\Theta_{i,j} = \theta_{i,j}e^{i\omega t}$, the Eq. (303) can be written in the matrix form as follows:

$$
\begin{pmatrix}
k_1\delta_{2j} + k_2\delta_{i2} + \rho A\omega^2 & k_d\delta_{11} & \mathrm{k}_s\delta_{i1} \\
k_d\delta_{11} & k_1\delta_{i2} + k_2\delta_{2j} + \rho A\omega^2 & -\mathrm{k}_s\delta_{1j} \\
\mathrm{k}_s\delta_{i1} & -\mathrm{k}_s\delta_{1j} & -\mathrm{k}_r\big(\delta_{2j} + \delta_{i2}\big) - 4\mathrm{k}_{od}\delta_{11} + \mathrm{k}_s\big(\delta_{0j} + \delta_{i0}\big) - \rho I\omega^2
\end{pmatrix}
\begin{pmatrix} u \\ v \\ \theta \end{pmatrix}
= \begin{pmatrix} 0 \\ 0 \\ 0 \end{pmatrix}
\tag{305}
$$

Denoting the following equivalence spring rigidity parameters as

$$
k_d = 2(k_{nd} + k_{td}),\ \ k_1 = k_n + 0.5k_d,\ \ k_2 = k_t + 0.5k_d,
\tag{306}
$$

$$
k_s = k_t + 2k_{td},\ \ k_r = k_o + 2k_{od},
$$

The following pseudodifferential operators could be expressed for continuum media with respect to Eq. (302):

$$
\delta_{0j} = \frac{e^{a\partial_x} + 2 + e^{-a\partial_x}}{4} = cosh^2\left(\frac{a\partial_x}{2}\right),\ \ \delta_{1j} = \frac{e^{a\partial_x} - e^{-a\partial_x}}{2a} = \frac{sinh\,(a\partial_x)}{a}\ ,\ \ \delta_{2j} = \frac{e^{a\partial_x} - 2 + e^{-a\partial_x}}{a^2} = \frac{4}{a^2}sinh^2\left(\frac{a\partial_x}{2}\right)
\tag{307}
$$

$$
\delta_{i0} = \frac{e^{a\partial_y} + 2 + e^{-a\partial_y}}{4} = cosh^2\left(\frac{a\partial_y}{2}\right),\ \ \delta_{i1} = \frac{e^{a\partial_y} - e^{-a\partial_y}}{2a} = \frac{sinh\,(a\partial_y)}{a}\ ,\ \ \delta_{i2} = \frac{e^{a\partial_y} - 2 + e^{-a\partial_y}}{a^2} = \frac{4}{a^2}sinh^2\left(\frac{a\partial_y}{2}\right)
\tag{308}
$$

$$
\delta_{11} = \frac{2\big(e^{a^2\partial_x\partial_y} - e^{-a^2\partial_x\partial_y}\big)}{4a^2} = \frac{sinh\,(a^2\partial_x\partial_y)}{a^2}
\tag{309}
$$

In which there is a relation between these operators as:

$$\delta_{2j}\delta_{0j} = \delta_{0j}\delta_{2j} = {\delta_1}^2 \, , \delta_{i2}\delta_{i0} = \delta_{i0}\delta_{i2} = {\delta_{i1}}^2 \tag{310}$$

For the continuum condition by assuming an infinite number of grains when the diameter of the grains converge to zero, the difference operators of Eq. (307), Eq. (308) and Eq. (309) could be continulized by keeping the first order development of Taylor series as follows:

$$\delta_{0j} \approx 1 \, , \;\; \delta_{1j} \approx \partial_x \;\; , \;\; \delta_{2j} \approx \partial_{xx} \tag{311}$$

$$\delta_{i0} \approx 1 \, , \;\; \delta_{i1} \approx \partial_y \, , \;\; \delta_{i2} \approx \partial_{yy} \tag{312}$$

$$\delta_{11} \approx \partial_{xy} \tag{313}$$

In order to obtain the nonzero solutions for Eq. (305) considering the determinant of the coefficient matrix equal to zero, yields:

$$\begin{gathered}
[k_r k_1 k_2]\left({\delta_{2j}}^3 + {\delta_{i2}}^3\right) \\
+ \left[(I\, k_1 k_2 + A\, k_2 k_r + A\, k_1 k_r)\rho\omega^2 - k_1 k_2 k_s(\delta_{i0} + \delta_{0j})\right]\left({\delta_{i2}}^2 + {\delta_{2j}}^2\right) \\
+ \left[k_r\left({k_1}^2 + {k_2}^2 + k_1 k_2\right)\delta_{2j}\delta_{i2} + (k_1 I + k_2 I + k_r A)\rho^2 A\omega^4\right]\left(\delta_{i2} + \delta_{2j}\right) \\
+ [(k_1^2 + k_2^2)\rho I\omega^2 + (k_1 + k_2)2k_r\rho A\omega^2]\left(\delta_{2j}\delta_{i2}\right) + [k_1 k_s^2]\left(\delta_{i1}^2\delta_{i2} + \delta_{1j}^2\delta_{2j}\right) \\
- [k_s(k_1^2 + k_2^2 - k_2 k_s)]\left(\delta_{1j}^2\delta_{i2} + \delta_{i1}^2\delta_{2j}\right) - [(k_1 + k_2)k_s\rho A\omega^2]\left(\delta_{2j}\delta_{i0} + \delta_{0j}\delta_{i2}\right) \\
- [(k_1 + k_2 - k_s)k_s\,\rho A\omega^2]\left({\delta_{1j}}^2 + {\delta_{i1}}^2\right) \\
- \left[\left(\delta_{2j} + \delta_{i2}\right)k_d^2 k_r - \left(\delta_{i0} + \delta_{0j}\right)k_d^2 k_s + I\, k_d^2\omega^2\rho\right](\delta_{11}^2) - \left[2k_d {k_s}^2\right]\left(\delta_{i1}\delta_{1j}\delta_{11}\right) \\
- [k_s\rho^2 A^2\omega^4]\left(\delta_{i0} + \delta_{0j}\right) + [A^2 I\,\omega^6\rho^3] = 0
\end{gathered} \tag{314}$$

For static condition and by assuming $\omega = 0$:

$$\begin{gathered}
[k_r k_1 k_2]\left({\delta_{2j}}^3 + {\delta_{i2}}^3\right) + \left[-k_1 k_2 k_s(\delta_{i0} + \delta_{0j})\right]\left({\delta_{i2}}^2 + {\delta_{2j}}^2\right) \\
+ \left[k_r\left({k_1}^2 + {k_2}^2 + k_1 k_2\right)\delta_{2j}\delta_{i2}\right]\left(\delta_{i2} + \delta_{2j}\right) + [k_1 k_s^2]\left(\delta_{i1}^2\delta_{i2} + \delta_{1j}^2\delta_{2j}\right) \\
- [k_s(k_1^2 + k_2^2 - k_2 k_s)]\left(\delta_{1j}^2\delta_{i2} + \delta_{i1}^2\delta_{2j}\right) \\
- \left[\left(\delta_{2j} + \delta_{i2}\right)k_d^2 k_r - \left(\delta_{i0} + \delta_{0j}\right)k_d^2 k_s\right](\delta_{11}^2) - \left[2k_d {k_s}^2\right]\left(\delta_{i1}\delta_{1j}\delta_{11}\right) = 0
\end{gathered} \tag{315}$$

Omitting the rotational and diagonal terms ($k_r = k_d = 0$):

$$\left[k_1 k_s^2(\delta_{i0} + \delta_{0j})\right]\left(\delta_{i2}{}^2 + \delta_{2j}{}^2\right) - \left[k_1 k_s^2\right]\left(\delta_{i1}^2\delta_{i2} + \delta_{1j}^2\delta_{2j}\right) + \left[k_s k_1^2\right]\left(\delta_{1j}^2\delta_{i2} + \delta_{i1}^2\delta_{2j}\right) = 0 \tag{316}$$

Using the properties of Eq. (310) and considering a continuum media using Eq. (307), (308) and (309) leads to:

$$\left[\left(\boldsymbol{\partial_x^2} + \boldsymbol{\partial_y^2}\right) + \left(\mathbf{2}\frac{E}{K_s G}\right)\boldsymbol{\partial_x^2}\boldsymbol{\partial_y^2}\right]u = \mathbf{0} \tag{317}$$

The Lagrangian equation of the equivalent continuum system could be obtained as follows

$$\begin{aligned}
\boldsymbol{L} &= \frac{\mathbf{1}}{\mathbf{2}}\left(\boldsymbol{m}(\boldsymbol{\partial_t U})^2 + \boldsymbol{I_m}(\boldsymbol{\partial_t \Theta})^2 + \boldsymbol{m}(\boldsymbol{\partial_t V})^2\right) \\
&-\frac{\mathbf{1}}{\mathbf{2}}\Big[(\boldsymbol{k_n} + \boldsymbol{k_{nd}} + \mathbf{2}\boldsymbol{k_{td}})\left((\boldsymbol{\partial_x U})^2 + (\boldsymbol{\partial_y V})^2\right) + (\boldsymbol{k_{nd}} + \boldsymbol{k_t} + \mathbf{2}\boldsymbol{k_{td}})\left((\boldsymbol{\partial_x V})^2 + (\boldsymbol{\partial_y U})^2\right) \\
&+\left(\frac{\boldsymbol{k_t}}{\mathbf{4}} + \frac{\boldsymbol{k_{td}}}{\mathbf{2}} + \boldsymbol{k_o} + \mathbf{2}\boldsymbol{k_{od}}\right)\left((\boldsymbol{\partial_x \Theta})^2 + (\boldsymbol{\partial_y \Theta})^2\right) + (\mathbf{2}\boldsymbol{k_{nd}} - \mathbf{2}\boldsymbol{k_{td}})\left(\boldsymbol{\partial_x U}\boldsymbol{\partial_y V} + \boldsymbol{\partial_x V}\boldsymbol{\partial_y U}\right) \\
&+ (\mathbf{2}\boldsymbol{k_t} + \mathbf{4}\boldsymbol{k_{td}})\left(\boldsymbol{\partial_y U} - \boldsymbol{\partial_x V}\right)\boldsymbol{\Theta} + (\boldsymbol{k_t} + \mathbf{2}\boldsymbol{k_{td}})\left(\boldsymbol{\partial_y U}\boldsymbol{\partial_y \Theta} - \boldsymbol{\partial_x V}\boldsymbol{\partial_x \Theta}\right) \\
&+ (\mathbf{2}\boldsymbol{k_{td}})\left(\boldsymbol{\partial_x U}\boldsymbol{\partial_x \Theta} - \boldsymbol{\partial_y V}\boldsymbol{\partial_y \Theta}\right) + (\mathbf{2}\boldsymbol{k_t} + \mathbf{4}\boldsymbol{k_{td}})\left(\boldsymbol{\partial_y \Theta}\right)\boldsymbol{\Theta} + (\mathbf{2}\boldsymbol{k_t})(\boldsymbol{\partial_x \Theta})\boldsymbol{\Theta} + (\mathbf{2}\boldsymbol{k_t} + \mathbf{2}\boldsymbol{k_{td}})\boldsymbol{\Theta}^2\Big]
\end{aligned} \tag{318}$$

Besides, the governing equations of the two-dimensional continuum for in-plane deformation could be obtained through the continualization of Eq. (305) as follows

$$\begin{pmatrix} k_1\partial_{xx} + k_2\partial_{yy} + \rho A\omega^2 & k_d\partial_{xy} & k_s\partial_y \\ k_d\partial_{xy} & k_1\partial_{yy} + k_2\partial_{xx} + \rho A\omega^2 & -k_s\partial_x \\ k_s\partial_y & -k_s\partial_x & -\mathrm{k}_r\left(\partial_{xx} + \partial_{yy}\right) - 4\mathrm{k}_{od}\partial_{xy} + 2k_s - \rho I\omega^2 \end{pmatrix}\begin{pmatrix} u \\ v \\ \theta \end{pmatrix} = \begin{pmatrix} 0 \\ 0 \\ 0 \end{pmatrix} \tag{319}$$

This system of equations is almost the same as the one of Suiker et al. [142] for nine-cell square lattice. Also omitting the diagonal shear and rotation springs ($\mathrm{k}_{od} = 0$, $\mathrm{k}_{td} = 0$) leads to the model studied by Pavlov et al. [143]. Neglecting all the diagonal

springs ($k_{nd} = 0$, $k_{td} = 0$ and $k_{od} = 0$) leads to the governing equations obtained by Pasternak and Dyskin [144]. It is noteworthy to mention that neglecting rotational springs ($k_r = 0$) and shear springs ($k_s = 0$), the abovementioned equation of motion leads to the ones obtained by Navier with the assumption of plane strain by

$$(\lambda + 2\mu)\partial_{xx}U + (\lambda + \mu)\partial_{xy}V + (\mu)\partial_{yy}U = \rho\partial_{tt}U; \quad (320)$$
$$(\lambda + 2\mu)\partial_{yy}V + (\lambda + \mu)\partial_{xy}U + (\mu)\partial_{xx}V = \rho\partial_{tt}V$$

where λ and μ are Lamé parameters. The micro parameters of the model are then defined

$$k_1 = \lambda + 2\mu, \;\; k_d = \lambda + \mu, \;\; k_2 = \mu \quad (321)$$

where the property of $k_d = k_1 - k_2$ is true. Substituting Eq. (306) leads to

$$k_n = 2k_{nd} \quad (322)$$

While the macro parameters would be expressed by

$$\lambda = \mu = k_{nd} \quad (323)$$

Or in terms of Young's modulus (E) and Poisson's ratio (ϑ)

$$\vartheta = \frac{\lambda}{2(\lambda + \mu)} = \frac{1}{4}, \;\; E = \frac{\mu(3\lambda + 2\mu)}{\lambda + \mu} = \frac{5}{2}k_{nd} \quad (324)$$

3. Linear Isotropic Micropolar Elasticity Theory

Nowacki [4] studied the linear elastic isotropic Cosserat continuum model, which has 6 independent parameters. In a linear micropolar continuum, a micropolar deformation is described by asymmetric strain and twist tensors which might be defined respectively as follows

$$\varepsilon_{ij} = U_{j,i} - \epsilon_{ijk}\theta_k \quad (325)$$
$$\tau_{ij} = \theta_{j,i}$$

where U is displacement field vector and θ is microrotation field vector. The strain tensor can be decomposed into a symmetric and antisymmetric part

$$\varepsilon_{ij} = \varepsilon_{ij}^{s} + \varepsilon_{ij}^{a} \tag{326}$$

$$\varepsilon_{ij}^{s} = \frac{1}{2}(U_{j,i} + U_{i,j}) \ , \quad \varepsilon_{ij}^{a} = \epsilon_{ijk}(\varphi_k - \theta_k)$$

where ϵ_{ijk} is the antisymmetric Levi-Civita (alternating or permutation) tensor, φ_k is the macro rotation vector and is defined by $\varphi_k = \frac{1}{2}\left(U_{j,i} - U_{i,j}\right) = 0.5\epsilon_{ijk}U_{j,i}$.

The associated internal energy of the system is expressed by (Nowacki [4]):

$$U_{internal} = \mu\varepsilon_{ij}^{s}\varepsilon_{ij}^{s} + \kappa\varepsilon_{ij}^{a}\varepsilon_{ij}^{a} + \frac{\lambda}{2}\varepsilon_{kk}\varepsilon_{nn} + \gamma\tau_{ij}^{s}\tau_{ij}^{s} + \beta\tau_{ij}^{a}\tau_{ij}^{a} + \frac{\alpha}{2}\tau_{kk}\tau_{nn} \tag{327}$$

Denoting that $\mu, \lambda, \kappa, \gamma, \alpha$ and β are six material parameters from which μ (shear modulus) and λ are the classical Lame coefficients. κ is Cosserat couple modulus γ, α and β are Cosserat twist coefficients, which are four new elastic constants referred to as the micropolar (Cosserat elastic constants).

The internal loads in a micropolar continuum are definable in terms of a classical force stress tensor (σ) and a micropolar couple stress tensor (C) which should satisfy the balance of linear and angular momentum as

$$\sigma_{ji,j} + f_i^{v} = \rho A\ddot{U}_{\iota}; \tag{328}$$

$$\mathsf{C}_{ji,j} + \epsilon_{ijk}\sigma_{jk} + l_i^{v} = \rho I\ddot{\theta}_{\iota}$$

Denoting that f_i^{v} and l_i^{v} are respectively the body force and body moment. The constitutive relations for a homogeneous, isotropic, and centrally symmetric elastic body is considered by

$$\sigma_{ij} = (\mu + \kappa)\varepsilon_{ij} + (\mu - \kappa)\varepsilon_{ji} + \lambda\varepsilon_{kk}\delta_{ij} \tag{329}$$

$$\mathsf{C}_{ij} = (\gamma + \beta)\tau_{ij} + (\gamma - \beta)\tau_{ji} + \alpha\tau_{kk}\delta_{ij}$$

where δ_{ij} is the Kronecker delta tensor (dyadic). Assuming a simple case by uniform tensile test along x_{11}, leads to the classical strain Poisson's ratio (ϑ) and the classical tensile or Young's modulus (E) as follows

$$\vartheta = -\frac{\varepsilon_{22}}{\varepsilon_{11}} = -\frac{\varepsilon_{33}}{\varepsilon_{11}} = \frac{\lambda}{2(\mu+\lambda)} \tag{330}$$

$$E = \frac{\sigma_{11}}{\varepsilon_{11}} = \frac{\mu(2\mu+3\lambda)}{\mu+\lambda}$$

The equations of motion in terms of displacements and rotations for the micropolar two-dimensional system with six material parameters could be obtained by substituting Eq. (325) and Eq. (329) in Eq. (328) as follows (Cosserat and Cosserat [3], Nowacki [4] and Schaefer [145]):

$$(\mu+\kappa)U_{i,jj} + (\mu-\kappa+\lambda)U_{j,ji} + 2\kappa\epsilon_{ijk}\theta_{k,j} + f_i^v = \rho A\ddot{U}_i; \tag{331}$$

$$(\gamma+\beta)\theta_{i,jj} + (\gamma-\beta+\alpha)\theta_{j,ji} + 2\kappa(\epsilon_{ijk}U_{k,j} - 2\theta_i) + l_i^v = \rho I\ddot{\theta}_i$$

Assuming plane strain conditions by $U_i = (U, V, 0)$ and $\theta_i = (0, 0, \theta)$ and neglecting the body forces and moments, it could be obtained ($\epsilon = \gamma + \beta$):

$$(\lambda+2\mu)\partial_x^2 U + (\mu-\kappa+\lambda)\partial_{xy}V + (\mu+\kappa)\partial_y^2 U + 2\kappa\partial_y\theta = \rho A\partial_t^2 U; \tag{332}$$

$$(\lambda+2\mu)\partial_y^2 V + (\mu-\kappa+\lambda)\partial_{xy}U + (\mu+\kappa)\partial_x^2 V - 2\kappa\partial_y\theta = \rho A\partial_t^2 V;$$

$$(\epsilon)\left(\partial_x^2\theta + \partial_y^2\theta\right) - (2\kappa)\left(\partial_y U - \partial_x V\right) - (4\kappa)\theta = \rho I\partial_t^2\theta$$

Going back to the discrete granular model, the micro parameters of the system might be determined by comparing Eq. (332) and Eq. (319) as follows

$$k_n = \frac{\lambda}{2} + \frac{3\mu}{2} + \frac{\kappa}{2},\ \ k_t = -\frac{\lambda}{2} + \frac{\mu}{2} + \frac{3\kappa}{2},\ \ k_{nd} = \frac{\lambda}{4} + \frac{3\mu}{4} - \frac{3\kappa}{4},\ \ k_{td} = \frac{\lambda}{4} - \frac{\mu}{4} + \frac{\kappa}{4}, \tag{333}$$

$$\mathrm{k}_{od} = 0,\ k_o = \epsilon$$

In the view of abovementioned equation, the following property could be obtained between the microparameters of the system

$$k_n - k_t = 2(k_{td} + k_{nd}) \tag{334}$$

Assuming $k_{td} = 0$ ($\kappa = \mu - \lambda$) (Pavlov et al. [143]), leads to the comparison results of Suiker et al. [142]

$$k_n = 2\mu, \;\; k_t = 2(\mu - \lambda), \;\; k_{nd} = \lambda, \;\; k_{td} = 0, \mathrm{k}_{od} = 0, \;\; k_o = \epsilon \tag{335}$$

4. Two-dimensional Micropolar Continuum Model

A micropolar plate $\mathcal{L} \subset R^2$ deform in the two-dimensional Euclidean space $\mathcal{E} \subset R^2$. In the reference placement, the state of a material particle is described by a position vector $X \in \mathcal{L}$ and by a local reference system defined by two vectors

$$\boldsymbol{E'_{1'}(X) = H(X)E_1}, \;\; \boldsymbol{E'_{2'}(X) = H(X)E_2} \tag{336}$$

where $E_1, E_2 \in \mathcal{L}$ are orthonormal base vectors; the application $H \in Ort(\mathcal{L}, \mathcal{L})$ is such that

$$\boldsymbol{H^{-1} = H^T}, \;\; \mathbf{det}(\boldsymbol{H}) = \mathbf{1} \tag{337}$$

The tensor *Q* with four components for the 2D plates describes microrotations, i.e. the differences between the initial and the actual orientation of the local reference system jointed to each particle

$$\boldsymbol{e'_{1'}(X) = QE'_{1'}}, \;\; \boldsymbol{e'_{2'}(X) = QE'_{2'}} \tag{338}$$

where $e'_{1'}(X) = h(X)e_1, \;\; e'_{2'}(X) = h(X)e_2$; e_1 and e_2 are orthonormal base vectors of $\mathcal{E}$; $h \in Ort(\mathcal{E}, \mathcal{E})$ and $\det(h) = 1$; the application $Q \in Ort(\mathcal{L}, \mathcal{E})$ has the following properties

$$\boldsymbol{Q^{-1} = Q^T}, \;\; \boldsymbol{det(Q)} = \mathbf{1} \tag{339}$$

It is noteworthy to mention that assuming only an orthogonal structure for *H* and *Q* imply their determinants equal to ±1: fixing these two scalar quantities to 1 avoid numerical fluctuations and physical inconsistencies.

4.1. The Cauchy-Green Strain Tensor

Let $F = \nabla\chi$ be the placement gradient that belongs to $Lin(\mathcal{L};\mathcal{E})$. The polar decomposition theorem ensures the existence of only one couple of linear applications $(R,U) \in Ort(\mathcal{L};\mathcal{E}) \times Sym(\mathcal{L},\mathcal{L})$ such that $F = RU$: R and U are respectively the rotation and strain tensors. The Cauchy-Green tensor C is defined by the product between the transpose of F and F itself: $C = F^T F$. Thus, the Cauchy-Green measure of deformation is defined as follows

$$\boldsymbol{G} = \frac{\mathbf{1}}{\mathbf{2}}(\boldsymbol{F^T F} - \boldsymbol{I}) \tag{340}$$

4.2. Relative Rotation Tensor

The presence of a microrotation implies the necessity to define another deformation tensor that takes into account the differences between macro and microrotations: indeed if the microrotation R is equal to the microrotation Q, the abovementioned new deformation tensor needs to be zero. Many authors consider the tensors R, Q and F in a unique deformation tensor $\mathcal{C} = Q^T F = Q^T RU$ which replaces also the Cauchy-Green tensor. It is noteworthy to mention that although $\mathcal{C}$ is really useful from a computational point of view, it does not allow to divide the energy contributions linked respectively to strain, curvature and relative rotation. As an alternative method, it could be possible to introduce the tensor $Q^T R$ which is objective and also depending only on R and Q; even if this new term would allow identifying each energy contribution, it would be almost impossible to evaluate and to define in a FEM code due to the structure of R:

$$\boldsymbol{R} = \boldsymbol{FU^{-1}} = \boldsymbol{F}(\boldsymbol{F^T F})^{-\mathbf{1/2}} \tag{341}$$

Keeping in mind all the aforementioned remarks, here, we decide to define a new relative rotation tensor $\mathcal{R}$ as the difference between $(Q^TF)^2$ and $(R^TF)^2$

$$\boldsymbol{\mathcal{R}} = (\boldsymbol{Q^TF})^2 - (\boldsymbol{R^TF})^2 = (\boldsymbol{Q^TF})^2 - \boldsymbol{C} \tag{342}$$

4.3. The Wryness Tensor

To contribute the gradient of the microrotation tensor Q in the deformation energy functions, it is essential to define the third measure of deformation namely the wryness tensor Γ. This tensor could be expressed as follows:

$$\boldsymbol{\Gamma} = \frac{\mathbf{1}}{\mathbf{2}}\boldsymbol{\epsilon}\colon\boldsymbol{\nabla Q^TQ} \tag{343}$$

5. Energy Approach

The energetic approach is indeed the most powerful tool to derive new mechanical models and to perform numerical applications. The principle of least action leads to fix a suitable action functional based on the kinematic assumptions introduced in Section 1:

$$\boldsymbol{A} = \int_{\mathcal{L}} (-\boldsymbol{W}(\boldsymbol{\chi}, \boldsymbol{Q}, \boldsymbol{C}, \boldsymbol{\mathcal{R}}, \boldsymbol{\Gamma}, \boldsymbol{X}))\, \boldsymbol{dA} + \int_{\partial\mathcal{L}} (-\boldsymbol{W}_s(\boldsymbol{\chi}, \boldsymbol{Q}, \boldsymbol{X}))\, \boldsymbol{dl} \tag{344}$$

where the field χ denotes the placement function between $\mathcal{L}$ and $\mathcal{E}$; the potential W is relative to the surface actions inside $\mathcal{L}$ and the potential W_s is relative to the edge actions externally applied at the boundary $\partial\mathcal{L}$: all the external actions are defined consistently with the internal work.

The internal energy W can be split into two addends, the first one representing the deformation energy satisfying the principle of material frame indifference, the second one an external conservative action of surface loads expressed as

$$\boldsymbol{W}(\boldsymbol{\chi},\boldsymbol{Q},\boldsymbol{C},\boldsymbol{\mathcal{R}},\boldsymbol{\Gamma},\boldsymbol{X}) = \boldsymbol{W}^{\boldsymbol{def}}(\boldsymbol{C},\boldsymbol{\mathcal{R}},\boldsymbol{\Gamma},\boldsymbol{X}) + \boldsymbol{U}^{\boldsymbol{ext}}(\boldsymbol{\chi},\boldsymbol{Q},\boldsymbol{X}) \tag{345}$$

The objectivity of $C, \mathcal{R}$ and Γ ensures the objectivity of the deformation energy W^{def} . The first variation of the action functional gives the minimum of the action functional itself and, consequently, the solution of the elastic problem in exam.

5.1. Deformation Energy Function for Isotropic Materials

For an isotropic material, the deformation energy function can be approximated up to quadratic terms in the non-linear case as follows (see La-Valle and Massoumi [44] and Massoumi and La-Valle [146])

$$\boldsymbol{W_{iso}} = \frac{\boldsymbol{1}}{\boldsymbol{2}}\boldsymbol{\lambda_G}[\boldsymbol{I^G}]^{\boldsymbol{2}} + \boldsymbol{\mu_G}\boldsymbol{II^G} + \frac{\boldsymbol{1}}{\boldsymbol{2}}\boldsymbol{\lambda_{\mathcal{R}}}[\boldsymbol{I^{\mathcal{R}}}]^{\boldsymbol{2}} + \boldsymbol{\mu_{\mathcal{R}}}\boldsymbol{II^{\mathcal{R}}} + \boldsymbol{\mu_{\Gamma\Gamma^T}}\boldsymbol{I^{\Gamma\Gamma^T}} + \boldsymbol{\gamma_{G\mathcal{R}}}\boldsymbol{I^{G\mathcal{R}}} \tag{346}$$

where $\lambda_G, \mu_G, \lambda_{\mathcal{R}}, \mu_{\mathcal{R}}, \mu_{\Gamma\Gamma^T}$ and $\gamma_{G\mathcal{R}}$ are six material parameters. The operators $I^{(*)}$ and $II^{(*)}$ represent the first and second invariants of the tensors assigned that are expressed by

$$\boldsymbol{I^{(*)}} = \boldsymbol{Tr}(*), \quad \boldsymbol{II^{(*)}} = \frac{\boldsymbol{1}}{\boldsymbol{2}}\left[\left(\boldsymbol{I^{(*)}}\right)^{\boldsymbol{2}} - \boldsymbol{I^{((*)^2)}}\right] \tag{347}$$

An alternative enriched deformation with eight material parameters could be considered as follows:

$$\begin{aligned}\boldsymbol{W_{iso}} \\ = \frac{\boldsymbol{1}}{\boldsymbol{2}}\boldsymbol{\lambda_G}[\boldsymbol{I^G}]^{\boldsymbol{2}} + \boldsymbol{\mu_{GG}}\boldsymbol{II^{GG}} + \boldsymbol{\mu_{GG^T}}\boldsymbol{I^{GG^T}} + \frac{\boldsymbol{1}}{\boldsymbol{2}}\boldsymbol{\lambda_{\mathcal{R}}}[\boldsymbol{I^{\mathcal{R}}}]^{\boldsymbol{2}} + \boldsymbol{\mu_{\mathcal{R}\mathcal{R}}}\boldsymbol{I^{\mathcal{R}\mathcal{R}}} + \boldsymbol{\mu_{\mathcal{R}\mathcal{R}^T}}\boldsymbol{I^{\mathcal{R}\mathcal{R}^T}} + \boldsymbol{\mu_{\Gamma\Gamma^T}}\boldsymbol{I^{\Gamma\Gamma^T}} \\ + \boldsymbol{\gamma_{G\mathcal{R}}}\boldsymbol{I^{G\mathcal{R}}}\end{aligned} \tag{348}$$

5.2. Boundary Conditions

Since it has not been considered a rotation angle as in all the common Cosserat models, we need to analyze the correct way to fix boundary conditions. To model a

constrain which acts on a part of the boundary ∂L and which is able to block each degree of freedom, it is necessary to impose the initial placement equal to the actual placement and the initial orientation equal to the actual orientation. The boundary conditions of the displacement for clamped ends could be considered as

$$\boldsymbol{u_1 = 0},\ \ \boldsymbol{u_2 = 0}, \tag{349}$$

Also regarding Eq. (338), the microrotations are assumed by

$$\boldsymbol{e'_{1'}(X) = E'_{1'}},\ \ \boldsymbol{e'_{2'}(X) = E'_{2'}}\ \rightarrow \boldsymbol{Q = I} \tag{350}$$

6. Numerical Simulations

In this section, several applications of the energy model which was given by equation (Eq. (346)) for the isotropic materials are investigated numerically. This sensitive numerical analysis is based on standard energy minimization techniques through the applications of the standard FEM packages in COMSOL Multiphysics. In detail, a 2D planar square of length $L = 0.5m$ with a single square hole of length l is chosen. The defect is half size of the specimen dimensions and is located at the center of the model. The material parameters of the model are defined in Table 3. Many researchers investigated the efficient methods for determining material parameters which are mainly the micro-macro identifications (see for instance Misra and Poorsolhjouy [147], Giorgio et al. [148], Angelo et al. [149] and Turco [150]). The number of the mesh elements must be large enough to assure smooth convergence of the results for the discrete finite element approximation. The model is meshed through 1046 free quad elements corresponding to 47560 degrees of freedom. A usual Lagrange quadratic shape function of quartic order for displacement and quadratic order for microrotation is considered to discretize the weak formulations.

6.1. Compression Test

The first test is set up by applying a vertical compression displacement to the top edge while the bottom edge is assumed to be clamped. Thus, the micro rotations and displacements of the bottom side are null. Accordingly, the boundary conditions are specified as follows:

$$\begin{gathered} \boldsymbol{u_2(X_1, L) = -0.01L,\ \ u_1(X_1, L) = 0,} \\ \boldsymbol{Q_{12}(X_1, L) = Q_{21}(X_1, L) = 0,\ \ Q_{11}(X_1, L) = Q_{22}(X_1, L) = 1,} \\ \boldsymbol{u_1(X_1, 0) = u_2(X_1, 0) = 0,} \\ \boldsymbol{Q_{12}(X_1, 0) = Q_{12}(X_1, 0) = 0,\ \ Q_{11}(X_1, 0) = Q_{22}(X_1, 0) = 1} \end{gathered} \tag{351}$$

The results are shown in Figure 30 It is noteworthy to mention that the maximum energy is stored near the corner of the hole which could be predicted also regarding the stress concentration. The variation of the shear and macro rotation distribution is nearly ignorable in contrast to the distribution of the microrotation which affects severely the domain. The compression test allows for the analysis of properties having a broad range of applications. The horizontal and vertical displacements obtained in Figure 30 are predictable and not so far from the classical one stating the reliability of the proposed theoretical model.

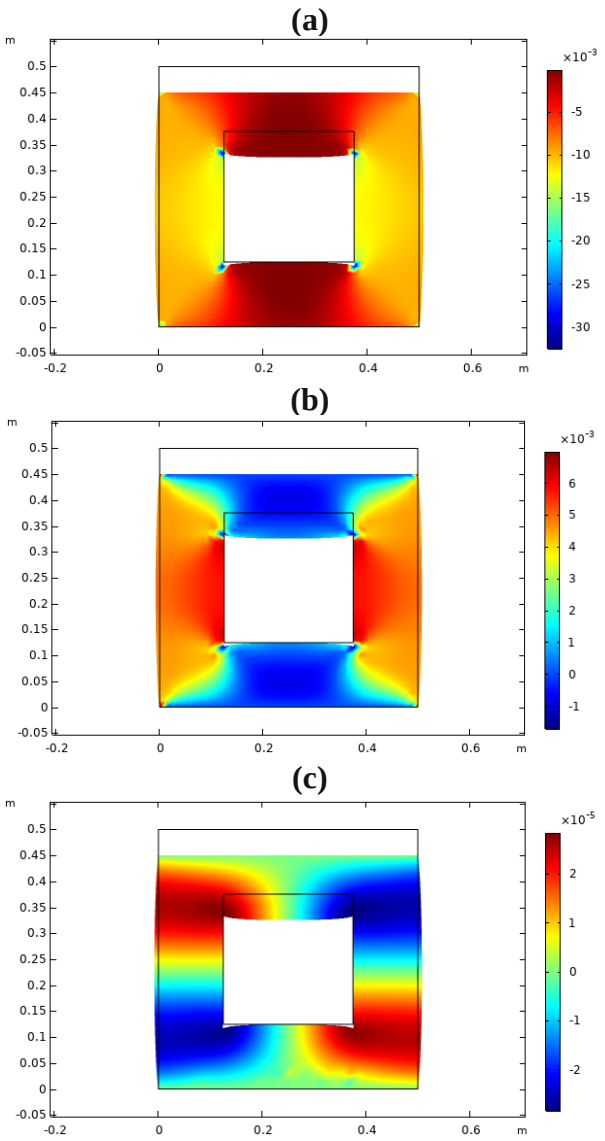

Figure 30. Compression test with a clamped bottom side **(a)** distribution of the vertical strain **(b)** distribution of the horizontal strain **(c)** distribution of the microrotation

6.2. Biaxial Shear Test

This test is performed by imposing parallel displacements of 1% of the square dimension which we apply to each side of the square but in opposite direction with respect to the opposite side. The microrotations of all edges are clamped. Briefly, these conditions could be expressed as

$$\boldsymbol{u_1(X_1, L) = -u_1(X_1, 0) = u_2(L, X_2) = -u_2(0, X_2) = 0.01L} \tag{352}$$

$$\boldsymbol{Q_{12}(X_1,0) = Q_{21}(X_1,0) = Q_{12}(0,X_2) = Q_{21}(0,X_2) = Q_{12}(X_1,L) = Q_{21}(X_1,L)}$$

$$\boldsymbol{= Q_{12}(L,X_2) = Q_{21}(L,X_2) = 0}$$

Some important results of this test are shown in Figure 31**.** The shear strain applied to the system is 1% and the numerical results clarify this value as well. The maximum values of the micro and macrorotations happen at the middle of each hole side with the same orientation.

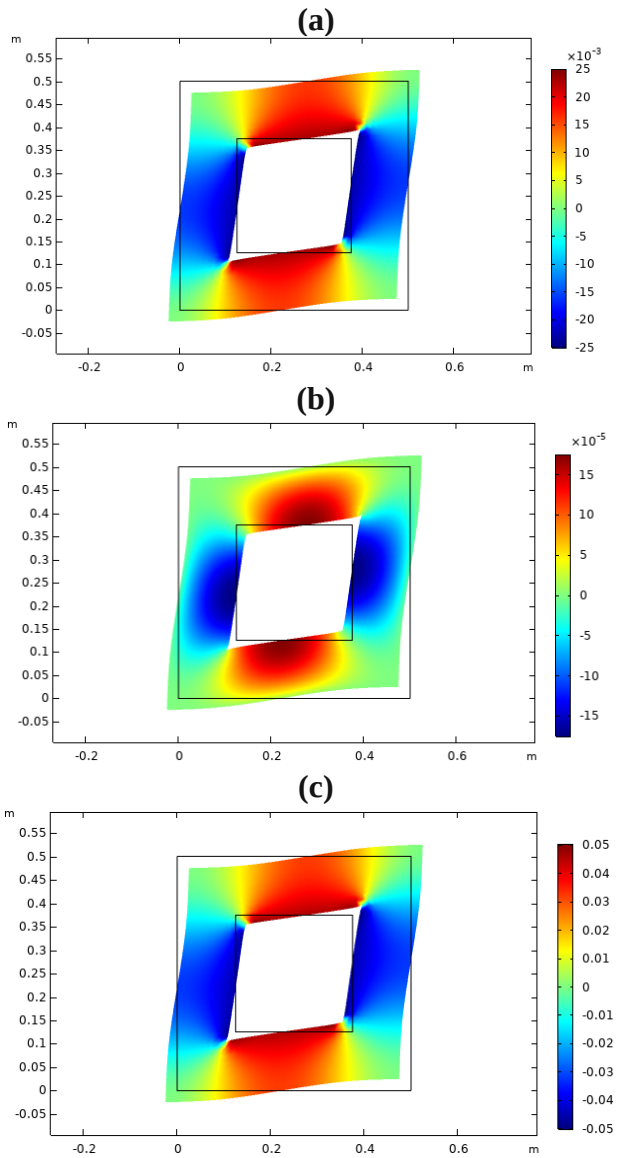

Figure 31. Biaxial shear test with fixed microrotation on the sides (a) distribution of the macro-rotation (b) distribution of the micro-rotation Q_{21} (c) distribution of the relative rotation $\mathcal{R}_{21}$

6.3. Parametric Analysis for Tensile Test

This section focuses on analyzing the effects of additional terms corresponding to the gradient of the microrotation in the energy equation with respect to the classical model. A sensitive parametric analysis has been done for $\mu_{\Gamma\Gamma^T}$ which controls mainly the amount of microrotation stored in the system. This test is set up by applying a horizontal tensile displacement equal to 1% of the model width. The constant displacement is applied to the top side of the square while the bottom side is clamped. For this setup, it is assumed also that the microrotations of the top and bottom sides are fixed. The boundary conditions could be specified as follows:

$$\boldsymbol{u_2(X_1, L) = 0.01L,\ \ u_1(X_1, L) = 0}\,, \tag{353}$$

$$\boldsymbol{Q_{12}(X_1, L) = Q_{21}(X_1, L) = 0}\,,\ \ \boldsymbol{Q_{11}(X_1, L) = Q_{22}(X_1, L) = 1}$$

$$\boldsymbol{u_1(X_1, 0) = u_2(X_1, 0) = 0},$$

$$\boldsymbol{Q_{12}(X_1, 0) = Q_{12}(X_1, 0) = 0},\ \ \boldsymbol{Q_{11}(X_1, 0) = Q_{22}(X_1, 0) = 1}$$

The effect of material parameter $\mu_{\Gamma\Gamma^T}$ on the distribution of the lateral displacement u_1 is presented in Figure 32 for two typical values of $0.001\mu_{\Gamma\Gamma^T{}_0}$ and $0.1\mu_{\Gamma\Gamma^T{}_0}$ in which $\mu_{\Gamma\Gamma^T{}_0}$ is presented in Table 3. The results are shown for a scale factor of 5 to magnify the deformation changes. For small values of $\mu_{\Gamma\Gamma^T}$, the effect of the poison ratio is dominant and leads to the larger values of the lateral displacement and thus increasing the curvature of the sample. This condition converges to the classical model by neglecting the microrotations. Another interesting difference is the distribution of u_1 between the corners of the sample and the ones of the squared hole. It can be noticed that for the great values of $\mu_{\Gamma\Gamma^T}$ the displacement distribution in these zones is not linear but curved.

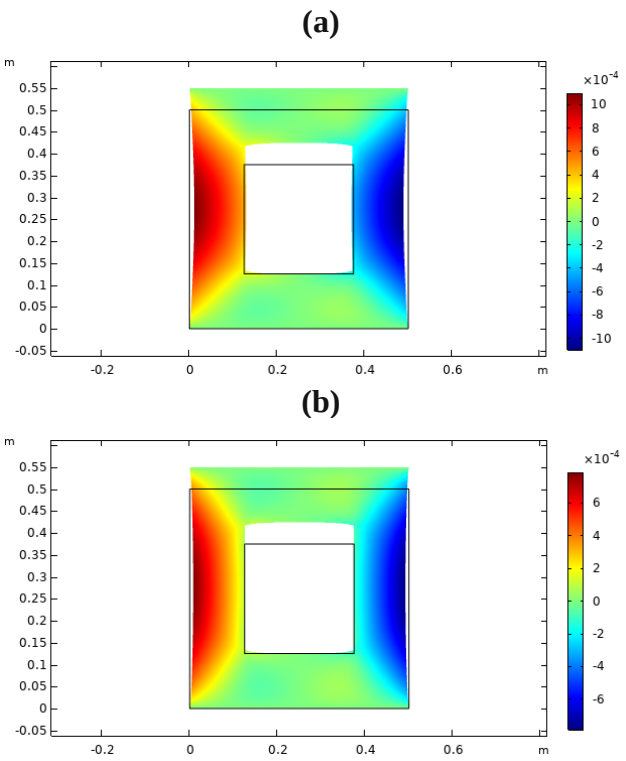

Figure 32. Distribution of the lateral displacement for parametric analysis on $\mu_{\Gamma\Gamma^T}$ for tensile test (a) $\mu_{\Gamma\Gamma^T}/\mu_{\Gamma\Gamma^T}{}_0 = 0.001$ (b) $\mu_{\Gamma\Gamma^T}/\mu_{\Gamma\Gamma^T}{}_0 = 0.1$

Figure 33 presents the effects of the $\boldsymbol{\mu_{\Gamma\Gamma^T}}$ changes on the microrotations distribution. This figure shows that an antisymmetric microrotation field is created for the tensile test. Increasing the value of the $\boldsymbol{\mu_{\Gamma\Gamma^T}}$ leads to the smaller values of the micro rotation proportionally. The maximum values occur at the corners of the squared defect. It is

noteworthy to emphasize that the decrease of this material parameter leads to the concentration of the microrotation field at the corners of the hole.

The distributions of the reaction forces in the clamped boundary are plotted in Figure 34. The horizontal rection is distributed anti-symmetrically which refers to zero in total.

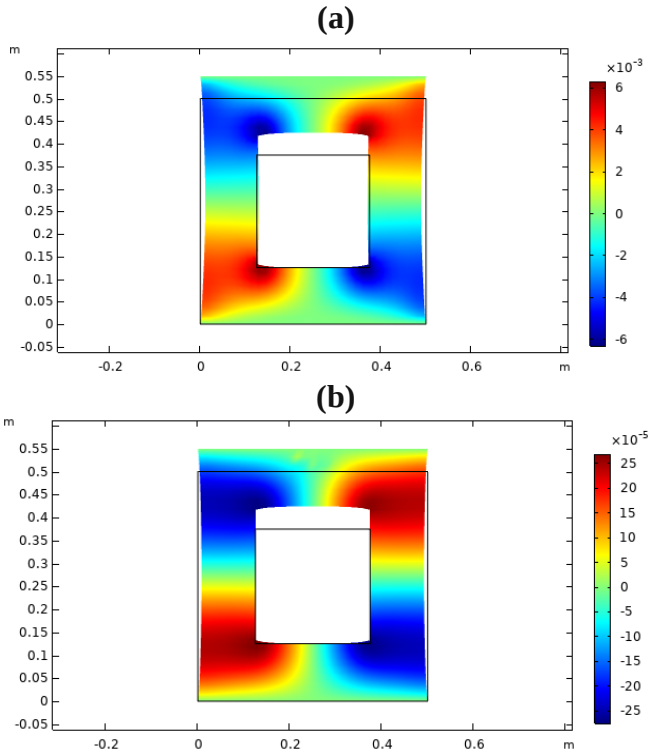

Figure 33. Distribution of the micro rotation for parametric analysis on $\mu_{\Gamma\Gamma^T}$ for tensile test (a) $\mu_{\Gamma\Gamma^T}/\mu_{\Gamma\Gamma^T}{}_0 = 0.001$ (b) $\mu_{\Gamma\Gamma^T}/\mu_{\Gamma\Gamma^T}{}_0 = 0.1$

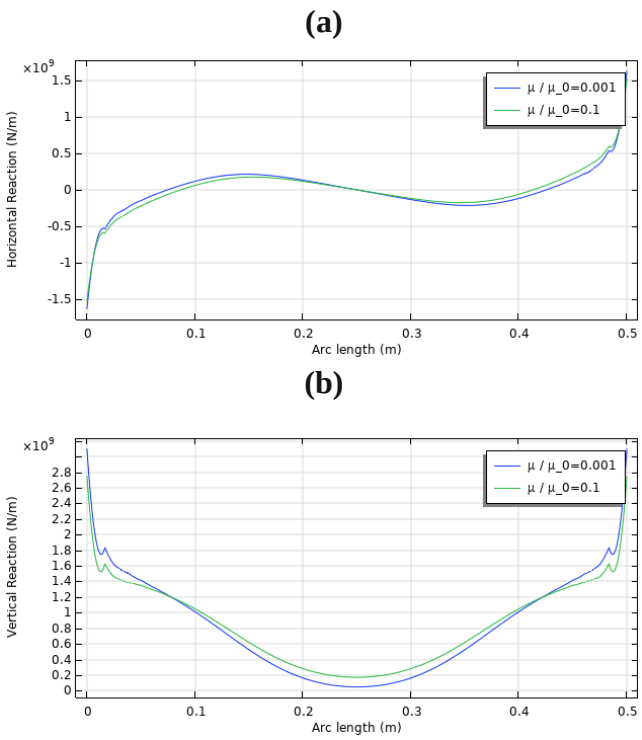

Figure 34. Distribution of reactions along the clamped boundary (a) Horizontal reaction (along x-direction) (b) Vertical reaction (along y-direction)

7. Conclusion and Summary

First, a 2D discrete granular model was proposed to investigate the in-plane deformations. The micro parameters of the model were evaluated through the linear isotropic micropolar model for the plane strain conditions with four material parameters. The main outcome of the presented work is a new non-linear micropolar continuum model which could be applied for two-dimensional isotropic plates. The need of such an enriched model is motivated for studying in a better way the 2D granular material arrangement in a continuum framework. The total deformation energy function of the proposed theory involves the contribution of a new measure of deformation which account for the relative rotation between the macro and micro rotations. Unlike all the other models findable in the literature, it aims to clearly distinguish each energetic contribution. The latter aspect could

facilitate the conception of a discrete model converging to the proposed continuum approach, in addition to a better understanding of the mechanical behavior. Consequently, there are several implications for the study of granular, porous and composite material such as rocks, concrete, soil and biological tissues: nowadays, the application of generalized theories and second gradient models for the analysis of this kind of complex materials has been embraced by a large number of scientists. The approach proposed in this paper has been formulated for 2D plates subjected to in-plane loads through the three measures of deformation with the coupling's terms. The enriched deformation energy depends on eight material parameters from which three correspond to the contributions of the new relative rotation. The derivation is purely kinematic and energetic: the authors recognize themselves as belonging to the group of analytical continuum mechanics and not continuum thermodynamics. Few applications of the model are studied for a squared plate with a central squared hole to depict some new functional aspects. Accordingly, the deformation energy equation has been implemented through the standard FEM in COMSOL Multiphysics. Parametric simulations are presented to expound the effect of microrotation on response. Decreasing the value of the microrotation material parameter results more dominancy of the Poisson's ratio in the medium. This leads consequently to the higher values of the lateral displacement as well as the curvature.

CHAPTER 6

Conclusion and Perspective

1. Conclusion and Summary

This thesis represents an effort to investigate theoretically the scale effect upon the bending deformation of a granular beam which can be viewed as a discrete Bresse-Timoshenko beam in both static and dynamic conditions. Furthermore, the presented work introduces a new non-linear micropolar continuum model which could be applied for two-dimensional isotropic elastic system. The need for such an enriched model is motivated for studying in a better way the 2D granular material arrangement in a continuum framework. A unidimensional granular chain consisting of rigid grains connected elastically with rotation and shear springs is considered. Thus, the mechanical properties of the system are characterized by the grain diameter (length scale). The proposed system can be considered as a discrete Cosserat chain with two independent degrees of freedom, namely the deflection and the rotation of each grain. Once the kinematics and Lagrangian energy of the model have been introduced, we have obtained the general solutions of the static granular chain under distributed vertical loads ruled by a coupled system of difference equations. It is shown that the discrete deflection equation of this granular system (Cosserat chain) is mathematically equivalent to the finite difference formulation of a shear deformable Bresse-Timoshenko beam resting on Winkler foundation.

Then, the gradient elasticity Cosserat continuum is developed through the continualization of the difference equations using two equivalent strategies based on the Taylor series and Padé approximants (nonlocal continuum). The nonlocal models are able to reproduce the scale effects. The distinguishing features of these two refined continuous

models basically stem from the continualization of the bending moment valid for the discrete Cosserat media which could be defined either by displacement or rotation parameters. It was shown that both nonlocal solutions coincide with the exact discrete one. A numerical asymptotic problem of a cantilever beam under distributed loading is studied for various boundary conditions. The problem is simulated by the open-source framework of Yade based on DEM. The DEM numerical results are exactly the same as the ones obtained by the exact analytical discrete approach. As the relevance of this discrete numerical model was checked for elementary cases, it would be of great interest to use it for investigating more complicated problems involving disordered discrete structures subjected to various types of loading including dynamic and vibration effects in 2D and 3D.

Next, the natural frequencies of such a granular model with simply supported ends were analytically investigated, whatever considered modes through the resolution of a linear difference equation. The eigenfrequencies obtained from the continualized beam using the Padé approximation have shown a good performance if compared to the corresponding one from the Taylor approximation. Nevertheless, it has been shown that in some cases the approach based on the Taylor approximant provides imaginary values for the two eigenfrequencies branches without a physical sense for the homogenized continuum. The dependency of the beam dynamic responses to its length ratio is clarified and the equations of the eigenfrequencies are obtained regarding the discrete Cosserat model, local and nonlocal continuous ones. It was found that the shear stiffness (represented by shear springs) has a significant effect on the vibration frequencies. Furthermore, the scale effects of the granular chain are captured by the continuous gradient

elasticity model. This scale effect is related to the grain size with respect to the total length of the Cosserat chain.

It is noteworthy to be summarized that for a S-S discrete beam modeled by granular elements, we obtained three critical frequencies. It was shown that the two higher critical frequencies are actually the natural frequencies of the system (one belongs to the mechanical branch of frequencies and the other belongs to the optical one). Notably, the corresponding mode shapes are the pure shear ones which represent that the grains are only rotating without displacing. As it was already mentioned for an infinite number of grains, the discrete model converges toward the continuum beam of Bresse and Timoshenko. For the continuum case, two of the critical frequencies which are depending on the length scale lead to zero. Thus, it could be predicted that the only critical frequency of the system $\left(\omega = \sqrt{\frac{K_S\, GA}{\rho I}}\right)$ refers to the one pure shear mode in simply supported boundary conditions. For this frequency, it could be imagined that although the deflection of the beam is zero, but the beam is vibrating through the rotations of the microstructure elements in the same orientation and with identical values.

In order to capture the wave dispersion effect, the same model has been used to analyze the wave propagation in one dimensional discrete granular chain. Using the exact resolution of the difference equation of the discrete system, it has been clarified that the two branches of eigenfrequencies exist for the granular model which leads to the ones obtained in the literature, namely by Bresse and Timoshenko for an infinite number of grains. It has been shown that the dispersion behavior of higher-order continuous models is improved by considering additional gradient enrichments terms, as compared to the initial discrete one. It can be also concluded that, as observed for the dispersion curves of

the discrete granular chain, the continuous approximation issued of a Padé approximant is always stable.

In the end, a new non-linear micropolar continuum model for two-dimensional isotropic plates was studied. The need for such an enriched model is motivated to study better the 2D granular material arrangement in a continuum framework. The total deformation energy function of the proposed theory involves the contribution of a new measure of deformation which accounts for the relative rotation between the macro and micro rotations. Unlike all the other models findable in the literature, it aims to clearly distinguish each energetic contribution. The latter aspect could facilitate the conception of a discrete model converging to the proposed continuum approach, in addition to a better understanding of the mechanical behavior. Consequently, there are several implications for the study of granular, porous and composite material such as rocks, concrete, soil and biological tissues: nowadays, the application of generalized theories and second gradient models for the analysis of this kind of complex materials has been embraced by a large number of scientists. The approach proposed in this study has been formulated for 2D plates subjected to in-plane loads through the three measures of deformation with the coupling terms. The enriched deformation energy depends on eight material parameters of which three of them correspond to the contributions of the new relative rotation. Few applications of the model are studied for a squared plate with a central squared hole to depict some new functional aspects. Accordingly, the deformation energy equation has been implemented through the standard FEM in COMSOL Multiphysics. Parametric simulations are presented to expound on the effect of microrotation on response.

2. Outlook

The results of the presented thesis will serve as a preamble to the further investigations on passage from discrete to continuum mechanics specifically in static deformation, vibration analysis and wave dispersion for metamaterials and granular structures. Nowadays, the advancements in additive manufacturing technology clarify the importance of analyzing the characteristics of granular microstructures.

Here, I would like to identify a few numbers of potential perspectives of the current thesis which will be useful for future works:

First, the discrete granular model presented for one-dimensional analysis can be extended by incorporating the effects of more neighbors which are not just in the vicinity of the subject grain. One challenge would be how to define the proper interactions and resolve the problem through an exact solution.

Another outlook might be working on the continualization approaches. To this aim, in truncation of the Padé approximant or Taylor's series expansion, higher order developments in terms of the kinematic parameters can be considered. This leads to higher-order gradient continuum theories. Also, it might be interesting to study the effects of the other continualization approximations for difference operators.

The model can be extended to an anisotropic one by considering different mechanical properties in different orientations. Imagine a discrete system connected elastically through various types of springs with different rigidity.

The proposed model motivates to study the nonlinear discrete systems which permits to analyze of further nonlinear plane waves, instability, buckling and post-buckling analysis. The nonlinearity may be considered in the geometry (geometrical nonlinear discrete

problem) or the constitutive law (nonlinear elasticity) and interactions. Random packed three-dimensional granular media are highly nonlinear according to the nonlinearity of the Hertz Law and the structural rearrangements of the structure when subjecting to dynamic loads. Wave propagation in nonlinear discrete systems leads to the failure of the continuum approximation which is evident in the acoustic diode behavior.

The verification of the numerical simulations for the static and dynamic linear problem of the one-dimensional discrete model can be a prelude to study more complex systems such as discrete systems with different elastic foundations, intricate external loading, 2D and 3D dimensions discrete media, disordered discrete structures and nonlinear problems.

For 2D planar problems, an interesting perspective might be considering various arrangements of the granular packing. Also, the influence of the further neighbors on the representative grain can be investigated. On the other hand, the interactions can be defined in such a way that lead to include more coupling effects between the kinematic descriptors.

The next research track might be studying the problem experimentally by designing grain pair interactions using 3d printing. This allows studying different coupling effects between the degrees of the freedom of the system.

APPENDIX A. Exact solution of the static deflection of the discrete granular beam – General solution

Basically, the general solutions of Eq. (12) could be considered as

$$\boldsymbol{W_i = W_i^h + W_i^p}\,;$$
$$\boldsymbol{\theta_i = \theta_i^h + \theta_i^p} \tag{A.1}$$

Note that W_i^h and θ_i^h are the homogenous solutions of the associated homogenous equations of Eq. (12) and W_i^p and θ_i^p are the particular solutions depending on the loading type. The homogenous parts admit the cubic polynomial solution:

$$\boldsymbol{W_i^h = A_1 + B_1(ai) + C_1\left(\frac{a^2}{2}i^2\right) + D_1\left(\frac{a^3}{6}i^3\right)};$$
$$\boldsymbol{\theta_i^h = A_2 + B_2(ai) + \bar{C}\left(\frac{a^2}{2}i^2\right) + D_2\left(\frac{a^3}{6}i^3\right)} \tag{A.2}$$

where A_i, B_i, C_i and D_i are constants. Eq. (A.2) could be simplified as follows by substituting in the homogenous difference equation system of Eq. (5).

$$\boldsymbol{W_i^h = W_0 + \left(a\theta_0 + \left(\frac{a}{6} - \frac{2k_r}{k_s a}\right)\beta\right)i + \left(\frac{a}{2}\alpha\right)i^2 + \left(\frac{a}{3}\beta\right)i^3};$$
$$\boldsymbol{\theta_i^h = \theta_0 + \alpha i + \beta i^2} \tag{A.3}$$

Where W_0, θ_0, α and β are constants that are obtained through the boundary conditions. A particular solution of Eq. (11) for a uniform loading can be found as:

$$\boldsymbol{W_i^p = \left(\frac{a^2 Q}{24k_r} - \frac{Q}{2k_s}\right)i^2 + \frac{a^2 Q}{24k_r}i^4};$$
$$\boldsymbol{\theta_i^p = \frac{aQ}{6k_r}i^3} \tag{A.4}$$

APPENDIX B. Exact solution of the static deflection of the discrete granular beam for various boundary conditions

I. Clamped-Simply (C-S) Supported Granular Beam

Considering the clamped condition located at the left and the simply support boundary at the right end. Thus, the boundary conditions for such a beam are given by

$$\boldsymbol{W_0 = 0\,,\ \theta_0 = 0\,;\ W_n = 0\,,} \tag{B.1}$$

$$\boldsymbol{M_{n-1/2} - \left(\frac{a}{2}\right) V_{n-1/2} = 0 \rightarrow -ak_s W_{n-1} - \frac{a^2}{2} k_s(\theta_{n-1} + \theta_n) + 2k_r(\theta_{n-1} - \theta_n) = 0}$$

By replacing the general solutions of the discrete beam (Eq. (13)) into the aforementioned set of exact boundary conditions, the deflection and rotation can be obtained readily by:

$$\begin{aligned}
&\boldsymbol{W_i} \\
&= \left(\left(\frac{2k_r}{k_s a^2} - \frac{1}{6}\right)\frac{a^2 nQ\left(5k_s L^2 - 2k_s a^2 + 12k_r\right)}{4k_r(4k_s a^2 n^2 - k_s a^2 + 12k_r)}\right) i \\
&+ \left(\frac{6k_s a^2 n^4 - 2k_s a^2 n^2 - k_s a^2 + 12k_r}{24k_r(4k_s a^2 n^2 - k_s a^2 + 12k_r)} a^2 Q\right) i^2 - \left(\frac{a^2 nQ\left(5k_s L^2 - 2k_s a^2 + 12k_r\right)}{12k_r(4k_s a^2 n^2 - k_s a^2 + 12k_r)}\right) i^3 \\
&+ \left(\frac{a^2 Q}{24k_r}\right) i^4 + \left(\frac{a^2 Q}{24k_r} - \frac{Q}{2k_s}\right) i^2;
\end{aligned} \tag{B.2}$$

$$\begin{aligned}
&\boldsymbol{\theta_i} \\
&= \frac{6k_s a^2 n^4 - 2k_s a^2 n^2 - k_s a^2 + 12k_r}{12k_r(4k_s a^2 n^2 - k_s a^2 + 12k_r)} aQi - \frac{anQ\left(5k_s a^2 n^2 - 2k_s a^2 + 12k_r\right)}{4k_r(4k_s a^2 n^2 - k_s a^2 + 12k_r)} i^2 \\
&+ \frac{aQ}{6k_r} i^3
\end{aligned}$$

For an infinite number of grains, the aforementioned discrete solutions could be compared well by the ones of Wang et al. [111] as follows

$$\begin{aligned}
&\boldsymbol{W(x)} \\
&= \left(\frac{Lq\left(5\mathcal{K}GAL^2 + 12EI\right)}{2\mathcal{K}GA(4\mathcal{K}GAL^2 + 12EI)}\right) x + \left(\frac{6\mathcal{K}GAL^4}{24EI(4\mathcal{K}GAL^2 + 12EI)} q\right) x^2 \\
&- \left(\frac{Lq\left(5\mathcal{K}GAL^2 + 12EI\right)}{12EI(4\mathcal{K}GAL^2 + 12EI)}\right) x^3 + \left(\frac{q}{24EI}\right) x^4 + \left(-\frac{q}{2\mathcal{K}GA}\right) x^2;
\end{aligned} \tag{B.3}$$

$$\boldsymbol{\theta(x) = \frac{6\mathcal{K}GAL^4}{12EI(4\mathcal{K}GAL^2 + 12EI)} qx - \frac{L\left(5\mathcal{K}GAL^2 + 12EI\right)}{4EI(4\mathcal{K}GAL^2 + 12EI)} x^2 + \frac{q}{6EI} x^3}$$

Once the solutions of the discrete beam have been obtained, the shear and bending interactions of the boundary grains could be expressed readily by using Eq. (B.2) in Eq. (7) as follows

$$\begin{aligned} V_{1/2} &= \frac{Q}{2}\left(\frac{5k_s a^2 n^2 - 2k_s a^2 + 12k_r}{4k_s a^2 n^2 - k_s a^2 + 12k_r} n - 1\right); \\ M_{1/2} &= \frac{aQ}{4}\left(\frac{n(k_s a^2 n^2(2n-5) - 2k_s a^2(n-1) - 12k_r)}{4k_s a^2 n^2 - k_s a^2 + 12k_r} + 1\right); \\ V_{n-1/2} &= -\frac{Q}{2}\left(\frac{3n(k_s a^2 n^2 + 4kr)}{4k_s a^2 n^2 - k_s a^2 + 12kr} - 1\right); \\ M_{n-1/2} &= -\frac{aQ}{4}\left(\frac{3n(k_s a^2 n^2 + 4kr)}{4k_s a^2 n^2 - k_s a^2 + 12kr} - 1\right) \end{aligned} \tag{B.4}$$

The reaction forces could be obtained through the equilibrium conditions of the granular beam as follows

$$\begin{aligned} &F^1_{ry} - \frac{Q}{2} - V_{1/2} = 0, \quad M^1_{rz} - \left(\frac{a}{2}\right)V_{1/2} - M_{1/2} = 0; \\ &F^2_{ry} - \frac{Q}{2} + V_{n-1/2} = 0, \quad M_{n-1/2} - \left(\frac{a}{2}\right)V_{n-1/2} = 0 \end{aligned} \tag{B.5}$$

which leads to

$$\begin{aligned} F^1_{ry} &= \frac{5k_s a^2 n^2 - 2k_s a^2 + 12k_r}{4k_s a^2 n^2 - k_s a^2 + 12k_r}\left(\frac{nQ}{2}\right), \quad M^1_{rz} = \frac{an^2 Q(k_s a^2 n^2 - k_s a^2)}{8k_s a^2 n^2 - 2k_s a^2 + 24k_r}; \\ V_{n-1/2} &= \frac{k_s a^2 n^2 + 4kr}{4k_s a^2 n^2 - k_s a^2 + 12kr}\left(\frac{3nQ}{2}\right) \end{aligned} \tag{B.6}$$

Thus, the bending moment and shear equations are given by

$$\begin{aligned} V_{i+1/2} &= -Q\left(i + \frac{1}{2} - \frac{5k_s a^2 n^2 - 2k_s a^2 + 12k_r}{8k_s a^2 n^2 - 2k_s a^2 + 24k_r} n\right); \\ M_{i+1/2} &= \frac{aQ}{2}\left(\left(i + \frac{1}{2}\right)^2 - \frac{5k_s a^2 n^2 - 2k_s a^2 + 12k_r}{4k_s a^2 n^2 - k_s a^2 + 12k_r} n\left(i + \frac{1}{2}\right) + \frac{n^2(k_s a^2 n^2 - k_s a^2)}{4k_s a^2 n^2 - k_s a^2 + 12k_r} + \frac{1}{4}\right) \end{aligned} \tag{B.7}$$

Replacing the continuum terms and neglecting the length scale leads to following continuum local equations

$$V(x) = -q\left(x - \frac{5\mathcal{K}GAL^2 + 12EI}{8\mathcal{K}GAL^2 + 24EI}L\right);$$

$$M(x) = \frac{q}{2}\left(x^2 - \frac{5\mathcal{K}GAL^2 + 12EI}{4\mathcal{K}GAL^2 + 12EI}Lx + \frac{L^2(\mathcal{K}GAL^2)}{4\mathcal{K}GAL^2 + 12EI}\right) \quad \textbf{(B.8)}$$

These results converge to the ones of the C-S Timoshenko beam (Wang et al. [111]).

II. Clamped – Clamped (C-C) Granular Beam

The exact conditions of the clamped ends beam can be considered with

$$W_0 = 0\,,\ \theta_0 = 0\,;$$
$$W_n = 0\,,\ \theta_n = 0 \quad \textbf{(B.9)}$$

With regards to the general solutions form of granular beam for deflection and rotation of Eq. (13), the deformation of C-C discrete beam could be obtained by:

$$W_i = \left(\left(\frac{2k_r}{k_s a} - \frac{a}{6}\right)\frac{anQ}{4k_r}\right)i + \left(\frac{a^2n^2Q}{24k_r}\right)i^2 - \left(\frac{a^2nQ}{12k_r}\right)i^3 + \left(\frac{a^2Q}{24k_r}\right)i^4 + \left(\frac{a^2Q}{24k_r} - \frac{Q}{2k_s}\right)i^2;$$
$$\theta_i = \frac{an^2Q}{12k_r}i - \frac{anQ}{4k_r}i^2 + \frac{aQ}{6k_r}i^3 \quad \textbf{(B.10)}$$

For an infinite number of grains, the solutions of the Bresse-Timoshenko beam on clamped ends might be considered as follows

$$W(x) = \left(\frac{Lq}{2\mathcal{K}GA}\right)x + \left(\frac{L^2q}{24EI}\right)x^2 - \left(\frac{Lq}{12EI}\right)x^3 + \left(\frac{q}{24EI}\right)x^4 - \left(\frac{q}{2\mathcal{K}GA}\right)x^2;$$
$$\theta(x) = \frac{L^2q}{12EI}x - \frac{Lq}{4EI}x^2 + \frac{q}{6EI}x^3 \quad \textbf{(B.11)}$$

The recent results could be compared well with the ones proposed by Wang et al. [111]. The maximum values are given by

$$W_{max} = \left(\frac{qL^4}{24EI}\right)\left[\frac{1}{8} - \frac{a^2}{4L^2} + \frac{3EI}{\mathcal{K}GAL^2}\right] < f_{CC}^{\infty};$$
$$\theta_{max} = \theta\left(\frac{3 \pm \sqrt{3}}{6}L\right) = \left(\frac{3 \pm \sqrt{3}}{36}\frac{qL^3}{EI}\right)\left[\frac{1}{2} - \frac{3 \pm \sqrt{3}}{4} + \left(\frac{3 \pm \sqrt{3}}{6}\right)^2\right] \quad \textbf{(B.12)}$$

where f_{CC}^{∞} represents the maximum displacement of the continuum beam which was obtained by Timoshenko [110] as follows

$$f_{CC}^{\infty} = \left(\frac{qL^4}{24EI}\right)\left[\frac{1}{8} + \frac{3EI}{\mathcal{K}GAL^2}\right] \tag{B.13}$$

These two equations Eq. (B.12) demonstrate that the length scale influence only the maximum values of beam deflection. This predicts that the granular beam behaves more rigidly than the equivalent local continuum one. The interaction shear and bending moment could be obtained for the boundary grains by using Eq. (B.10) in the definitions of Eq. (7)

$$\begin{aligned} V_{1/2} &= \frac{Q}{2}(n-1), \;\; M_{1/2} = -\frac{aQ}{4}\left(-\frac{n^2}{3} + n - \frac{2}{3}\right) \\ V_{n-1/2} &= -\frac{Q}{2}(n-1), \;\; M_{n-1/2} = -\frac{aQ}{4}\left(-\frac{n^2}{3} + n - \frac{2}{3}\right) \end{aligned} \tag{B.14}$$

Also, the reaction forces of the boundary would be obtained by using the equilibrium conditions for the boundary grains as follows

$$\begin{aligned} &F_{ry}^1 - \frac{Q}{2} - V_{1/2} = 0\,, \;\; M_{rz}^1 - \left(\frac{a}{2}\right)V_{1/2} - M_{1/2} = 0\,; \\ &F_{ry}^2 - \frac{Q}{2} + V_{n-\frac{1}{2}} = 0\,, \;\; -M_{rz}^2 + M_{n-1/2} - \left(\frac{a}{2}\right)V_{n-1/2} = 0 \end{aligned} \tag{B.15}$$

Note that F_{ry}^1 and M_{rz}^1 are the vertical force and moment reaction of the left clamped end and F_{ry}^2 and M_{rz}^2 are the reactions of the right clamped boundary which are obtained by

$$F_{ry}^1 = F_{ry}^2 = \frac{nQ}{2}\,, \;\; M_{rz}^1 = M_{rz}^2 = \frac{aQ}{12}(n^2 - 1)\,; \tag{B.16}$$

The distribution of bending moment and shear forces for clamped ends beam could be found eventually by applying the conditions of Eq. (B.14) the discrete general solutions of Eq. (18),

$$V_{i+1/2} = -Q\left(i + \frac{1}{2} - \frac{n}{2}\right), \;\; M_{i+1/2} = \frac{aQ}{2}\left((i+\frac{1}{2})^2 - n(i+\frac{1}{2}) + \frac{1}{12} + \frac{n^2}{6}\right) \tag{B.17}$$

It could be concluded that, for an infinite number of grains, the distribution of bending moment and shear forces converge to the ones that refer to the local continuum model of Bresse-Timoshenko as follows (Wang et al. [111]).

$$V(x) = -q\left(x - \frac{L}{2}\right), \quad M(x) = \frac{q}{2}\left(x^2 - Lx + \frac{L^2}{6}\right) \tag{B.18}$$

These equations are almost the same for the Euler-Bernoulli beam subjected to uniformly distributed load.

III. Clamped-Free (C-F) Granular Beam

We assumed here that the 2 DOF of the clamped boundary (for instant left side) are blocked while for the free side, there is no constraint. The reaction forces could be found through the application of the equilibrium equations of the whole system by

$$F_{ry}^{1} - nQ = 0\,, \quad M_{rz}^{1} - (\frac{an}{2})(nQ) = 0 \tag{B.19}$$

F_{ry}^{1} and F_{ry}^{1} are respectively the vertical reaction and the bending reaction of the clamped end. Applying the equilibrium conditions to the individual boundary grains

$$F_{ry}^{1} - \frac{Q}{2} - V_{1/2} = 0\,, \quad M_{rz}^{1} - \left(\frac{a}{2}\right)V_{1/2} - M_{1/2} = 0\,;$$

$$V_{n-1/2} - \frac{Q}{2} = 0\,, \quad M_{n-1/2} - \left(\frac{a}{2}\right)V_{n-1/2} = 0 \tag{B.20}$$

In view of Eq. (B.19) and Eq. (B.20), the shear and bending interactions of the boundaries might be obtained by

$$V_{1/2} = \frac{Q}{2}(2n-1), \quad M_{1/2} = \frac{aQ}{4}\left(2n^2 - 2n + 1\right)$$

$$V_{n-1/2} = \frac{Q}{2}, \quad M_{n-1/2} = \left(\frac{a}{2}\right)V_{n-1/2} = \frac{aQ}{4} \tag{B.21}$$

Applying these conditions in the discrete general form solutions of the shear and bending moment distribution (Eq. (18)) leads to

$$V_{i+1/2} = -Q\left(i + \frac{1}{2} - n\right), \quad M_{i+1/2} = \frac{aQ}{2}\left((i+\frac{1}{2})^2 - 2n(i+\frac{1}{2}) + \frac{1}{4} + n^2\right) \tag{B.22}$$

Ignoring the length scale for an infinite number of grains refers to the Bresse-Timoshenko beam which has the same moment and shear distributions as the Euler-Bernoulli for the C-

F conditions. Furthermore, the bending moment and shear equations could be found for the local continuum model as

$$\boldsymbol{V(x) = -q(x-L),\ \ M(x) = \frac{q}{2}\left(x^2 - 2Lx + L^2\right)} \tag{B.23}$$

substituting the shear and bending moment interactions through the kinematics terms (Eq. (7)) into Eq. (B.20) leads to

$$\boldsymbol{W_0 = 0\,,\ \ \theta_0 = 0\,;}$$
$$\boldsymbol{k_r(\Theta_n - \Theta_{n-1}) - \frac{a}{4}Q = 0\,,\ \ k_s\left(W_n - W_{n-1} - \frac{a}{2}(\Theta_n + \Theta_{n-1})\right) - \frac{1}{2}Q = 0} \tag{B.24}$$

The solutions could be found by replacing the general solutions of Eq. (13) in the aforementioned boundary conditions. Thus, the deflection and micro rotations of the system are given by

$$\boldsymbol{W_i} = \left(\left(\frac{2k_r}{k_s a} - \frac{a}{6}\right)\frac{anQ}{2k_r}\right)i + \left(\frac{6a^2n^2Q + a^2Q}{24k_r}\right)i^2 - \left(\frac{a^2nQ}{6k_r}\right)i^3 + \left(\frac{a^2Q}{24k_r}\right)i^4 + \left(\frac{a^2Q}{24k_r} - \frac{Q}{2k_s}\right)i^2; \tag{B.25}$$

$$\boldsymbol{\theta_i = \frac{6aQn^2 + aQ}{12k_r}i - \frac{anQ}{2k_r}i^2 + \frac{aQ}{6k_r}i^3}$$

These converge asymptotically to the ones obtained by Bresse-Timoshenko (Timoshenko [110] and Wang et al. [111]) for continuum beam assuming an infinite number of grains as follows

$$\boldsymbol{W(x) = \left(\frac{Lq}{\mathcal{K}GA}\right)x + \left(\frac{L^2q}{4EI}\right)x^2 - \left(\frac{Lq}{6EI}\right)x^3 + \left(\frac{q}{24EI}\right)x^4 - \left(\frac{q}{2\mathcal{K}GA}\right)x^2;} \tag{B.26}$$

$$\boldsymbol{\theta(x) = \frac{6qL^2}{12EI}x - \frac{Lq}{2EI}x^2 + \frac{q}{6EI}x^3}$$

The maximum deflection and micro angle occur at $i = na$ and obtained as follows

$$\boldsymbol{W_{max} = \frac{qL^4}{8EI}\left[1 + \frac{4EI}{\mathcal{K}GAL^2}\right] = f_{CF}^{\infty};} \tag{B.27}$$

$$\boldsymbol{\theta_{max} = \frac{qL^3}{6EI}\left[1 + \frac{a^2}{2L^2}\right]}$$

f_{CF}^{∞} refers to the maximum displacement of the C-F continuum beam which was obtained by Timoshenko [110]. It could be concluded that the length scale only affects θ_{max} for clamped-free boundary conditions while W_{max} is independent of the grain dimension. The maximum values of micro-rotation are estimated bigger than the local continuum ones for this case.

APPENDIX C. Exact solution of the static deflection of the continuous nonlocal granular beam

The development of the difference operators is done neglecting the higher-order terms in $\boldsymbol{a^4}$ for deflection and rotation field as follows:

$$\boldsymbol{\mathcal{K}GA\left(1+\frac{a^2D_x^2}{12}\right)D_x^2W(x)-\mathcal{K}GA\left(1+\frac{a^2D_x^2}{6}\right)D_x\Theta(x)=-q} \tag{C.1}$$

$$\boldsymbol{\mathcal{K}GA\left(1+\frac{a^2D_x^2}{6}\right)D_xW(x)+\left(EI\left(1+\frac{a^2D_x^2}{12}\right)D_x^2-\mathcal{K}GA\left(1+\frac{a^2D_x^2}{4}\right)\right)\Theta(x)=0} \tag{C.2}$$

Here, a is the characteristic length of the nonlocal model which can be computed from the microstructure cell size (grain diameter for instance). Multiplying Eq. (C.2)(C.2) by the term $-\left(1-\frac{a^2D_x^2}{12}\right)D_x$ with neglecting the higher order terms in a^4 leads to

$$\boldsymbol{-\mathcal{K}GA\left(1+\frac{a^2D_x^2}{12}\right)D_x^2W(x)-\left(EID_x^3-\mathcal{K}GA\left(1+\frac{a^2D_x^2}{6}\right)D_x\right)\Theta(x)=0} \tag{C.3}$$

Summing the previous equation with Eq. (C.1) leads to

$$\boldsymbol{EI\Theta'''=q} \tag{C.4}$$

On the other hand, the following auxiliary equation could be obtained with the multiplication of Eq. (C.1) by the term $\left(1-\frac{a^2D_x^2}{12}\right)D_x^2$ and ignoring the higher-order terms in a^4

$$\boldsymbol{\mathcal{K}GAD_x^4W(x)-\mathcal{K}GA\left(1-\frac{a^2D_x^2}{12}\right)D_x^3\Theta(x)=-q\left(1-\frac{a^2D_x^2}{12}\right)D_x^2} \tag{C.5}$$

Thus, the deflection differential equations of the nonlocal system for the displacement could be obtained for a uniform constant distributed loading through the application of relation Eq. (C.4) as follows

$$\boldsymbol{EIW''''=q} \tag{C.6}$$

APPENDIX D. Alternative methods of the static analysis of the continuous nonlocal granular beam

I. Continualization of Discrete Bending Moment

The nonlocal bending moment and shear distribution of the S-S continuum beam could be obtained from the continualization of Eq. (22) by substituting $x = ai, L = an$ and $Q = qa$ as follows

$$\boldsymbol{V(x) = -q\left(x - \frac{L}{2}\right)}\ ,\ \ \boldsymbol{M(x) = \frac{q}{2}\left(x^2 - Lx + \frac{a^2}{4}\right)} \tag{D.1}$$

According to Eq. (52) and Eq. (C.1) by considering the corresponding bending moments on the boundaries, the nonlocal conditions could be obtained the same as Eq. (55).

II. Continualization of the Kinematic Boundary Conditions

This method is based on the continualization of the cinematic boundary conditions presented for the discrete system by Eq. (24). This could be expressed for the nonlocal beam as

$$\begin{aligned} &\boldsymbol{W(0) = 0,\ \ aKGAW(a) - \frac{a^2}{2}KGA\big(\theta(a) + \theta(0)\big) + 2EI(\theta(a) - \theta(0)) = 0}\ ; \\ &\boldsymbol{W(L) = 0,\ \ -aKGAW(L-a) - \frac{a^2}{2}KGA\big(\theta(L-a) + \theta(L)\big) + 2EI\big(\theta(L-a) - \theta(L)\big) = 0} \end{aligned} \tag{D.2}$$

Using the general nonlocal continuum solutions of Eq. (49) in the abovementioned conditions reflects the same nonlocal solutions that have been obtained by Eq. (56).

III. Continualization of Discrete Bending Moment

Another approach to continualize the cinematic conditions could be done by applying the polynomial expansions. Developing the difference terms using the Taylor series up to the quartic order a^4 for displacement and cubic order a^3 for rotation in Eq. (D.2) leads to

$$
\begin{aligned}
&W(0) = 0,\\
&a\mathcal{K}GA\left(aW'(0) + \frac{a^2}{2}W''(0) + \frac{a^3}{6}W'''(0) + \frac{a^4}{24}W''''(0)\right)\\
&-\frac{a^2}{2}\mathcal{K}GA\left(2\theta(0) + a\theta'(0) + \frac{a^2}{2}\theta''(0) + \frac{a^3}{6}\theta'''(0)\right)\\
&+2EI\left(a\theta'(0) + \frac{a^2}{2}\theta''(0) + \frac{a^3}{6}\theta'''(0)\right) = 0\,;\\
&W(L) = 0,\\
&-a\mathcal{K}GA\left(aW'(L) + \frac{a^2}{2}W''(L) + \frac{a^3}{6}W'''(L) + \frac{a^4}{24}W''''(L)\right)\\
&-\frac{a^2}{2}\mathcal{K}GA\left(2\theta(L) - a\theta'(L) + \frac{a^2}{2}\theta''(L) - \frac{a^3}{6}\theta'''(L)\right)\\
&-2EI\left(a\theta'(L) - \frac{a^2}{2}\theta''(L) + \frac{a^3}{6}\theta'''(L)\right) = 0
\end{aligned}
\qquad \textbf{(D.3)}
$$

The aforementioned developed conditions again lead to the solutions of Eq. (56).

IV. Continualization of the Static Boundary Conditions with Cinematic Variables

The equilibrium of the bending moment for the boundaries of the nonlocal beam could be considered by

$$
M\left(\frac{a}{2}\right) + \frac{a}{2}V\left(\frac{a}{2}\right) = 0\,,\quad M\left(L - \frac{a}{2}\right) - \frac{a}{2}V\left(L - \frac{a}{2}\right) = 0 \qquad \textbf{(D.4)}
$$

Substituting Eq. (50) and Eq. (51) in these equations leads to

$$
\begin{aligned}
&\left(EI\theta'\left(\frac{a}{2}\right) + \frac{a^2}{24}q\right) + \frac{a\mathcal{K}GA}{2}\left(W'\left(\frac{a}{2}\right) - \theta\left(\frac{a}{2}\right) - \frac{a^2}{12}W'''\left(\frac{a}{2}\right)\right) = 0\,;\\
&\left(EI\theta'\left(L - \frac{a}{2}\right) + \frac{a^2}{24}q\right) - \frac{a\mathcal{K}GA}{2}\left(W'\left(L - \frac{a}{2}\right) - \theta\left(L - \frac{a}{2}\right) - \frac{a^2}{12}W'''\left(L - \frac{a}{2}\right)\right) = 0
\end{aligned}
\qquad \textbf{(D.5)}
$$

The constants of the general solutions of Eq. (49) could be obtained the same as the ones that have been expressed by Eq. (56).

APPENDIX E. Nonlocal static analysis of the granular beam for various boundary conditions

I. Clamped-Simply Nonlocal Model

For C-S boundary conditions, ones could be obtained for the bending moment and shear distribution, through the continualization of the corresponding discrete equations. These are given respectively as follows

$$\begin{aligned} \boldsymbol{V(x)} &= \boldsymbol{-q\left(x-\frac{5\mathcal{K}GAL^2-2\mathcal{K}GAa^2+12EI}{8\mathcal{K}GAL^2-2\mathcal{K}GAa^2+24EI}L\right)}, \\ \boldsymbol{M(x)} &= \boldsymbol{\frac{q}{2}\left(x^2-\frac{5\mathcal{K}GAL^2-2\mathcal{K}GAa^2+12EI}{4\mathcal{K}GAL^2-\mathcal{K}GAa^2+12EI}Lx+\frac{L^2\left(\mathcal{K}GAL^2-\mathcal{K}GAa^2\right)}{4\mathcal{K}GAL^2-\mathcal{K}GAa^2+12EI}+\frac{a^2}{4}\right)} \end{aligned} \tag{E.1}$$

The nonlocal C-S boundary conditions could be considered in view of Eq. (52) and Eq. (E.1), by:

$$\boldsymbol{W(0)=0\,;\quad \Theta(0)=0\,;\quad W(L)=0\,;\quad \Theta'(L)=\frac{a^2q}{12EI}} \tag{E.2}$$

Thus, ones could be obtained for the deflection and rotation of the nonlocal beam by replacing the nonlocal general solutions (Eq. (49))

$$\begin{aligned} &\boldsymbol{W(x)} \\ &\boldsymbol{=\left(\left(\frac{2EI}{\mathcal{K}GA}-\frac{a^2}{6}\right)\frac{Lq\left(5\mathcal{K}GAL^2-2\mathcal{K}GAa^2+12EI\right)}{4EI(4\mathcal{K}GAL^2-\mathcal{K}GAa^2+12EI)}\right)x} \\ &\boldsymbol{+\left(\frac{6\mathcal{K}GAL^4-2\mathcal{K}GAa^2L^2-\mathcal{K}GAa^4+12EIa^2}{24EI(4\mathcal{K}GAL^2-\mathcal{K}GAa^2+12EI)}q\right)x^2} \\ &\boldsymbol{-\left(\frac{Lq\left(5\mathcal{K}GAL^2-2\mathcal{K}GAa^2+12EI\right)}{12EI(4\mathcal{K}GAL^2-\mathcal{K}GAa^2+12EI)}\right)x^3+\left(\frac{q}{24EI}\right)x^4+\left(\frac{qa^2}{24EI}-\frac{q}{2\mathcal{K}GA}\right)x^2}; \end{aligned} \tag{E.3}$$

$$\begin{aligned} &\boldsymbol{\Theta(x)} \\ &\boldsymbol{=\frac{6\mathcal{K}GAL^4-2\mathcal{K}GAa^2L^2-\mathcal{K}GAa^4+12EIa^2}{12EI(4\mathcal{K}GAL^2-\mathcal{K}GAa^2+12EI)}qx-\frac{L\left(5\mathcal{K}GAL^2-2\mathcal{K}GAa^2+12EI\right)}{4EI(4\mathcal{K}GAL^2-\mathcal{K}GAa^2+12EI)}x^2} \\ &\boldsymbol{+\frac{q}{6EI}x^3} \end{aligned}$$

These could be also obtained from the continualization of the corresponding discrete solutions (Eq. (B.2)).

II. Clamped-Clamped Nonlocal Model

The shear and bending distribution of the nonlocal continuum beam could be obtained by continualizing the ones which were found for the discrete system. This could be done by considering the continuum terms $x = ai, L = an$ and $Q = qa$. Accordingly, Eq. (B.14) leads to

$$\boldsymbol{V(x) = -q\left(x - \frac{L}{2}\right),\ \ M(x) = \frac{q}{2}\left(x^2 - Lx + \frac{a^2}{12} + \frac{L^2}{6}\right)} \tag{E.4}$$

For this case, the boundary conditions might be defined the same as the discrete or local ones by

$$\boldsymbol{W(0) = 0\,;\ \ \theta(0) = 0\,;\ \ W(L) = 0\,;\ \ \theta(L) = 0} \tag{E.5}$$

Applying the aforementioned set of boundary conditions in the general solutions of the nonlocal beam (Eq. (49)) leads to:

$$\boldsymbol{W(x) = \left(\frac{Lq}{2\mathcal{K}GA}\right)x + \left(\frac{L^2q}{24EI} - \frac{q}{2\mathcal{K}GA}\right)x^2 - \left(\frac{Lq}{12EI}\right)x^3 + \left(\frac{q}{24EI}\right)x^4 + \left(\frac{a^2q}{24EI}\right)(x - L)x;}$$

$$\boldsymbol{\theta(x) = \frac{L^2q}{12EI}x - \frac{Lq}{4EI}x^2 + \frac{q}{6EI}x^3} \tag{E.6}$$

Similarly, an alternative method to obtain these results is through the continualization of the corresponding discrete solutions of Eq. (B.10). The maximum displacement occurs at the middle of the beam and is given by

$$\boldsymbol{W_{max} = W(L/2) = \left(\frac{qL^4}{24EI}\right)\left[\frac{1}{8} - \frac{a^2}{4L^2} + \frac{3EI}{\mathcal{K}GAL^2}\right]} \tag{E.7}$$

It is noteworthy to state that the maximum value is equal to Eq. (B.12). Although the boundary conditions and the governing differential equations of the local and nonlocal beam are the same, the scale effect appears (only in the displacement equation) in the results. This stems from the nonlocal gradient coupled differential equations system expressed by Eq. (C.1) and Eq. (C.2).

III. Clamped-Free Nonlocal Model

Replacing $x = ai, L = an$ and $Q = qa$ in Eq. (B.22) leads to the moment and shear equations of the nonlocal continuum beam as follows

$$\boldsymbol{V(x) = -q(x - L),\ \ M(x) = \frac{q}{2}\left(x^2 - 2Lx + \frac{a^2}{4} + L^2\right)} \tag{E.8}$$

For the free boundary, we have $V(L) = 0$ and $M(L) = \frac{a^2 q}{8}$. Applying Eq. (50) and Eq. (51) leads to the following nonlocal variational boundary conditions

$$\boldsymbol{W(0) = 0\ ;\ \ \Theta(0) = 0\ ;} \tag{E.9}$$

$$\boldsymbol{\Theta'(L) = \frac{a^2 q}{12EI}\ ;\ \ W'(L) - \Theta(L) - \frac{a^2}{12}W'''(L) = 0}$$

Also, regarding Eq. (52) and knowing $M'(L) = -V(L) = 0$, an equivalent boundary conditions could be assumed

$$\boldsymbol{W(0) = 0\ ;\ \ \Theta(0) = 0\ ;} \tag{E.10}$$

$$\boldsymbol{\Theta'(L) = \frac{a^2 q}{12EI}\ ;\ \ \Theta''(L) = 0}$$

On the other hand, defining the bending moment and shear force of the free end through the cinematic parameters leads to an alternative set of boundary conditions for C-F nonlocal beam

$$\boldsymbol{W(0) = 0\ ;\ \ \Theta(0) = 0\ ;}$$

$$\boldsymbol{\Theta(L) - \Theta(L - a) = \frac{a^3 q}{4EI}\ ;\ \ W(L) - W(L - a) - a\frac{\Theta(L) + \Theta(L - a)}{2} = \frac{a^2 q}{2\mathcal{K}GA}} \tag{E.11}$$

Applying the nonlocal beam solutions of Eq. (49) in one of the aforementioned boundary conditions (e.g. Eq. (E.9)) leads to:

$$\boldsymbol{W(x)} = \left(\frac{\boldsymbol{Lq}}{\boldsymbol{\mathcal{K}GA}}\right)\boldsymbol{x} + \left(\frac{\boldsymbol{L^2q}}{\boldsymbol{4EI}} - \frac{\boldsymbol{q}}{\boldsymbol{2\mathcal{K}GA}}\right)\boldsymbol{x^2} - \left(\frac{\boldsymbol{Lq}}{\boldsymbol{6EI}}\right)\boldsymbol{x^3} + \left(\frac{\boldsymbol{q}}{\boldsymbol{24EI}}\right)\boldsymbol{x^4} + \left(\frac{\boldsymbol{a^2q}}{\boldsymbol{12EI}}\right)\boldsymbol{(x-L)x};$$

$$\boldsymbol{\theta(x)} = \frac{\boldsymbol{6L^2q + a^2q}}{\boldsymbol{12EI}}\boldsymbol{x} - \frac{\boldsymbol{Lq}}{\boldsymbol{2EI}}\boldsymbol{x^2} + \frac{\boldsymbol{q}}{\boldsymbol{6EI}}\boldsymbol{x^3} \qquad \textbf{(E.12)}$$

These results coincide with the ones that could be found from the continualization of the discrete solutions which have been presented in Eq. (B.25). The maximum deflection happens at the free side of the beam and is obtained as follows

$$\boldsymbol{W_{max} = W(L)} = \frac{\boldsymbol{qL^4}}{\boldsymbol{8EI}}\left[\boldsymbol{1} + \frac{\boldsymbol{4EI}}{\boldsymbol{\mathcal{K}GAL^2}}\right] \qquad \textbf{(E.13)}$$

This equation reflects also the same values as Eq. (B.27).

APPENDIX F. Comparison of the numerical DEM model and the exact discrete approach of the static deflection of the granular beam

Table 1: Comparison of the maximum deflection values (μm) for the discrete granular beam with simply supported (S-S), clamped-simply (C-S), clamped-clamped (C-C) and clamped-free (C-F); exact analytical solutions and the numerical ones (DEM)

	DEM Results			**Exact Analytic Results**			
Boundary Conditions	Number of Grain $n = \frac{L}{a}$						
	5	11	21	5	11	21	∞
S-S	0.2261	0.2366	0.2381	0.2261	0.2366	0.2381	0.2386
C-S	0.1709	0.1788	0.1799	0.1709	0.1788	0.1799	0.1808
C-C	0.1326	0.1379	0.1386	0.1326	0.1379	0.1386	0.1388
C-F	0.1653	0.1653	0.1653	0.1653	0.1653	0.1653	0.1653

Table 2: Comparison of the maximum rotation values ($\mu\ degree$) for the discrete granular beam with simply supported (S-S), clamped-simply (C-S), clamped-clamped (C-C) and clamped-free (C-F); exact analytical solutions and the numerical ones (DEM)

	Numerical DEM Results			**Exact Analytic Results**			
Boundary Conditions	Number of Grain $n = \frac{L}{a}$						
	5	11	21	5	11	21	∞
S-S	0.3742	0.3951	0.3981	0.3742	0.3951	0.3981	0.3991
C-S	-0.3063	-0.3282	-0.3314	-0.3063	-0.3282	-0.3314	-0.3324
C-C	0.7483	0.7663	0.7663	0.7483	0.7663	0.7663	0.7681
C-F	-0.1646	-0.1604	-0.1598	-0.1646	-0.1604	-0.1598	-0.1596

Table 3: Material parameters used in energy definition of the medium

λ_{G_0}	μ_{GG_0}	$\mu_{GG^T{}_0}$	λ_{R_0}
$85.52\ kN.mm^{-1}$	$32.50\ kN.mm^{-1}$	$25.35\ kN.mm^{-1}$	$40.12\ kN.mm^{-1}$
$\mu_{\mathcal{R}\mathcal{R}_0}$	$\mu_{\mathcal{R}\mathcal{R}^T{}_0}$	$\mu_{\Gamma\Gamma^T{}_0}$	$\gamma_{G\mathcal{R}_0}$
$15.85\ kN.mm^{-1}$	$20.40\ kN.mm^{-1}$	$25.36 \times 10^6\ kN.mm$	$20.25\ kN.mm^{-1}$

BIBLIOGRAPHY

[1] F. Nicot and F. Darve, The H-microdirectional model: accounting for a mesoscopic scale, Mechanics of Materials, 43 (2011) 918–929. https://www.sciencedirect.com/science/article/abs/pii/S0167663611001232

[2] I. Vardoulakis., Cosserat continuum mechanics with applications to granular media, Lecture Notes in: Applied and Computational Mechanics, Springer, Berlin, 2019.

[3] E. Cosserat and F. Cosserat, Theories of the deformable bodies, A. Herrmann et Fils, Paris, 1909.

[4] W. Nowacki, The linear theory of micropolar elasticity, W. Nowacki and W. Olszak (eds.), Micropolar Elasticity. Wien, New-York (Springer-Verlag) (1974) 1-43.

[5] W. Voigt, Theoritical studies on the elasticity relationships of cristals, Abh. Gesch. Wissenschaften, Göttingen, 1887.

[6] R. D. Mindlin, Micro-structure in linear elasticity, Archive for Rational Mechanics and analysis, 16 (1964) 51-78. https://doi.org/10.1007/BF00248490

[7] E. C. Aifantis, On the role of gradients in the localization of deformation and fracture, Journal of Engineering Science, 30 (10) (1992) 1279-1299. https://www.sciencedirect.com/science/article/abs/pii/0020722592901413

[8] C. Truesdell and W. Noll, The non-linear field theories of mechanics, Springer-Verlag, Flügge S. (Ed.), Handbuch der Physik, Berlin, 1965.

[9] R. A. Toupin, Elastic materials with couple-stress, Archive for Rational Mechanics and analysis, 17 (1962) 385-414. https://doi.org/10.1007/BF00253945

[10] C. Truesdell, A First Course in Rational Continuum Mechanics (second ed.), vol. I, Academic Press, Boston, 1991.

[11] E. Pasternak and H. B. Mühlhaus, Generalized homogenization procedures for granular materials, Journal of Engineering Mathematics, 51 (1) (2005) 199-229. https://doi.org/10.1007/s10665-004-3950-z

[12] W. H. Duan, N. Challamel, C. M. Wang and Z. Ding, Development of analytical vibration solutions for microstructured beam model to calibrate length scale coefficient in nonlocal Timoshenko beams, Journal of Applied Physics, 114 (2013) 104312-104323. https://doi.org/10.1063/1.4820565

[13] N. Challamel, J. Lerbet, F. Darve and F. Nicot, Buckling of granular systems with discrete and gradient elasticity Cosserat continua, Annals of Solid Structural Mechanics, 12 (2020) https://doi.org/10.1007/s12356-020-00065-5

[14] P. Poorsolhjouy and A. Misra, Grain-size Effects on Mechanical Behavior and Failure of Dense Cohesive Granular Materials, KONA Powder and Particle Journal, (2020) https://doi.org/10.14356/kona.2022001

[15] A. Misra, L. Placidi and T. Matsushima, Granular Material Models across Scales, mechanics Research Communications, (2019) https://doi.org/10.1016/j.mechrescom.2019.103405

[16] J. A. C. Bresse, Cours de mécanique appliquée – Résistance des matériaux et stabilité des constructions Gautier-Villars, Paris, 1859.

[17] S. P. Timoshenko, On the correction for shear of the differential equation for transverse vibrations of prismatic bars, Philosophical Magazine, 41 (1921) 744-746.

[18] S. P. Timoshenko, On the transverse vibration of bars with uniform cross-section, Philosophical Magazine, 43 (1922) 125-131.

[19] A. G. Bagdoev, V. I. Erofeev and A. V. Shekoyan, Wave Dynamics of Generalized Continua, Springer-Verlag Berlin Heidelberg, 2016.

[20] I. Vardoulakis, Cosserat Continuum Mechanics With Applications to Granular Media, Springer International Publishing, 2019.

[21] P. A. Cundall and O. D. L. Strack, A discrete numerical model for granular assemblies, Geotechnique, (1979) 47–65. https://www.icevirtuallibrary.com/doi/10.1680/geot.1979.29.1.47

[22] A. A. Serrano and J. M. Rodriguez-Ortiz, A contribution to the mechanics of heterogeneous granular media, Proc. Symp. Plasticity and Soil Mechanics, Palmer A.C. (Ed.), Cambridge University Engineering Department, pp. 215-227, 13-15 September 1973, Cambridge, 1973.

[23] A. Eringen, Microcontinuum field theories, Springer, New York, 1999.

[24] A. Eringen, Nonlocal continuum field theories, Springer, New York, 2002.

[25] S. Forest, Generalized continua, In: Buschow, K., Cahn, R., Flemings, M., Ilschner, B., Kramer, E., Mahajan, S. (Eds.), Encyclopedia of Materials: Science and Technology Updates, Elsevier, 2005.

[26] S. Feng, Percolation properties of granular elastic networks in two dimensions, Physical Review B, 32 (1) (1985) 510-513. https://journals.aps.org/prb/abstract/10.1103/PhysRevB.32.510

[27] S. Massoumi et al., Static bending of granular beam: Exact discrete and nonlocal solutions, submitted for publication, Meccanica, (2021)

[28] T. Matsushima, H. Saomoto, Y. Tsubokawa and Y. Yamada, Grain rotation versus continuum rotation during shear deformation of granular assembly, Soils Found, 43 (4) (2003) 95–106. https://doi.org/10.3208/sandf.43.4_95

[29] F. Bourrier, F. Kneib, B. Chareyre and T. Fourcaud, Discrete modeling of granular soils reinforcement by plant roots, Ecological Engineering., 61 (2013) 646-657. https://doi.org/10.1016/j.ecoleng.2013.05.002

[30] E. Barchiesi, M. Spagnuolo and L. Placidi, Mechanical metamaterials: a state of the art, Journal of Mathematics and Mechanics of Solids, 24 (1) (2019) 212-234 https://doi.org/10.1177/1081286517735695

[31] D. D. Vescovo and I. Giorgio, Dynamic problems for metamaterials: review of existing models and ideas for further research, International Journal of Engineering Science, 80 (2014) 153-172. https://doi.org/10.1016/j.ijengsci.2014.02.022

[32] I. Giorgio et al., In-depth gaze at the astonishing mechanical behavior of bone: A review for designing bio-inspired hierarchical metamaterials, Mathematics and Mechanics of Solids, 26 (7) (2021) 1074-1103. https://doi.org/10.1177/1081286520978516

[33] A. Misra, N. Nejadsadeghi, M. D. Angelo and L. Placidi, Chiral metamaterial predicted by granular micromechanics: verified with 1D example synthesized using additive manufacturing, Continuum Mechanics and Thermodynamics, 32 (2020) 1497-1513. https://doi.org/10.1007/s00161-020-00862-8

[34] E. Cosserat and F. Cosserat, Sur la théorie de l'elasticité, Toulouse, 1896.

[35] C. Truesdell and R. Toupin, The classical field theories. In: Flügge, S. (ed.) Handbuch der Physik, vol. III/, 226–793, Springer, Berlin, 1960.

[36] E. L. Aero and E. V. Kuvshinskii, Fundamental equations of the theory of elastic media with rotationally interacting particles, Soviet physics solid state, 2 (7) (1961) 1272–1281.

[37] E. L. Aero and E. V. Kuvshinskii, Continuum theory of asymmetric elasticity. Equilibrium of an isotropic body (in Russian), Fizika Tverdogo Tela, 6 (1964) 2689–2699.

[38] R. D. Mindlin and H. F. Tiersten, Effects of couple stresses in linear elasticity, Archive for Rational Mechanics and analysis, 11 (1962) 415. https://doi.org/10.1007/BF00253946

[39] A. C. Eringen, Linear theory of micropolar elasticity, Journal of Mathematics and Mechanics, 15 (6) (1966) 909–923. https://www.jstor.org/stable/24901442

[40] A. C. Eringen, Linear theory of micropolar viscoelasticity, International Journal of Engineering Science, 5 (2) (1967) 191–204. https://doi.org/10.1016/0020-7225(67)90004-3

[41] R. A. Toupin, Theories of elasticity with couple-stress, Archives for Rational Mechanics and Analysis, 17 (1964) 85–112. https://doi.org/10.1007/BF00253050

[42] W. Pietraszkiewicz and V. A. Eremeyev, On natural strain measures of the non-linear micropolar continuum, International Journal of Solids and Structures, 46 (3-4) (2009) 774-778. https://doi.org/10.1016/j.ijsolstr.2008.09.027

[43] V. A. Eremeyev and W. Pietraszkiewicz, Material symmetry group and constitutive equations of micropolar anisotropic elastic solids, Mathematics and Mechanics of Solids, 21 (2) (2016) 210-221. https://doi.org/10.1177/1081286515582862

[44] G. La-Valle and S. Massoumi, A new deformation measure for micropolar plates subjected to in-plane loads, Continuum Mechanics and Thermodynamics, (2021) https://doi.org/10.1007/s00161-021-01055-7

[45] G. Grioli, Elasticita asimmetrica, Annali di Matematica Pura ed Applicata, 50 (1960) 389–417

[46] C. B. Kafadar and A. C. Eringen, Micropolar media—I. The classical theory, International Journal of Engineering Science, (1971) 271–305.

[47] S. Ramezani and R. Naghdabadi, Energy pairs in the micropolar continuum, International Journal of Solids and Structures, 44 (2007) 4810–4818. https://doi.org/10.1016/j.ijsolstr.2006.12.006

[48] A. C. Eringen and C. B. Kafadar, Polar field theories. In: Eringen, A.C. (Ed.), Continuum Physics, vol. 4. Academic Press, New York, 1976.

[49] Z. P. Bažant and M. Christensen, Analogy between micropolar continuum and grid frame- works under initial stress, Journal of Solids Structure, 8 (1972) 327–346. https://www.sciencedirect.com/science/article/abs/pii/0020768372900935

[50] A. Bacigalupo and L. Gambarotta, Identification of non-local continua for lattice-like materials, Journal of Engineering Science, 159 (2021) https://www.sciencedirect.com/science/article/abs/pii/S0020722520302172?via%3Dihub

[51] A. Bacigalupo and L. Gambarotta, Enhanced dynamic homogenization of hexagonally packed granular materials with elastic interfaces, Computers and Geotechnics, 137 (104102) (2021) https://doi.org/10.1016/j.compgeo.2021.104102

[52] V. Picandet, B. Hérisson, N. Challamel and A. Perrot, On the failure of a discrete axial chain using a continualized nonlocal Continuum Damage Mechanics approach, International Journal for Numerical and Analytical Methods in Geomechanics, 40 (2016) 436–466. https://onlinelibrary.wiley.com/doi/abs/10.1002/nag.2412

[53] J. Duffy, Stress–strain relations and vibrations of granular medium, Colombia Univ, New York, 1957.

[54] P. J. Digby, The effective elastic moduli of porous granular rock, Journal of Applied Mechanics, 48 (1981) 803-808. https://scinapse.io/papers/1991585306

[55] C. S. Chang, Micromechanical modelling of constitutive relations for granular material, Micromechanics of granular material, (1988) 271-279. https://www.sciencedirect.com/science/article/pii/B9780444705235500382

[56] H. B. Mühlhaus and I. Vardoulakis, The thickness of shear bands in granular materials, Geotechnique, 37 (3) (1987) 271-283. https://www.icevirtuallibrary.com/doi/10.1680/geot.1987.37.3.271

[57] A. S. J. Suiker, C. S. Chang, R. D. Borst and C. Esveld, Surface waves in a stratified half space with enhanced continuum properties, Journal of Applied Mechanics, 18 (1999) 749–768. https://www.sciencedirect.com/science/article/pii/S0997753899001072

[58] C. S. Chang and L. Ma, Elastic material constants for isotropic granular solids with particle rotation, Journal of Solids Structure, 29 (1992) 1001-1018. https://www.sciencedirect.com/science/article/abs/pii/002076839290071Z

[59] L. M. Schwartz, D. L. Johnson and S. Feng, Vibrational modes in granular materials, Physical Review, 52 (10) (1984) 831-834. https://journals.aps.org/prl/abstract/10.1103/PhysRevLett.52.831

[60] H. Pichard et al., Localized transversal-rotational modes in linear chains of equal masses, Physical Review, 89 (2014) https://doi.org/10.1103/PhysRevE.89.013201

[61] A. A. Vasiliev, A. E. Miroshnichenko and M. Ruzzene, A discrete model and analysis of one-dimensional deformations in a structural interface with micro-rotations, mechanics Research Communications, 37 (2) (2010) 225-229. https://www.sciencedirect.com/science/article/abs/pii/S0093641309001669

[62] M. Ostoja-Starzewski, Lattice models in micromechanics, Journal of Applied Mechanics, 55 (1) (2002) 35-60. https://asmedigitalcollection.asme.org/appliedmechanicsreviews/article-abstract/55/1/35/458978

[63] M. Attar, A. Karrech and K. Regenauer-Lieb, Free vibration analysis of a cracked shear deformable beam on a two-parameter elastic foundation using a lattice spring model, Journal of Sound and Vibration, 333 (2014) 2359-2377. https://www.sciencedirect.com/science/article/abs/pii/S0022460X13009267

[64] T. M. Wang and J. E. Stephens, Natural frequencies of Timoshenko beams on Pasternak foundations, Journal of Sound and Vibration, 51 (2) (1977) 149-155. https://www.sciencedirect.com/science/article/abs/pii/S0022460X77800291

[65] A. I. Manevich, Dynamics of Timoshenko beam on linear and nonlinear foundation: phase relations, significance of the second spectrum, stability, Journal of Sound and Vibration, 344 (2015) 209-220. https://www.sciencedirect.com/science/article/abs/pii/S0022460X15000735

[66] I. Elishakoff, G. M. Tonzani and A. Marzani, Three alternative versions of Bresse-Timoshenko theory for beam, International Journal of Mechanic Science, 149 (2018) 402-412. https://www.sciencedirect.com/science/article/pii/S0020740317302278

[67] I. Elishakoff, Handbook on Timoshenko-Ehrenfest and Uflyand-Mindlin plate theories, World Scientific Publishing Company, 2019.

[68] N. Challamel and I. Elishakoff, A brief history of first-order shear-deformable beam and plate models, mechanics Research Communications, 102 (103389) (2019) 1-8. https://www.sciencedirect.com/science/article/abs/pii/S0093641319302289

[69] M. B. Rubin, On the quest for the best Timoshenko shear coefficient, Journal of Applied Mechanics, 70 (2003) 154-158. https://asmedigitalcollection.asme.org/appliedmechanics/article-abstract/70/1/154/447384/On-the-Quest-for-the-Best-Timoshenko-Shear?redirectedFrom=fulltext

[70] G. Exadaktylos, Overview of micro-elasticity theories with emphasis on strain gradient elasticity: part I – Theoretical considerations, CTU, Prague, 2017.

[71] A. Eringen, On differential equations of nonlocal elasticity and solutions of screw dislocation and surface waves, Journal of Applied Physics, 54 (1983) 4703-4710. https://aip.scitation.org/doi/10.1063/1.332803

[72] M. D. Kruskal and N. J. Zabusky, Stroboscopic perturbation for treating a class of nonlinear wave equations, Mathematics and Physics, 5 (1964) 231-244. https://aip.scitation.org/doi/10.1063/1.1704113

[73] U. Gul, M. Aydogdu and G. Gaygusuzoglu, Axial dynamics of a nanorod embedded in an elastic medium using doublet mechanics, Composite Structures, 160 (2017) 1268-1278. https://www.sciencedirect.com/science/article/abs/pii/S026382231631916X

[74] H. Askes and A. V. Metrikine, Higher-order continua derived from discrete media: continualization aspects and boundary conditions, journal of Solids and Structures, 42 (2005) 187–202. https://www.sciencedirect.com/science/article/abs/pii/S0020768304001714

[75] I. V. Andrianov, G. A. Starushenko and D. Wiechert, Numerical investigation of 1D continuum dynamical models of discrete chain, ZAMM Z Angew Math Mech, 92 (2012) 945–954. https://onlinelibrary.wiley.com/doi/abs/10.1002/zamm.201200057

[76] N. Challamel, M. Aydogdu and I. Elishakoff, Statics and dynamics of nanorods embed- ded in an elastic medium: nonlocal elasticity and lattice formulations, European Journal of Mechanics- A/Solids, 67 (2018) 254–271. https://www.sciencedirect.com/science/article/abs/pii/S0997753817301900

[77] H. Hencky, Über die angenäherte lösung von stabilitätsproblemen im raummittels der elastischen gelenkkette, Der Eisenbau, 11 (1920) 437–452 (in German).

[78] M. S. E. Naschie, Stress, stability and chaos in structural engineering: An energy approach, McGraw-Hill, New York., 1990.

[79] N. Challamel, J. N. Reddy and C. M. Wang, Eringen's stress gradient model for bending of nonlocal beams, Engineering Mechanic, 142 (12) (2016) 1-9. https://ascelibrary.org/doi/abs/10.1061/%28ASCE%29EM.1943-7889.0001161

[80] F. Gomez-Silva and R. Zaera, Analysis of low order non-standard continualization methods for enhanced prediction of the dispersive behaviour of a beam lattice, Journal of Mechanical Science, 196 (2021) https://www.sciencedirect.com/science/article/abs/pii/S002074032100031X

[81] N. Nejadsadeghi, L. Placidi, M. Romeo and A. Misra, Frequency band gaps in dielectric granular metamaterials modulated by electric field, mechanics Research Communications, 95 (2019) 96-103. https://doi.org/10.1016/j.mechrescom.2019.01.006

[82] A. Misra and N. Nejadsadeghi, Longitudinal and transverse elastic waves in {1D} granular materials modeled as micromorphic continua, Wave Motion, 90 (2019) 175-195. https://doi.org/10.1016/j.wavemoti.2019.05.005

[83] N. Nejadsadeghi and A. Misra, Role of higher-order inertia in modulating elastic wave dispersion in materials with granular microstructure, International Journal of Mechanical Sciences, 185 (2020) https://doi.org/10.1016/j.ijmecsci.2020.105867

[84] S. Massoumi, N. Challamel and J. Lerbet, Bending/Shear wave dispersion analysis of granular chains – discrete and enriched continuous Cosserat modelling, International Journal of Solids Structures, 1-16 (111355) (2022) 236-237. https://doi.org/10.1016/j.ijsolstr.2021.111355

[85] Y. Starosvetsky, K. R. Jayaprakash and A.F. Vakakis, J. Appl. Mech. 79, 011001 (2012). Scattering of solitary waves and excitation of transient breathers in granular media by light intruders and no precompression, Journal of Applied Mathematics, 79 (2012) 11001-11013. https://asmedigitalcollection.asme.org/appliedmechanics/article-

abstract/79/1/011001/475144/Scattering-of-Solitary-Waves-and-Excitation-of?redirectedFrom=fulltext

[86] V. F. Nesterenko, Propagation of nonlinear compression pulses in granular media, Journal of Applied Mechanics and Technical Physics, 24 (1984) 733-743. https://link.springer.com/article/10.1007/BF00905892

[87] E. B. Herbold et al., Pulse propagation in a linear and nonlinear diatomic periodic chain: effects of acoustic frequency band-gap, Acta Mechanica, 205 (2009) 85-103. https://link.springer.com/article/10.1007/s00707-009-0163-6

[88] S. Massoumi, N. Challamel and J. Lerbet, Exact solutions for the vibration of finite granular beam using discrete and gradient elasticity Cosserat models, Journal of Sound and Vibration, 494 (2021) 115839. https://doi.org/10.1016/j.jsv.2020.115839

[89] R. D. Gauthier and W. E. Jahsman, A quest for micropolar elastic constants, Journal of Applied Mechanics, 42 (1975) 369-374.

[90] R. S. Lakes, Experimental methods for study of Cosserat elastic solids and other generalized continua. In: Mühlhaus, H. (ed.) Continuum Models for Materials with Micro-Structure, Wiley, New York 1995.

[91] R. Mora and A. M. Waas, Measurement of the Cosserat constant of circular-cell polycarbonate honeycomb, Philosophical Magazine a-Physics of Condensed Matter Structure Defects, 80 (7) (2000) 1699–1713. https://doi.org/10.1080/01418610008212145

[92] A. J. Beveridge, M. A. Wheel and D. H. Nash, The micropolar elastic behaviour of model macroscopically heterogeneous materials, International Journal of Solids and Structures, 50 (1) (2013) 246-255. https://www.sciencedirect.com/science/article/pii/S0020768312004076

[93] R. S. Lakes, D. Gorman and W. Bonfield, Holographic screening method for microelastic solids, Journal of Materials Science, 20 (8) (1985) 2882-2888. https://doi.org/10.1007/BF00553052

[94] I. Cielecka, M. Wo´zniak and C. Wo´zniak, Elastodynamic behaviour of honeycomb cellular media, Journal of Elasticity, 60 (2000) 1-17. https://doi.org/10.1023/A:1007634916326

[95] R. Larsson and Y. Zhang, Homogenization of microsystem interconnects based on micropolar theory and discontinuous kinematics, Journal of the Mechanics and Physics of Solids, 55 (4) (2007) 819–841 https://doi.org/10.1016/j.jmps.2006.09.010

[96] A. C. Eringen, Theory of micropolar plates, ZAMP, 18 (1) (1967) 12–30. https://doi.org/10.1007/BF01593891

[97] A. C. Eringen, Microcontinuum Field Theory. I. Foundations and Solids. Springer, New York, 1999.

[98] H. Altenbach and V. A. Eremeyev, On the linear theory of micropolar plates, ZAMM Z Angew Math Mech, 89 (4) (2009) 242–256. https://doi.org/10.1002/zamm.200800207

[99] H. Altenbach and V. Eremeyev, On the constitutive equations of viscoelastic micropolar plates and shells of differential type, Mathematics and Mechanics of Complex Systems, 3 (3) (2015) 273-283. DOI: 10.2140/memocs.2015.3.273

[100] I. Giorgio, F. dell'Isola and A. Misra, Chirality in 2D Cosserat media related to stretch-micro-rotation coupling with links to granular micromechanics, International Journal of Solids and Structures, 202 (2020) 28-38. https://doi.org/10.1016/j.ijsolstr.2020.06.005

[101] S. Casolo, Macroscopic modelling of structured materials: Relationship between orthotropic Cosserat continuum and rigid elements, International Journal of Solids and Structures, 43 (2006) 475-496. https://doi.org/10.1016/j.ijsolstr.2005.03.037

[102] M. O. Ouali, P. Poorsolhjouy, L. Placidi and A. Misra, Evaluation of the effects of stress concentrations on plates using granular micromechanics, Construction and Building Materials, 290 (2021) https://doi.org/10.1016/j.conbuildmat.2021.123227

[103] E. Turco, F. dell'Isola and A. Misra, A nonlinear Lagrangian particle model for grains assemblies including grain relative rotations, International Journal for Numerical and Analytical Methods in Geomechanics, 43 (5) (2019) 1051-1079. https://doi.org/10.1002/nag.2915

[104] L. Placidi, E. Barchiesi, A. Misra and D. Timofeev, Micromechanics-based elasto-plastic–damage energy formulation for strain gradient solids with granular microstructure, Continuum Mechanics and Thermodynamics, (2021) 1-29. https://doi.org/10.1007/s00161-021-01023-1

[105] D. Timofeev, E. Barchiesi, A. Misra and L. Placidi, Hemivariational continuum approach for granular solids with damage-induced anisotropy evolution, Mathematics and Mechanics of Solids, 26 (2021) 738-770. https://doi.org/10.1177/1081286520968149

[106] A. D. Hasanyan and A. M. Waas, On the Buckling of a Two-Dimensional Micropolar Strip, Journal of Applied Mechanics, 82 (4) (2015) https://asmedigitalcollection.asme.org/appliedmechanics/article-abstract/82/4/041006/443704/On-the-Buckling-of-a-Two-Dimensional-Micropolar?redirectedFrom=fulltext

[107] A. Misra and P. Poorsolhjouy, Elastic behavior of 2D grain packing modeled as micromorphic media based on granular micromechanics, Journal of Engineering Mechanics, 143 (1) (2016) C4016005. https://doi.org/10.1061/(ASCE)EM.1943-7889.0001060

[108] I. Giorgio, M. D. Angelo, E. Turco and A. Misra, A Biot–Cosserat two-dimensional elastic nonlinear model for a micromorphic medium, Continuum Mechanics and Thermodynamics, 32 (2020) 1357–1369. https://doi.org/10.1007/s00161-019-00848-1

[109] G. R. Cowper, The shear coefficients in Timoshenko's beam theory, Journal of Applied Mechanics, 33 (1966) 335-340. https://asmedigitalcollection.asme.org/appliedmechanics/article-abstract/33/2/335/386601/The-Shear-Coefficient-in-Timoshenko-s-Beam-Theory?redirectedFrom=fulltext

[110] S. P. Timoshenko, Strength of materials, D. Van Nostrand Company, New York, 1930.

[111] C. M. Wang, J. N. Reddy and K. H. Lee, Shear deformable beam and plates – Relationships with classical solutions, Elsevier, 2000.

[112] V. Šmilauer et al., Yade Documentation 2nd ed, (2015) http://yadedem.org/doc/. doi:10.5281/zenodo.34073.

[113] L. Verlet, Computer ‘‘experiments” on classical fluids. i. thermodynamical properties of lennard-jones molecules, Physical Review, 159 (1967) 98. https://journals.aps.org/pr/abstract/10.1103/PhysRev.159.98

[114] E. Winkler, The doctrine of elasticity and strength, Dominicus, Prague, 1867.

[115] A. Bacigalupo and C. Gambarotta, Generalized micropolar continualization of 1D beam lattices, Journal of Mechanic Science, 155 (2019) 554-570. https://www.semanticscholar.org/paper/Generalized-micropolar-continualization-of-1D-beam-Bacigalupo-Gambarotta/cdfa099a77c74e0b898f3c4e8c7f9d763a8f0986

[116] N. Challamel, J. Lerbet and C. M. Wang, On buckling of granular columns with shear interaction: discrete versus nonlocal approaches, Journal of Applied Physics, 115 (2014) 234902. https://aip.scitation.org/doi/abs/10.1063/1.4883540

[117] N. Challamel, J. Lerbet, F. Darve and F. Nicot, Buckling of granular systems with discrete and gradient elasticity Cosserat continua, Annals of Solid and Structural Mechanics, 12 (2020) 7-22. https://doi.org/10.1007/s12356-020-00065-5

[118] F. Y. Cheng and C. P. Pantelides, Dynamic Timoshenko beam-columns on elastic media, Journal of Structure Engineering, 114 (1988) 1524-1550. https://ascelibrary.org/doi/10.1061/%28ASCE%290733-9445%281988%29114%3A7%281524%29

[119] S. Goldberg, Introduction to difference equations: with illustrative examples from economics, psychology, and sociology, Dover publications, New-York, 1958.

[120] S. Elaydi, An introduction to difference equations, Springer, New York, 2005.

[121] I. Elishakoff and R. Santoro, Error in the finite difference based probabilistic dynamic analysis: analytical evaluation, Journal of Sound and Vibration, 281 (2005) 1195-1206. https://www.researchgate.net/publication/238951362_Error_in_the_finite_difference_based_probabilistic_dynamic_analysis_Analytical_evaluation

[122] I. Elishakoff and R. Santoro, Accuracy of the finite difference method in stochastic setting, Journal of Sound and Vibration, 2911 (2006) 275-284. https://www.sciencedirect.com/science/article/abs/pii/S0022460X05004049

[123] G. W. Hunt, A. Tordesillas, S. C. Green and J. Shi, Force-chain buckling in granular media: a structural mechanics perspective, Philos Trans A Math Eng Sci, 368 (2010) 249-262. https://www.ncbi.nlm.nih.gov/pubmed/19948554

[124] Z. Zhang, C. M. Wang, N. Challamel and I. Elishakoff, Obtaining Eringen′s length scale coefficient for vibrating nonlocal beams via continualization method, Journal of Sound and Vibration, 333 (2014) 4977-4990. https://www.sciencedirect.com/science/article/abs/pii/S0022460X1400371X

[125] R. W. Traill-Nash and A. R. Collar, The effects of shear flexibility and rotory inertia of the bending vibrations of beams, Journal of Mechanics and Applied Math, 6 (2) (1953) 186-222. https://academic.oup.com/qjmam/article-abstract/6/2/186/1823872?redirectedFrom=fulltext

[126] M. G. Salvadori, Numerical computation of buckling loads by finite differences, ASCE, 116 (1951) 590-624. https://www.semanticscholar.org/paper/Closure-of-%22Numerical-Computation-of-Buckling-Loads-Salvadori/ffdb1fa7e0721241a49968b54e74fae5ed518eb1

[127] A. G. Baker and P. Graves-Morris, Pade approximants, Cambridge University Press, 1996.

[128] E. Winkler, Die Lehre von der Elasticitaet und Festigkeit, Prague, Dominicus, (1867)

[129] D. D. Domenico and H. Askes, Nano scale wave dispersion beyond the First Brillouin Zone simulated with inertia gradiant continua, Journal of Applied Physics, 124 (2018) https://aip.scitation.org/doi/10.1063/1.5045838

[130] P. Lu, H. P. Lee and C. Lu, Dynamic properties of flexural beams using a nonlocal elasticity model, Journal of Applied Physics, 99 (2006) 073510-073519. https://www.semanticscholar.org/paper/Dynamic-properties-of-flexural-beams-using-a-model-Lu-Lee/b164e6fb5c0d2a1b0e8a725a9b78c7870ba6721d

[131] N. Challamel, C. M. Wang and I. Elishakoff, Discrete systems behave as nonlocal structural elements: Bending, buckling and vibration analysis, European Journal of Mechanics A/Solids, 44 (2014) 125-135. https://www.sciencedirect.com/science/article/abs/pii/S0997753813001204

[132] M. D. Kruskal and N. J. Zabusky, Stroboscopic perturbation for treating a class of nonlinear wave equations, Journal of Mathematical Physics, 5 (1964) 231-244. https://aip.scitation.org/doi/10.1063/1.1704113

[133] L. Wang and H. Hu, Flexural wave propagation in single-walled carbon nanotubes, Physical Review B, 71 (195412) (2005) https://journals.aps.org/prb/abstract/10.1103/PhysRevB.71.195412

[134] T. Vodenitcharova and L. C. Zhang, Effective wall thickness of a single-walled carbon nanotube, Physical Review B, 68 (165401) (2003) https://journals.aps.org/prb/abstract/10.1103/PhysRevB.68.165401

[135] A. W. Bojanczyk and A. Lutoborski, Computation of the Euler angles of a symmetric 3x3 matrix, Journal on Matrix Analysis and Applications, 12 (1991) 41-48. https://doi.org/10.1137/0612005

[136] V. A. Eremeyev, L. P. Lebedev and H. Altenbach, Foundations of micropolar mechanics, Springer, 2013.

[137] F. dell'Isola and S. L. Gavrilyuk, Variational models and methods in solid and fluid mechanics, CISM International Centre for Mechanical Sciences, Springer-Verlag Wien, Vienna, 2012.

[138] P. Steinmann and E. Stein, A uniform treatment of variational principles for two types of micropolar continua, Acta Mechanica, 121 (1997) 215–232

[139] I. Nistor, Variational principles for Cosserat bodies, International Journal of Non-Linear Mechanic, 37 (2002) 565–569. https://doi.org/10.1016/S0020-7462(00)00113-X

[140] Z. Hashin and S. Shtrikman, A variational approach to the theory of the elastic behaviour of multiphase materials, Journal of the Mechanics and Physics of Solids, 11 (2) (1963) 127-140. https://doi.org/10.1016/0022-5096(63)90060-7

[141] A. S. J. Suiker, A. V. Metrikine and R. Borst, Dynamic behaviour of a layer of discrete particles, Part 1: Analysis of body waves and eigenmodes, Journal of Sound and Vibration, 240 (2001) 1-18. 1

[142] A. S. J. Suiker, A. V. Metrikine and R. Borst, Comparison of wave propagation characteristics of the Cosserat continuum model and corresponding discrete lattice models, Journal of Solids Structure, 38 (2001) 1563–1583.

[143] I. S. Pavlov, A. I. Potapov and G. A. Maugin, A 2D granular medium with rotating particles, Journal of Solids Structure, 43 (2006) 6194-6207.

[144] E. Pasternak and A. V. Dyskin, On a possibility of reconstruction of Cosserat moduli in particulate materials using long waves, Acta Mechanica, DOI 10.1007/s00707-014-1132-2 (2014)

[145] H. Schaefer, Versuch einer Elastizitätstheorie des zweidimensionalen ebenen Cosserat-Kontinuums, Berlin: Akademie-Verlag, 1962.

[146] S. Massoumi and G. La-Valle, Static analysis of 2D micropolar model for describing granular media by considering relative rotations, mechanics Research Communications, (2021)

[147] A. Misra and P. Poorsolhjouy, Identification of higher-order elastic constants for grain assemblies based upon granular micromechanics, Mathematics and Mechanics of Complex Systems, 3 (3) (2015) 285-308. https://msp.org/memocs/2015/3-3/p04.xhtml

[148] I. Giorgio et al., Wrinkling in engineering fabrics: a comparison between two different comprehensive modelling approaches, Proceedings of the Royal Society A: Mathematical, Physical and Engineering Sciences, 474 (2216) (2018) https://doi.org/10.1098/rspa.2018.0063

[149] M. D. Angelo, E. Barchiesi, I. Giorgio and B. E. Abali, Numerical identification of constitutive parameters in reduced-order bi-dimensional models for pantographic structures: application to out-of-plane buckling, Archive of Applied Mechanics, 89 (7) (2019) 1333-1358. https://doi.org/10.1007/s00419-018-01506-9

[150] E. Turco, Identification of axial forces on statically indeterminate pin-jointed trusses by a nondestructive mechanical test, The Open Civil Engineering Journal, 7 (1) (2013) DOI: 10.2174/1874149501307010050